THE UNIVERSITY OF HUDDERSFIELD

Photophysics and Applications of Triazole Complexes

By

SALEM ALI ELHADI OMAR

A thesis submitted in partial fulfilment for the

Degree of Doctor of Philosophy

In the

School of Applied Sciences.

Department of Chemical and Biological Sciences

December 2017

1

Copyright Statement

Abstract

1,2,3-Triazoles have proven to be highly successful in ligand design due to their facile synthesis owing to the advent of the copper-catalyzed azide-alkyne cycloaddition (CuAAC) reaction. The Cu(I) species necessary for the CuAAC reaction can be generated in situ with simple purification of the resulting 1,4-disubstituted products and has proven to be an outstanding method to prepare triazole-containing ligands.

The present work focuses on the synthesis, characterization and photophysical investigation of triazole-containing transition metal complexes and their possible use in applications, such as LECs and biological cell imaging. To explore this wide topic different types of 1,2,3-triazole containing ligands including 2-(1-benzyl-1H-1,2,3-triazol-4-yl)pyridine as a bidentate ligand, 2,6-bis(1-phenyl-1H-1,2,3-triazol-4-yl)pyridine as a tridentate ligand and 1,4-bis((4-(pyridin-2-yl)-1H-1,2,3-triazol-1-yl)methyl)benzene as a bridging ligand. were prepared and used with Re(I), Os(II), Ru(II) and Ir(III) transition metals.

Chapter 2 deals with rhenium complexes $[Re(CO)_3(Bn-pytz)(X)]^{+/0}$ (X = Cl or substituted pyridine). The photophysical investigation indicates that the emission can be further shifted towards the blue by replacing the Cl^- ligand with pyridine. Two of these complexes were utilised in preliminary tests as the phosphor in light-emitting electrochemical cell LEC devices.

In Chapter 3 a series of osmium(II) complexes $[Os(bpy)_{3-n}(Bn-pytz)_n](PF_6)_2$ (where bpy = bipyridine, n = 1, 2, 3) were prepared and characterised. The progressive replacement of bpy by Bn-pytz leads to blue-shifted UV-visible electronic absorption and emission spectra. Successful separation of the *fac* and *mer* isomers of $[Os(Bn-pytz)_3](PF_6)_2$ complexes was achieved, which exhibits phosphorescence (λ_{em} = 615 nm, in degassed acetonitrile). $[Os(Bn-pytz)_3][PF_6]_2$ was shown to exhibit significant quenching of luminescence intensity in the presence of oxygen (K_{sv} = 83 atm^{-1}). The water soluble chloride form of the complexes were prepared and were subjected to preliminary cellular uptake and luminescence imaging microscopy studies. The results from these studies reveal that the $[Os(Bn-pytz)_3]^{2+}$ is successfully taken up by two cancer cell lines. Bright emission from $[Os(Bn-pytz)_3]^{2+}$ can be seen by

confocal microscopy with localisation at the lysosomes, however, no photodynamic therapy (PDT) activity is observed.

Described in Chapter 4 is the synthesis, characterisation and photophysical investigation of an osmium(II) 2,6-bis(1-phenyl-1H-1,2,3-triazol-4-yl)pyridine (btzpy) complex. From photophysical investigations [Os(btzpy)$_2$](PF$_6$)$_2$ exhibits phosphorescence (λ_{em} = 595 nm, τ = 937 ns, φ_{em} = 9.3% in degassed acetonitrile). The complex undergoes significant oxygen-dependent quenching of emission with a 43-fold reduction in luminescence intensity between degassed and aerated acetonitrile solutions (K_{sv} = 110 atm^{-1}), demonstrating its capability as a singlet oxygen sensitiser. The water soluble chloride form of the complex was prepared on the basis of the photophysical properties and was subject to preliminary cellular uptake and luminescence microscopy imaging studies. The complex easily entered the HeLa and U2OS cancer cell lines with mitochondrial localisation observed with intense emission permitting imaging at reduced concentrations up to 1 µM. Long-term dose toxicity results show low toxicity in HeLa cells with LD$_{50}$ >100 µM.

Described in Chapter 5 is the synthesis and characterisation of a range of dinuclear supramolecular complexes, containing a bridging ligand incorporating the 1,2,3-triazole moiety. The homonuclear complexes ([Ir(ppy)$_2$-L-Ir(ppy)$_2$](PF$_6$)$_2$, [Ru(bpy)$_2$-L-Ru(bpy)$_2$](PF$_6$)$_4$, [Os(bpy)$_2$-L-Os(bpy)$_2$](PF$_6$)$_4$ and [Os(Bn-pytz)$_2$-L-Os(Bn-pytz)$_2$](PF$_6$)$_4$ and heteronuclear complex ([Ru(bpy)$_2$-L-Ir(ppy)$_2$](PF$_6$)$_3$ (where L = 1,4-{bis-4-(pyrid-2-yl)-1,2,3-triazol-1-yl methyl}benzene) were prepared. Photophysical studies show that the dinuclear species display greater luminescence intensities than their mononuclear model complexes. The emission spectra of the heteronuclear complex [Ru(bpy)$_2$-L-Ir(ppy)$_2$](PF$_6$)$_3$, exhibits features similar to those observed in the emission spectra of the mononuclear complexes [Ir(ppy)$_2$-L](PF$_6$) and [Ru(bpy)$_2$-L](PF$_6$)$_2$. This indicates dual emission occurs from both the Ir- and Ru-centred chromophores (φ_{em} = 0.33% in acetonitrile). Interestingly the emission from the Ru-centred chromophore seems greatly enhanced relative to the emission of the Ru mononuclear analogue. This indicates partial energy transfer from Ir to Ru. The dual emission results in near white light emission and could be used for the devolpment of single component white light emitting phosphors.

Acknowledgements

In the name of Allah the most Beneficent, the most Merciful

Contents

VIII

IX

X

List of Figures

XIII

XIV

XV

XVI

List of Schemes

List of Tables

XIX

Abbreviations

°	**Degrees**
°C	**Degrees Celsius**
^{13}C NMR	**Carbon-13 nuclear magnetic resonance**
^{1}H NMR	**Proton nuclear magnetic resonance**
^{1}MLCT	**Singlet metal-to-ligand charge transfer**
^{1}O$_2$	**singlet oxygen**
2D	**2-dimensional**
^{3}MLCT	**Triplet metal-to-ligand charge transfer**
acac	**acetylacetone**
aq	**Aqueous**
Bn-pytz	**(1-benzyl-1H-1,2,3-triazol-4-yl)pyridine**
bpy	**2,2'-bipyridyl**
Btzpy	**2,6-bis(1-phenyl-1H-1,2,3-triazol-4-yl)pyridine**
CDCl$_3$	**Deuterated chloroform**
CH$_3$CN	**Acetonitrile**
cm^{-1}	**Wavenumbers**
CNS	**Central Nervous System**
COSY	**Correlation Spectroscopy**
Cp	**Cyclopentadienyl**
CuAAC	**Copper catalysed azide-alkyne cycloaddition**
DCM	**Dichloromethane**
DFT	**Density functional theory**
DMF	**Dimethyl formamide**
DMSO	**Dimethyl sulfoxide**
DPEPhos	**bis{2-(diphenylphos-phanyl)phenyl} ether]**
DSSCs	**Dye-sensitized solar cells**
ESI-MS	**Electrospray ionization mass spectrometry**
eV	**Electron-volt**
FT-IR	**Fourier transform infra-red**
g	**Grams**
HOMO	**Highest occupied molecular orbital**
HRMS	**High resolution mass spectrometry**
Hz	**Hertz**
J	**Coupling Constant**
K	**Kelvin**
Kcal mol^{-1}	**Kilocalories per molecule**
L	**1,4-bis((4-(pyridin-2-yl)-1H-1,2,3-triazol-1-yl)methyl)benzene**
LC	**Ligand centred**
LEEC	**Light emitting electrochemical cell**

LF	ligand field
LUMO	Lowest unoccupied molecular orbital
M	Molarity/Molar
m/z	mass/charge
MC	Metal centred
mg	Milligram
mins	Minutes
ml	Millilitre
MLCT	Metal-to-ligand charge transfer
MLLCT	Metal-to-ligand-to-ligand charge transfer
mmol	Millmole
mtpy =L2	4'-(p-tolyl)-2,2':6',2''-terpyridine
nm	Nanometer
nOe	Nuclear Overhauser effect
NOESY	Nuclear Overhauser effect spectroscopy
ns	Nanosecond
OLED	Organic light emitting diode
PDT	Photodynamic Therapy
pic	picolinic acid
PLED	Polymer light emitting diode
ppm	Parts per million
ppy	2-phenylpyridine
PS	photosensitizer
py	Pyridine
pytz	2-(1,2,3-triazol-4-yl)pyridine
RuACC	Ruthenium catalysed azide alkyne cycloaddition
S_0	Singlet ground state
T_1	Lowest triplet excited state
TBTA	Tris-(benzyltriazolymethyl)amine
THF	Tetrahydrofuran
TMS	Trimethylsilyl
tpy	2,2':6',2''-terpyridine
UV-vis	Ultraviolet-visible
V	Volts
δ	Delta (chemical shift)
τ	Lifetime

Chapter 1:   Introduction

1.1 **Introduction**

Transition metal complexes occupy a prominent position in photophysics and photochemistry because of their remarkable properties and stability.[1] The field of photophysics and photochemistry of coordination complexes of transition metals has received increasing interest in the last few decades for the understanding of the excited state properties and photochemical reactions.[2] In the earlier studies, transition metal complex photochemistry was mainly confined to and dominated by photosubstitution reactions typical of ligand field (LF) excited state reactivates of chromium(III) complexes[3] and metal carbonyls.[4] In 1971 photoredox reactivities characteristic of the metal-to-ligand charge transfer (MLCT) excited states of ruthenium(II) bipyridine complexes became apparent.[5] This has also eventually led to the emergence of a new branch of supramolecular photochemistry.[6] d^6 transition metal complexes which demonstrate luminescence have been utilized as probes in photosensitizers developed for conversion of solar energy[7] and electron transfer reactions.[8] Although most of these applications use Ru(II) complexes, researchers have been exploring the excited state characteristics of Re(I),[9] Ir(III),[10] Mo(O),[11] W(O), Os(II)[12] and Pt(II)[13] complexes. Control of the photophysical and photochemical properties of the complex can be achieved by manipulating ligands and metal. The ligand design was perhaps the most important step in the development of metal complexes which display unique properties and novel reactivity. The full potential of color tuning of complexes can be controlled by ligand design. Therefore reactions that enable the facile routes to the modular construction of new ligands and these architectures are particularly useful in the development of such materials. The structure of the complex is important for development of the solar energy conversion device that relates to the different applications such as luminescent sensors, dyesensitised solar cells DSSCs, light-emitting electrochemical cells LECs and OLEDs.[14] Over the last 40 years, transition metal- complexes

have been realized for their therapeutic properties in several fields of medicine. Since phosphorescence is longer-lived than the autofluorescence from biological organic compounds, emissive complexes are amenable to use in time-gated imaging microscopy.[15] A combination of rich photophysical and electrochemical properties of the metal complexes has led to their use in numerous applications, covering a wide range such as photocatalysis, luminescent sensors, DSSCs, LECs and OLEDs

1.2 Photophysics of d^6 transition metal complexes

Octahedral d^6 transition metal complexes have received attention in the past few decades due to their rich photophysical, photochemical and redox properties. These characteristics make them amenable to application in artificial photosynthesis,[16] solar fuels catalysis,[17] electroluminescent devices,[18] dyesensitised solar cells (DSSCs),[19] molecular sensors,[20] luminescence live-cell imaging,[21] photoinitiated anticancer agents and singlet oxygen sensitisation for photodynamic therapy.[22] It is essential to describe the energy levels involved in electronic transitions for better understanding of the photophysics of this type of complex. Molecules have many occupied and empty molecular orbitals, for this, there are many possible transitions to elevate an electron from an occupied low-energy orbital to the empty higher-energy orbital. For d^6 transition metal complexes, the π^* ligand orbitals are typically lower in energy than $d\sigma^*$ orbitals. The highest occupied molecular orbital (HOMO) is localised on the metal center and the lowest unoccupied molecular orbital (LUMO) localised on the ligand. The lowest-energy electronic transition corresponds to a transition of an electron from the HOMO to the LUMO. The HOMO-LUMO energy gap (ΔE) usually determines the color of light we see transmitted through a solution. Transitions of an electron from lower-energy occupied orbitals or into higher-energy empty orbitals will essentially need higher-energy photons. The $[Ru(bpy)_3]^{2+}$ complex, displys all the general properties of the d^6 complexes, making it the most

studied complex in transition metal complexes since the 70s. It is used here as an example to describe the energy levels which are involved in the electronic transitions that occur as a result of absorption or emission of light. In this type of d^6 complex the HOMO is dominated by metal d-orbital and the LUMO has predominantly ligand-based π* character. Above the LUMO lie dπLπ* orbitals which are mostly ligand-based π* character. At higher energies are the antibonding dσ* orbitals related to the metal-ligand σ-bonding interactions. (Figure 1.1).
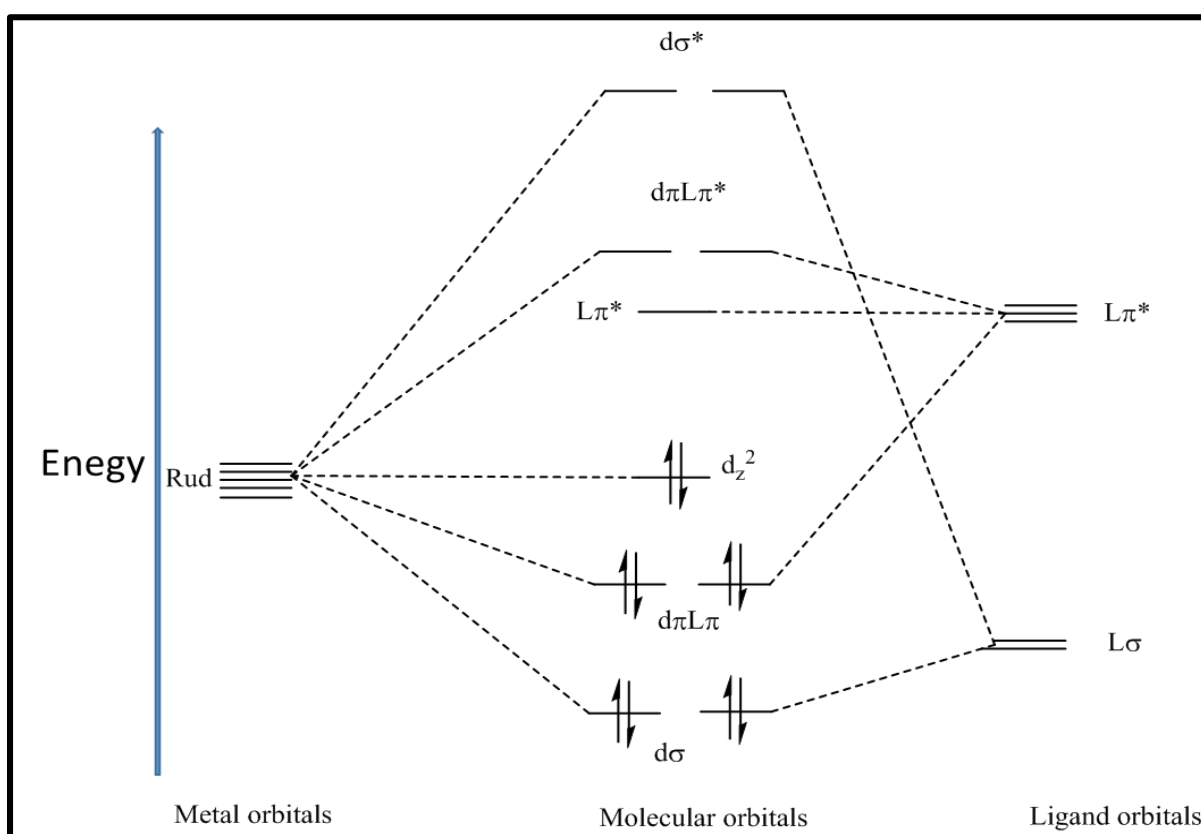
Figure 1-1 Simplified molecular orbital energy diagram for [Ru(bpy)₃]²⁺ transition Metal Complexes

The ground state of transition metal complexes is usually studied by absorption spectroscopy where the spectra are characterized by a low energy MLCT band and some higher energy ligand cantered bands. According to the nature of frontier orbitals, three main optical transitions may arise: (1) the lower energy parity forbidden, metal-centered transition ³MC (the d-d transition) (2) the higher energy π-π* transition localized on the ligand, and (3) the ¹MLCT transition (d-

4

π^*). All these transitions are spin allowed, but only the latter two are observed in the UV-vis absorption spectrum of most of the transition metal complex. Note that in some transition metal complexes the ^{3}MLCT band also exhibits as a low energy tail that stems from the spin-forbidden ^{3}MLCT transitions. The spin forbidden absorption populates the ^{3}MLCT directly from the ground state and is readily observed because of the large spin-orbital coupling effect that results from the heavy metal atom.[23-25]

At ambient temperatures solutions of $[Ru(bpy)_3]^{2+}$ exhibit a broad absorption band centered at 450 nm (MLCT) corresponding to a transition from one of the d-orbitals of Ru^{2+} ion to the ligand π^*-orbitals. During this transition the electron is moved from the HOMO, which is the t_{2g} metal orbital in this case into the LUMO which is a ligand π^* orbital. As a result, the transition metal ion oxidation state changes to Ru^{3+}. The UV range (200-300 nm) is dominated by strong transitions involving ligand orbitals (π and π^* orbitals). They can be grouped into ligand-centered (LC, < 300 >260 nm) and (LMCT, 220-260 nm) transitions. In the case of LMCT transition, the absorption involves the π orbital and the antibonding metal d-orbitals . According to von Zelewsky, the 300-360 nm band can be assigned to the MC states,[25] which strongly overlaps with the MLCT states. Therefore, the MC absorption bands are hidden below the strong background absorption of the MLCT states (which in general have larger absorption cross sections than MC states).[26] Upon photoexcitation in the region 380-490 nm into MLCT band, the long-lived triplet ^{3}MLCT state is formed, which exhibits visible luminescence centered at 620 nm, as shown in Figure 1.2.
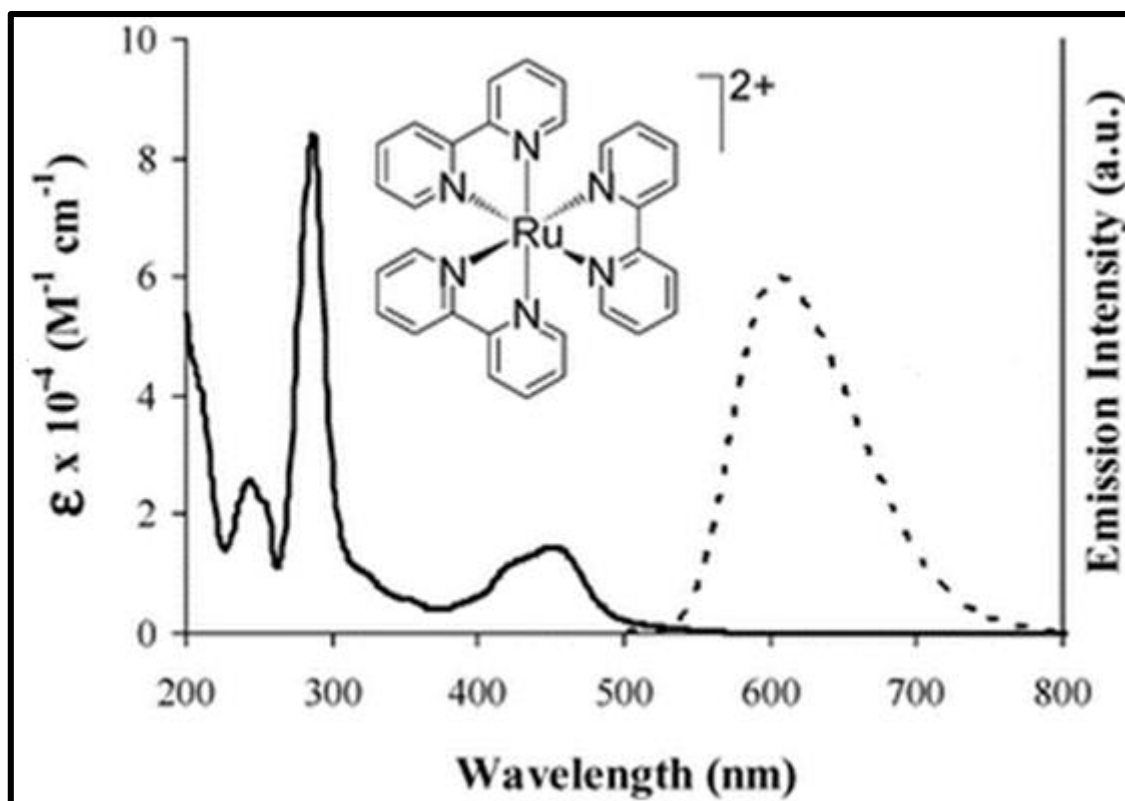
Figure 1-2 Electronic absorption (solid line) and emission spectra (dotted line) of $[Ru(bpy)_3]^{2+}$ in acetonitrile at room temperature. Reprinted from Ref,[27] with permission from Energy & Environmental Science .

The effective population of the ^{3}MLCT state becomes possible due to a large spin-orbit coupling, which results in the significant mixing of the singlet and triplet states. The studies on Ru complexes opened the approach to the design of luminescent complexes based on other d^6 metal complex systems. A very typical example comes from cyclometalated iridium(III) systems. Even these species are very similar from the assembly point of view to the Ru complexes but are more emissive and tunable. Cyclometalated iridium(III) complexes have some important features over classical ruthenium complexes that allow for further development and the amendment of their optical characteristics. As $[Ru(bpy)_3]^{2+}$ is used to represent the ruthenium polypyridine complexes, $Ir(ppy)_3$ may be used to represent the cyclometalated iridium(III) complexes. While the LUMO is localised on the neutral pyridine fragment, the HOMO of this type of complexes have metallic d-orbital character with a significant

contribution from the π-system of the aryl rings.[28] An electronic absorption spectrum of Ir(ppy)$_3$ exhibits an intense LC transition in the UV region with two MLCT (^{1}MLCT and ^{3}MLCT) transitions in the visible region. The complex displays a visible broad and asymmetric emission centred at 515 nm,[29] as shown in Figure 1.3.
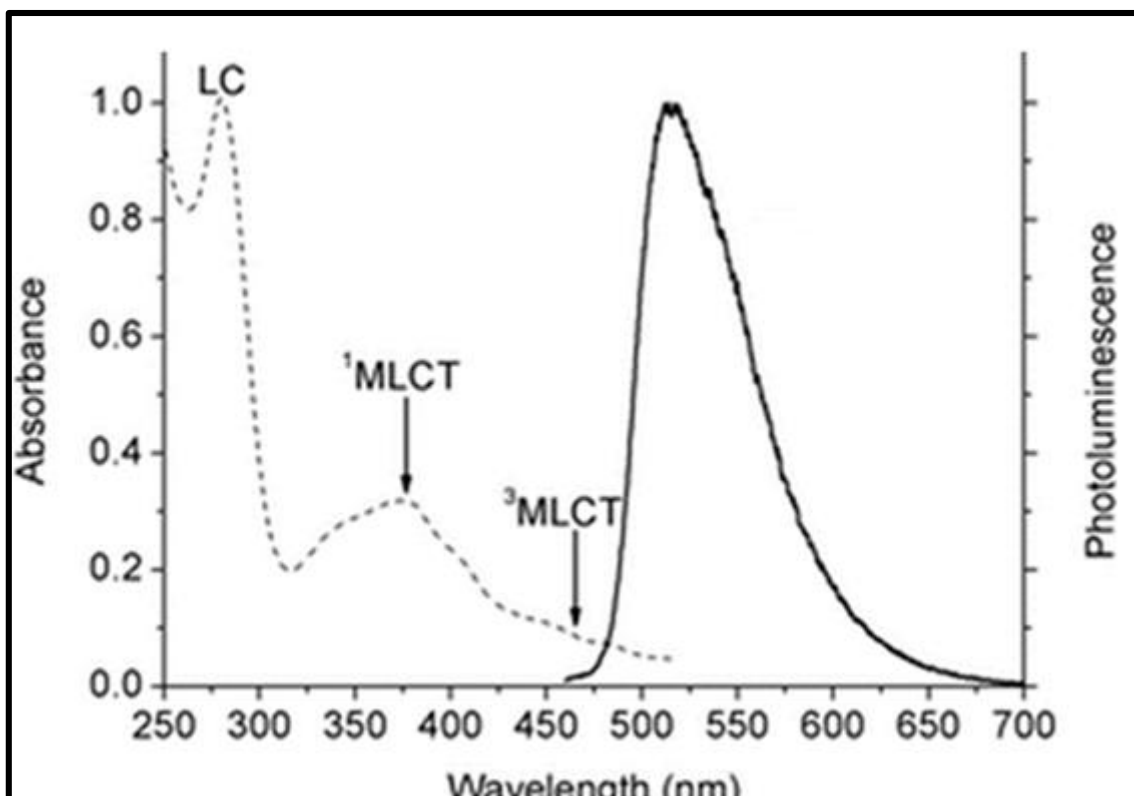
Figure 1-3 Electronic absorption (dotted line) and emission spectra (solid line) of Ir(ppy)$_3$ in dichloromethane at room temperature. Reprinted from Ref,[29] with permission from the Royal society of chemistry.

It is possible to modulate the optical features of Ir complexes by moving from neutral Ir(ppy)$_3$ to cationic [Ir(ppy)$_2$(bpy)]$^+$. This varying in ligand will permit a modification of the HOMO-LUMO energy gap (ΔE). In these type of complexes the HOMO is localised across the metal center and the (C^N) ligand while the LUMO is localised on the 2,2'-bipyridine ancillary ligand.[30] The orbital distribution is the key for predictable and accessible tuning of [Ir(ppy)$_2$(bpy)]$^+$ based hetroleptic complexes, due to the ability to functionalise individually the two types of ligands.[31] Alexander Jablonski (1898-1980) came up with the Jablonski-Diagram[32] which assists with the process through which the theoretical concept for

7

comprehending photophysical features as explained in Figure 1.4 The traditional Jablonski diagram generally assumes a largely isostructural set of ground and excited states and does not take into account changes in the geometry of the complex. According to Jablonski theory, when irradiated with light the complex absorbs energy and the electrons are excited from lower singlet state (S_0) to higher singlet excited state orbital (S_1), which is the lowest energy features in the visible region of the optical absorption spectra of d^6 metal complexes (^{1}MLCT) character. The initial photoexcited singlet state undergoes rapid intersystem crossing (ISC) which is a process where there is a crossover between different multiplicity electronic states such as the singlet state ^{1}MLCT to a triplet state ^{3}MLCT (S_1 to T_1). The photo excited state is generally short lived (10^{-12} s). The complex will relax from the ^{3}MLCT state to the ground state (S_0), which is observed as emission exhibited by these complexes. The emissive states for cyclometalated complexes will also have additional ^{3}ILCT, this process occurs when there is the movement of an electron within one ligand, mostly referred to as $\pi \rightarrow \pi^*$ and/or ^{3}LLCT character, which takes place when an electron moves from one coordinated ligand to another ligand. The relaxation to the ground state takes place with the excited energy being lost by either I) Radiative decay, II) Non-radiative decay.[33]
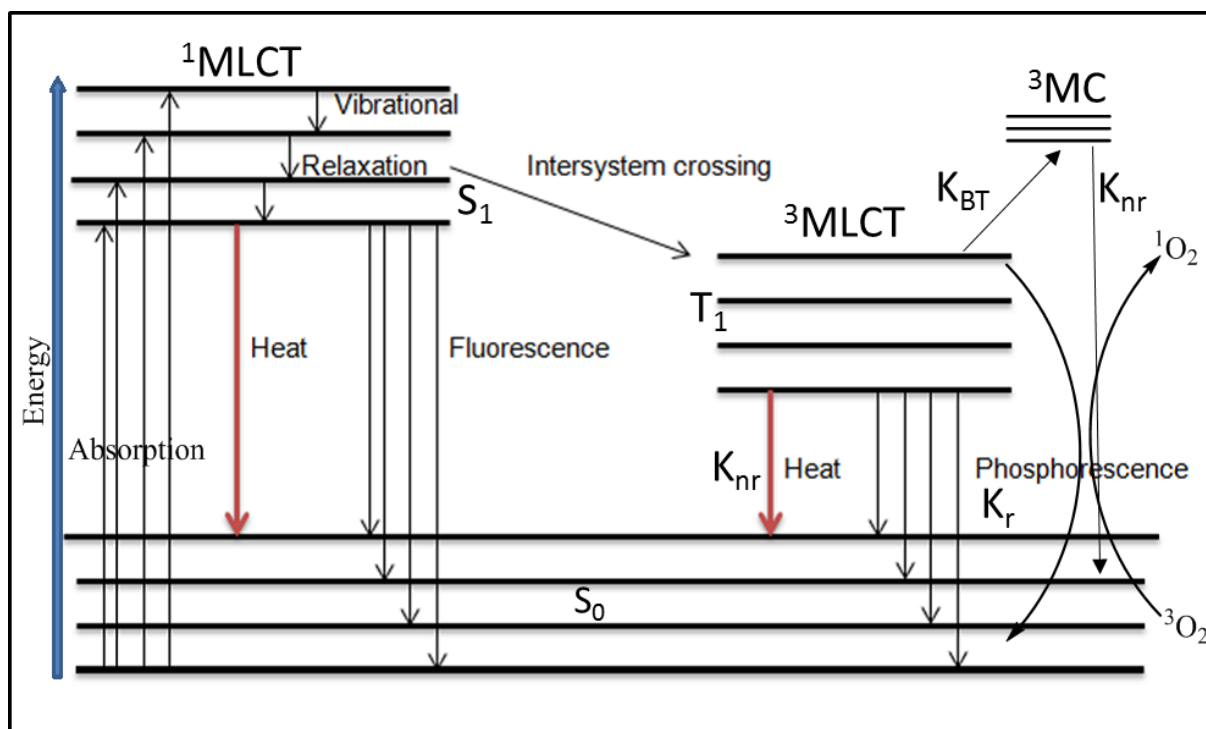
Figure 1-4 Summary of the Various Pathways Available to an Excited Molecule as From Jablonski Diagram.-

1.2.1 Radiative Decay

Luminescence (radiative decay) is a process when the excited electrons relax from their excited state to the ground state and emit a photon of light. In general, luminescence can be categorized by looking at a way through which it is generated. [33] These can be of two types, and that are the fluorescence and phosphorescence.

1.2.1.1 Fluorescence:

 Is a process through which there is the emission of a photon coming from an electronic state to one that has the same multiplicity. When looking at Figure 1.4 it is evident that this process in solution occurs from the first singlet excited state to the ground state, which is also singlet excited state multiplicity. It can be explained as ($S_1 \rightarrow S_0$). The excited mode is seen to relax at a point of the lowest vibration state of S_1. Because the singlet excited state and the ground

9

state have the same multiplicity (spin-allowed), the lifetime of this specific emission is usually very short being at a scale of about 10^{-9} s or shorter. The fluorescence process comes from a thermal equilibrated excited state which is at the lowest energy vibration state. This type of radiative decay mostly occurs within the organic compounds and is not often seen for late transition metal complexes.

1.2.1.2 Phosphorescence:

Is the process through which there is the emission of a photon while electrons move between states of different multiplicity such as ($T_1 \rightarrow S_0$). There is a parallel spin of electrons in the ground state to the excited represented as either ($\uparrow\uparrow$) or ($\downarrow\downarrow$). Even though we have a forbidden spin population of a triplet state, where there are heavy atoms in the spin-orbit coupling. Phosphorescence is a spin forbidden process. Therefore decay rate is several orders of magnitude smaller than those for fluorescence. Figure 1.4 shown in Jablonski diagram and has been stated in Hund's rule. S_1 a singlet state will be of higher energy than a triplet state T_1 in the same configuration. That, therefore, states that phosphorescence will come about at lower energy, therefore, having the longer wavelength that than fluorescence from a given molecule.

1.2.1.3 Excited state lifetime:

As mentioned before for $[Ru(bpy)_3]^{2+}$ complex absorption of a photon elevates an electron from the ground state (GS) to the spin-allowed ^{1}MLCT level. Then intersystem crossing allows for population of the ^{3}MLCT level. The excited electrons may relax back to the GS either without emission (non-radiative decay) or with emission (phosphorescence) or populate the ^{3}MC level (non-radiative decay). Because phosphorescence is spin forbidden, it is longer lived than fluorescence. There is also the rate constant that is found helpful while characterizing every

step of decay experienced by an excited molecule. Lifetime (τ_0) is also seen describing the excited state and can be well expressed as:

$$(\tau_0) = \frac{1}{k_r + k_u + k_{nr}}$$

This equation has k_r, k_u, and k_{nr} which refers to the rate constant for radiative deactivation unimolecular photoreaction and non-radiative deactivation respectively.

1.2.1.4 Quantum yield ϕ:

Quantum yield (ϕ): is the ratio of photons absorbed to photons emitted through radiative decay (e.g Phosphorescence in metal complexes). When the complex absorbs a photon of light, the excited state is formed, with the end of result being that, the electron loses energy and returns to the GS. Some of this energy is lost through intersystem crossing (ISC) or through internal conversion (IC) and vibration relaxation as heat (non-radiative decay) but deactivation also takes place through emission (phosphorescence).

For the $[Ru(bpy)_3]^{2+}$ complex which is used as a standard complex, the quantum yield ϕ can be calculated as a ratio of radiative and total non-radiative decays

$$(\phi) = \frac{k_r}{k_r + k_{nr} + k_u}$$

The absolute value of quantum yield ϕ for any complex can be expressed as:

$$\phi_x = \phi_{ST}\left(\frac{E_x}{E_{ST}}\right)\left(\frac{1 - 10^{AST}}{1 - 10^{Ax}}\right)\left(\frac{\eta^2 x}{\eta^2 ST}\right)$$

Where X and ST, refer to the tested and standard complexes respectively, E refer to the emission intensity of the complexes, A refer to the absorbance and η refractive index of the

solvent. k_{nr} include the deactivation by means of ^{3}MC state, which can be thermally accessed from the ^{3}MLCT state and will give rise to rapid excited state decay and photochemical instability. It is important that any ^{3}MC state is at a higher level than the emitting level when photoluminescence is desired.

1.2.2 Non-Radiative Decay:

The process through which an excited molecule emits heat while resuming to the lower energy state or the ground state is referred to as non-radiative decay. This process can be classified into three types: Internal conversion (IC) is composed of non-emissive relaxation between two states that have equivalent spin multiplicity; it may involve relaxation of the vibrationally excited state to vibrational levels of the ground state; intersystem crossing (ISC) which involves the non-emissive relaxation between states with non-equivalent spin multiplicity. It is a process where there is a crossover between different multiplicity electronic states as revealed in the singlet state ^{1}MLCT to a triplet state ^{3}MLCT (S_1 to T_1) on Figure 1.4. (^{3}MC) states which lie at higher energies and accompany population of the dσ* ligand-field antibonding orbitals, this occurs readily. If the energy barrier on the triplet potential energy surface to their population from ^{3}MLCT states is low enough.

1.2.2.1 O₂ quenching:

One of the important additional non-radiative proceses is quenching of the MLCT state in the presence of molecular oxygen. Because the ground state of oxygen is triplet state ($^3O_2$), it can quench the triplet state of the metal complex, which deactivates the complex and produces singlet oxygen ($^1O_2$). This character gives advantage for transition metal complexes to act as photosensitizer (PS) in photodynamic therapy (PDT). Photodynamic therapy (PDT) uses light to activate a photosensitizer (PS) which is an otherwise nontoxic drug as seen from scheme

below. This technique has advantage over other available therapies due to its inherent ability to induce highly localized cytotoxicity by a point at which photosensitizer and light spatially overlap. The process paves the way for the removal of unwanted cells with little to no damage to the surrounding tissue.[34]

$$PS + hv \rightarrow PS^* + {}^3O_2 \rightarrow PS + {}^1O_2$$
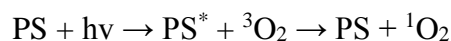
1.3 Application of d^6 transion metal complexes

Due to their attractive photophysical and photochemical properties, d^6 transition metal complexes have been of extensive interest in a number of areas for the past few decades. Applications of the transition metal complexes can be divided in to several sections according to the way they are used.

1.3.1 Transition metal complexes in photocatalysis

Due to their high thermal stability, electronic and electrochemical properties, metal complexes can act as a catalyst.[35] The reduction of CO_2 and photoproduction of hydrogen from the splitting of water using solar energy as the driving force, has been a goal of scientists and engineers since the early 1970s when Fujishima and Honda (1972) reported the generation of hydrogen and oxygen in a photoelectrochemical cell. [36] Since then there has been an explosion of scientific interest and experiments. Now that more than 45 years has elapsed, it is appropriate to take a critical look at the prospects for the solar generation of hydrogen fuel from water. [Re(bpy)(CO)$_3$Cl][37] and [Re(bpy)(CO)$_3${P(OEt)$_3$}]$^{+}$[38] complexes were applied by Raymond Ziessel and Ibusuki as a photocatalyst for the reduction of CO_2 to CO. The complexes indicate high chemical specificity under visible light with quantum yield of CO production of 14 % and 38 % respectively. Morimoto and co-worker[39] investigated the photocatalytic abilities of a Ru(II)−Re(I) binuclear complex (RuReCl) in an aqueous solution, where Ru(II) acts as a

photosensitizer and Re(I) catalyst units were connected with a bridging ligand. The complex showed low photocatalytic efficiency. Further studies of the photochemical electron-transfer process revealed back-electron transfer from the one-electron-reduced species (OERS) of the photosensitizer unit to an oxidized ascorbate proceeded efficiently, and this should be one of the main reasons why the photocatalytic efficiency was lower in the aqueous solution.
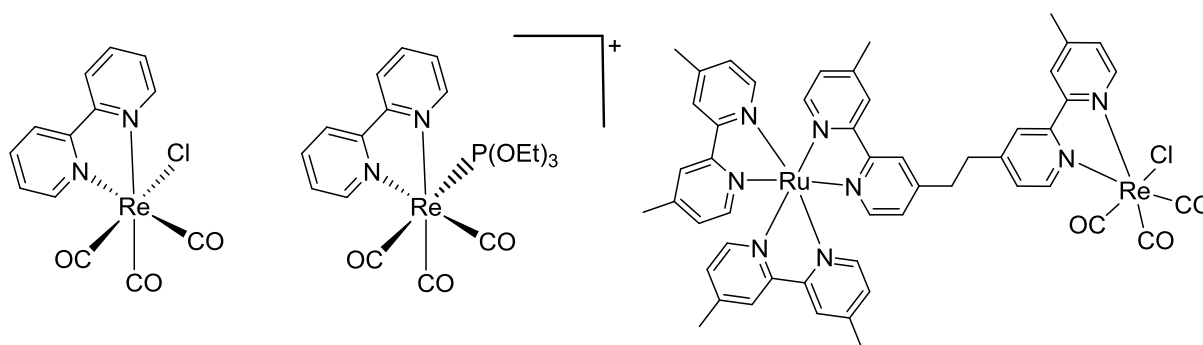
Figure 1-5 Examples of metal complexes used as photocatalysts

1.3.2   Transition metal complexes in light-emitting electrochemical cells LEECs and OLEDs

Light-emitting electrochemical cells LEECs were introduced in 1995 by Pei et al., who mixed a conjugated luminescent polymer with an inorganic salt and an ionic conductive polymer.[40] In 1996 Maness et al., applied [Ru(vbpy)$_3$](PF$_6$)$_2$ complex (vbpy = 4-vinyl-4′-methyl-2,2′-bipyridine) as the single active component in the light-emitting layer.[41] Nowadays, ionic transition metal complex LEECs are mostly based on luminescent ionic biscyclometalated Ir(III) complexes, which like the original Ru(II) complex, may sustain charge injection and transport while affording light emission at the same time.[42] The use of ionic transition metal

complexes in LEECs allows novel device fabrication developments, such as soft contact lamination,[43] as well as the development of large-area illumination panels.[44]
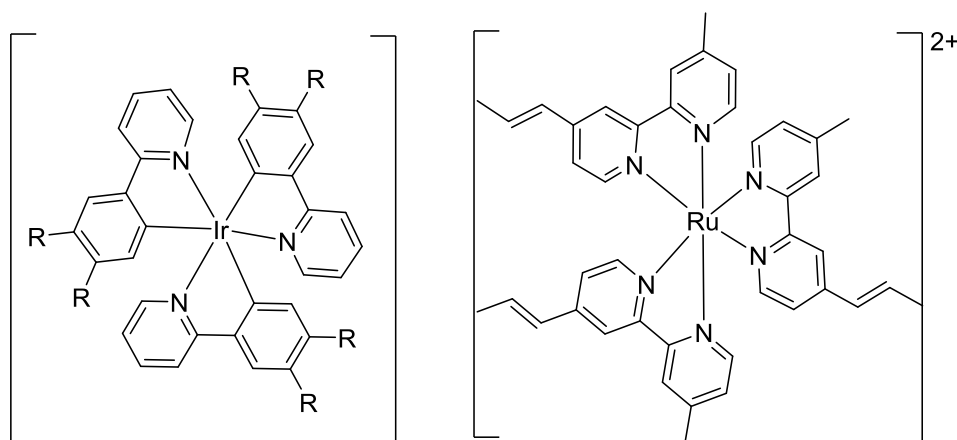
Figure 1-6 Examples of metal complexes used in LEECs

1.3.3 Transition metal complexes in photovoltaic applications

The luminescent properties of d^6 transition metals complexes has also allowed for use in photovoltaic applications like dye-sensitized solar cells (DSSCs),[45] as they allow for a light-driven charge separation by a metal-to-ligand charge transfer (MLCT) to exploit the charge-separated triplet excited state (^{3}MLCT), photo- and redox-stability as well as sufficiently long excited-state lifetimes.[46] DSSCs have a possibility of generating photovoltaic energy with a very low cost. DSSCs belong to a group of solar cells with thin films. The dye in Dye-sensitized solar cells can be modified to improve the performance of DSSCs. The *cis*-[Ru(dcb)$_2$(NCS)$_2$] (referred to as N3) (λ_{em} = 715 nm, ϕ = 0.4 %) was the first ruthenium complex used in DSSCs. A thin-layer photoelectrochemical cell based on this system reached a η = 10% solar-to-electric conversion yield when applied in a DSSC device on laboratory scale.[47] The most efficient dyes reach values of around 10-12%. The benchmark dye used in DSSC is N749 (referred to as black dye) with (η = 10.4%).[48] Figures 1.7
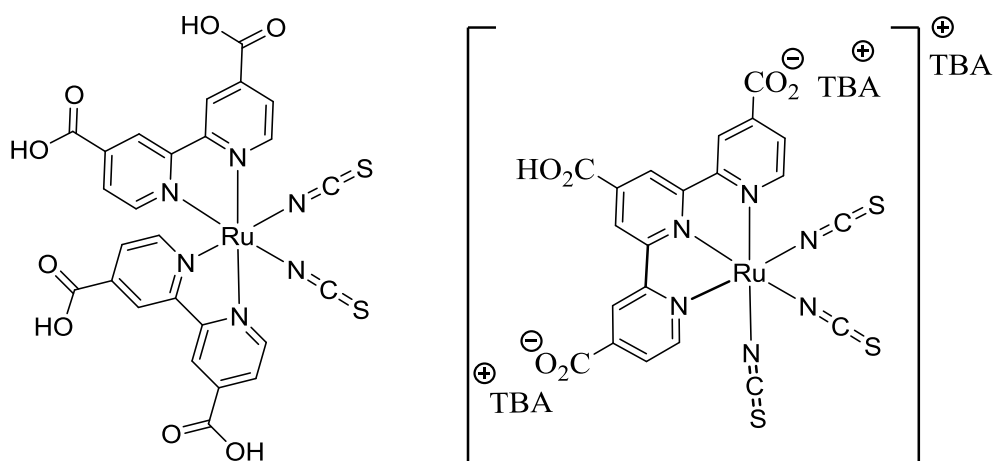
Figure 1-7 Examples of metal complexes used in DSSCs

1.3.4 Transition metal complexes in cell imaging and PDT

Transition metal complexes have a remarkable place within medicinal biochemistry.[49] Research has revealed significant progress in application of transition metal complexes as drugs to treat several human diseases like lymphomas, carcinomas, infection control, anti-inflammatory, diabetes, and neurological disorders. Transition metal complexes have been applied in the inorganic medical field including diagnostic or therapeutic purposes.[50] The results observed from metal complexes in medical field show that metals can play an increasingly important role of in the design of anticancer agents.[51] There has been a suggestion that derivatives of such d^6 polypyridyl complexes would assist with the process lumphores in fluorescence cell microscopy. However, until recently there were a few reported examples of this kind of applications. Fluorescent imaging offers a one of a kind course to identify metal cation in cells through a contactless and harm free route. Cellular imaging probes have been examined based on d^6 transition metals such as iridium,[52, 53] ruthenium,[54, 55] rhenium[56, 57] and Osmium poly pyridyl.[58] Osmium(II) polypyridyl complexes share many of the photophysical advantages of their ruthenium(II) analogues.[12]

16
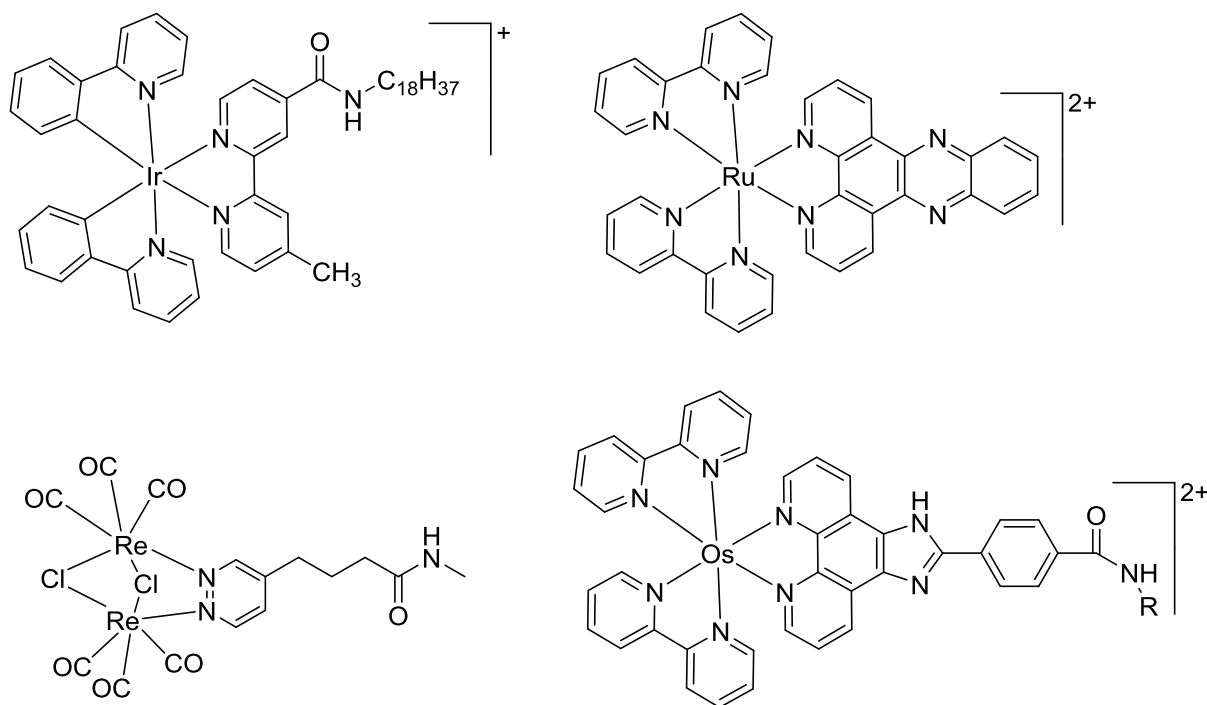
Figure 1-8 Examples of successful therapeutic and diagnostic metal complexes

Although their emission quantum yields and lifetimes tend to be lower, they have two key additional benefits; firstly, osmium(II) polypyridyl complexes typically exhibit emission maxima in the NIR spectral region below 700 nm, i.e. strongly coincident with the biological optical window. Secondly, because of their increased crystal field that splits the osmium d-d states, they lack the ability to gain access to the metal centered excited state by a thermal crossover that originates from the MLCT as in cases for ruthenium,[59] therefore, this implies that osmium(II) polypyridyl complexes show exceptional photostability and favorable luminescence properties.[60] This condition is necessary when referring to cell imaging, especially when there is cell incubation at 37 °C. Ever since the discovery of cisplatin more than four decades ago, there has been great achievement in cancer therapy and some efforts that investigate other non-platinum and platinum metal complexes for their potential use in the treatment of cancer.[61] The success of platinum complex in cancer therapy brings about

17

increased interests associated with coming up with a new metal complex that shows anti-cancer activity reported by Sadler and Lippard,[62, 63] the chemistry community have had a lot of growing interest that assist with examination of anti-cancer activities of ruthenium(II, III), gold(I-II), iron(II), platinum(II) complexes and antiviral activities of vanadium(IV) complexes. Some metals have improved to a level that they reach clinical trials.Anticancer therapy has metal-based therapeutics at the forefront having compounds such as that have proven essential in the chemotherapy treatments.[64] Anti-proliferative and potent cytotoxic complexes have been developed based on some transition metals involving iridium,[65] ruthenium,[66] osmium,[67] cobalt,[68] vanadium,[69] and platinum.[70] The desired photophysical and photochemical properties can be achieved by manipulating both ligands and metal, for this reason several ligands have been developed that bear extended π systems. There are several synthetic strategies available for the development of ligands. The intense studies relies on the reaction of CuAAC (Copper Catalysed Azide-Alkyne Cycloaddition) to produce the 1,2,3-triazole in regulating solar radiation conversion process into electrical energy in the device.[71] A wide range of triazole-based ligands are avialable, and this makes it possible to have a wide range of information in metal coordination chemistry. 1,2,3-Triazole and its derivatives are an important class of nitrogen containing aromatic heterocyclic compounds and have attracted a great deal of interest due to their diverse biological activities.

1.4 **Click-Chemistry**

Click Chemistry explains the reaction of a pair of functional groups which react rapidly and selectively with each other in mild and aqueous conditions[72]. The concept of Click Chemistry reactions is based on the activation and click coupling of compatible click-functional groups because of their high selectivity. The possible plethora of reactions that fit the required reactivity, biocompatibility and selectivity for the Click Chemistry include Cu (I) catalyzed Azide-Alkyne Click Chemistry reaction (CuAAC), the Strain-promoted Azide-Alkyne Click Chemistry (SPAAC) and the Tetrazine-Alkene Ligation reactions. Click Chemistry, as first coined by Sharpless and co-workers in the year 2001 defined stringent principles for a reaction to be called a "click" chemistry reaction.[73] According to Sharpless and co-workers, a click reaction produces high yields with high efficiency, modular and wide scope and the products can be isolated with ease.[72] 1,2,3-Triazoles have become the most recent product in Click Chemistry also forming the new advances and applications of the chemical agent in photodynamic therapy and imaging microscopy. The click chemistry approach is based on the Huisgen's dipolar cycloaddition reactions in which an alkyne and an azide is reacted to form the 1,4 and 1,5-triazole regioisomers.[74] The click –chemistry has been used to control the regioselectivity and also to improve the conditions of the reaction. Many of the products have been used for photodynamic therapy and imaging microscopy, these one of the recent applications.[75]
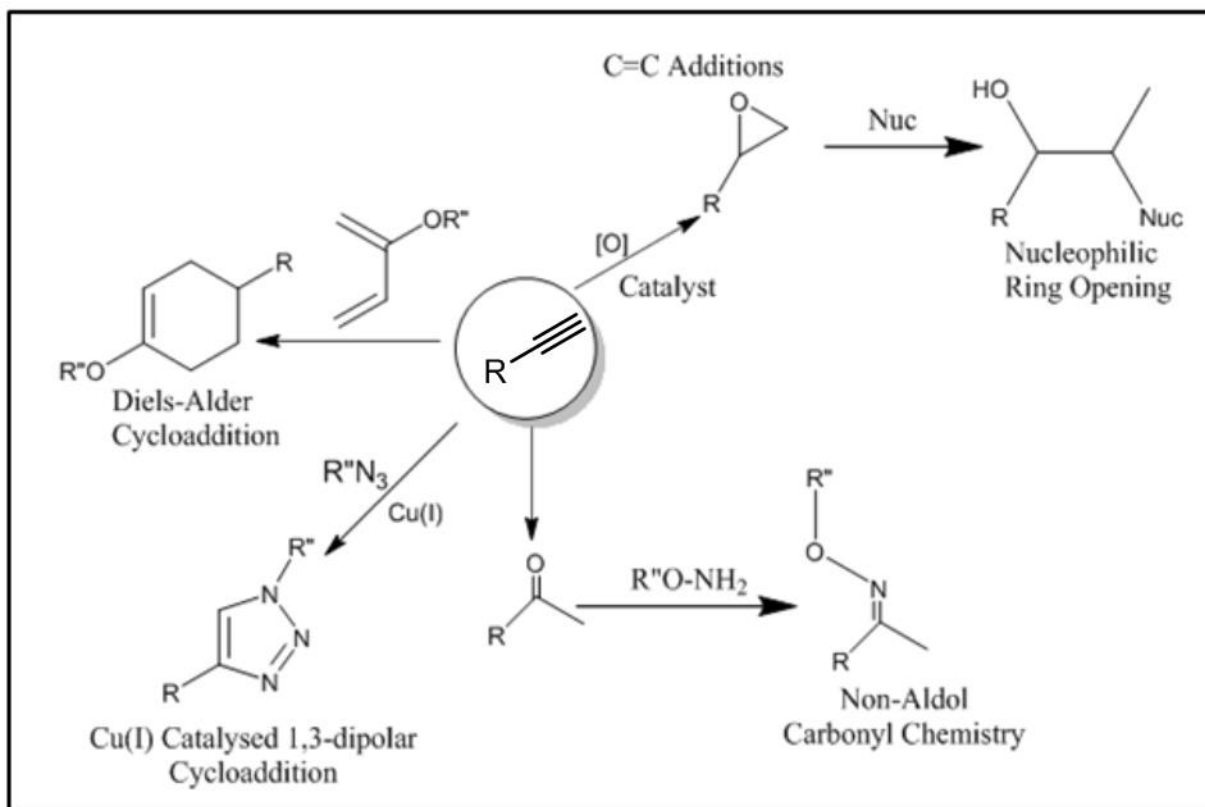
Figure 1-9 Some of the reactions which match the "click chemistry" standard[75]

1.4.1 Copper catalysed azide-alkyne cycloaddition (CuAAC)

(CuAAC) reaction for the synthesis of 1,2,3-triazoles which occurs by the 1,3-dipolar cycloaddition of organic azides to terminal alkynes is the most widely known and utilised 'click' reaction. The use of copper-based reducing agent as a stabilizing ligand improves the reaction outcome supported by different solvents such as water, with a miscible organic solvent while stating the reagent needs for the successful reaction process that produces pure filtration solution as the primary purification steps.[76-79] Since the middle of the 20th Century, the use of copper as a catalyst as a reagent in the organic synthesis experiments has been documented as it also underwent rapid development. Copper(I) had observed to be the most effective catalysts in the click chemical reactions that lead to the formation of 1,2,3-triazoles.[80] For instance, when forming allenyl azide, a methanesulfonate form 3-hydroxyl-1,3-diphenylprop-1-yne is reacted

20

with lithium azide at low temperature and catalyzed by copper(I) chloride. In their experiment, Sharpless and the Fokin group made use of copper(II) sulfate and sodium ascorbate and also included the copper(I) acetylides.[81] The functionalized azide molecules react with the functional terminal alkyne molecule to form a stabilized conjugate of both molecules through the triazole moiety as illustrated below.

$$R-\!\!\!\equiv \; + \; R''\!-\!N\!=\!N^+\!\!:\!N^- \; \xrightarrow{\;Cu\;}$$
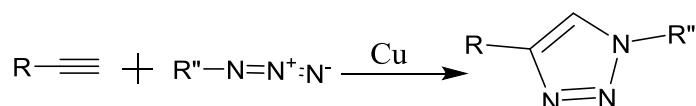
Scheme 1-1 The copper catalysed azide-alkyne cycloaddition (CuAAC) resulting in the formation of exclusively the 1,4-disubstituted-1,2,3-triazole regioisomer.

The efficiency of the CuAAC reaction increases because the alkynes and the azides are relatively unreactive and also depends on the metal catalyst present. Depending on the copper source available, the reaction completion varies with the concentration and source of copper catalyst. The toxicity of the copper(I) ions prevents the use of the copper(I)-catalyzed alkyne-azide reactions in live cells during photodynamic therapy and because of this the use of copper(I) chelating ligands has been implemented to overcome the problem.[82] Copper-Catalysed Azide-Alkyne Cycloaddition reaction (CuAAC) is used to produce a better reaction with enormous reaction acceleration and also with few or no side products.[83]

1.4.2 General CuAAC reaction conditions

The copper (I) catalyzed click chemistry reaction has frequently been utilized in connecting the molecular entities of all sizes in copper- catalyzed azide-alkyne cycloaddition reaction. A CuAAC reaction occurs under special conditions which qualify the reaction to be a good "click" chemistry reaction that reacts with high efficiency without a co-catalyst to produce the desired product.[83] This type of click reaction is highly robust which has numerous successful experiments that have been carried out proving the efficiency of the methodology. The general

conditions; i) copper(I) salts or complexes which act as a catalyst of this reaction. ii).[84] room temperature reaction, although microwave heating can be used to improve the reaction.[85] The aqueous copper(II) ascorbate methodology is simple, efficient and an economical way of preparing 1,4-disubstituted-1,2,3-triazoles.[86] The regiospecific copper(I)-catalysed azide-alkyne cycloaddition (CuAAC) click chemistry reaction has attracted considerable interest as more other researchers look onto it. The characteristics of the reaction include high yield, presence of mild conditions and also it has an excellent functional group tolerance regarding functionality. The triazole is easy to prepare and also offers the ability of a fully functional group of substituents proving a good route for the ligand design. There is a capability of the triazoles derived from copper(I) azide-alkyne cycloaddition reaction to having two nitrogen atoms and also an essential N3-position in its structural composition.[80]

1.4.3   One-Pot CuAAC reactions

In the CuAAC click chemistry reaction, the mild and aqueous Cu(I)-catalyzed 1,3 – cycloaddition reaction of the alkynes and organic azides result been the formation of the functional groups of 1,4-disubstitured-1,2,3-triazole.[87] The reactions of CuAAC considers the nature and properties of the reactions of the Cu(I) species and the different kinds of alkynes in a click chemistry reaction. In the Cu(I)-catalyzed 1,3-cycloadition reaction, the alkynes and organized azides are thermally induced using the Huisgen's approach leading to the synthesis of a mixture of the 1,4-disubstited-1,2,3-triazole and other products. As a result, it is possible to exploit the CuAAC "click" chemistry reaction so as to generate the functionalized groups of ligand architectures essential for their numerous potential uses.[80] The one-pot CuAAC method is one of the "click" methodologies that has been established so as to increase the levels of efficiency and safety of the CuAAC reaction during the synthesis of the copper(I) azide-alkyne cycloaddition or click chemistry reaction. In one-pot CuAAC methodologies either the reactant from the alkyne or the azide is generated during the reaction promptly and it does not require

an isolation or purification process.[88] According to Fletcher and co-workers, it is possible to deprotect the TMS-protected alkynes and react in a click reaction with azides generating bi-ligand triazoles that produce excellent yields of the product.[89]
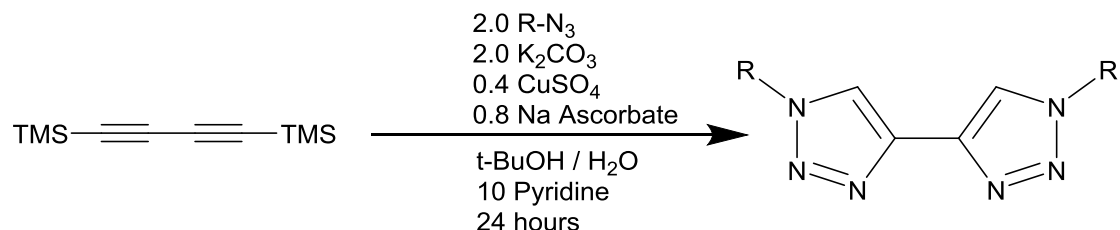
Scheme 1-2 Tandem in situ deprotection of bis(trimethylsilyl)butadiyne and "click" reaction to synthesise 4,4'-bis-1,2,3-triazolyl ligands

Initially, the azide and alkyne reactants were prepared separately for the use in the CuAAC reactions but in the One-Pot CuAAC methodology there is no isolation or separation of the reactants prior to the click chemistry reaction. The One-Pot CuAAC "Click" methodologies have proved successful especially due to their recent application in generating benzyl-, alkyl-, and the aryl-substituted 2-(1H-1,2,3-triazol-4-yl) pyridine (pytz) and 2,6-bis(1H-1,2,3-triazol-4-yl) pyridine ligands[83] (dtzpy) Figure 1-10.
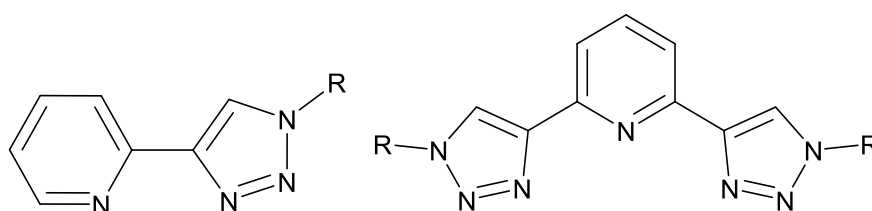
Figure 1-10 Structures of pyridyltriazole (pytz) and ditriazolylpyridine (dtzpy) ligands

1.5   Coordination chemistry and photophysics of CuAAC derived ligands

The coordination chemistry of 1,2,4-triazoles and the unsubstituted parent 1H-1,2,3-triazole are rich and extensive.[86] Figure 1.11
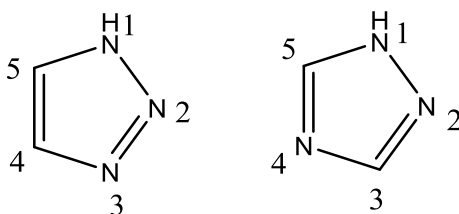
Figure 1-11 The two isomers of triazole 1,2,3-triazole (left), and 1,2,4-triazole (right)

Discovery of the CuAAC reaction, synthetic approaches to substituted 1,2,3-triazoles led to production of one isomer. The most significant property of the mild and modular copper(I)-catalyzed alkyne-azide cycloaddition click chemistry with organic azides is that it readily allows the functionalized regiospecific 1,4-disubstituted-1,2,3-triazole. As a result of this vital property has triggered the rapid and increased interested in the coordination chemistry of these ligands.[83] Many reports of the CuAAC reaction had used the 1,2,3-triazole moiety as a stable linker unit for two chemical or biochemical components, with little attention being paid to the heterocycle itself.[83] The triazole can participate in hydrogen bonding interactions as a donor or acceptor depending on the interacting partner. The weakly hydrogen bond donating property of the C5-H group is evident in interactions with anions[90] and intramolecularly with methoxy or tert-butoxy groups.[91] Exceedingly more common is the hydrogen bond accepting nature of the N2/ N3 atoms. Additionally, the Lewis basic nature of N2 and N3 allows for 1,2,3- triazoles to behave as efficient coordination ligands with a range of different metal ions.[92] Simple pyridyl-conjugated 1,2,3-triazoles have been shown to form metallic complexes that display intricate supramolecular interactions in the solid state. The simplicity involved in preparing the various varieties of 1,2,3-triazole-based ligands makes it possible to have a wide range of metal

coordination chemistry. The chemical coordination of triazole can act as an N-donor ligand at

the N3 position or at the N2 atom as illustrated below
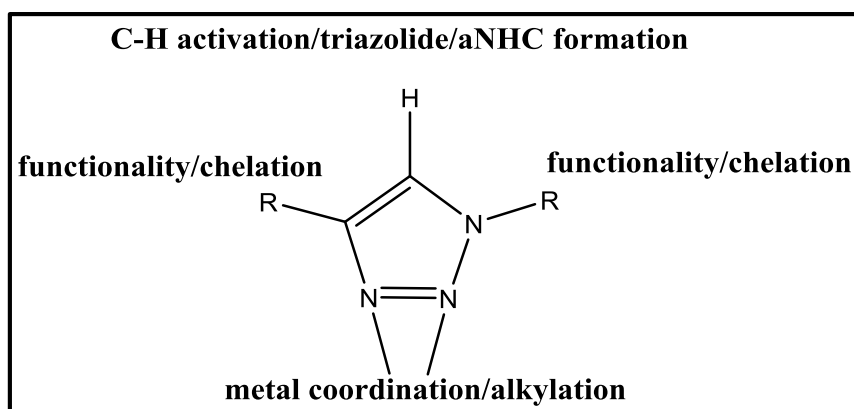
Figure 1-12 Copper (I)-catalysed 1,3-dipolar alkyne/azide cycloaddition to form 1,4-disubtitued 1,2,3-triazoles. Functional potential of 1,2,3-triazoles for coordation chemistry[83].

The diagram shows the possible metal coordination site of the 1,4-disubstituted -1,2,3-riazole

ligands. Additionally, there is also a potential that the bonding can take place at the C5 position,

C5 is deprotonated as the ionic triazolylides and also when it is the mesoionic triazolylide

NHCs as illustrated in Figure 1- 12. The area of "Click" chemistry especially the CuAAC has

undergone tremendous development with an increased application of the CuAAC derived

ligands such as 1,4-disubstituted-1,2,3-triazole. Because of the attractive photophysical

properties of their resultant complexes, a number of reports on the coordination chemistry of

triazole ligand have appeared.[83] Numerous[83, 86, 93] groups have compared metal triazole

complexes to bipyridyl (bpy) and terpyridyl (tpy) complexes. Complexes of the bidentate (pytz,

btz) and terdentate ligands (dtzpy) have been prepared with a set of transition metals including

Ru(II) ,Re(I), and Ir(III). The electron rich triazole moiety in these ligands leads to higher

energy LUMOs. This subsequently leads to destabilised MLCT excited states for their

complexes when related to well-known bpy and tpy analogues.[94] Largely or totally quenched

phosphorescence and a blue shift in MLCT absorption bands resulted when bpy ligand changed

to pytz in $[Ru(bpy)_{3-n}(ptz)_n]^{2+}$ complexes. This quenching of emission is possible due to the

destabilised MLCT states approaching into closer energy to non-radiative metal-centred (MC) states, allowing for efficient thermal population.[95] A good luminescent performance is observed from complexes with metals that have a larger ligand field and hence higher energy MC states. Luminescence of [Re(pytz)(CO)$_3$Cl] complexe is higher in energy than its bpy analogue, with longer lifetime and higher quantum yield when recorded under same conditions.[96] Even with a blue-shifted and hence diminished optical absorption in the visible region, pytz complexes of ruthenium have demonstrated to produce efficient dye-sensitised solar cells (DSSC).[97]

The rest of this section forms a systematic review of the employment of triazole based "click" chemistry in coordination chemistry. Various researchers and scientists have come up with some reports on the coordination chemistry of ligands especially those derived from copper (I)-catalyzed Alkyne-Azide cycloaddition click chemistry reactions. For instance, the N^C^N pincer platinum(II) and palladium(II) complexes which has a series of the monodentate triazole ligands that show a coordination at N3-Position.[80]

1.5.1 1,4-Disubstituted-1,2,3-Triazoles as N-Donor Ligands

1.5.1.1 1,4-Disubstituted-1,2,3-Triazoles as Monodentate N-Donor Ligands

In 2011 Elliott and coworkers[98] applied the 1,4- disubstituted-1,2,3-triazole unit as a monodentate ligand in a series of cationic Re(I) complexes. Cationic Re(I) complexes were prepared by stirring [Re(bpy)(CO)$_3$Cl] with AgPF$_6$ in dichloromethane in the presence of ligands. The complexes were characterised by NMR, UV-visible absorption spectroscopy, IR, mass spectra and luminescent lifetime measurements. X-ray crystal structures were obtained, which confirm that the coordination of the Re(I) is through the N3 nitrogen. IR spectra suggest that the 1,4-disubstituted-1,2,3-triazole ligands are marginally stronger donors than pyridine. The complexes are luminescent in aerated dichloromethane at room temperature with emission

maxima at 542 to 552 nm, while the emission is blue-shifted relative to the parent chloride

complex (612 nm). Luminescent lifetimes observed for complexes are 475 to 513 ns.

R_1	R_2
Me	H
Pr	H
Bz	H
Br	Me
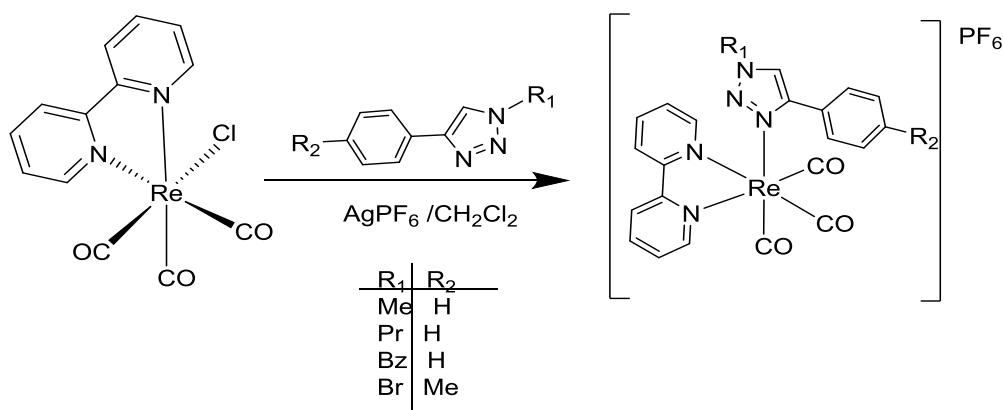
Scheme 1-3 - Preparation of [Re(bpy)$_2$(CO)$_3$(pytz)](PF$_6$)

In general the complexes show similar photophysical properties compared with the

monodentate pyridine (py) complex [Re(bpy)(CO)$_3$(py)]$^+$. This means that the 1,4-

disubstituted-1,2,3-triazole unit as a monodentate ligand has a limited influence on the

photophysical properties of the complex. Without photophysical investigation, other research

studies in the same area have also been carried out by various researchers such as Van Koten

and coworkers who applied the Copper(I)-catalyzed alkyne-azide cycloaddition reaction to

synthesize the 1,4-disubstituted-1,2,3-triazoles which acted as the monodentate ligands for the

aryl diamine cyclometalation pincer complexes of palladium and platinum.[99]
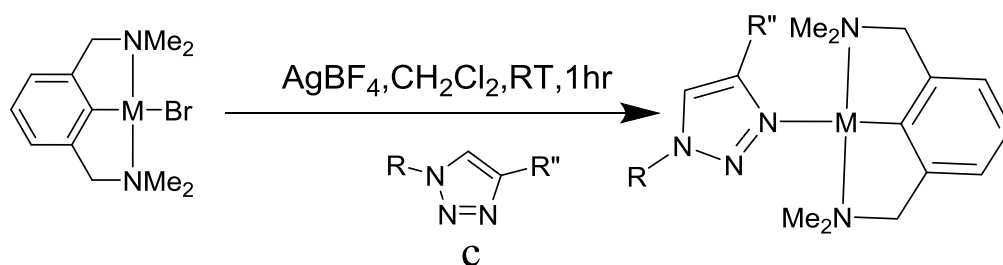
Scheme 1-4 metal complexes containing monodentate 1,4-disubstituted-1,2,3-triazole ligand N^C^N pincer complexes (M = Pd , Pt)[99]

On follow-up studies made by Astruc[100] and Crowley[101] on Van Koten's work, the two found that the 1,4-disubstituted-1,2,3-triazole ligands could coordinate and integrate with the palladium(II) ion in a monodentate way using the N3 nitrogen of the triazole product. When the two were mixed, the 1,4-disubstituted-1,2,3-triazole ligand formed the palladium(II)-1,4-disubstituted-1,2,3-triazole complexes.
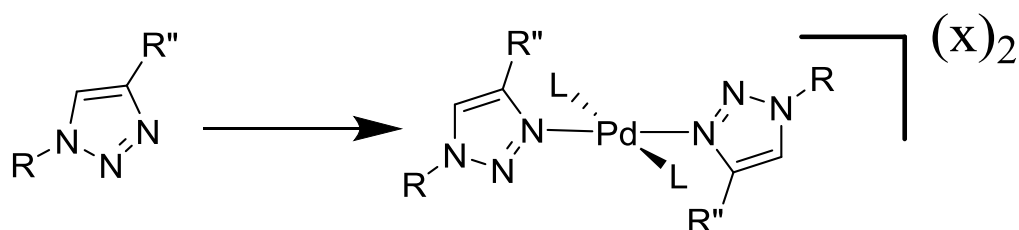
Scheme 1-5 Pd(II) complexes containing monodentate 1,4-disubstituted-1,2,3-triazole ligands,

In Astruc's experiment, they used azido methylbenzene and ethynyl ferrocene was used for the synthesis of the three novel ligands which comprised of the 1, 2 or 3 ferrocenyl triazole moieties. The ferrocenyl triazole ligand was mixed with $PdCl_2(C_6H_5CN)_2$ which led to the production of a triazole complex. Osuka, Shinokuno and coworkers[102] prepared the 1,4-disubstituted-1,2,3-triazole using zinc (II)-porphyrin. The ion and metal complex coordination during the click chemistry reaction caused the dimerization as the 1,4-disubstituted-1,2,3-triazole donor on the porphyrin and zinc(II) ion are brought closer to the poryphyrin. The X-ray crystallographic studies showed coordination from the 1,4-disubstituted-1,2,3-triazole unit to the metal at the N3 nitrogen of the triazole. There was a wide variety of presumption of the number of 1,4-disubstituted-1,2,3-triazole metal complexes during the monodentate binding of the metal complexes, although none of them has been structurally characterized in the studies since the coordination occurs through the N2 nitrogen and N3 nitrogen atoms of the 1,2,3-triazole unit.[74]

1.5.1.2 Bidentate Ligands Containing 1,4-disubstituted-1,2,3-Triazole Units

In the copper(I)-catalyzed alkyne-azide cycloaddition derived ligand systems, the bidentate ligands which have 1,4-disubstituted-1,2,3-triazole ligands have been studied widely. The other well-known ligands include the 2-pyridine and pyridyle-1,2,3-triazole frameworks. As shown in the diagrams below of the 1,4-disubstituted-1,2,3-triazoles.
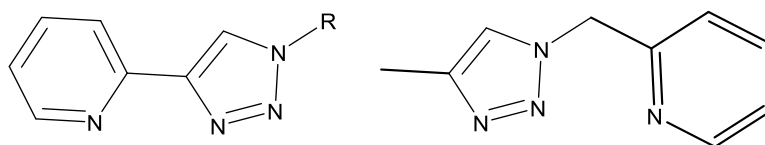
Figure 1-13- Bidentate ligands containing 1,4-disubstituted-1,2,3-triazoles 2-(1-R-1H-1,2,3-triazol-4-yl)pyridine and [2-(4-R-1H-1,2,3-triazol-1- yl)methyl]pyridine

1.5.1.2.1   Ligands Containing One 1,4-Disubstituted-1,2,3-Triazole Unit

The 2-(1,2,3-triazol-4-yl) pyridine type ligands have also been a subject of research studies, especially in finely tuneable analogues. The influence of the triazole moiety is apparent when combined as the chelating N^N ligand in complexes. In this type it has a direct impact on the energy of the LUMO and hence the energies of the ^{1}MLCT and ^{3}MLCT states. In most studies, the 2-(1-R-1H-1,2,3-triazol-4-yl)pyridine complexes of ligands have been compared to the 2,2′-bipyridine complexes, despite the presence of the additional nitrogen donor atom (N2) within the ligand scaffold, all of these studies proved that the 2-(1-R-1H-1,2,3-triazol-4-yl)pyridine acting as bpy-like N^N five-membered chelates. The triazole ligand coordinate through the pyridyl and N3 nitrogen of the 1,2,3-triazole unit with a wide range of metals ions including those with octahedral complexes (Re(I), Tc(I),[103] Ru(II),[104] Ir(III).[105] Figure 1.14.
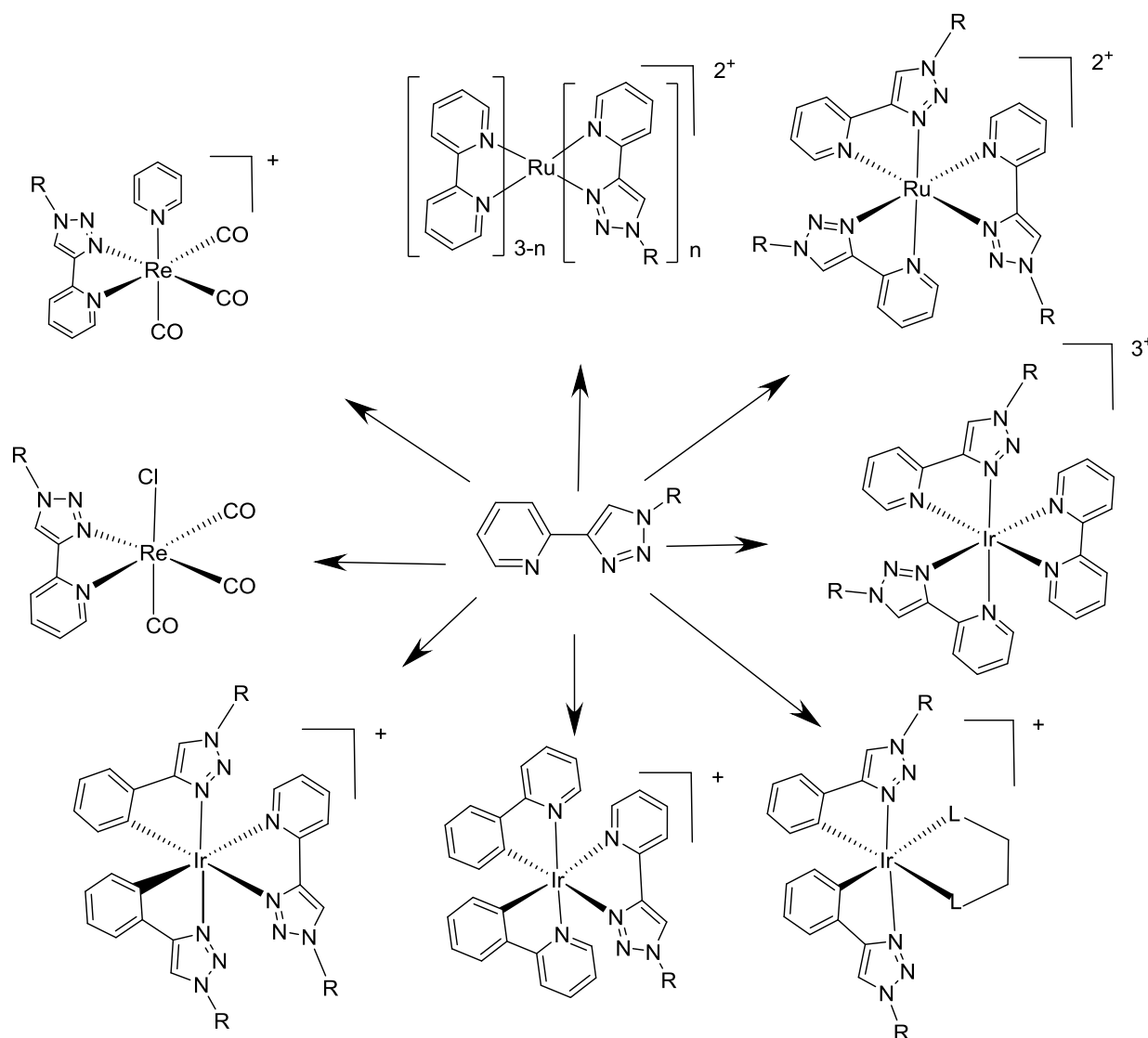
Figure 1-14- Some metal complexes containing the 2-(1-R-1H-1,2,3-triazol-4-yl)pyridine

Rhenium complexes [Re(Bn-pytz)(CO)$_3$Cl][96, 103, 106] showed a blue-shifted electronic absorption and emission (λ_{abs}= 333 nm, λ_{em} = 538 nm) compared with [Re(bpy)(CO)$_3$Cl] complexes (λ_{abs}= 371 nm, λ_{em} = 633 nm) with emission coming from the mixed metal-to-ligand-to-ligand charge transfer (MLLCT) state. Both complexes have the same HOMO level of energy, so the blue-shift of the MLCT means that the [Re(Bn-pytz)(CO)$_3$Cl] has a higher energy level of LUMO than [Re(bpy)(CO)$_3$Cl]. Similarly, in the excited state at room

temperature [Re(pytz)(CO)$_3$Cl] showed the blue-shifted luminescence compared to [Re(bpy)(CO)$_3$Cl] complex, This was further supported by the radiative lifetimes of the complexes. The luminescence lifetime of [Re(Bn-pytz)(CO)$_3$Cl] (τ/μs = 8.90) is longer than [Re(bpy)(CO)$_3$Cl] (τ/μs = 3.17). Changing the π-donor axial chloride ligand by a neutral pyridine donor leads to further blue-shift in the emission maximum to the blue-green region of the spectrum (496 nm).[107] 2-(1-R-1H-1,2,3-triazol-4-yl)pyridine technetium-99 complexes were prepared by Benoist, Machura and coworkers[103] which presented a suitable lipophilic character for its use as a CNS imaging agent.

 [Ru(pytz)$_3$]$^{2+}$ was prepared and compared with [Ru(bpy)$_3$]$^{2+}$ independently by Fletcher[89] and Schubert.[94] Because of the asymmetry of the pytz ligands in the homoleptic complex the product results in a mixture of the *fac* and *mer* isomers which are difficult to separate, being possible only if a bulky substituent is present at the N1 position of the triazole heterocycle. Comparing with their bpy analogues the [Ru(pytz)$_3$]$^{2+}$, it was found that the homoleptic complexes are only modestly coloured and are not emissive. A family of complexes [Ru(bpy)$_{3-n}$(pytz)$_n$](PF$_6$)$_2$ (n = 1 to 3) were prepared, and the photophysical and electrochemical properties were characterised. Complexes show a progressive blue-shift in the UV-visible absorption spectra on increasing the pytz ligand content, [Ru(pytz)$_3$](PF$_6$)$_2$ exhibits a very large blue shift (λ_{abs}= 384 nm) compared with [Ru(bpy)$_3$](PF$_6$)$_2$ (λ_{abs}= 461 nm) and the energy of the LUMO is increased, as observed by cyclic voltammetry.[94, 108] Cyclometallated Ir(III) complexes with pytz ancillary ligands of type [Ir(ppy)$_2$(pytz)]$^+$ and [Ir(F$_2$ppy)$_2$(pytz)]$^+$ (where ppy = 2-phenylpyridine and F$_2$ppy = 2-(2,4- difluorophenyl)pyridine) have been prepared and their photophysical and electrochemical properties have been examined by De Cola and coworkers.[105, 109-111] The compounds display excellent structured emission bands, often indicative of the presence of a large amount of ligand-centred character in the emissive excited states, with emission maxima at (λ_{max} =475) for [Ir(ppy)$_2$(pytz)]$^+$ and (λ_{max} =450 nm)

for $[Ir(F_2ppy)_2(pytz)]^+$ and quantum yields, (0.16-0.23 in degassed dichloromethane) for both complexes respectively, long luminescent lifetimes, (0.53-1.3 μs) and reversible oxidation behaviour observed from these complexes. Emission is also blue shifted through perturbation of the bpy-centred LUMO to higher energy when compared with $[Ir(ppy)_2(bpy)]^+$ complex which displays emission maxima at (λ_{max} =580 nm). Also, compounds exhibited electrochemiluminescence where the emission colour can be modulated from green to blue by ligand modification, and authors suggest that this can be exploited in the development of eugenic labels for bioanalytical applications.[105]

Square planar complexes of 2-(1,2,3-triazol-4-yl) pyridine type ligands with Pd and Pt have been prepared and crystallographically characterized.[112-114]Palladium "click" complexes, which were prepared by Milani and coworkers[113] demonstrated the ability to act as an active catalyst for styrene carbonylation producing low-molecular-weight products. In general complexes display absorption spectra, with bands in the region 270–285 nm being associated with π-π* pytz-localised IL transitions and weaker absorbances at lower energy (360–380 nm) which are assigned to MLCT transitions with a degree of chloride-to-pytz charge transfer contributions. These features are also shifted to higher energy, $[Pt(Bn-pytz)Cl_2]$ (λ_{abs} = 330 nm) compared with $[Pt (bpy)Cl_2]$ (λ_{abs} = 389 nm). The other well-known ligand is [2-(4-R-1H-1,2,3-triazol-1-yl) methyl]pyridine frameworks Figure 1-15. Complexes based on this ligand have a higher energy LUMO over that of complexes with bpy ligand. The ^{1}MLCT absorption and ^{3}MLCT emission bands are observed to blue-shift on increasing pytz ligands comparing with bpy based ligand complexes.[115, 116]
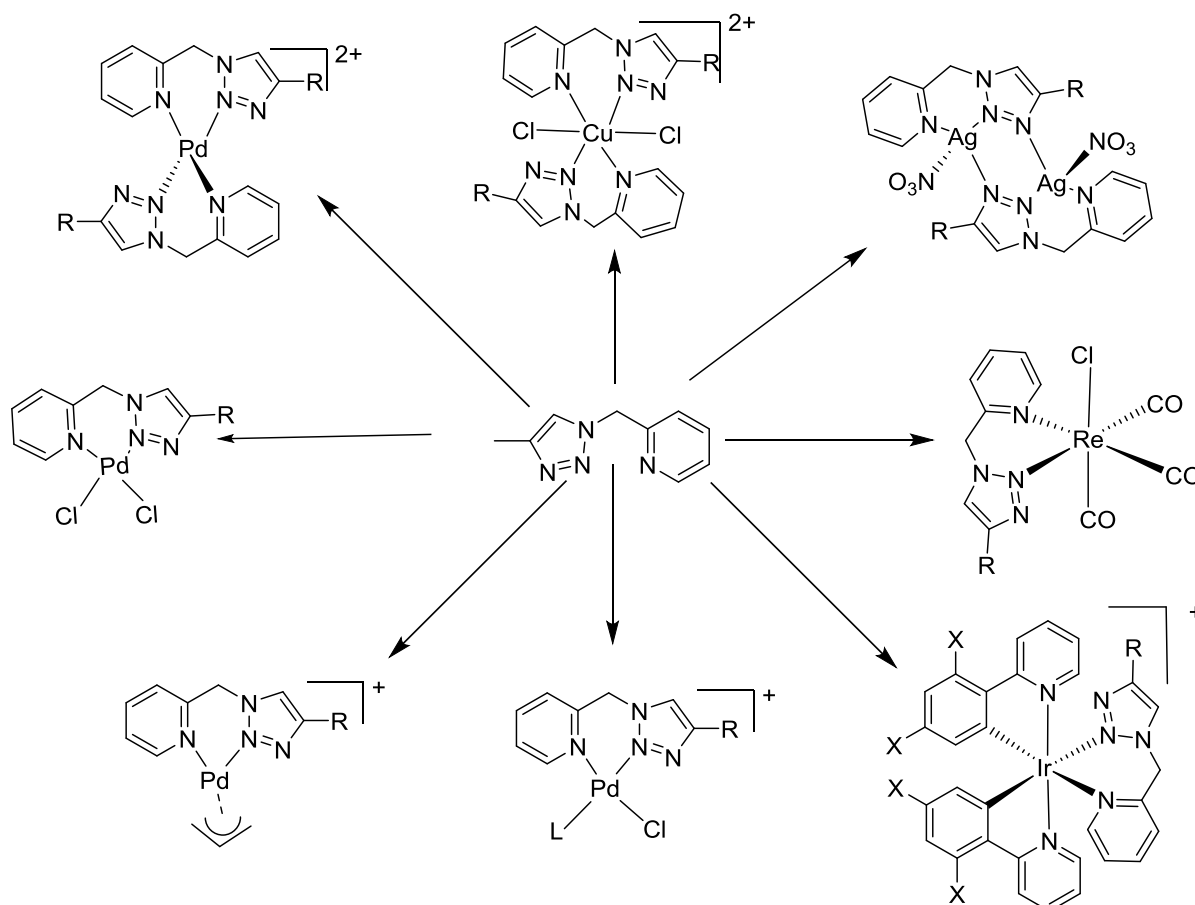
Figure 1-15- some metal complexes containing the [4-R-1H-1,2,3-triazol-1-yl)methyl]pyridine ligand.[86]

1.5.1.2.2 Bidentate Ligands Containing Two 1,4-Disubstituted-1,2,3-Triazole Units

The last class of this type of ligands which has received keen interest in is the ligands that are bi-1,2,3-triazoles.[89, 117-121] Most researchers have therefore attempted to examine the symmetrical structure of the ligands which have portrayed the stable metal complexes. The ligands have five membered rings.
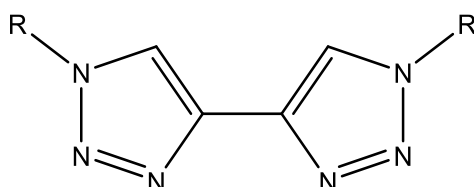
Figure 1-16- Structure of bidentate 4,4'-bis-1,2,3-triazolyl ligands
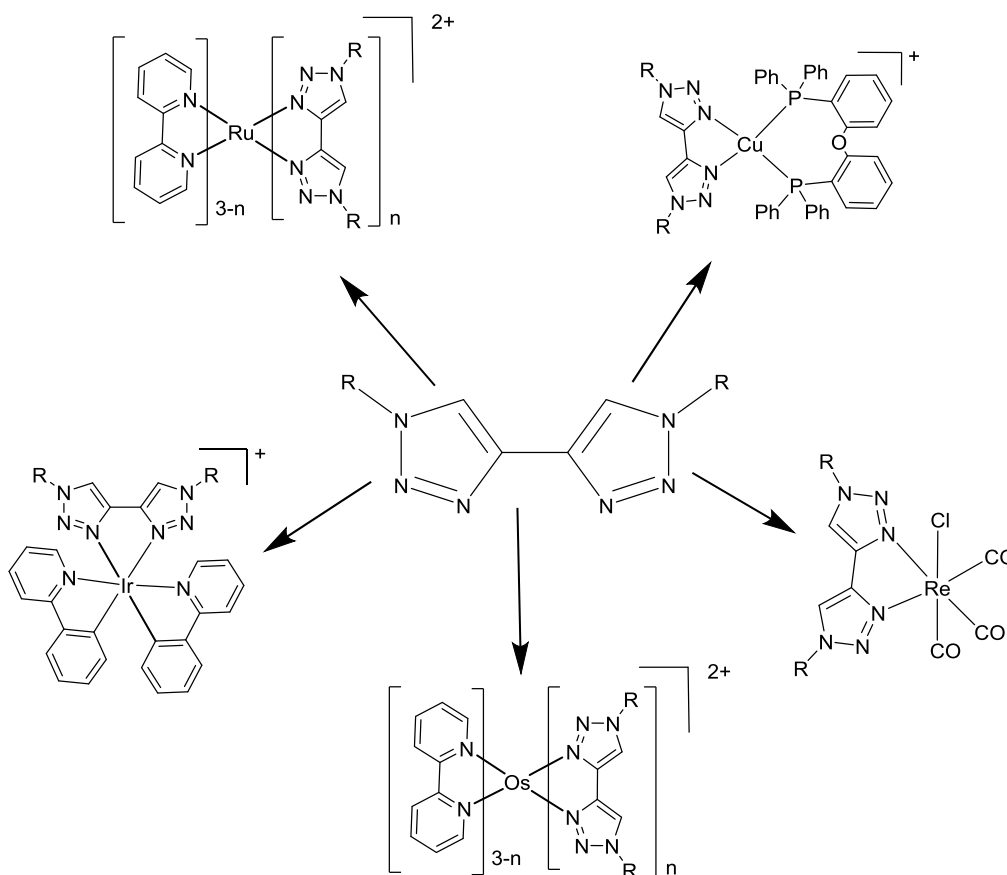
Figure 1-17 Some metal complexes containing the 4,4'-bis-1,2,3-triazolyl ligands

With the bis-triazole ligands Konig, Monkowius, and coworkers formed stable complexes with Ru(II), Cu(I), and Re(I).[118] They confirmed the bidentate coordination of the ligands through the N3 atoms of the triazoles to form five-membered chelate rings. The bi-1,2,3-triazole complex's electronic absorptions are significantly higher in energy than the corresponding bpy complexes, but they are not emissive in solution or the solid state. A family of complexes $[Ru(bpy)_{3-n}(btz)_n](PF_6)_2$ (n = 1 to 3) were prepared by the Elliott group.[119] The photophysical and electrochemical properties were characterised. Complexes show a progressive blue-shift in the UV-visible absorption spectra on increasing the btz ligand content with a very large blue-shift observed on replacement of the final bpy ligand by btz when compared to $[Ru(bpy)_3].^{2+}$ The energy of the LUMO is increased as observed by cyclic voltammetry. The Elliott group applied the same ligand to prepare and characterised a series of osmium(II) complexes[120] $[Os(bpy)_{3-n}(btz)_n](PF_6)_2$. These Os complexes also show a progressive blue-shift in the UV-

visible absorption and in the photoluminescence emission spectra on increasing the btz ligand content with a very large blue-shift observed on replacement of the final bpy ligand by btz when compared to $[Os(bpy)_3]$,[2+] which indicates the much higher energy LUMO of the btz ligand over that of bpy. The homoleptic complex appears to display extremely weak room temperature emission, but on cooling to 77 K the complex exhibits highly intense blue emission. The complexes were used in light-emitting electrochemical cell (LEEC) devices. All LEECs display electroluminescence in the deep-red/near-IR. Elliott[121] used the same ligand to synthesise complexes of the form $[Ir(R-ppy)_2(btz)]PF_6$,(R-ppy = 4-(pyrid-2-yl)benzaldehyde, 2-phenylpyridine and 2-(2,4-difluorophenyl)pyridinethe complexes. The complexes show luminescence with emission wavelengths tunable through variation of the aryl substituents of the cyclometalated ligands but are independent of the ancillary btz ligand with emission maxima about (λ max = 452-500 nm). The authors suggest that this type of complex are promising candidates for further development as phosphors in light emitting devices and in other applications such as biological imaging. Table 1-1 summarises the absorption and emission data of some metal complexes based on the 4,4'-bis-1,2,3-triazolyl ligand compared to the bpy based ligand complexes.

Table 1-1: Absorption and emission data of some metal complexes based on the 4,4'-bis-1,2,3-triazolyl ligand compared to the bpy based ligand complexes.

Complex	λ_{abs} /nm	λ_{em}/ nm
$[Ru(bpy)_3]^{2+}$	452	610
$[Ru(btz)_3]^{2+}$	303	Not observed
$[Cu(phen)(DPEphos)]^+$	391	700
$[Cu(btz)(DPEPhos)]^+$	307	Not observed
$[Re(bpy)(CO)_3Cl]$	371	633
$[Re(btz)(CO)_3Cl]$	302	Not observed
$[Os(bpy)_3]^{2+}$	450	732
$[Os(btz)_3]^{2+}$	422	Not observed
$[Ir(ppy)_2(bpy)]^+$	405, 377	580
$[Ir(ppy)_2(btz)]^+$	382, 332	476, 508

1.5.1.3 Tridentate Ligands Containing 1,4-Disubstituted-1,2,3-Triazole Units

Some the tridentate "click" ligands have also been a subject of scholarly work and research studies and experiments aiming at the synthesis and characterization of their structural formation and also coordination. Although most of the ligands have two or three 1,4-disubstituted-1,2,3-triazole units, some other tridentate ligands have only one triazole unit.

1.5.1.3.1 Tridentate Ligands Containing One 1,4-Disubstituted-1,2,3-Triazole Unit

The click-to-chelate concept was first written by Mindt and Shibli[122-127] who have synthesized a series of amino acids generated from the tridentate ligands that contain one 1,4-disubstituted-1,2,3-triazole. Complexes containing tridentate ligands of Re(I) and also [99]Tc(I) developed in radiopharmaceuticals (which can be used as potential imaging agents in PET scans). They generated both the 'regular' and the 'inverse' ligands although they realized that the regular ligands were more stable compared to the inverse ligands. However, no photophysical studies were revaled in this work. One of the methods used in the synthesis is the mild click method which enabled conjugation of a variety of biotargeting molecules such as phospholipids, carbohydrate, thymidine, bombesin, and folate.[128] Similar ligands used by Adolfsson and co-workers[129] to prepare rhodium complexes which have been shown to be effective as a catalyst in organic reactions. A hybrid NHC-1,2,3-triazole tridentate ligand and its Ag(I), Pt(II) and Pd(II) complexes were synthesized and characterised by Chen and coworkers[130] Figure 1-18. The palladium complex, was found to be a very active catalyst for the Suzuki-Miryaura cross-coupling reactions. The last example of the complexes that use this kind of ligands are "super-hybrid" Fe(II) complexes which prepared by Chandrasekher and co-workers[131] in this complex tridentate ligands contain pyridyl, pyrazolyl, and triazolyl N donors. X-ray crystal structures at 100 K (the temperature of the X-ray data collection) showed the octahedral Fe(II) complexes to be low spin and deep red. Photophysics of complexes using this type of ligand investigated by Strassert and co-workers[132] who used a triazole containing terdentate cyclometalate ligand (TzPyPh) in order to obtain room temperature luminescence in Pt(II) complexes. All complexes display absorption spectra band between 300 nm–450 nm, which are assigned to mixed singlet metal-to-ligand charge transfer/ligand-centred ([1]MLCT/LC) excitations. Complexes exhibit structured vibrational emissions at about 500 nm.
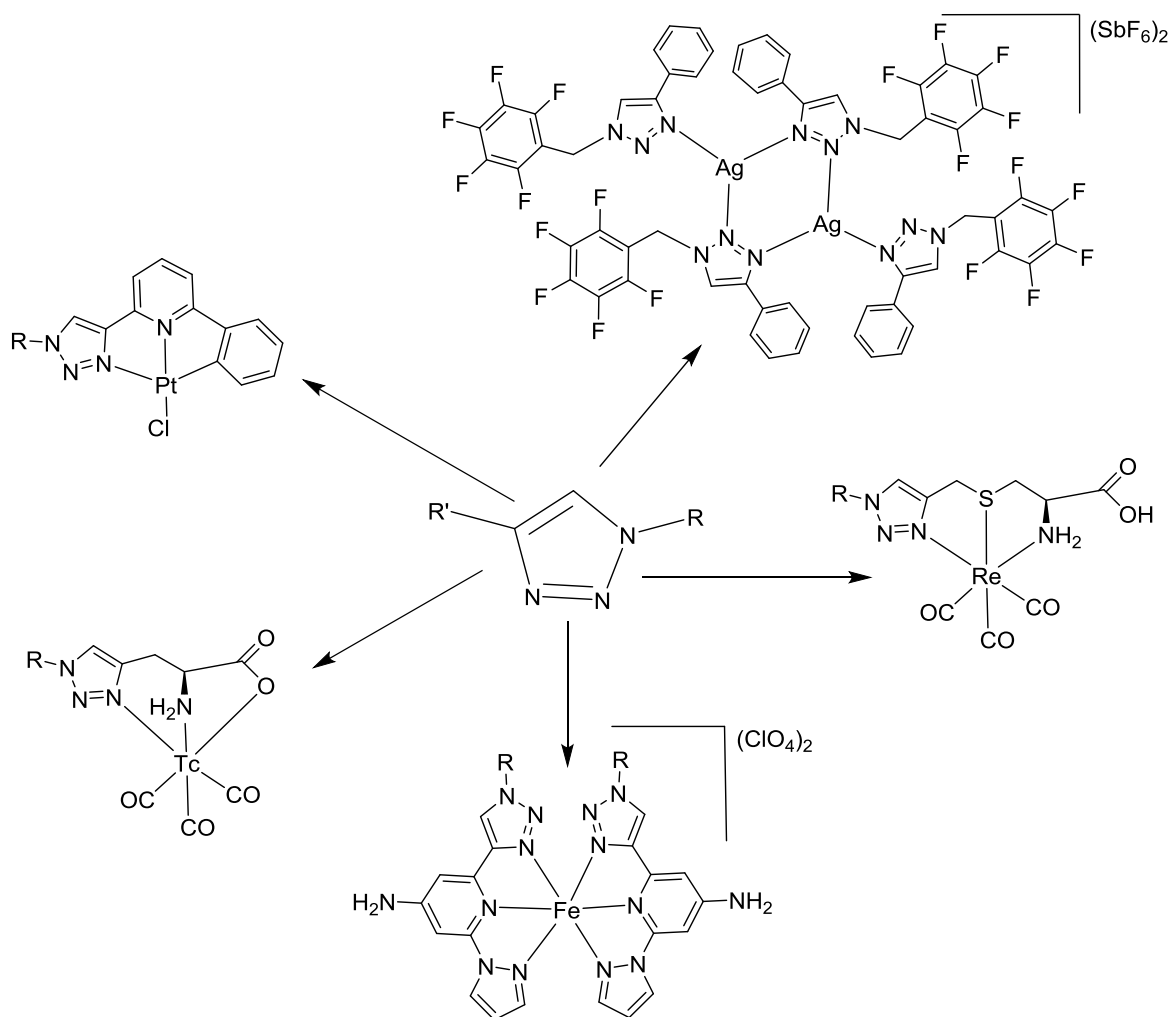
Figure 1-18 Some metal complexes containing One 1,4-Disubstituted-1,2,3-Triazole Unit

1.5.1.3.2 Tridentate Ligands Containing Two 1,4-Disubstituted-1,2,3-Triazole Units

The tridentate 2,2':6',2"-terpyridine ligads (tpy) is another ligand which has been widely studied in the area of coordination chemistry. This has triggered several researchers to apply the CuAAC reaction in the synthesis of analogues of this ligand starting from 2,6-diethynylpyridines. It has also been reported that most of these ligands behave like the tpy tridentate ligands bridging through the pyridyl and the N3 nitrogen atoms position of the triazole rings. Various metal ions have been found useful in the synthesis of tridentate 2,6-

bis(1,2,3-triazol-4-yl)pyridine (btzpy) metal complex such as Fe(II),[133-135] Cu(II),[88, 136] Ag(I)[88] and Ru(II), Figure 1-19.[135, 137, 138] The first synthesis of the 2,6-bis(1,2,3-triazol-4-yl) pyridine type of ligands was reported to have a coordination to the Eu(III) and the ferrous(II) metal ions.[133] The reaction of the ligands with the metal ions produced octahedral complexes which when characterized by the X-ray crystallography showed that they were less sterically strained compared to the tpy analogues. The photophysical and electrochemical properties were characterised. Complexes showed a blue-shift in the UV-visible absorption and in the emission spectra compared to tpy complexes, this is due to the LUMO of the btzpy ligand being higher in energy than the tpy ligand. $[Fe(btzpy)_2]^{2+}$ complex display a broad MLCT band at ($\lambda_{abs} = $ 432 nm), which is significantly shifted to the blue region of the visible spectrum compared to that of $[Fe(tpy)_2]^{2+}$ complex ($\lambda_{abs} = 552$ nm). A heteroleptic Ru(II) complexes containing a terpy and a 2,6-bis(1-R-1,2,3-triazol-4-yl)pyridine ligand, was synthesized in a stepwise manner via a $[Ru(L)Cl_3]^{2+}$ intermediate species by Schubert and coworkers.[137, 139] This octahedral complex displays intermediate electronic properties comparing to the related homoleptic species. The heteroleptic Ru(II) complex displays a band at ($\lambda_{abs} = 432$ nm) in absorption spectra, which is located between the MLCT bands of the homoleptic complexes $Ru(tpy)_2$ ($\lambda_{abs} = 475$) nm and $Ru(btzpy)_2$ ($\lambda_{abs} = 394$). The blue shift of the MLCT, when exchanging the tpy ligands by btzpy, can be attributed to energetically because the btzpy ligand has a higher energy π^* orbitals (lowest unoccupied molecular orbital, LUMO), which means bigger ΔE. Complexes are not emissive at room temperature, but bright orange emission has been observed for the heteroleptic complex at 77 K in a matrix of n-butyronitrile glass ($\lambda_{em} = $ 583). Which blue-shifted of about 20 nm, compared to the homoleptic Ru(tpy) complex ($\lambda_{em} = $ 604). O'Reilly[140] reported a similar approach to the synthesis of metallostar complexes of Ru(II) and Eu(III). Photophysical data for Ru(II) whith two 1,4-Disubstituted-1,2,3-triazole units based complexes summarised in Table 1-3.

Table 1-2: Photophysical data for Ru(II) whith two 1,4-Disubstituted-1,2,3-Triazole Units based complexes at room tempreture

Complex	λ_{abs} /nm	λ_{em}/ nm
$[Ru(tpy)_2]^{2+}$	475	604
$[Ru(tpy)(dpb)]^{2+}$	499	Not observed
$[Ru(tpy)(btzpy)]^{2+}$	432	583
$[Ru(btzpy)_2]^{2+}$	394	Not observed
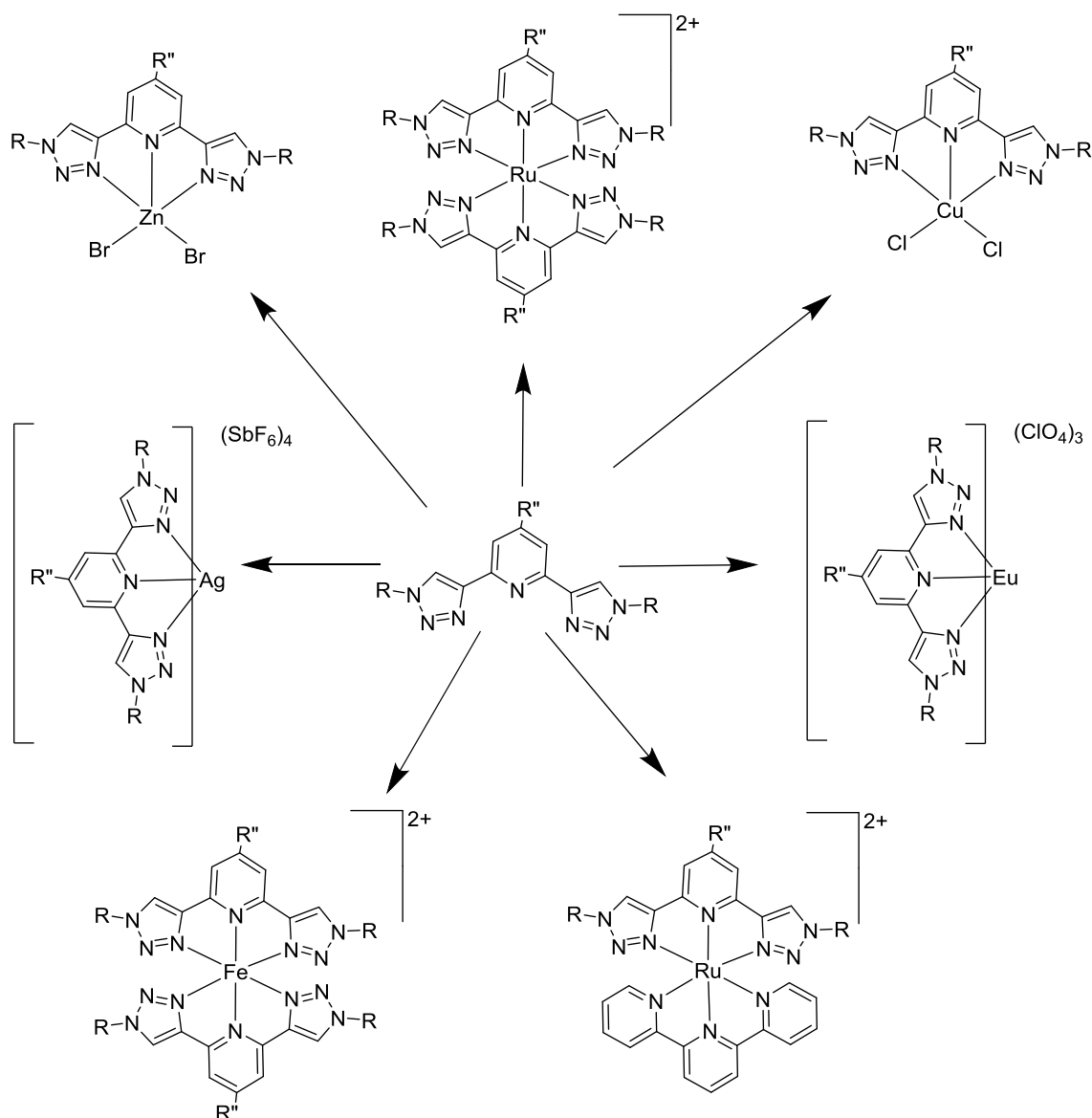
Figure 1-19- Some metal complexes containing 2,6-bis(1-R-1,2,3-triazol-4-yl)pyridine

The more flexible 2,6-bis(4-R-1,2,3-triazol-1-ylmethyl)pyridine ligands related to btzpy have also been studied by Crowley and co-workers[88] who explored the synthesis and characterization of their structural formation and also coordination of these types of ligands with Ag(I) and Cu(II), Figure 1-20. The silver complex was found to be polymeric in the solid state with the tetrahedral Ag(I) centres coordinated to the pyridyl and triazolyl nitrogens from one ligand along with the other two nitrogen donors from a second identical ligand resulting in a 4,4 net structure. From the same ligand Zhu and coworkers[141] prepared complexes of Cu(II),

Fe(II), and Co(II). X-ray structures of these showed them have the expected octahedral structures.
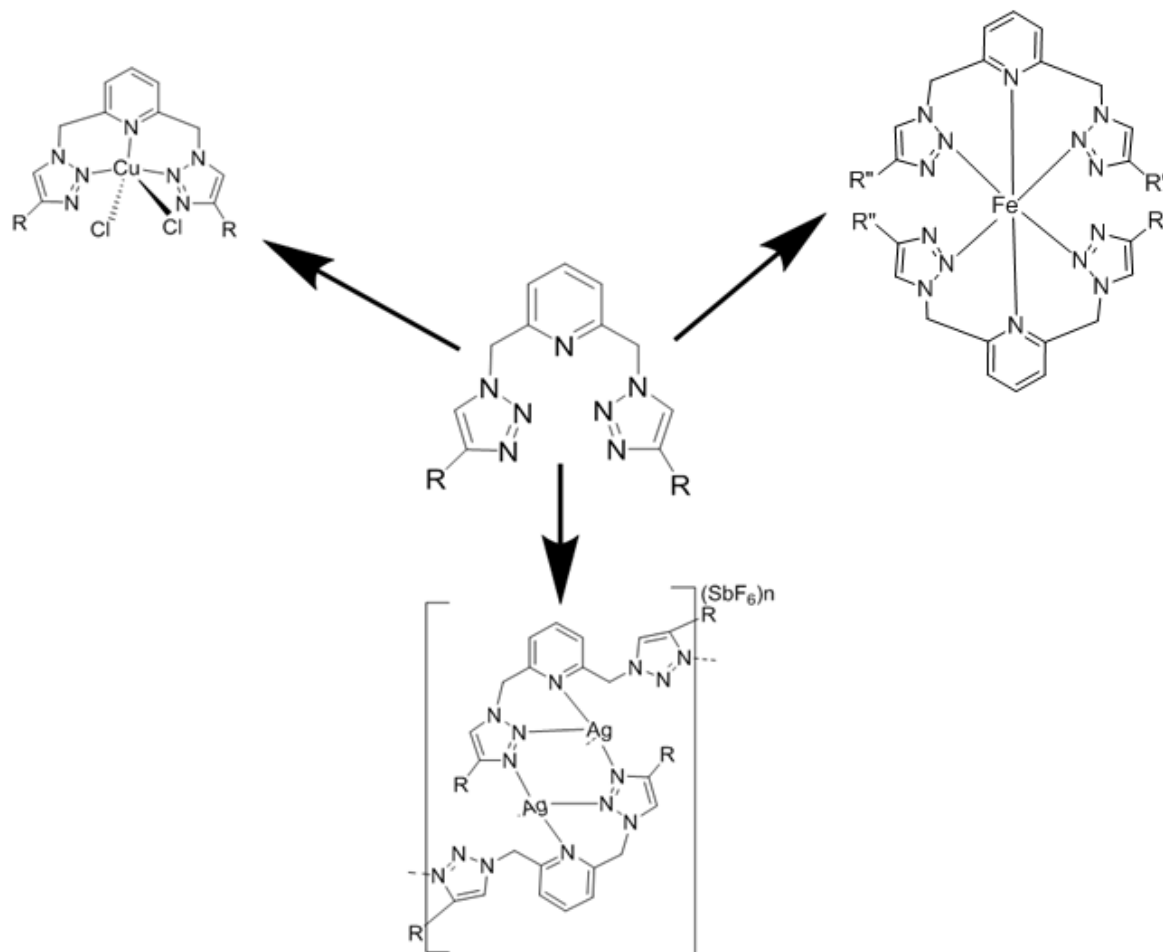
Figure 1-20- 2,6-bis(4-R-1,2,3-triazol-1-ylmethyl)pyridine inverse "click" metal complexes

1.5.1.3.3 Tridentate Ligands Containing Three 1,4-Disubstituted-1,2,3-Triazole Units

Another type of tridentate click chelates in click chemistry are the ligands with three 1,4-disubstituted-1,2,3-triazole units. In a research study conducted by Pericas and coworkers,[142] they prepared the copper chloride compound which demonstrated the excellent catalyst properties of CuAAC, Figure 1-21. Conclusively, based on the discussion and the review of literature in research studies conducted in the past by other researchers, it is evident that the

mild function group or CuAAC reaction has proven to be a reliable robust for the synthesis of the functionalized ligands.
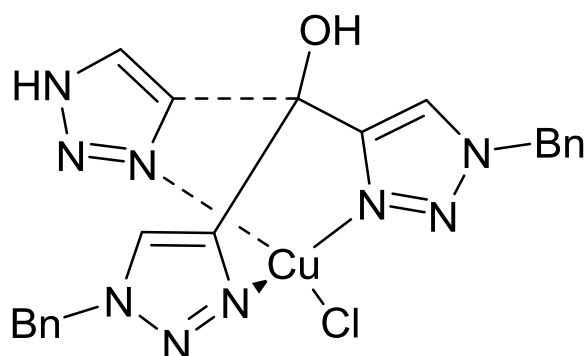
Figure 1-21- CuCl-tris(1-benzyl-1H-1,2,3-triazol-4-yl) methanol CuAAC catalyst

Recently Didier Astruc and co-workers[143] prepared tris-1,2,3-triazole-Stabilized Gold nanoparticles. The authors mentioned that a water-soluble complex contains amphiphilic ligand containing hydrophobic tris(1,2,3-triazolyl) on the one side and a hydrophilic polyethylene glycol 2000 chain on the other side to stabilize AuNPs. And the formation of the micellar AuNP catalyst, would further improved catalytic efficiency. The complexe exhibit absorption band at 515 nm.
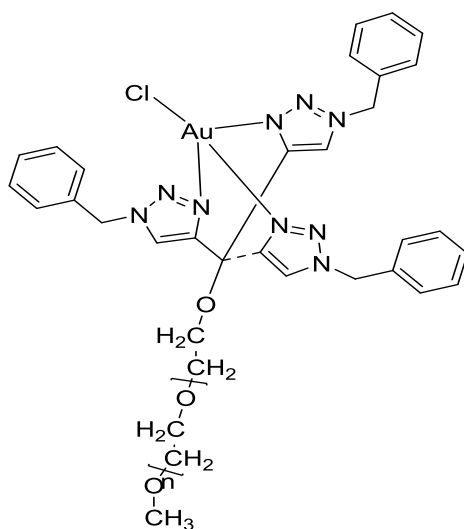
Figure 1-22- PEG-tristrzAu-Cl

1.5.2 1,4-Disubstituted-1,2,3-Triazoles as C^N-Donor and N^C^N-Donor Ligands

Another type of triazole ligand that has been widely studied is the C^N donor ligand such as the 4-phenyl-1,2,3-triazoles which researchers have extensively studied their application as precursors for cyclometallation. A experiment conducted by Schubert,[144] revealed that the reflux method in which 4-phenyl-1,2,3-triazole was heated at reflux with $IrCl_3 \cdot 3H_2O$ in ethoxyethanol led to the synthesis of the biscyclometalated chloro bridged dimer which could be treated with a wide variety of neutral and anion ligands such as acac and pic forming monomeric complexes.[110, 144] One of the optical-electronic characteristics and behavior of the complexes is the color-tuning of emission, which could be produced by changing the substituent on the ancillary ligand. Using functional groups with electron withdrawing on ancillary ligands leads to stabilisation of the LUMO. While applied functional groups with electron donating on ancillary ligands leads to higher energy in LUMO All the complexes exhibit blue shifted emission comparing with $Ir(ppy)_3$ complex (= 530) except the bpy complex. Emission was revealed to be easily tunable on the basis of the nature of the auxiliary ligand L^L, Figure1-23. Following the same reaction conditions, DeCola and coworkers[110, 145] synthesized and characterized the iridium dimers bearing 4-(2,4-difluorophenyl)-1,2,3-triazolyl)pyridine (dfptz) which contained an almost similar chemical structure and characteristics. Comparing with $Ir(ppy)_2$ complexes showed similar absorption features with strong π-π* transitions and weaker MLCT. Emission bands were significantly shifted to the blue region of the visible spectrum compared to that of the non-fluorinated analogue.

Cyclometalated ruthenium(II) complexes bearing aryltriazole-based ligands have been prepared and characterised by Wenwen Yang and Yuwu Zhong.[146] The complex showed red shifted in absorption relative to that of $[Ru(bpy)_2(pytz)](PF_6)_2$ and extends beyond 600 nm. The HOMO of this type of complexes is not localised on the metal centre only, but is localised over the ruthenium and cyclometalated ligand, therefore the HOMO energy can be controlled

by changing the R group on the cyclometalated ligand. In 2011, Yao, Zhong, and coworkers[138] reported heteroleptic Ru(II) complexes by reacting Ru(terpy)Cl$_3$ with the bis (triazolyl)benzene ligand, to give an octahedral cycloruthenated complex. 2,6-bis(1-R-1,2,3-triazol-4-yl)pyridine ligands, also used to prepare cyclometallated complexes and metallostar complexes. The UV/vis absorption spectra of cyclometallated complexes were compared with [Ru(tpy)$_2$](PF$_6$)$_2$ and [Ru((dpb)$_2$](PF$_6$)$_2$ where dpb = 1,3-di(2-pyridyl)benzene ligand. While [Ru(tpy)$_2$](PF$_6$)$_2$ complex shows (MLCT) transition at λ_{abs} = 475 nm, the MLCT absorptions of cyclometalated [Ru(tpy)(dpb)](PF$_6$)$_2$ complex are red shifted at λ_{abs} = 499 nm, extended, and slightly reduced in intensity. The complexes which contained 2,6-bis(1-R-1,2,3-triazol-4-yl) pyridine ligands, as cyclometallated triazole complexes display significantly different UV/vis absorption spectra. Blue shifted, the complexes exhibit absorption bands between 340 and 420 nm which are assigned as MLCT from metal center to N^C^N ligand. Obata, Kakuchi and co-workers[104] reported that they prepared a four-arm metallostar architecture from reacting Ru(II) with the ligand resulting from reaction of an azido functionalised polystyrene polymer with 2,6-diethynylpyridine.
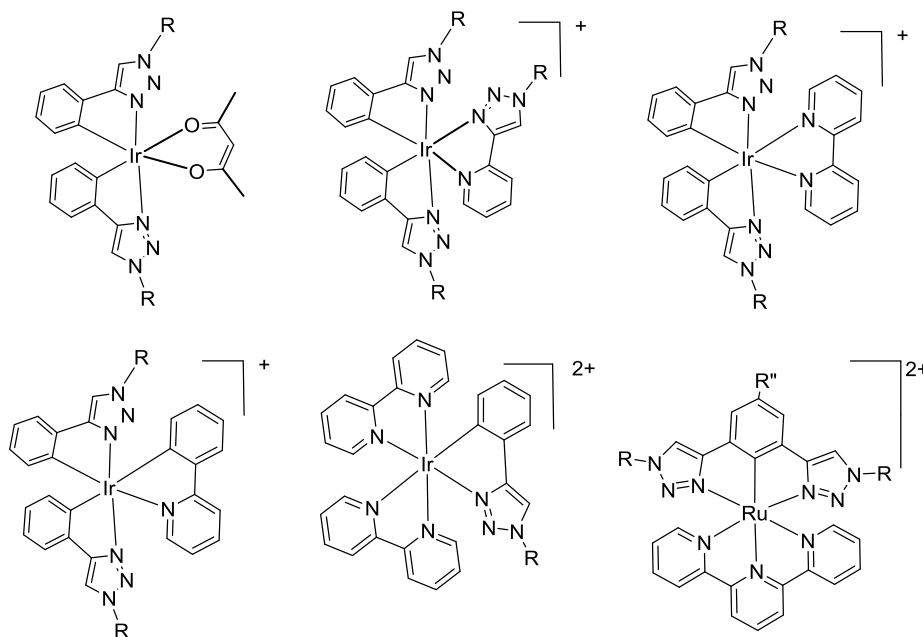
Figure 1-23 Some metal complexes containing the 4-phenyl-1,2,3-triazole ligands as C^N donor

45

Table 1-3: photoluminescence data of some iridium(III) and ruthenium(II) complexes containing the 4-phenyl-1,2,3-triazoles ligands as C^N and 2,6-bis(1-R-1,2,3-triazol-4-yl)phenyl ligand as N^C^N –donor at room temperature.

Complex	λ_{em}/ nm
$[Ir(ppy)_3]^+$	530
$[Ir(ppy)_2(bpy)]^+$	580
$[Ir(ptz)_2(bpy)]^+$	560
$[Ir(ptz)_2(acac)]^+$	435
$[Ir(dfptz)_3]^+$	392, 418
$[Ir(dfptz)_2(bpy)]^+$	514
$[Ir(dfptz)_2(ppy)]^+$	480, 510
$[Ir(dfptz)_2(dfppy)]^+$	465, 489
$[Ru(tpy)_2]^{2+}$	604
$[Ru(tpy)(dtab)]^{2+}$	Not observed
$[Ru(bpy)_2(Butab)](PF_6)$	Not reported

1.5.3 1,4-Disubstiuted-1,2,3-Triazoles as C-Donor Ligands

In most cases, the most preferred metal coordination sites are the N2 and N3 nitrogen atom positions of the 1,4-disubstituted-1,2,3-triazole although from the previous discussion there is a possibility for metal coordination at the C5 carbon position. Copper triazolide is thought to be key intermediates in CuAAC reaction. The formulation of a Cu(I) triazolide in the CuAAC

reaction gives rise to valuable modifications of the catalytic cycle. With stoichiometric quantities of Cu and in the protons absence, the Cu(I) triazolide is obtained as product, that permitting the following transmetalation of the triazolide to other metal centers.[147] The alkylation or protonation of 1,4-Disubstituted-1,2,3-triazole ligand occurs selectively at the N(3) position to make1,3,4-trisubstituted-1,2,3-triazolium salts, which are known as mesoionic or 'abnormal N-heterocyclic carbene (aNHC).

1.5.3.1 Triazolide complexes

The coordination of the triazole ring with C5 as a monodentate ligand demonstrated by Gray and coworkers who in their experiment synthesized a series of luminescent gold-1,2,3-triazolide complexes in a click chemistry reaction, Scheme 1-6. The complexes are luminescent in THF at room temperature and showed dual singlet- and triplet-state luminescence from excited states localized on the aromatic fragment with the shorter-wavelength emission peaks at 383 nm; and a longer-wavelength emission maxima at 498, 536, and 579 nm,. Luminescence lifetimes observed for complexes are from hundreds of microseconds to tens of milliseconds. [148]
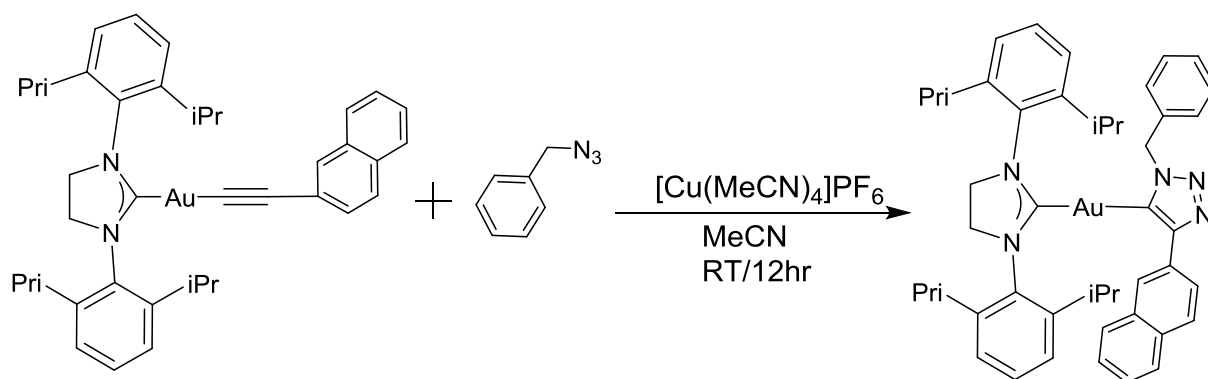
Scheme 1-6 Copper-Catalyzed Gold(I) Triazolide Synthesis[148]

Copper(I) triazolides that are typically formed as intermediates in CuAAC reactions, were generated and used as a bidentate C^N donor ligands in the formation of neutral iridium(III) pyridyltriazolide complexes by Swager and co-workers, Figure 1-24.[147] The complexes showed structured bands in their emission spectra indicating phosphorescence from ^{3}MLCT/^{3}ILCT states. These complexes were found not to be stable, and could be readily converted into their cationic N^N-pytz analogues through UV photolysis or through heating in glycerol solutions. By using RuAAC Schubert and his group prepared the ligand 6-(1-octyl-1,2,3-triazol-5-yl)-2,2-bipyridyl in which tridentate N^N^N coordination including to the triazole is not possible. Reaction with [Ru(tpy)(NCMe)$_3$]$^{2+}$ leads to cyclometalation to form the triazolide complex.[149] The absorption and emission bands are shifted to lower energy (λ_{abs} = 520 nm, λ_{em} = 730nm) compared to [Ru(tpy)$_2$]$^{2+}$ complex (λ_{abs} 452 = nm, λ_{em} =610). The HOMO of the triazolide complex has contributions from the metal as well as the triazolide p-system and is destabilised with respect to that of [Ru(tpy)$_2$]$^{2+}$. Methylation of the N(3) position of the triazolide complex using methyl iodide lead to production of the mesoionic triazolylidene complex .
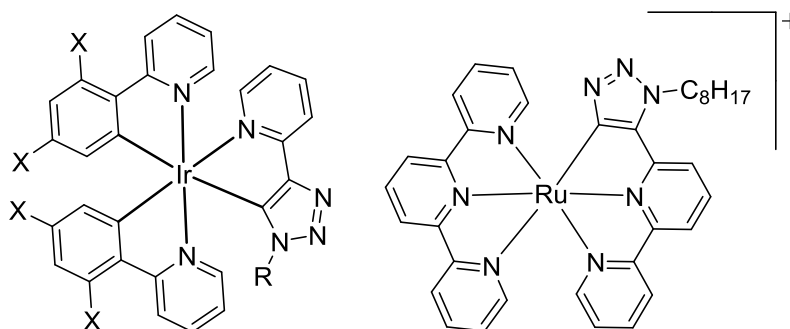
Figure 1-24 Structures of iridium(III), ruthenium(II) triazolide complexes.

1.5.3.2 Carbene complexes

As mentioned above, Schubert and his group prepared a mesoionic triazolylidene rhuthenium complex by methylation of the N(3) position of the triazolide complex using methyl iodide.

The HOMO is stabilised in 1,2,3-triazol-5-ylidene complexes relative to that of triazolide complexes, because of the overall charge neutrality of the carbene donor, and poor π-donor properties compared with triazolide complexes. This leads to shifted absorption and emission to higher energy.[83]

The increasing of the energy gap between the ^{3}MLCT and ^{3}MC states can be amended by using stronger σ-donating ligands as well as auxiliary substituents.[150] Also, using strong π-donors within the ligand set can be lead to deactivation of ^{3}MC states. Long lived phosphorescence from tpy based ^{3}MLCT states is observed as a result of the strong σ-donor character of the triazolylidene ligands and the consequential destabilisation of emission-deactivating ^{3}MC states. Protonation and deprotonation of triazolide complexes shift the ^{3}MLCT emission band to 648 nm. The absorption spectra of the complexes are shifted to higher energy (λ_{abs} = 480 nm) comparing to Ru(tpy)$_2$ (λ_{abs} = 474 nm) and triazolied complex (λ_{abs} =520 nm). While rhuthenium catalyzed Azide-Alkyne Cycloaddition (RuAAC) was chosen by Schubert to produce 1,5-disubstituted 1,2,3-triazolylidene,[149] CuAAC was selected by Berlinguette to prepare 1,4-disubstituted 1,2,3-triazolylidene ligands.[151] Berlinguette and his group reported the series of bi(triazolylidene) ruthenium(II) complexes, Figure 1-25. The two strong carbene donors in the complex leads to an extremely long lived ^{3}MLCT state (τ = 7.9 μs), amongst the longest recorded for a bis(tridentate) ruthenium(II) complex. A terdentate bis-2,6-(triazolylidene)pyridine Fe(II) complex has been synthesised by Sundström and coworkers.[152] The first known examples of bis(triazolylidene)pyridine coordination to Pt(II) have recently reported by Hwang et al.[153] These complexes which containing different X ligands (X = Cl, NCCH$_3$, CN) are emissive in MeCN solutions, with (X = Cl λ_{em} = 504 nm, τ= 6.93 μs) and X= NCCH$_3$ (λ_{em} = 494 nm, τ = 1.68 μs) giving broad bands while the complex with X= CN is more structured with λ_{max} = 490 nm and 522 nm (τ= 5.58 μs).
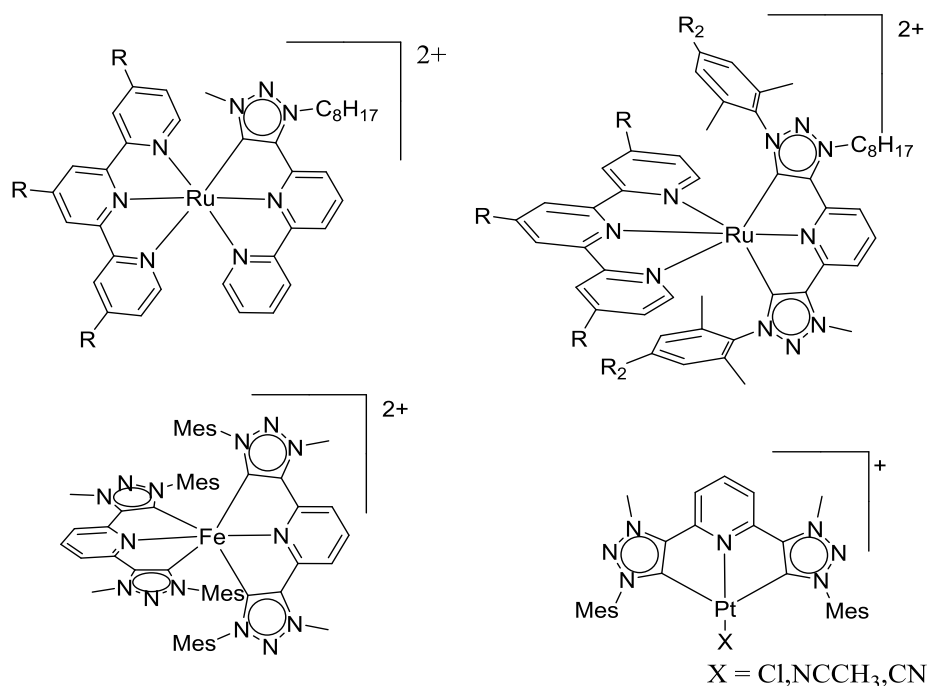
Figure 1-25-Some bis(tridentate) complexes based on 1,2,3-triazolylidene ligands

The bidentate triazolylidene ruthenium complex has been reported by Albrecht Figure 1-26.[154] Due to the slight anionic charge on the abnormal carbene ligand donor C-atom, this complex exhibits a slightly destabilised HOMO comparing to $[Ru(bpy)_3]^{2+}$ complex. The resultant reduction of the HOMO–LUMO gap results in a slight red-shift in the emission band, (λ_{em}= 648 nm). Bis(1,2,3-triazol-5-ylidene) Fe(II) complexes having been synthesised by Sundström.[155] The red-shift of the lowest-energy MLCT band observed in the visible region from 520 nm of $[Fe(bpy)_3][PF_6]_2$ to 609 nm, with long ^{3}MLCT lifetime of 13 ps, significantly longer than the lifetime of $[Fe(bpy)_3]^{2+}$ (τ = 130 fs). Recently Wärnmark and coworkers prepared bis(1,2,3-triazol-5-ylidene) ligands which have been used within low-spin complexes of Fe(III). Most remarkably, the resulting ^{2}LMCT excited states are emissive at room temperature (λ= 600 nm) with a lifetime of 100 ps. Albrecht reported BODIPY-functionalised triazolylidene complexes of Pd(II).[156] This complex displays BODIPY-derived photoluminescence (emission around 545 nm, quantum yields in the 0.35−0.7 range, and

excited-state lifetimes between 3 and 7 ns). Replacing DMAP ligand in this complex by acridine allows for an observation of the exchange of emission-quenching constants were determined as $K_{SV} = 0.86$
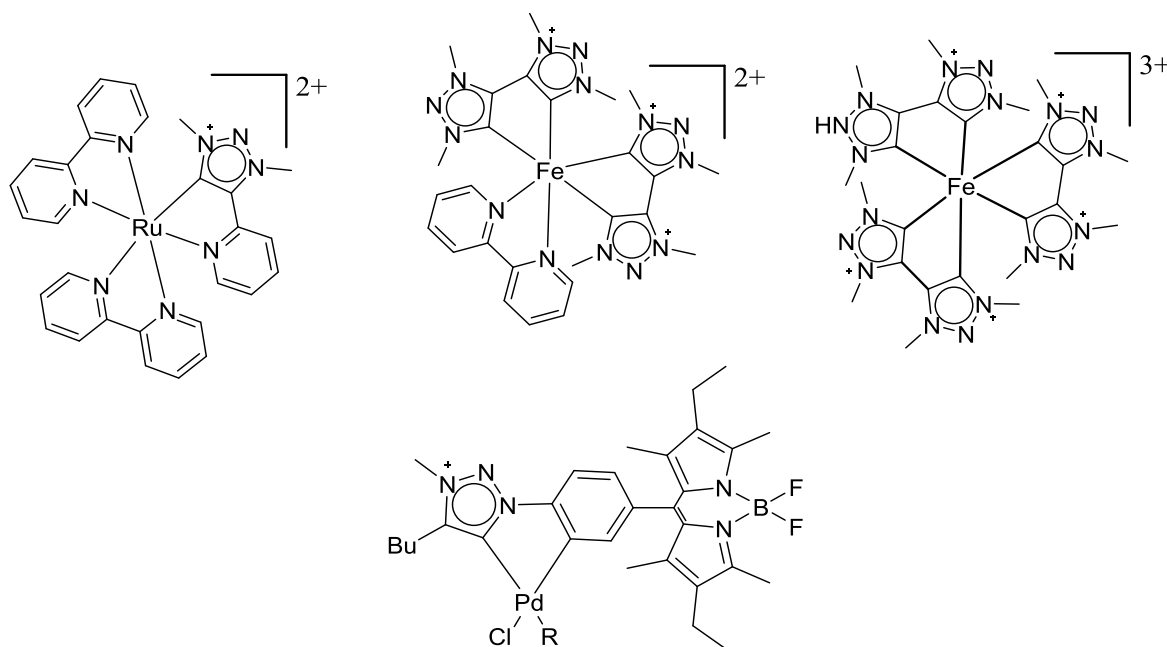
Figure 1-26 Some metal complexes 1,2,3-triazole-based aNHC ligands

1.5.4 1,2,3-triazole moiety as a supramolecular linking unit.

Synthesis of metallosupramolcular compounds has to be based on the preparation of bridging ligands with various coordination sites into which can then be incorporated metal centers. This methodology has major defects with complications in the selectivity and control of the metal binding when, for example, heterometallic complexes are demanded and where the bridging ligand is non-symmetric. "Expanded ligand" based approaches[157] have also been reported in the complexes that are prepared and modified at their periphery in order to graft onto the complex a second binding domain. One method for such architectures involves a separately preformed coupling of superamolecular complexes under mild conditions, which require as few as possible steps. Such process would necessitate a coupling reaction of high productivity

and highly efficient, for this, functional groups are required which can be easily inserted into the periphery of the metal complex components. With this methodology in place and a library of appropriately derivatised transition metal complex components, this would allow easy access to supramolecular architectures with remarkable diversity of structure. For this purpose The CuAAC reaction is an excellent candidate. A number of groups have reported "click" ligands[158-160] in the formation of coordination polymers.
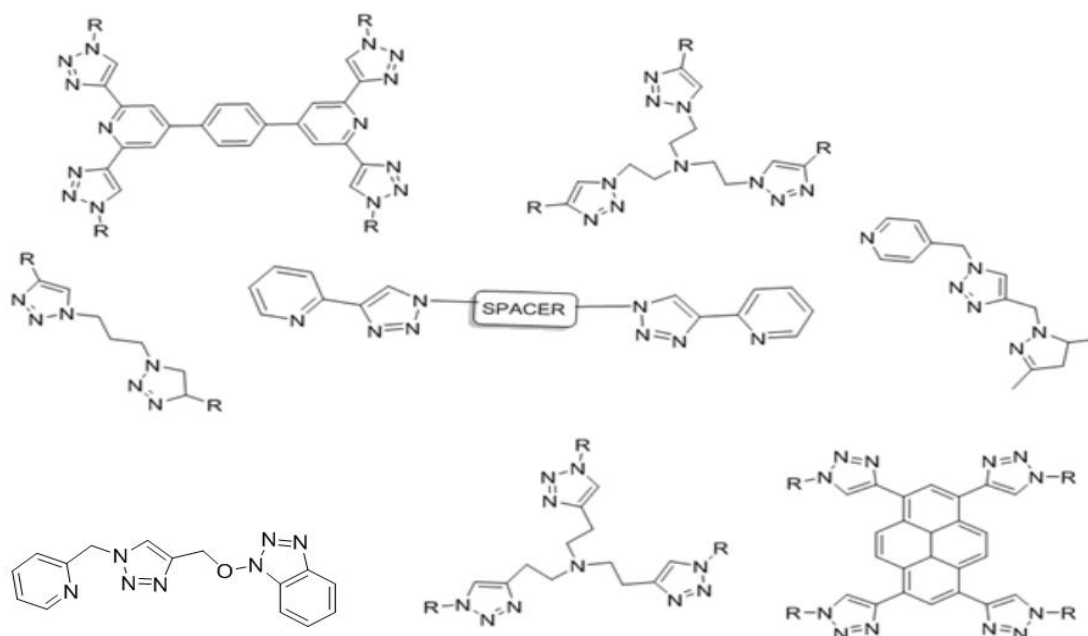
Figure 1-27- Click ligands used as bridging ligands on the preparation of metallosupramolcular materials

The tris(benzyltriazolylmethyl) amine (TBTA) which used as a co-ligand in CuAAC reaction is the most common ligand used in this type . Donnelly, Williams, and coworkers[161] have reacted The tris(benzyltriazolylmethyl)amine (TBTA) with [Cu(MeCN)$_4$]BF$_4$ in acetonitrile to give a dinuclear cation complex, Figure 1-28. From X-ray crystallography they found that each Cu(I) ion is coordinated by three N3 triazole donors from one ligand and an N2 donor from a second ligand.
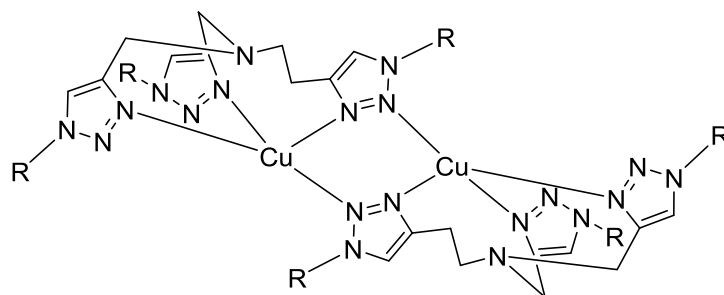
Figure 1-28- *Dinuclear cation complex of TBTA Cu^{II} complexes.*

Potential bis-tridentate ligands have been formed by incorporating triazole units into a pyrene skeleton by Yao, Zhong, and coworkers[162] by reacting two equivalents of dicycloruthenated complex, where each octahedral Ru(II) center is coordinated by three N donors from a terpy ligand and two triazole N donors as well as a carbon donor from the pyrene core Figure 1-29. The UV–visible absorption spectrum of the dinuclear complex is very like to that of its mononuclear complex proposing that in the ground state there is little communication between the two metal centres. Upon one-electron oxidation of the dinuclear complex there is a new LMCT band detected at around 730 nm along with an intervalence charge transfer (IVCT) transition. When a second electron is removed from the dinuclear complex, this IVCT band is noted to disappear.
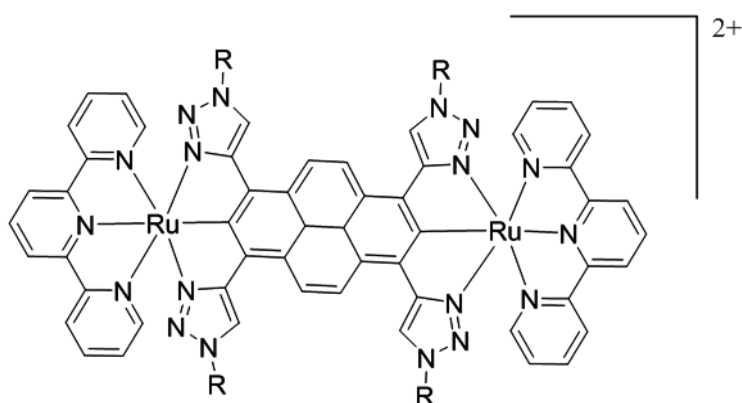
Figure 1-29- Linear dimetallic biscyclometalated Ru (II) complex using 1,3,6,8-tetrakis(1-butyl- 1H-1,2,3-triazol-4-yl)pyrene as bridging ligand

Ulrich S. Schubert and co-workers[163] apply [1,1′-(9,9-Dioctyl-9H-fluorene-2,7-diyl)bis(1H-1,2,3-triazole-4,1-diyl)]bis{3-[(4-nitrophenyl)ethynyl]pyridine}ligand as bridging ligand to synthesise the ruthenium dinuclear complex [Ru(dmbpy)$_2$]$_2${μ-2,2′-[1,1′-(9,9-dioctyl-9H-fluorene-2,7-diyl)bis(1H-1,2,3-triazole-4,1-diyl)](dipyridine)}(PF$_6$)$_4$, Figure 1-30. The complex shows a typical absorption band for ruthenium(II) polypyridine complexes around 450 nm, which assigned to MLCT transitions. Even though the pytz moiety and lead to quenched emission, this complex is emissive in dichloromethane solutions at room temperature (λ$_{em}$ = 593 nm).
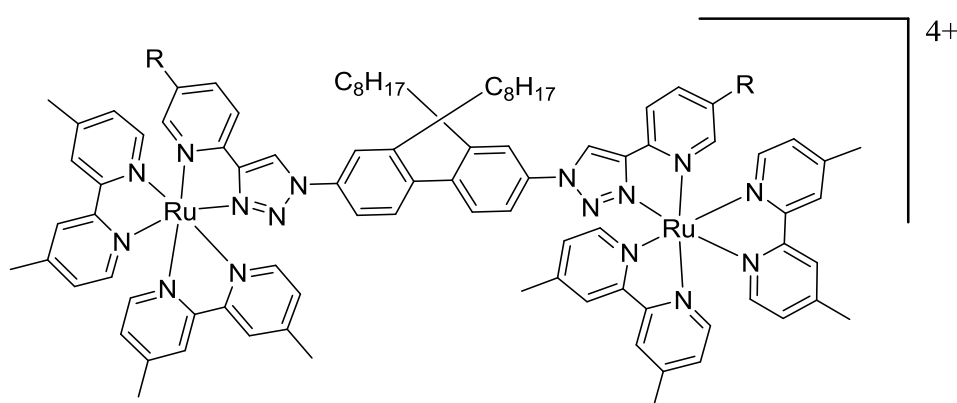
Figure 1-30 Heteroleptic ditopic ruthenium(II) complexes

Crowley and co-workers[164] have shown that poly-2-(1-R-1H-1,2,3-triazol-4-yl) pyridine ligands will form metallomacrocycles Figure 1-31. Crowley react of the ligands, with AgSbF$_6$ to form the metallosupramolecular architectures. Characterisation of complexes indicate that these complexes are stable in solution. The structure of the silver (I) metallomacrocycle, was confirmed using X-ray crystallography.
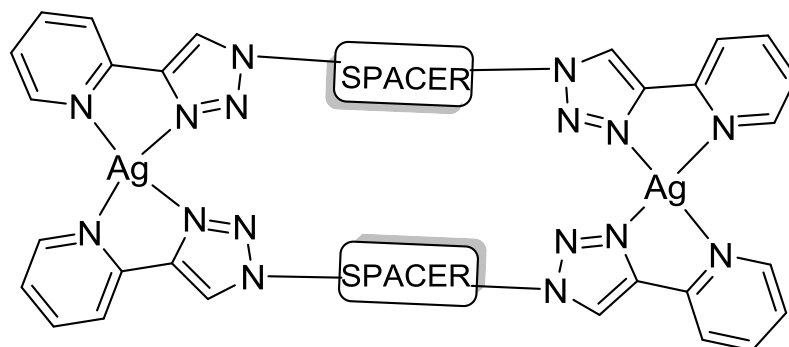
Figure 1-31 bis-bidentate "click" silver (I) metallomacrocycle

Crowley and co-workers[165] also applied the same ligand to prepare an iron complex. UV-vis absorption spectroscopy of the complex revealed absorption features in the UV-visible region of the spectrum (300–450 nm) with maxima observed at 420–430 nm. These absorption maxima are assigned as MLCT bands which are blue-shifted relative to related bipyridine based iron(II) complexes, (λmax = 500–540 nm) but occur in a similar region to complexes containing pyridylpyrazole chelators (λmax = 423 nm). This shift to lower wavelength for the MLCT band of the "click" complexes compared to these other systems is consistent with the reduced π-acceptor nature of the triazole unit. Hor and coworkers[159] have formed an elegant helical Cu(II) coordination polymer from reaction of 1-(2-picolyl)-4-(1-(methoxyl)-benzotriazole)-1H-1,2,3-triazole with CuCl$_2$. 2H$_2$O Addition of one equivalent of CuCl$_2$ gave a mixture of green and blue crystals, Figure 1-32.
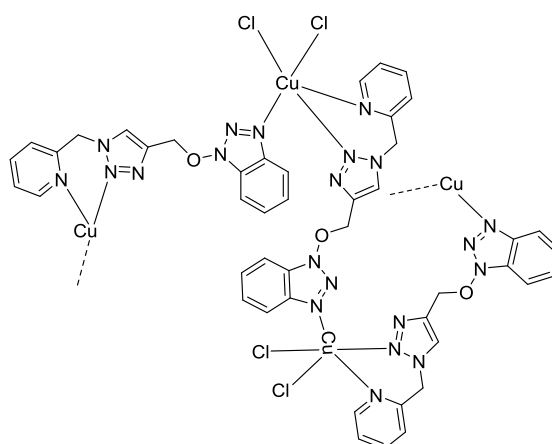
Figure 1-32- 1-(2-picolyl)-4-(1-(methoxyl)-benzotriazole)-1H- 1,2,3-triazole as bridging ligand in Helical Cu(II) Polymers

Recently A. Wiehe and co-workers[166] used the copper(I)-catalyzed 1,3-dipolar cycloaddition (CuAAC) to prepare a functionalized symmetric dimer as a biocompatible carrier system for photodynamic therapy (PDT).
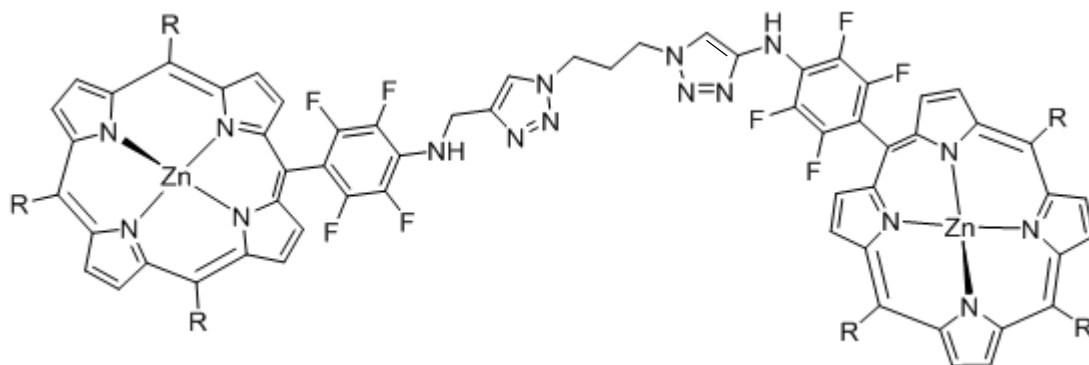
Figure 1-33- Structure of Porphyrin dimer using triazole ligand as bridging ligand

1.6   **Aim of the project**

The main goal of the project in this thesis is the synthesis, structural investigation, photophysical and electrochemical properties of new triazole-containing transition metal complexes and their possible use in applications, such as light-emitting diveces, imaging in living cells and photodynamic therapy (PDT) as photosensitizer (PS). The desired photophysical and photochemical properties of a complex can be achieved by use of synthetic chemistry and molecular design to manipulate ligands and metal. The increased used of luminescent complexes in these applications depend on the lifetime regarding biological applications for instance phosphorescence often displays a longer lifetime compared to autofluorescence emanating from the natural or organic compounds of emissive complexes amenable to time-gated imaging microscopy and therapy. In this project osmium(II) will be used as a central metal. The osmium(II) complexes allow excitation at lower energy. The principle sustains efficient excitation at low energies that eliminate the possibility of cellular damage and negates the auto-fluorescent and necessity of additional expensive time gated apparatus. The osmium(II) complexes are inert to ligand photo substitution. The intensity of phosphorescence is dependant upon the concentration of oxygen in the system due to quenching through conversion of ground state $^3O_2$ to the reactive $^1O_2$, thus supporting exploitation of the complex for photodynamic therapy (PDT). Therefore reactions that enable facile routes to the modular construction of new ligands and these architectures are particularly useful in the development of such materials. The influence of the supermolecular architecture is that it controls the photophysical properties of the complex which allows to design it for certain application. In this project 1,4-disubstituted 1,2,3-triazoles will be used as a ligand, prepared by the CuAAC reaction. In general, triazoles, which are formed from this reaction contain two nitrogen atoms that can coordinate with metals, with N3-position acting as the

more basic site. On the other hand, the R and R' groups of the alkyne and azide precursors can also feature coordinating fragments, which allows for the access to numerous chelating ligands, while C-H activation of position-5 gives access to anionic triazolides. Also triazoles can be used as a linker to develop di and trinuclear complexes (oligonuclear, organometallic) complexes of diverse architectures. The potential of the CuAAC in coordination chemistry has only just begun to be fully exploited. This work will investigate the following aims:

1- Synthesis and characterisation of different types of 1,2,3-triazole containing ligands including 2-(1-benzyl-1H-1,2,3-triazol-4-yl)pyridine as bidentate ligand , 2,6-bis(1-phenyl-1H-1,2,3-triazol-4-yl)pyridine as tridentate ligand and 1,4-bis((4-(pyridin-2-yl)-1H-1,2,3-triazol-1-yl)methyl)benzene which will be applied as a bridging ligand.
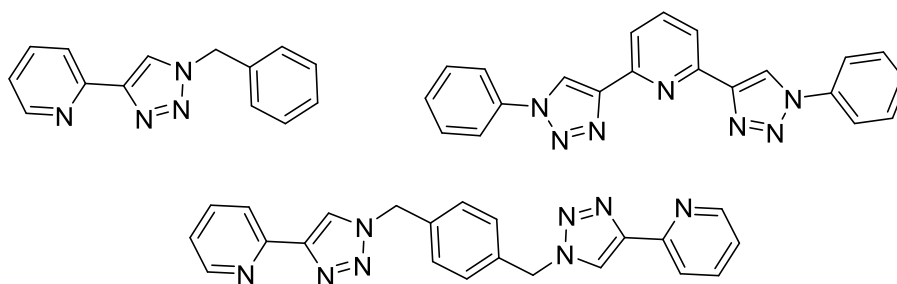
2- Investigation of the coordination of 2-(1-benzyl-1H-1,2,3-triazol-4-yl)pyridine and 2,6-bis(1-phenyl-1H-1,2,3-triazol-4-yl)pyridine as bidentate ligand with rhenium transition metal, then investigate the influence of (N^N) ligands on the photophysical and electrochemical characteristics of complexes comparing with bipyridine and terpyridine derivatives. In 2-(1-benzyl-1H-1,2,3-triazol-4-yl)pyridine rhenium complex, different types of monodentate pyridine based ligands as axial ligands (X) will be used, to investigate the effect of axial ligands on the photophysical properties of the complex. The potential of these complexes to be used in light-emitting devices will be assessed.
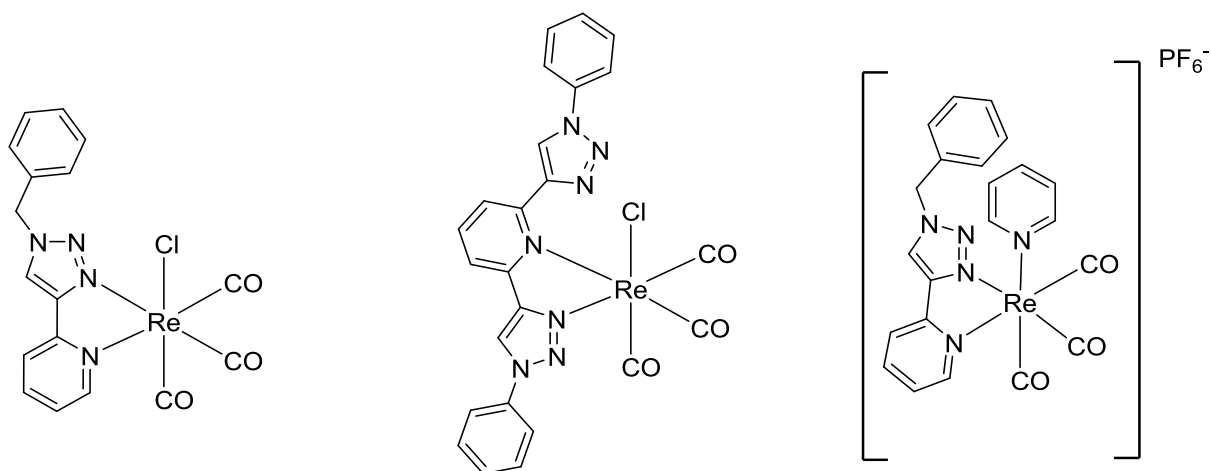
3- Prepare osmium complexes using triazole ligands of different types including 2-(1-benzyl-1H-1,2,3-triazol-4-yl)pyridine as a bidentate ligand and 2,6-bis(1-phenyl-1H-1,2,3-triazol-4-yl)pyridine as tridentate ligand as its hexafluorophosphate and chloride salts complex and study the photophysical and electrochemical properties of these complexes and ability to sensitise $^1O_2$ production.
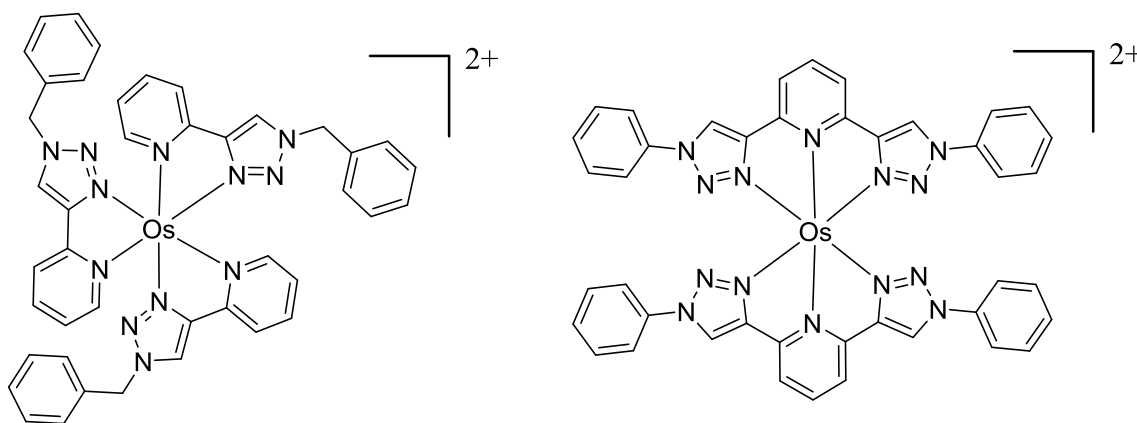
4- The water soluble chloride salts of these osmium(II) complexes will be subject to preliminary cellular uptake and luminescence imaging studies.

5- Formation of complexes using 1,4-bis((4-(pyridin-2-yl)-1H-1,2,3-triazol-1-yl)methyl)benzene as the bridging ligand to synthesize organometallic homodinuclear and heterodinuclear complexes of Ru, Os, and Ir, then characterize their photophysical as well as electrochemical properties. In the end, the products might find useful applications in catalytic reactions, and industrial as well as biological applications.

62
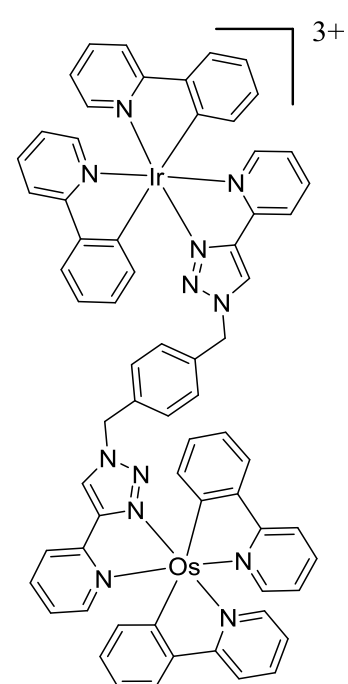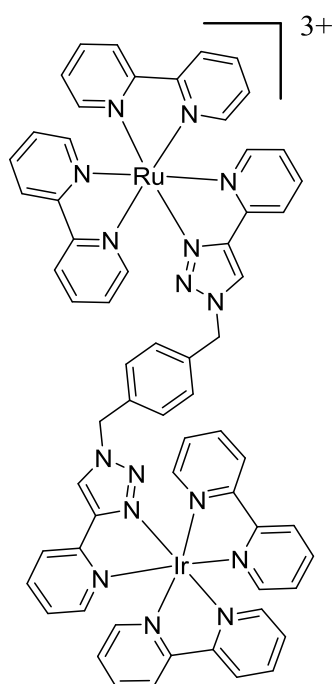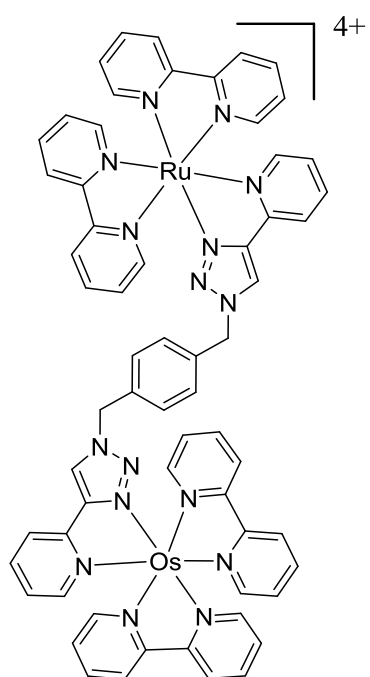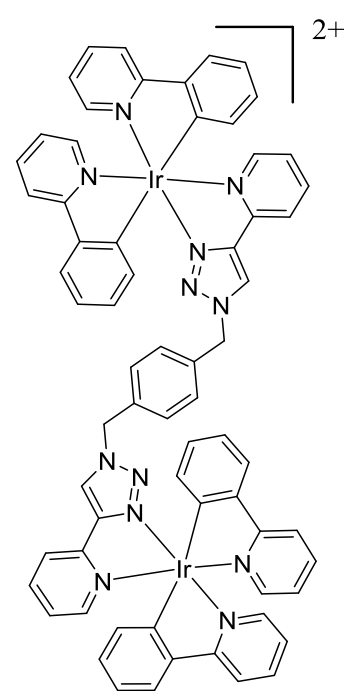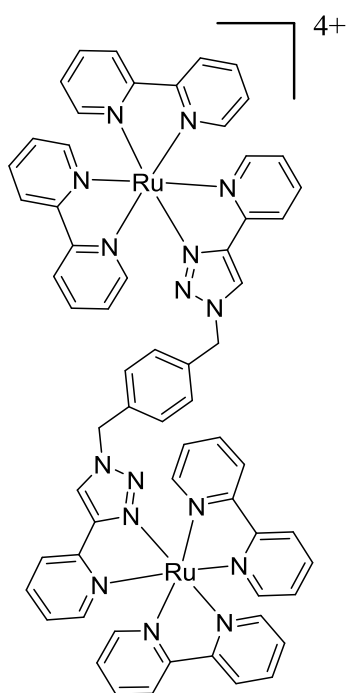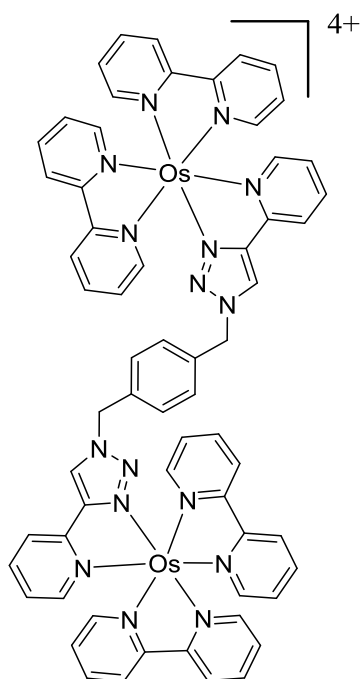
Chapter 2: Rhenium 4-(pyrid-2-yl)-1,2,3-triazole complexes

Synthesis, characterisation and photophysical investigation of Rhenium 4-(pyrid-2-yl)-1,2,3-triazole complexes

2.1 Introduction:

The d^6 metal/diimine combinations are valuable as they can allow: i) prolonged excited-state lifetimes, ii) strong absorption of light in visible-region, iii) photochemical stability and iv) noticeable visible-region luminescence. Substantial attention has been attracted by rhenium(I) tricarbonyl diimine complexes[167] in the last few decades for their luminescent and photophysical properties and the complexes have been used as photocatalysts for CO_2,[168-170] emitters for electroluminescent devices,[171, 172] biological imaging agents[173-175] and as supramolecular building blocks.[176] As a result many compounds of the form fac-[Re^I(CO)$_3$(N^N)(L)]^n have been studied in an effort to understand their photophysical processes and their functions.[177] Photophysical properties of rhenium(I) carbonyl complexes usually include tunable metal-ligand charge transfer (MLCT) (dπ(M) to π*(L)) and ^{3}MLCT emission wavelengths as well as their quantum yields and room-temperature luminescence[7] from low-lying states. Typically, in this type of complex fac-[Re(N^N)(CO)$_3$(X)]$^{0/+}$, the HOMO is dominated by a Re 5d-orbital (with additional carbonyl π* contributions as well as p-orbital contributions where X is a halide e.g. Cl). On the other hand, the LUMOs are essentially the π* orbital of diimine ligands. As these characteristics are influenced by solvent environment,[178] ligands and metal, desired photophysical and photochemical properties can be achieved by manipulating these factors, which can be modified by changing the electron donating character of ancillary ligands and/or diimine ligand substituents of these complexes. In particular, light-emitting electrochemical cells, LECs, and organic-light-emitting diodes, OLEDs, promise to be efficiently compared with incandescent and fluorescent lamps and can be exploited in

electroluminescent displays. The effective OLED requires facile and stable charge transfer as well as a high conversion efficiency of excitation to light.[179] As electrons and holes are transported through the LUMOs and HOMOs, respectively, in OLED components, the relative band gap ΔE, HOMO and LUMO energies of these materials is of critical importance to the efficiency of an OLED.[180] Due to their chemical stability, redox and luminescent properties, which can also be exploited on photoswitches, Re(I) complexes have attracted a great deal of recent attention and recently, have been used as emissive species due to their higher emission efficiency when compared to the polymers.[181-183] In order to achieve higher emission yields in metal complexes based OLEDs, two strategies have been employed: (i) use of different diimine ligands to tune the photophysical and electrochemical properties, (ii) attachment of electron-withdrawing or electron-donating groups to ligands.[184] Rhenium(I) coordination complexes of 1,2,3-Triazoles have been widely utilised within bidentate chelating ligands with *fac*-[Re(Bn-pytz)(CO)$_3$Cl] displaying an electronic absorption band with a maximum at 333 nm, slightly higher in energy than that observed for the bpy analogue (371 nm) and emission at 538 nm which is blue shifted compared with [Re(bpy)(CO)$_3$Cl] (633 nm).[96] Replacement of the halide ligand by a neutral pyridine donor in [Re(bpy)(CO)$_3$(py)]$^+$ complex results in a blue-shift in emission of 42 nm over that of [Re(bpy)(CO)$_3$Cl].[107] In this chapter the use of the 4-(pyrid-2-yl)-1,2,3 triazole and 2,6-bis(1-phenyl-1H-1,2,3-triazol-4-yl)pyridine ligands within bidentate donor ligand is explored to investigate the influence of (N^N) ligands on the photophysical and electrochemical characteristics of complexes; these are compared with bipyridine and terpyridine derivatives after synthesizing a series of rhenium(I) tricarbonyl diimine complexes *fac*-[Re(L)(CO)$_3$Cl], and [Re(L)(CO)$_3$(py)] (L= 1-benzyl-4-(2-pyridyl)-1,2,3-triazole, 2,6-bis(1-phenyl-1H-1,2,3-triazol-4-yl)pyridine, 2,2′-bipyridyl, 1,10-phenanthroline). Synthesis of rhenium (I) complexes having 1,2,3-triazole ligand as a bidentate donor ligand with different types of monodentate pyridine based ligands as axial ligands (X) (X = Pyridine, 4-tert-

Butylpyridine, 4-Methylpyridine, 3-Methylpyridine, 4-Dimethylaminopyridine, 3,5-Dimethylpyridine) to study the photophysical and electrochemical properties of the these complexes (study the effect of axial ligands on the photophysical properties. Some of these complexes will be subjected to preliminary tests, on their use in LEECs as blue emitting complexes

2.2 Synthesis and characterisation

2.2.1 Synthesis and characterisation of triazole Ligands

Ligand 1-benzyl-4-(2-pyridyl)-1,2,3-triazole (Bn-pytz) was prepared by a modification of the method[98] reported from isolated benzyl azide. Benzyl azide was synthesied through reaction of benzyl bromide with an excess of sodium azide in water and acetone. Upon completion, the reaction was quenched with water, and the azide extracted into diethyl ether. Benzyl azide was kept at -4°C and used in following reactions. In THF and water, with the presence of one equivalent of $CuSO_4$, two equivalents of sodium ascorbate and 2,6-lutidine, the benzyl triazole was prepared by reaction of the azide with an excess of 2-ethynylpyridine. After stirring at room temperature, isolation of the product was completed by partitioning between an aqueous ammonia and chloroform to remove copper (Scheme 2.1).
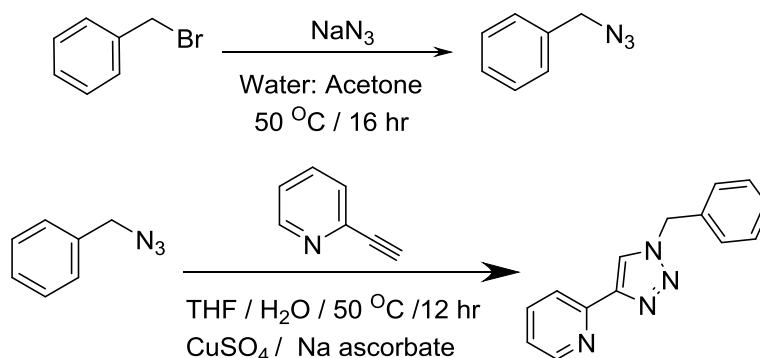
Scheme 2-1 Synthesis of triazole Ligand (bnpytz)

Column chromatography was used to purifiy the crude product which give a white solid isolated in good yield.

The ligand 2,6-bis(1-phenyl-1H-1,2,3-triazol-4-yl)pyridine, (btzpy)[88] was prepared in a two-step reaction (Scheme 2.2). Firstly 2,6-bis[(trimethylsilyl)ethynyl]pyridine was prepared through palladium-catalysd Sonogashira coupling of 2,6-dibromopyridine with ethynyl trimethylsilane. The crude product was purified by column chromatography to give a white solid.
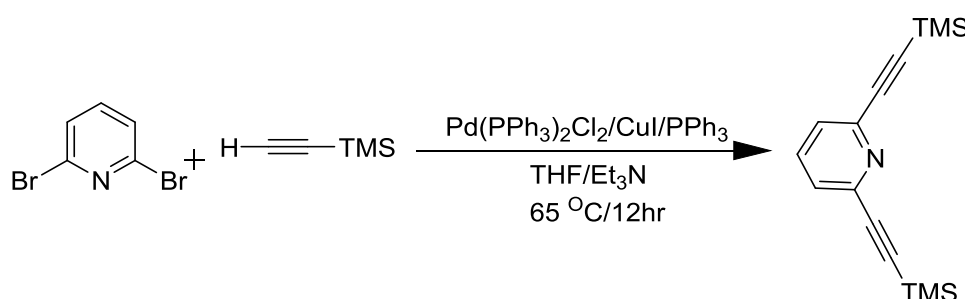
Scheme 2-2- Synthesis of 2,6-bis [(trimethylsilyl) ethynyl] pyridine

In the second step (Scheme 2.3) aniline was added to acetonitrile. The mixture stirred in ice bath then *tert* butyl nitrite and trimethylsilylazide were added to generate the corresponding phenyl azide *in-situ*. The mixture was then stirred for 2 hours and allowed to warm up to room temperature. Upon completion of the substitution reaction 2,6-bis[(trimethylsilyl)ethynyl]pyridine was added along with catalytic quantity of $CuSO_4$ and sodium ascorbate. The resulting precipitate of the Cu complex was decomposed by addition of aqueous ammonia. The product was extracted into $CHCl_3$, washed and drid. The solvent was removed under reduced pressure. The crude product was purified by column chromatography.

66
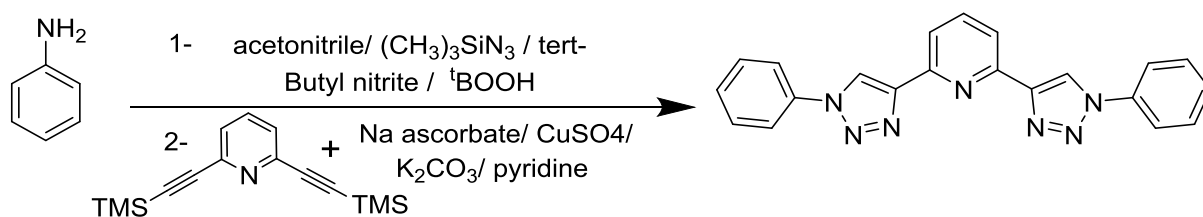
Scheme 2-3- Synthesis of 2,6-bis(1-phenyl-1H-1,2,3-triazol-4-yl)pyridine, (btzpy)

The triazole ligands 1-benzyl-4-(2-pyridyl)-1,2,3-triazole (Bn-pytz) and 2,6-bis(1-phenyl-1H-1,2,3-triazol-4-yl)pyridine (btzpy) were fully characterised by ^{1}H and ^{13}C NMR spectroscopy and mass spectrometry. The data are in agreement with a literature data.[98] The ^{1}H NMR spectrum for the (Bn-pytz) free ligand shows a distinct diagnostic signal for the C-H proton of the triazole ring (0) (Figures 2.1, 2.2).
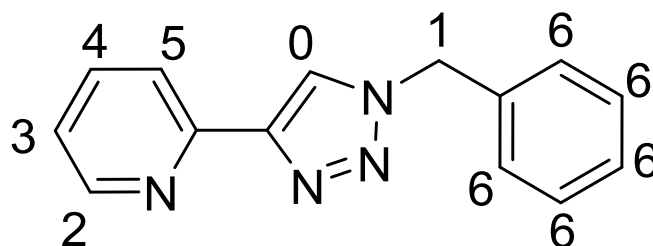
Figure 2-1-Number of protons of triazole Ligand (Bn-pytz)
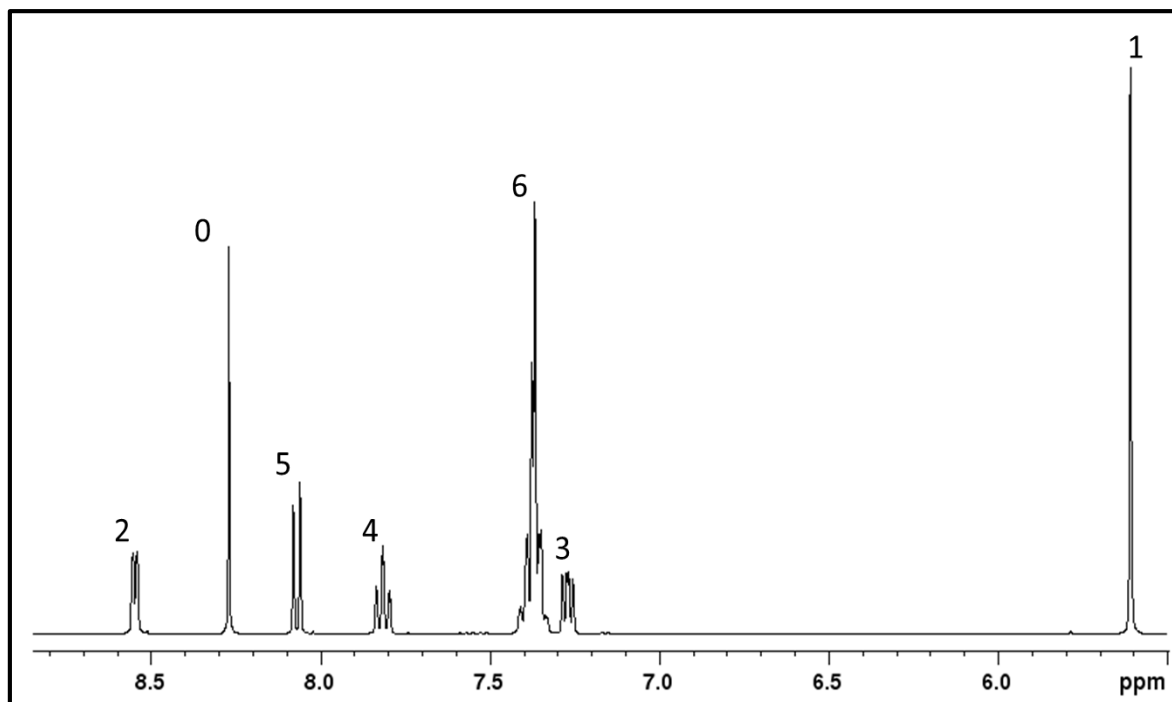
Figure 2-2-^{1}H NMR (400MHz) spectrum of free ligand (Bn-pytz) in CD$_3$CN

This appears as singlet resonances at δ 8.26. This signal shows nOe interactions in the two dimensional NOESY spectrum with correlation to the methylene protons of the benzyl substituent (1) which appears as a singlet resonance at δ 5.60. The methylene protons of the benzyl substituent (1) shows another nOe interactions in the two dimensional NOESY spectrum with correlation to the the phenyl protons which appears as multiplet at region δ 7.41–7.30 (6). (Figure 2.3)
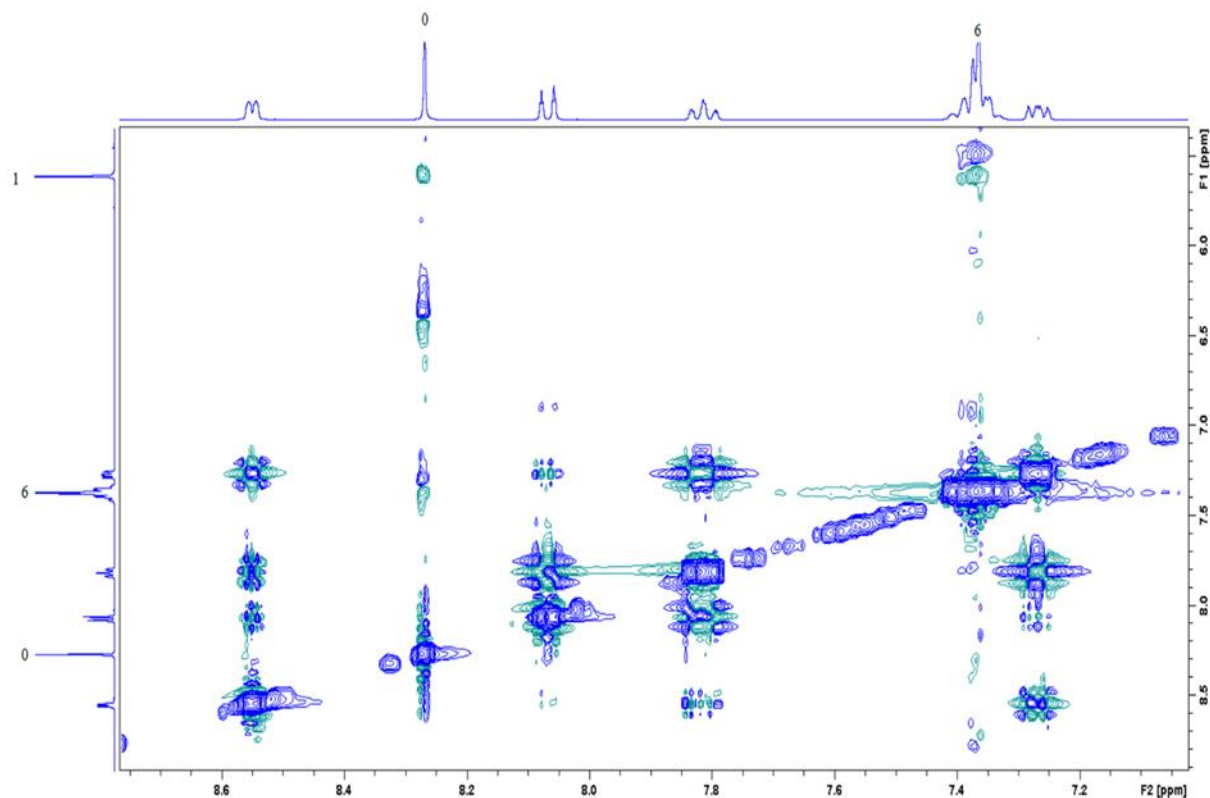
Figure 2-3-*2D H-H NOESY NMR spectrum of free ligand (Bn-pytz) in CD₃CN*

From the spectrum the proton next to the N atom of the pyridyl ring (2) is the most down field which appears as a doublet resonance at δ 8.53. This proton displays a COSY correlation with the signal which appears at region δ 7.28-7.24 (3). Proton (3) also displays strong COSY correlation with the signal appears at δ 7.76 (4). (Figure 2.4).
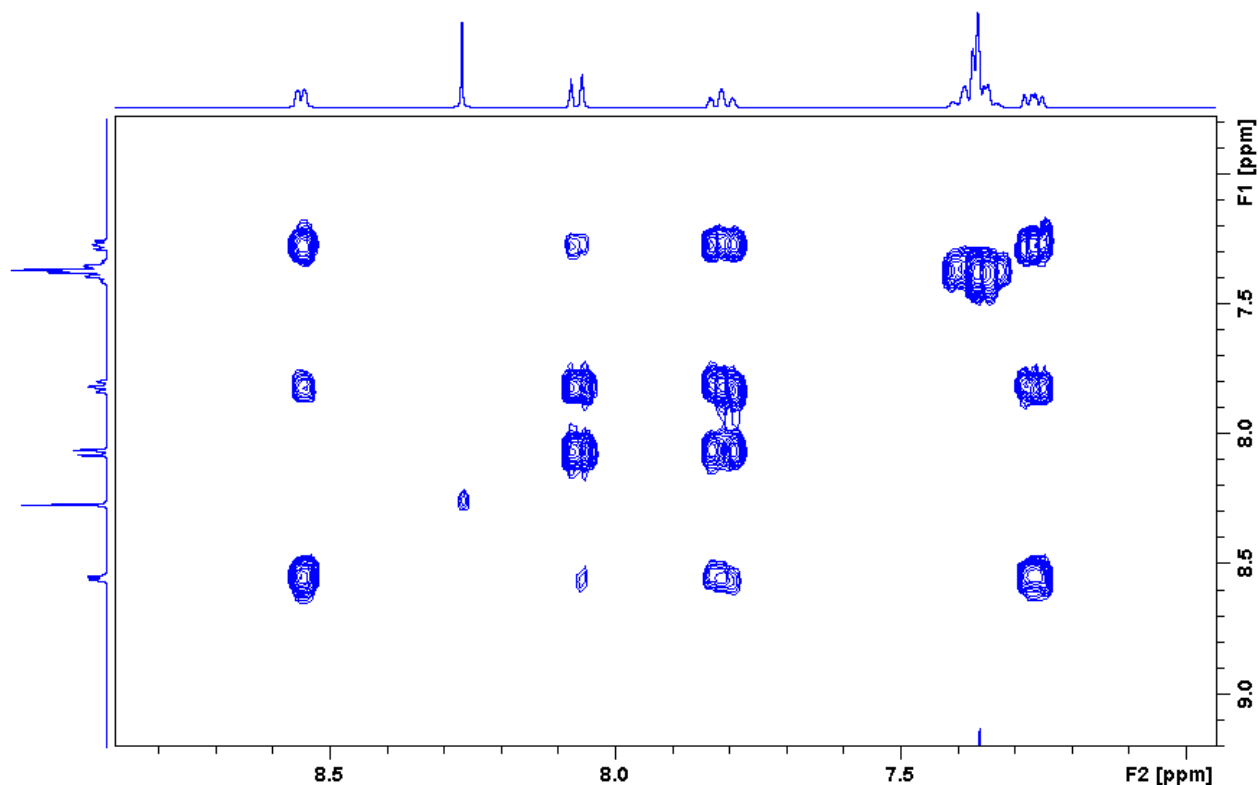
Figure 2-4-2D H-H COSY NMR spectrum of free ligand (Bn-pytz) in CD₃CN

In the ¹H NMR spectrum for 2,6-bis(1-phenyl-1H-1,2,3-triazol-4-yl)pyridine, contains a resonance for the triazole ring proton at δ 8.97, Figure 2.5 and resonance for the pyridyl protons in the range of δ 8.13–7.99, the phenyl rings shows 8 protons in the range of δ 7.93–7.63 and 2 protons at δ 7.53 The ESI mass spectrum of 2,6-bis(1-phenyl-1H-1,2,3-triazol-4-yl)pyridine, (btzpy) shows a peak at m/z = 388.1285, assignable to the species [M+Na]⁺. These results are in full agreement with previous results for the same compound.[88]

70
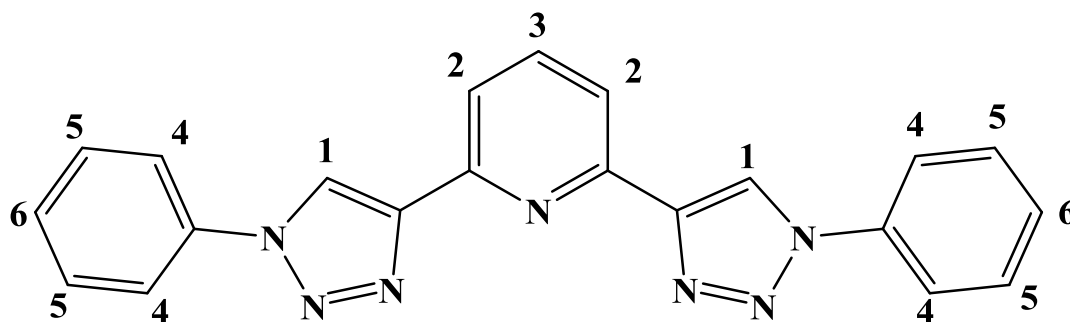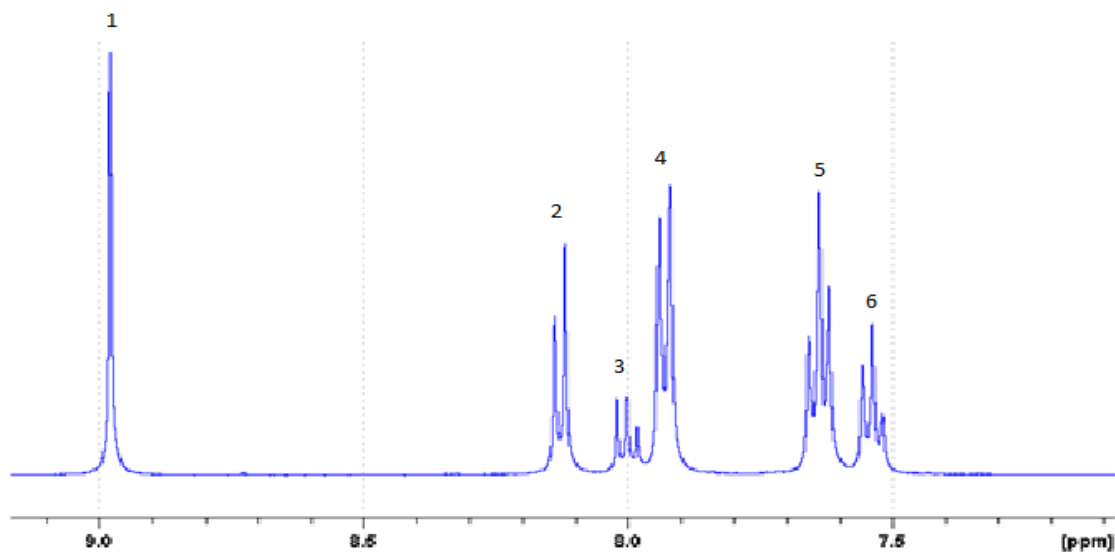
Figure 2-5- The 1H-NMR spectrum (400 MHz, CD₃CN) of free ligand *2,6-bis(1-phenyl-1H-1,2,3-triazol-4-yl)pyridine*

2.2.2 Synthesis and characterisation of cationic rhenium(I) triazole complexes

The rhenium(I) complexes, were prepared by firstly isolating the starting material *fac-*[Re(L)(CO)₃Cl] using a similar procedure to that of Meyer *et al.*[185] by heating rhenium pentacarbonylchloride with a slight excess of diimine ligand (L= 1-benzyl-4-(2-pyridyl)-1,2,3-triazole, 2,6-bis(1-phenyl-1H-1,2,3-triazol-4-yl)pyridine, 2,2′-bipyridyl and 1,10-phenanthroline) at reflux in toluene. The yellow precipitate was collected and used without further purification. The strongly bound Cl atom was removed by reaction of *fac-*[Re(L)(CO)₃Cl] with silver hexafluorophosphate (AgPF₆) in dichloromethane. The relevant of pyridine based ligands as axial ligand (X) (X=pyridine, 4-tert-butylpyridine, 4-methylpyridine, 3-methylpyridine, 4-dimethylaminopyridine, 3,5-dimethylpyridine) were added to the solution and the mixture was stirred in the dark at room temperature for 48 h. Pure complexes were obtained after purification by column chromatography and subsequent recrystallisation from hexane / dichloromethane and were isolated as yellow to green crystalline solids, depending on the nature of the N^N as well as X ligands. (Scheme 2-5)

71
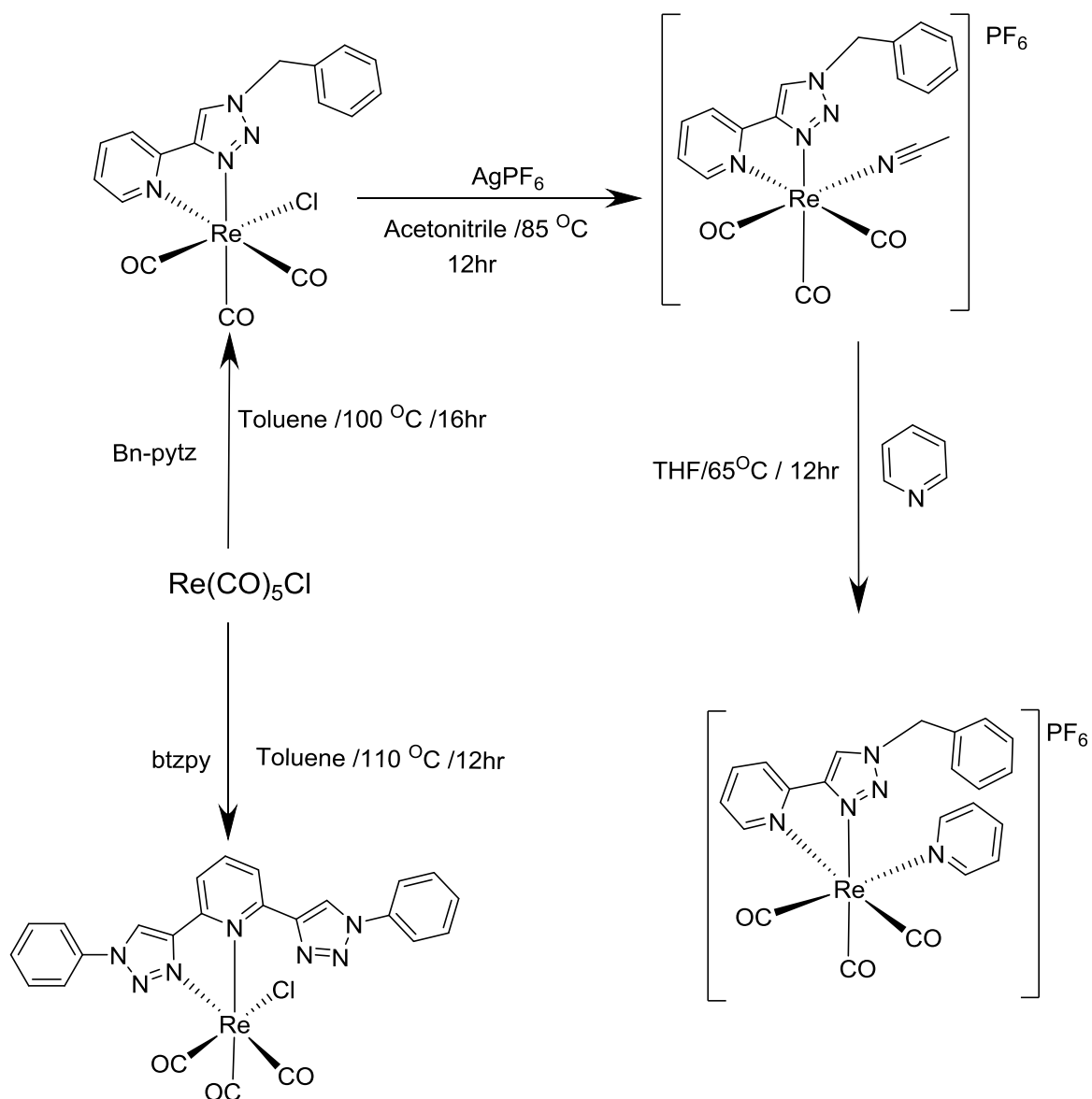
Scheme 2-4- Synthesis of cationic rhenium (I) triazole complexes

The identities of the complexes were confirmed by ^{1}H NMR, ^{13}C NMR, HRMS mass spectrometry and FT-IR spectroscopy. The free ligand Bn-pytz and corresponding Re complexes were characterised by ^{1}H NMR spectroscopy and the corresponding spectra are shown in Figure 2.6. The ^{1}H NMR spectra shows that the triazole proton resonance at δ 8.57 is shifted to higher field by 0.31 ppm for *fac*-[Re(Bn-pytz)(CO)₃Cl] complex comparative to the corresponding resonance for the free ligand at δ 8.27. While Replacement of Cl by pyridine

in *fac*-[Re(Bn-pytz)(CO)₃(py)]⁺ does not affect the triazole environment, a shift to higher field for other protons of pyridine of the pytz ligand.
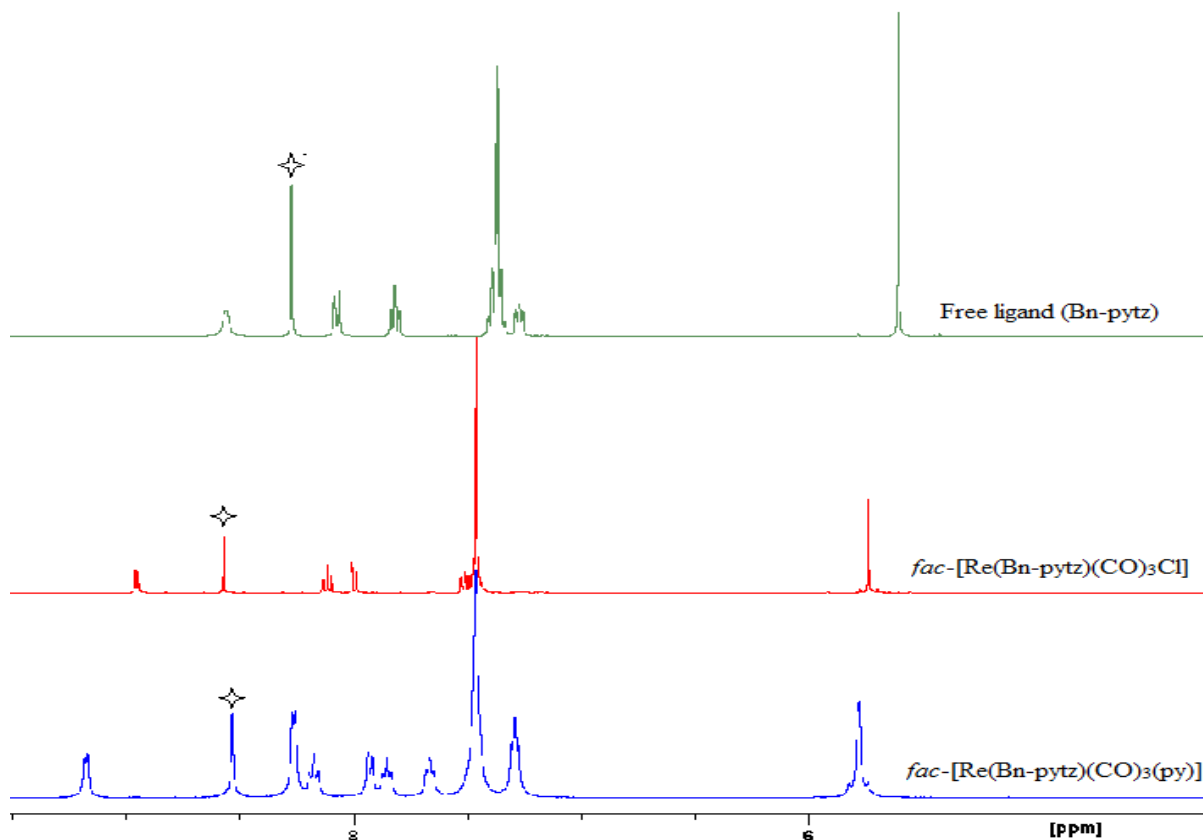
Figure 2-6-1H NMR (400MHz) spectrum of free ligand (Bn-pytz), *fac*-[Re(L)(CO)₃Cl], *fac*-[Re(L)(CO)₃(py)] in CD₃CN

While the btzpy ligand shows a one singlet resonances for the triazole ring protons at δ 9.40 in ¹H NMR spectrum in dimethyl sulfoxide-d6, as a result of the complexation split symmetry the ¹H NMR spectrum of [Re(CO)₃(btzpy)Cl] complex shows two singlets for the triazole ring proton at δ 10.08 and δ 9.33. This indicates that one of the triazole rings is coordinated to the metal center which appears at δ 10.08 and other one is free. This confirmed the expected bytz-like coordination mode with a pendant triazole. The corresponding spectra are shown in Figure 2.7.
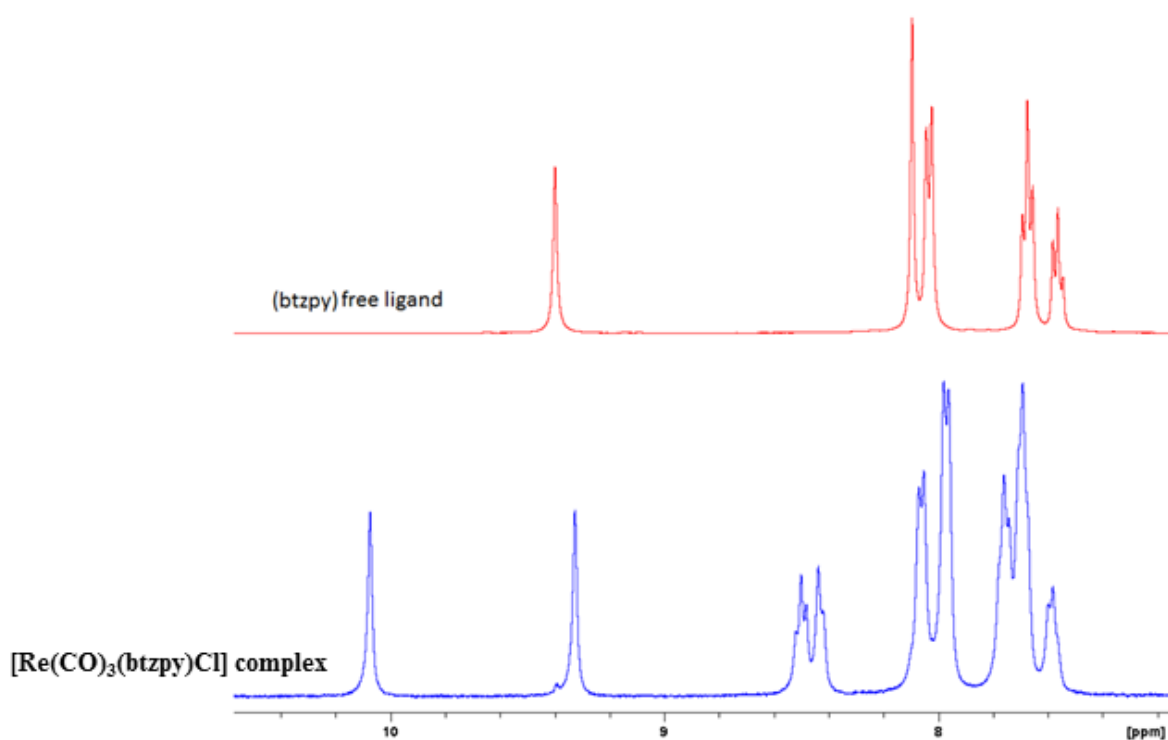
Figure 2-7-^{1}H NMR (400MHz) spectrum of free ligand (btzpy), [Re(btzpy)(CO)$_3$Cl], in DMSO

The infrared spectra of the rhenium chloride complexes which recorded in acetonitrile show three bands corresponding to the ν_{CO} stretching modes with the symmetric stretch appearing at ~2025 cm^{-1} with the closely spaced asymmetric stretches centred at ~1920 cm^{-1} and 1897cm^{-1}. (Figure 2.8). From the figure we can note that the Bn-pytz and btzpy ligands indeed appears to have little effect on the ν_{CO} when compared to bpy and phen.
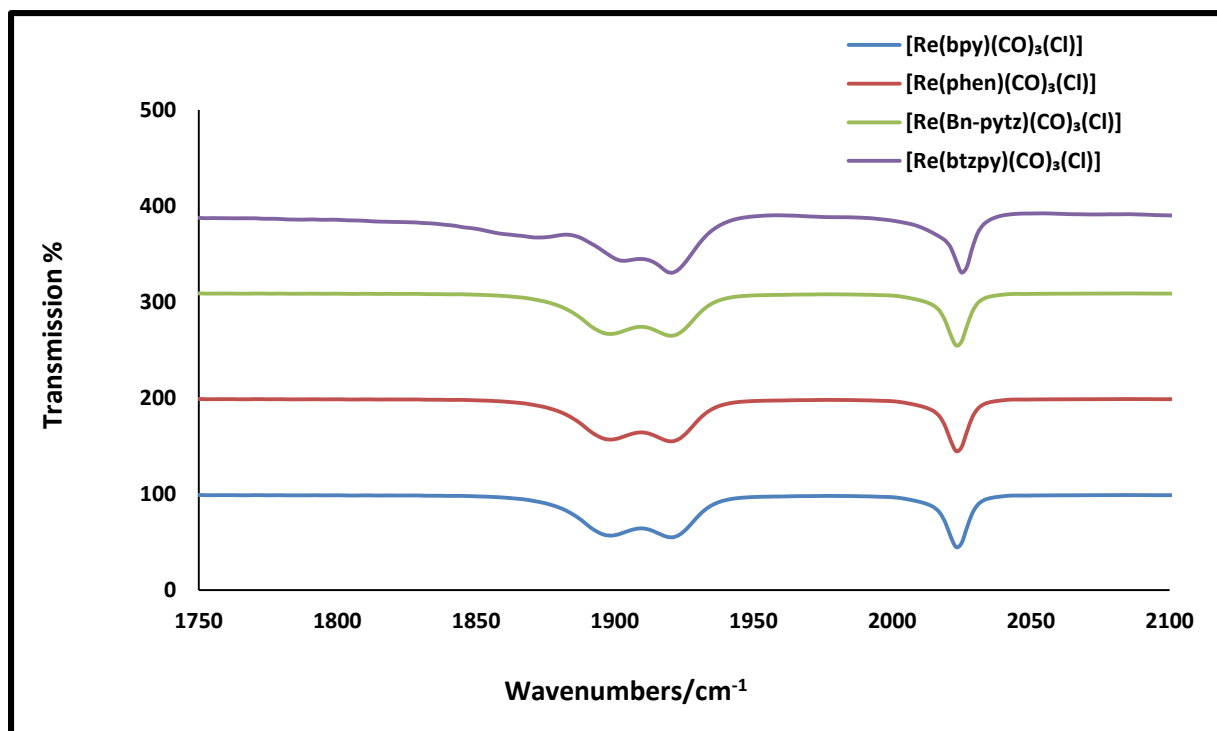
Figure 2-8-The infrared spectra of the complexes Re(N^N)(CO)$_3$Cl] in CH$_3$CN

The replacement of chloride in complex [Re(N^N)(CO)$_3$Cl] with pyridine in the complexes [Re(N^N)(CO)$_3$(py)]$^+$ results in the appearance of two bands corresponding to the ν_{CO} stretching modes with the symmetric stretches appearing at ~2036 cm^{-1} with the approximately coincident asymmetric stretches centred at ~1932 cm^{-1}, (Figure 2.9). These are slightly higher in energy than those observed for the chlorine complexes due to loss of the π-donor chloride for a π-acceptor pyridine leading to reduced e$^-$ density of the metal center. FT-IR data for all complexes are shown in Table 2.1.
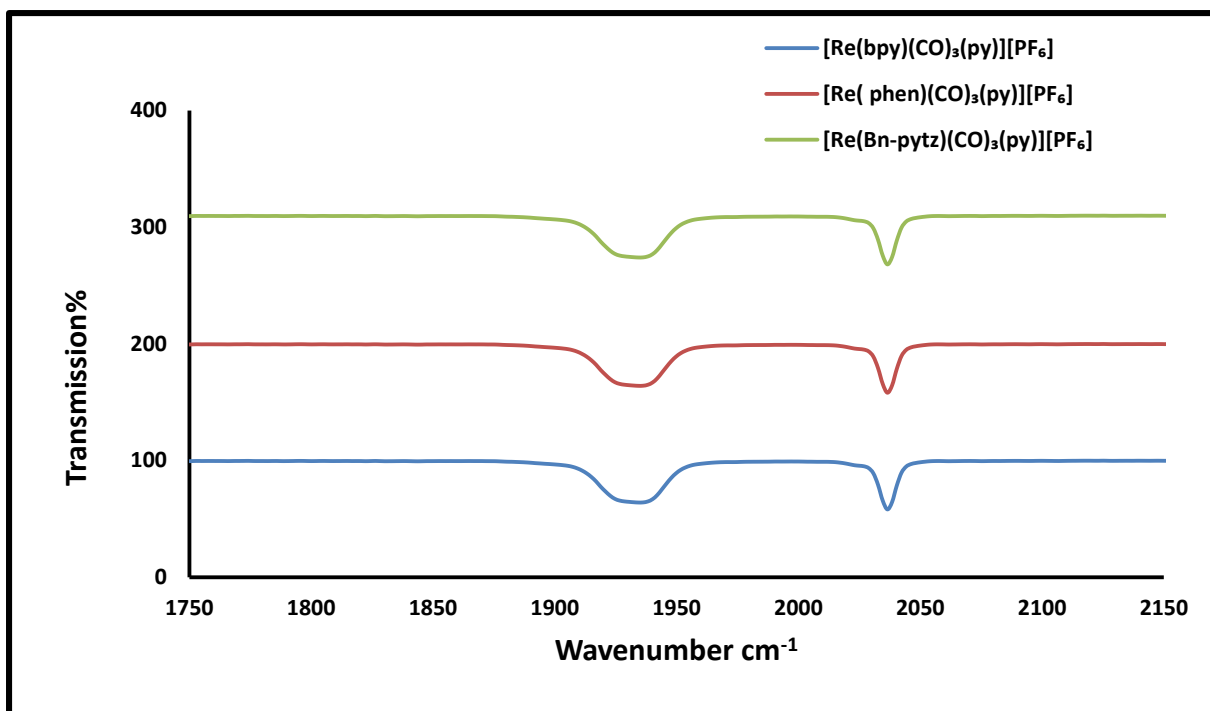
Figure 2-9- The infrared spectra of the complexes $[Re(N^N)(CO)_3(py)]^+$ in CH_3CN

Table 2-1: FT-IR data for complexes in acetonitrile

Complex	vCO (cm^{-1})
[Re(bpy)(CO)$_3$Cl]	2023, 1920, 1897
[Re(bpy)(CO)$_3$(py)]$^+$	2036, 1932
[Re(phen)(CO)$_3$Cl]	2024, 1920, 1897
[Re(phen)(CO)$_3$(py)]$^+$	2036, 1932
[Re(Bn-pytz)(CO)$_3$Cl]	2023, 1920, 1897
[Re(Bn-pytz)(CO)$_3$(py)]$^+$	2036, 1932
[Re(btzpy)(CO)$_3$Cl]	2025, 1920, 1903

The effect of changing the X group in X-py as an axial ligand was found to be minimal effect

with respect to the ν_{CO} stretching. All complexes of the type [Re(Bn-pytz)(CO)$_3$(X)]$^+$ showed

two bands corresponding to the ν_{CO} stretching modes with the symmetric stretches appearing

at ~2036 cm^{-1} with the approximately coincident asymmetric stretches centred at ~1932 cm^{-1}.

(Figure 2.10).
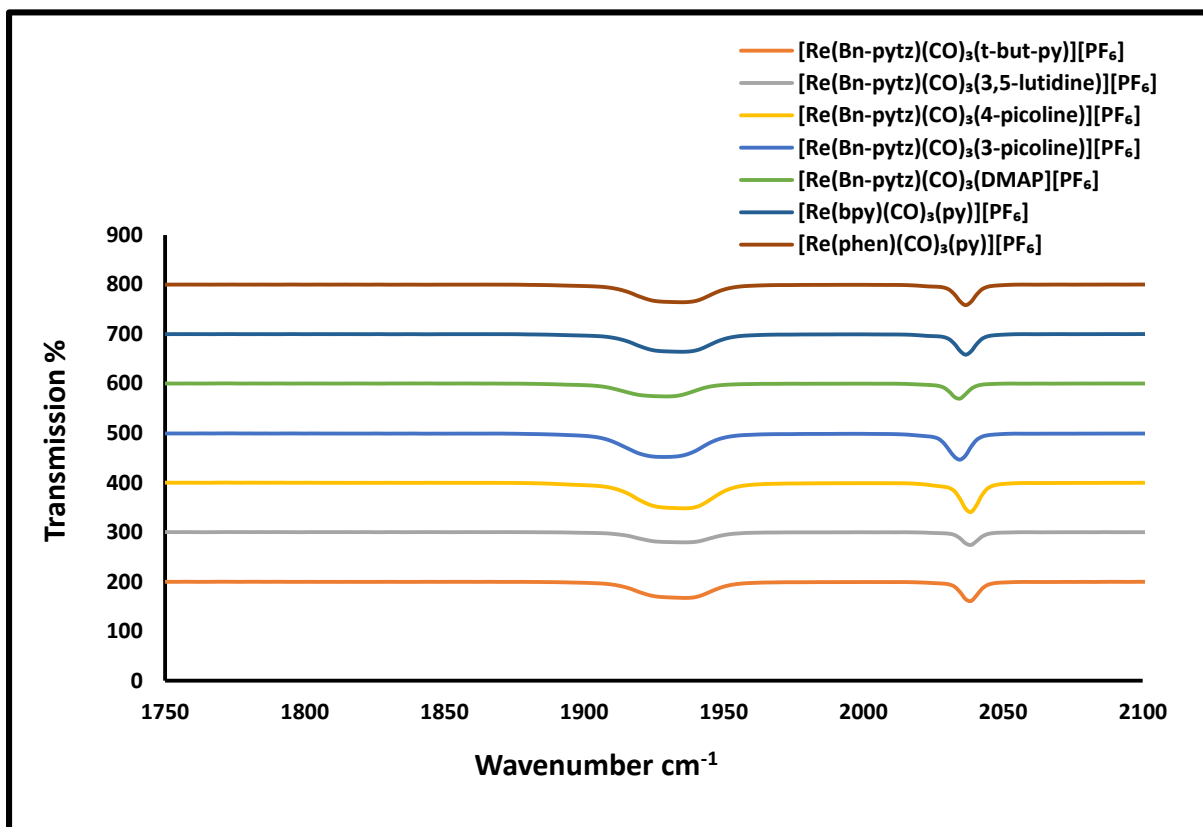
Figure 2-10- The infrared spectra of the complexes [Re(Bn-pytz)(CO)$_3$(X)]$^+$ in CH$_3$CN

2.3 **Electrochemical studies**

2.3.1 **Electrochemical properties of complexes with different diimine ligands**

The electrochemical properties of the complexes in distilled acetonitrile were investigated by cyclic voltammetry. Typically, for the known models of rhenium(I) complexes, the reversible redox wave can be attributed to the reduction of the ligand, [186] the wave at positive potential can be assigned as rhenium-based oxidation (Re^I/ Re^{II}) and that is observed in bpy and phen complexes. The electrochemical data for complexes [Re(N^N)(CO)$_3$Cl] are summarized in Table 2.2.

Table 2-2: electrochemical data for complexes [Re(N^N)(CO)$_3$Cl] IN acetonitrile, 0.2 M [NBu$_4$][PF$_6$], 100 mVs^{-1},at room temperature

No	Complex	Reduction E1/2 V vs. Fc/Fc$^+$	Oxidation E_{pa} V vs. Fc/Fc$^+$
2	[Re(bpy)(CO)$_3$Cl]	-1.78(0.066)^a	0.99
6	[Re(phen)(CO)$_3$Cl]	-1.73(0.091)^a	0.99
	Re(Bn-pytz)(CO)$_3$Cl]	-2.20	1.00
	Re(btzpy)(CO)$_3$Cl]	-2.00	0.95

E$_{1/2}$ = (Epa+ Epc) /2 , Epc are anodic and cathodic peak potentials respectively. a = reversible. ( ) = ΔEP^{a,c}

Figure 2.11 presents the cyclic voltammograms for the chloride complexes. Anodic scans reveal a single irreversible oxidation at about 1 V vs Fc/Fc$^+$ in acetonitrile. This is assigned to the Re(I)/Re(II) redox couple. Both [Re(bpy)(CO)$_3$Cl] and [Re(phen)(CO)$_3$Cl] complexs display quasi-reversible reduction couple which occurs at almost the same potential -1.8 V vs. Fc/Fc$^+$ which is assigned as N^N ligand centered reduction. The fact that the potentials for oxidation of Re are very similar for all complexes is reasonable in view of the fact that the HOMO is Re based with little influence from N^N ligands. This strongly suggests that any

differences in the MLCT absorption and emission energies (see later) between the complexes are primarily due to differences in the π^* level of the N^N ligands. The [Re(Bn-pytz)(CO)$_3$Cl] and [Re(btzpy)(CO)$_3$Cl] have a higher energy LUMO than another complexes including [Re(terpy)(CO)$_3$Cl] which displays ligand centered reduction at -1.74 V.[187] They are better σ-donorS compared to other N^N ligand.[188] Replacement of bpy by Bn-pytz or btzpy ligands result in more negative and irreversible reductions. The negative shift is due to the higher energy π^* ligand centred LUMOs localised on these ligands.
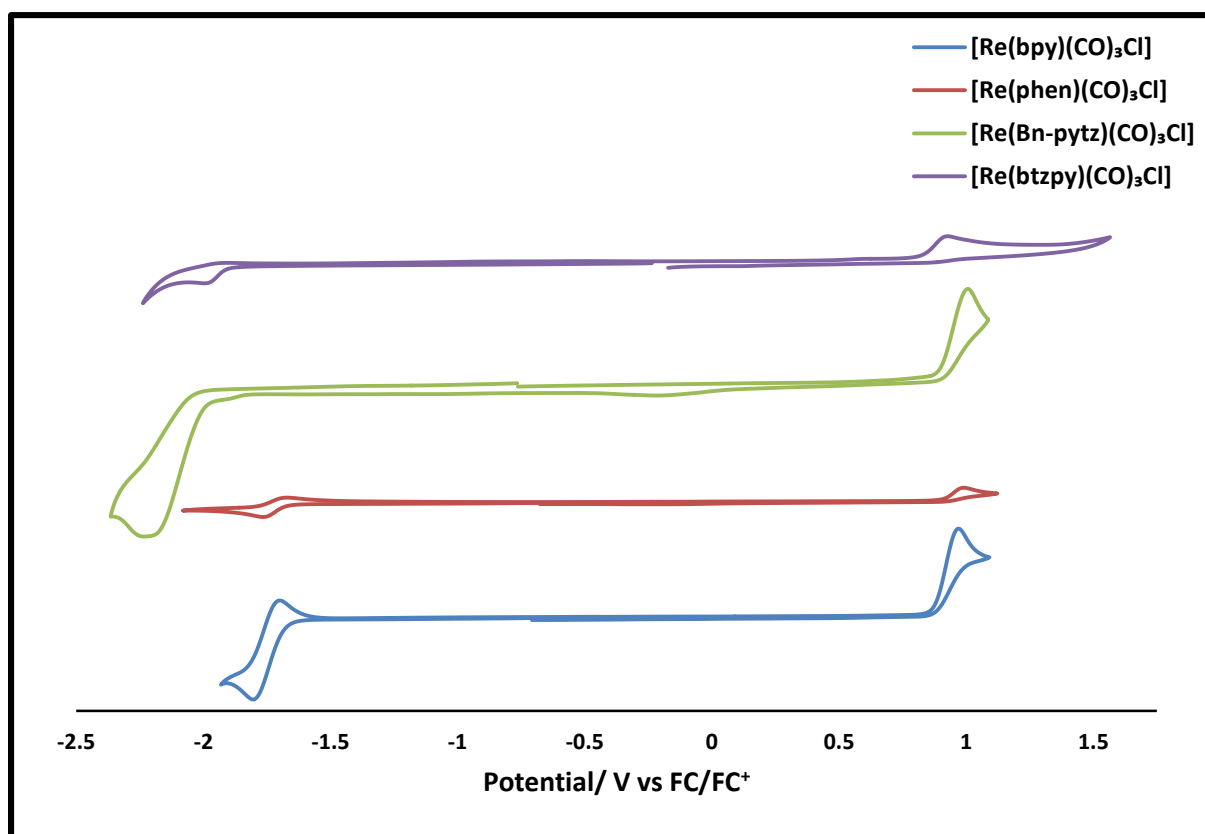
Figure 2-11- Cyclic voltammogram of complexes [Re(N^N)(CO)$_3$Cl] in CH$_3$CN /0.2 M NBu$_4$PF$_6$; scan rate (v) = 100 mV s^{-1} . Potentials V are reported against ferrocene (Fc/Fc $^+$ = 0.0 V)

 It is generally accepted that the main features include an irreversible anodic peak at vs Ag/AgCl, assigned to the one-electron oxidation, which was characteristic of all known

complexes of the type $[Re(N^{\wedge}N)(CO)_3Cl]$. Its production involves a unimolecular process in which the chloride ligand serves as a one-electron reductant toward the electrogenerated rhenium(II) center, resulting in the loss of chlorine radical from the complex (which then forms molecular chlorine) and subsequent coordination by the solvent . For all the rhenium complexes, the one-electron oxidation showen in the (eq 1) is followed by a rapid loss of a chlorine atom to form $[Re(N^{\wedge}N)(CO)_3(CH_3CN)]^+$.

$$Re(N^{\wedge}N)(CO)_3Cl \longrightarrow [Re(N^{\wedge}N)(CO)_3Cl]^+ + e^- \ldots\ldots\ldots(eq\,1)$$
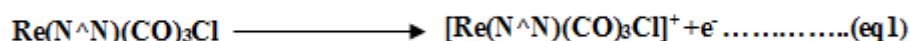
For the reduction process, a one-electron ligand based reductions leads to the loss of the chloride ligand. This is followed either by solvation or fast dimerization as follows:[189, 190]

The losing of a chloride ligand from the reduced Re complex to generate a 17-electron intermediate

$$[Re(N^{\wedge}N)(CO)_3Cl]^+ + e^- \longrightarrow [Re(N^{\wedge}N)(CO)_3Cl]^-$$

$$[Re(N^{\wedge}N)(CO)_3Cl]^- \longrightarrow [Re(N^{\wedge}N)(CO)_3] + Cl^-$$
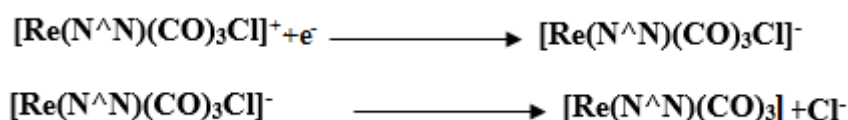
The resulting Re-carbonyl complex fragments can undergo in two possible reactions. (I) they can react with the solvent (CH_3CN) to form a solvent-coordinated complex:

$$[Re(N^{\wedge}N)(CO)_3] + CH_3CN \longrightarrow [Re(N^{\wedge}N)(CO)_3(CH_3CN)]$$

(II) The resulting Re-carbonyl complex fragments can also combine to form a Re-Re bonded dimer:

$$2\,[Re(N^{\wedge}N)(CO)_3] \longrightarrow [Re(N^{\wedge}N)(CO)_3]_2$$

Because these features are well known for bpy containing complexes, therefore, it is speculated that, this also acurs here for triazole containing complexes.

2.3.2 Electrochemical Properties of complexes with different axial ligands

The electrochemistry of the rhenium compounds $[Re(Bn\text{-}pytz)(CO)_3(X)]^+$ in using acetonitrile was probed using cyclic voltammetry and Bu_4NPF_6 as supporting electrolyte. Data are presented in Table 2.3.

Table 2-3: Electrochemical data for $[Re(Bn\text{-}pytz)(CO)3(X)]+$ complexes in acetonitrile, 0.2 M [NBu4][PF6], 100 mVs-1,at room temperature

No	Complex	Reduction $E_{1/2}$ V vs. Fc/Fc$^+$	Oxidation E_{pc} V vs. Fc/Fc$^+$
1	$[Re(Bn\text{-}pytz)(CO)_3(py)]^+$	-1.93 , -2.04	1.54
2	$[Re(Bn\text{-}pytz)(CO)_3(t\text{-}but\text{-}py)]^+$	-1.91 , -2.04	1.62
3	$[Re(Bn\text{-}pytz)(CO)_3(4\text{-}picoline)]^+$	-2.05, -2.26	1.59
4	$[Re(Bn\text{-}pytz)(CO)_3(3\text{-}picoline)]^+$	-1.93, -2.23	1.53
5	$[Re(Bn\text{-}pytz)(CO)_3(3,5\text{-}lutidine)]^+$	-1.95 , -2.04 , -2.23	1.52
6	$[Re(Bn\text{-}pytz)(CO)_3(DMAP)]^+$	-2.01	1.24

$E_{1/2}$ = (Epa+ Epc) /2 , Epc are anodic and cathodic peak potentials respectively.

Changing a chloride complex $[Re(Bn\text{-}pytz)(CO)_3Cl]$ with the $[Re(bn\text{-}pytz)(CO)_3(X)]^+$ led to a positive shift in the oxidation potential. N-donor axial pyridine ligands are strong π –acceptors, this reduces the electron density on a metal centre and thus results in a lower energy HOMO compared to π-donor chloride based complexes. Both reduction and oxidation couples were observed in the cyclic voltammograms upon reductive and oxidative scans, respectively. All samples display an irreversible one-electron oxidation associated with the Re(I)/Re(II) couple at about +1.5 V and (+1.24) for $[Re(Bn\text{-}pytz)(CO)_3(DMAP)]^+$ representative voltammograms in (Figure 2.12).
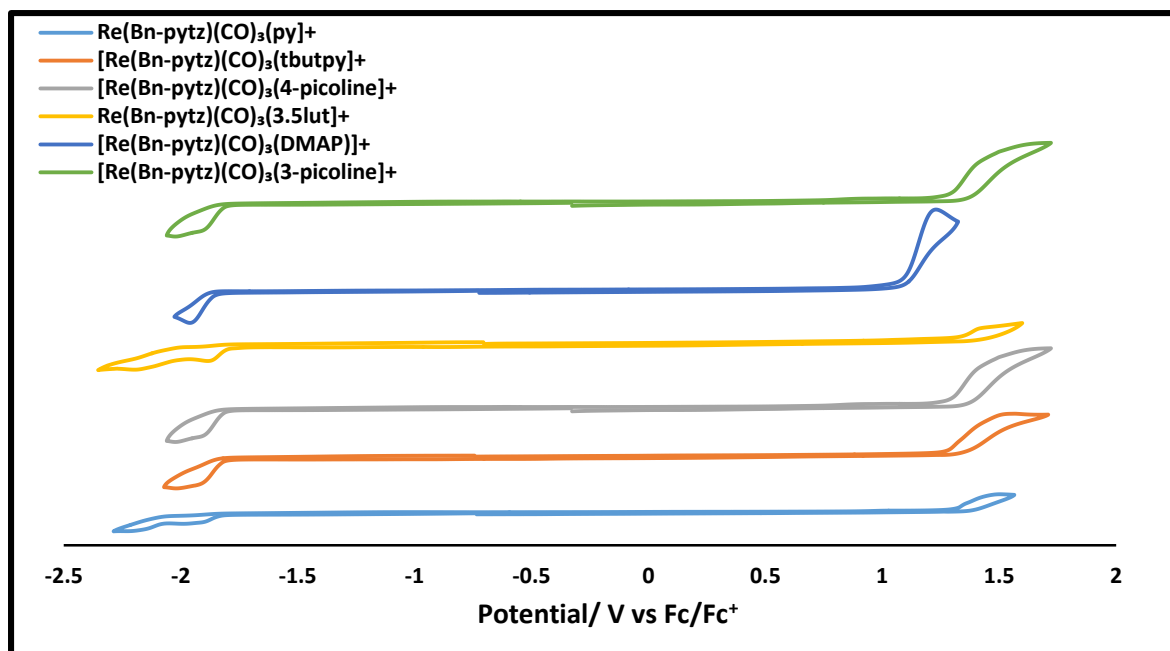
Figure 2-12-Cyclic voltammogram of complexes [Re(Bn-pytz)(CO)$_3$(X)] in CH$_3$CN /0.2 M NBu$_4$PF$_6$; scan rate (v) = 100 mV s^{-1} . Potentials V are reported against ferrocene (FC/FC + = 0.0 V)

All of the complexes display one oxidation and two reduction processes in the potential region from +2.5 to -2.5 V with exception of [Re(Bn-pytz)(CO)$_3$(DMAP)]$^+$ which is display one reduction processes in the potential at -2.01. The replacement of the chloride with a neutral axial ligand results in an anodic shift of E$_{ox}$. The nature of the N-based axial ligand affects the ease with which the metal is oxidized. The two irreversible reduction waves observed in the cyclic voltammograms of all of the complexes at the region of (2,-2.5 V). The variation of the axial ligand changes the reduction potentials less than the oxidation potentials of the complexes. All complexes approximately have the same reduction, meaning the reduction potential is unaffected by changing the nature of the N-based axial ligand, this is not surprising because all complexes have the same diimine ligand Bn-pytz which meane have the same LUMO. Except of DMAP complex, [Re(Bn-pytz)(CO)$_3$(DMAP)]$^+$ which has the strongly donating group (Me$_2$N) mostly the oxidation is also unaffected by changing the nature of the N-based axial ligand meaning that py ligand probably has little influence on the energy of the HOMO.

82

2.4 **Photophysical studies**

2.4.1 **Effect of chelate ligands**

Table (2.4) summarizes the UV-VIS absorption, emission, and life time data for the rhenium chloride complexes**.**

Table 2-4 : UV-vis Absorption, photoluminescence and lifetime data for the complexes [Re(N^N)(CO)$_3$Cl] in aerated acetonitrile

complex	λ / nm(ε/ dm^3.mol^{-1}cm^{-1})	Em λ(max) / nm	T/ns
[Re(bpy)(CO)$_3$Cl]	370(4041), 343(4086), 315(11145), 290(18741)	634	6 (26%), 29 (74%)
[Re(phen)(CO)$_3$Cl]	367(4752), 290(15210), 273(29558),	622	12 (2%), 66 (98%)
[Re(Bn-pytz)(CO)$_3$Cl]	346(5500), 337(9900), 296(20200),	545	47(100%)
[Re(btzpy)(CO)$_3$Cl]	345(3395), 295(18930), 247(29700), 224(34180)	586	68 (100%)

Figure 2.13 shows the UV-vis absorption spectra of the rhenium chloride complexes in acetonitrile at room temperature. From the figure it can be seen that all complexes have the dominant absorption bands in the UV region at 290- 310 nm which are assigned to intraligand (IL) $\pi \rightarrow \pi^*$ transitions localized on the chelate ligand. All of the complexes presented here have an absorption maximum around 335 - 370 nm. This transition is assigned to a metal-to-ligand charge transfer (^{1}MLCT) from Re to the chelate ligand as has been observed for other rhenium N^N complexes.[191-193] [Re(Bn-pytz)(CO)$_3$Cl] and [Re(btzpy)(CO)$_3$Cl] showed a blue-shifted electronic absorption. Both complexes exhibit an intense absorption band in the visible region at 335, 345 nm respectively assignable to the ^{1}MLCT (d$_\pi \rightarrow \pi^*$) transitions, at compared

with another complexes [Re(bpy)(CO)₃Cl]   370 nm and [Re(phen)(CO)₃Cl] 367 nm. The HOMO of all complexes is primarily localized on the Re(I) and Cl atoms, in both cases and so the energies of the HOMO orbitals for all complexes should not be expected to be significantly different. The large blue-shift observed for the [Re(Bn-pytz)(CO)₃Cl] and [Re(btzpy)(CO)₃Cl] complexes is therefore, consequence of the much higher energy of the LUMO associated with the triazole- containing ligand compared to the other diimine ligands.

©
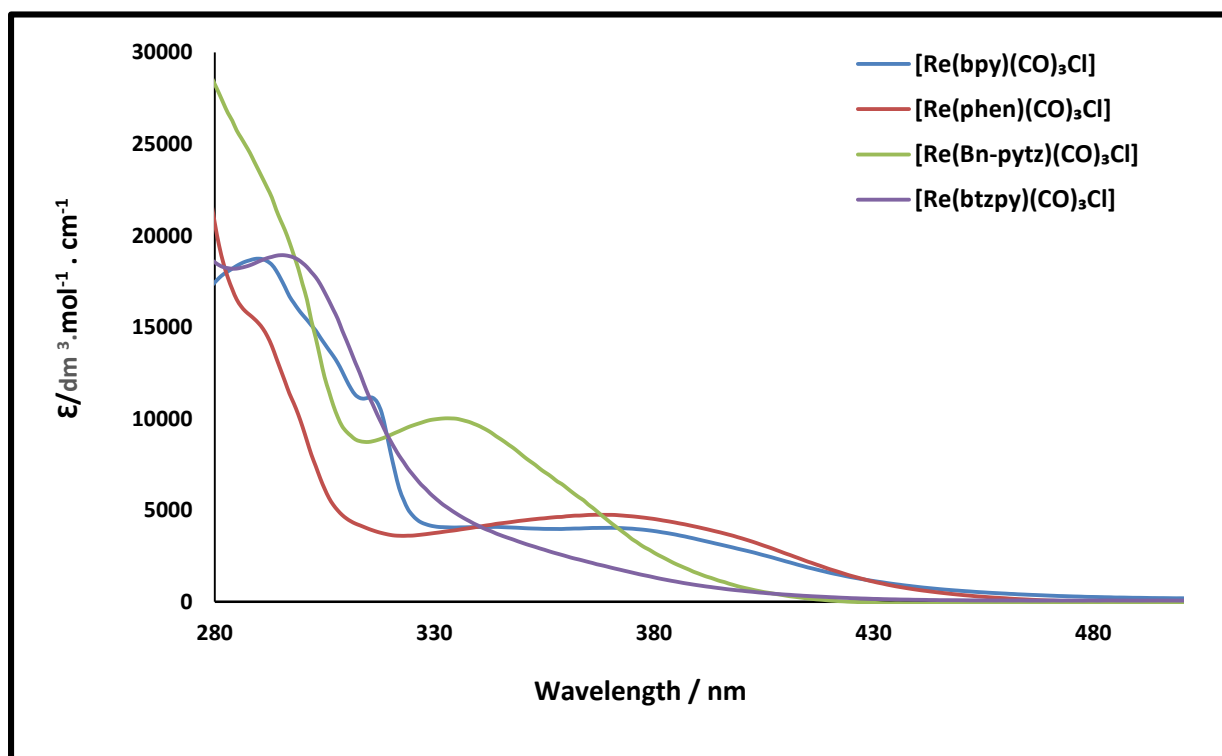
Figure 2-13-- UV-vis absorption spectra of complexes [Re(N^N)(CO)₃Cl]] in acetonitrile

While broad emission of around 620-640 nm was observed for the [Re(bpy)(CO)₃Cl] and [Re(phen)(CO)₃Cl] complexes at room temperature in aerated acetonitrile [Re(Bn-pytz)(CO)₃Cl] and [Re(btzpy)(CO)₃Cl] showed blue-shifted luminescence with a maxima at 545 nm and 586 nm respectively (Figure 2.14). This was accompanied with increased radiative decay lifetimes of the complexes. This is consistent with the energy gap law.[185]
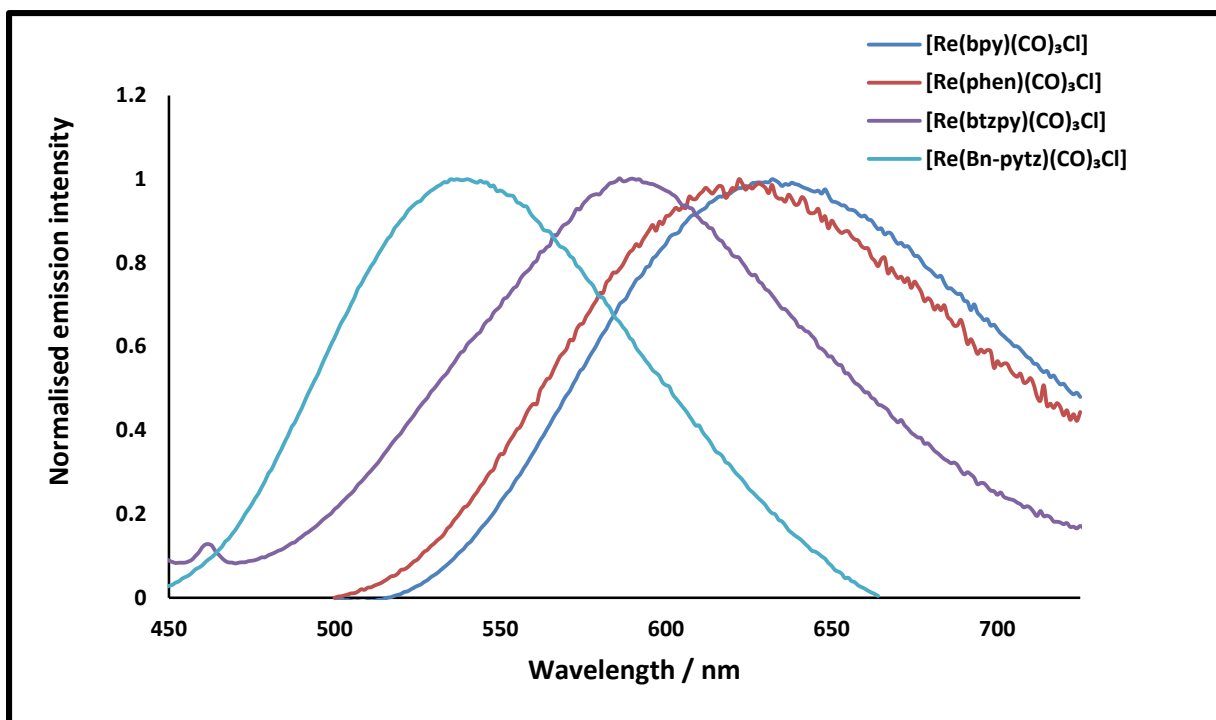
Figure 2-14-Room-temperature emission of complexes [Re(N^N)(CO)$_3$Cl] in aerated acetonitrile

Compared with [Re(terpy)(CO)$_3$Cl] which has been reported as non-luminescent in in aerated acetonitrile[194] but showed weakly luminescent in degassed acetonitrile at room temperature centred at 506 nm.[187] [Re(btzpy)(CO)$_3$Cl] at room temperature in aerated acetonitrile showed red-shifted luminescence at 586 nm.

2.4.2 Effect of axial ligands.

All the UV-vis absorption, emission and life time data for complexes [Re(Bn-pytz))(CO)$_3$(X)]$^{+/0}$ are listed in Table 2.5

Table 2-5 : UV-vis absorption, photoluminescent, data for the complexes [Re(Bn-pytz)(CO)$_3$(X)]$^+$ in acetonitrile

No	Compound	λ / nm(ε/ dm^3.mol^{-1}cm^{-1}))	Em λ(max) / nm	Φ%	Ţ/ns
1	[Re(Bn-pytz)(CO)$_3$Cl]	346(5500), 337(9900), 296(20200), 276(29900), 251(40600)	545	0.3	47
2	[Re(Bn-pytz)(CO)$_3$(py)]$^+$	354(2000), 322(5700), 296(12400), 262(19900), 251(23000)	499	0.7	60
3	[Re(Bn-pytz)(CO)$_3$(t-but-py)]$^+$	346(1900), 322(4000), 296(9200), 262(16100), 251(17800)	499	0.76	66
4	[Re(Bn-pytz)(CO)$_3$(4-picoline)]$^+$	354(2000), 322(5700)296(9100)	499	1.59	67
5	[Re(Bn-pytz)(CO)$_3$(3-picoline)]$^+$	347(1700),326(3500), 297(8500)287(9500), 261(15600), 251(17600))	499	1.6	61
6	[Re(Bn-pytz)(CO)$_3$(3,5-lutidine)]$^+$	322(2800), 298(6200)278(8600), 262(11600), 251(12700)	499	0.71	61
7	[Re(Bn-pytz)(CO)$_3$(DMA-py)]$^+$	347(1700), 306(9800), 288(18900), 251(12300)	526	0.74	61

A blue-shift of MLCT bands are deserved in UV-vis absorption spectra by changing the chloride ligand in [Re(N^N)(CO)₃Cl] (335-370 nm) with neutral axial ligand in the [Re(N^N)(CO)3(X)]⁺ (340-360 nm) (X = pyridine, 4-*tert*-butylpyridine, 4-picoline, 3-picoline, 4-dimethylaminopyridine, 3,5-lutidine) (Figure 2.14). The dominant absorption bands in the UV region at 290 nm are assigned to intraligand $\pi \rightarrow \pi^*$ transitions localized on Bn-pytz ligand. From Figure 2.15 we can see that all of the complexes presented here had an absorption maximum around 340 -360 nm. This transition is assigned to a metal-to-ligand charge transfer (MLCT) from dπ (Re) to π^* (Bn-pytz). The replacement of a π-donor with a π-accepting ligand is leading to stabilisation of the HOMO relative to the LUMO. This replacement increases the MLCT energy. With the exception of [Re(Bn-pytz)(CO)₃(DMAP)]⁺, all the complexes exhibt similar UV-vis absorption spectra because all of them using the same ligand Bn-pytz and the same metal centre, which indicated that the axial ligand has little impact on the spectroscopic properties.
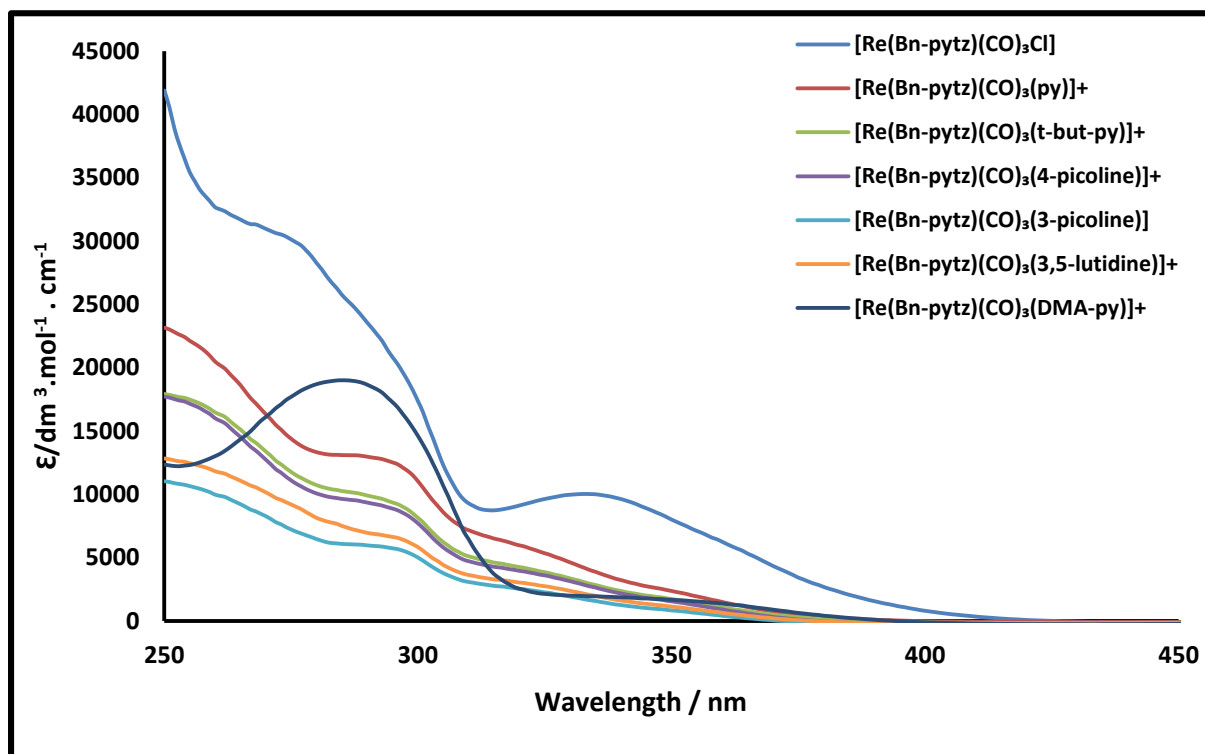
Figure 2-15-Room-temperature emission of complexes [Re(Bn-pytz)(CO)₃(X)] in aerated acetonitrile

There is a significant blue-shift of approxmately 50 nm for all complexes, as a result of changing the chloride ligand in [Re(Bn-pytz)(CO)$_3$Cl] with pyridine based ligand in the [Re(Bn-pytz)(CO)$_3$(X)].
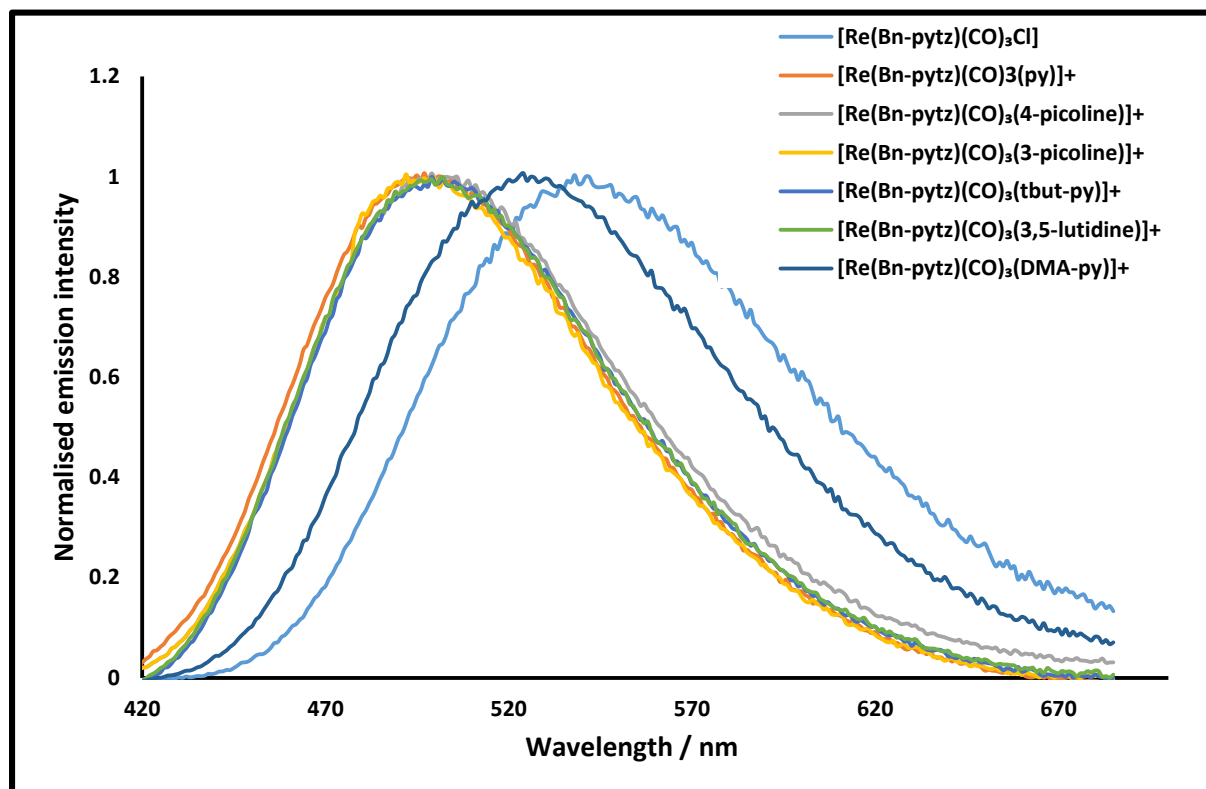
Figure 2-16-Room-temperature emission of complexes [Re(Bn-pytz)(CO)$_3$(X)] in aerated acetonitrile

A broad emission of around 540 nm (Figure 2.16) was observed from the [Re(Bn-pytz)(CO)$_3$Cl] in aerated acetonitrile at room temperature. The emission bands of [Re(Bn-pytz)(CO)$_3$(X)]$^+$ are significantly blue-shifted to 490-500 nm as a result of replacement of a π-donor with a π-accepting ligand which leads to stabilisation of the HOMO relative to the LUMO. As for the effect of the pyridine substituents on the absorption and emission properties, an increase in the electron accepting strength of the substituent caused shorter MLCT absorption and emission wavelengths (λ_{MLCT} and λ_{em}). Although the lifetime of the complexes is shorter for [Re(Bn-pytz)(CO)$_3$Cl] comparing with [Re(Bn-pytz)(CO)$_3$(X)]$^+$ because the MLCT state is higher in energy than the ^{3}MLCT in the chloride complexes in totally agreement

with the energy gap law. Except in the case of the dimethyl amino pyridine, changing the substituent on the axial pyridine has no significant effect on the emission spectra. The strongly electron donating dimethyl amino group results in destabilisation of the HOMO with respect to the LUMO and the lower energy ^{3}MLCT state.

2.5 Density functional theory (DFT) studies

These calculations were carried by Dr Alessandro Sinopoli. DFT calculations were carried out using the NWChem 6.3 software package. Calculations were carried out using the B3LYP hybrid functional (20% Hartree–Fock). Benzyl side chains ligand were simplified to methyl groups to reduce computational expense. Stuttgart-Dresden- relativistic small core pesedo potentials ECP for the metal and 6-311G* basis sets used for all other atoms. Molecular structures and molecular orbitals were visualized by means of the ccp1 graphical user interface. The ground state geometries of all complexes were first optimized and molecular orbital energies determined. At the ground state geometries DFT calculations were then used to derive vertical excitation energies and hence simulated absorption spectra. DFT calculations on optimised structures in CH$_3$CN by using the COSMO solvation model, built into the NWChem software, were used to determine the molecular orbital energy levels and localisations.

2.5.1 Ground state properties

In order to further understand the electronic transitions of the complexes and validate the interpretation of the photophysical and electrochemical results, the localisation and energies of the molecular orbitals were calculated by DFT and absorption spectra simulated with time-dependent density functional theory (TDDFT). Table 2.6 shows energies of the HOMO and LUMO of complexes [Re(Bn-pytz)(CO)$_3$(X)]$^+$ as well as the HOMO – LUMO gap. The HOMO of [Re(Bn-pytz)(CO)$_3$(X)]$^+$ is dominated by Re d-orbital character. For the DMAP complex there is a significant contribution of the π system of the monodentate pyridine based

ligand (Figure 2.17). On the other hand, the LUMOs of all complexes are essentially the lowest

energy π^* orbital of the Bn-pytz ligands. Hence the electronic transition at the lowest energy

region is clearly assigned to the mixed metal to ligand charge transfer ([1]MLCT). The HOMO

and LUMO provide some useful insight as to the atomic contributions. Here the density

functional calculations indicate that for all the complexes in the singlet state the LUMO orbital

is nearly in the same energy level and the significantly higher energy level of HOMO in

[Re(Bn-pytz)(CO)$_3$(DMAP)]$^+$ (Figure 2.18). Changing of X ligand substituent genaraly results

in no significant difference in changing in band gap between the HOMO and LUMO which

means that these substituent have minimum electronic effect on the spectroscopic properties.

Table 2-6: Selected Calculated energies of the HOMO and LUMO orbitals of complexes [Re(Bn-pytz)(CO)$_3$(X)]$^+$

Complex	HOMO E/eV	LUMO E/eV	ΔE/eV
[Re(Bn-pytz)(CO)$_3$(py)]$^+$	-9.308	-5.465	3.843
[Re(Bn-pytz)(CO)$_3$(^{t}But-py)]$^+$	-9.169	-5.368	3.801
[Re(Bn-pytz)(CO)$_3$(4-picoline)]$^+$	-9.220	-5.406	3.814
[Re(Bn-pytz)(CO)$_3$(3-picoline)]$^+$	-9.246	-5.424	3.822
[Re(Bn-pytz)(CO)$_3$(3,5lutidine)]$^+$	-9.198	-5.386	3.812
[Re(Bn-pytz)(CO)$_3$(DMAP)]$^+$	-8.674	-5.219	3.455
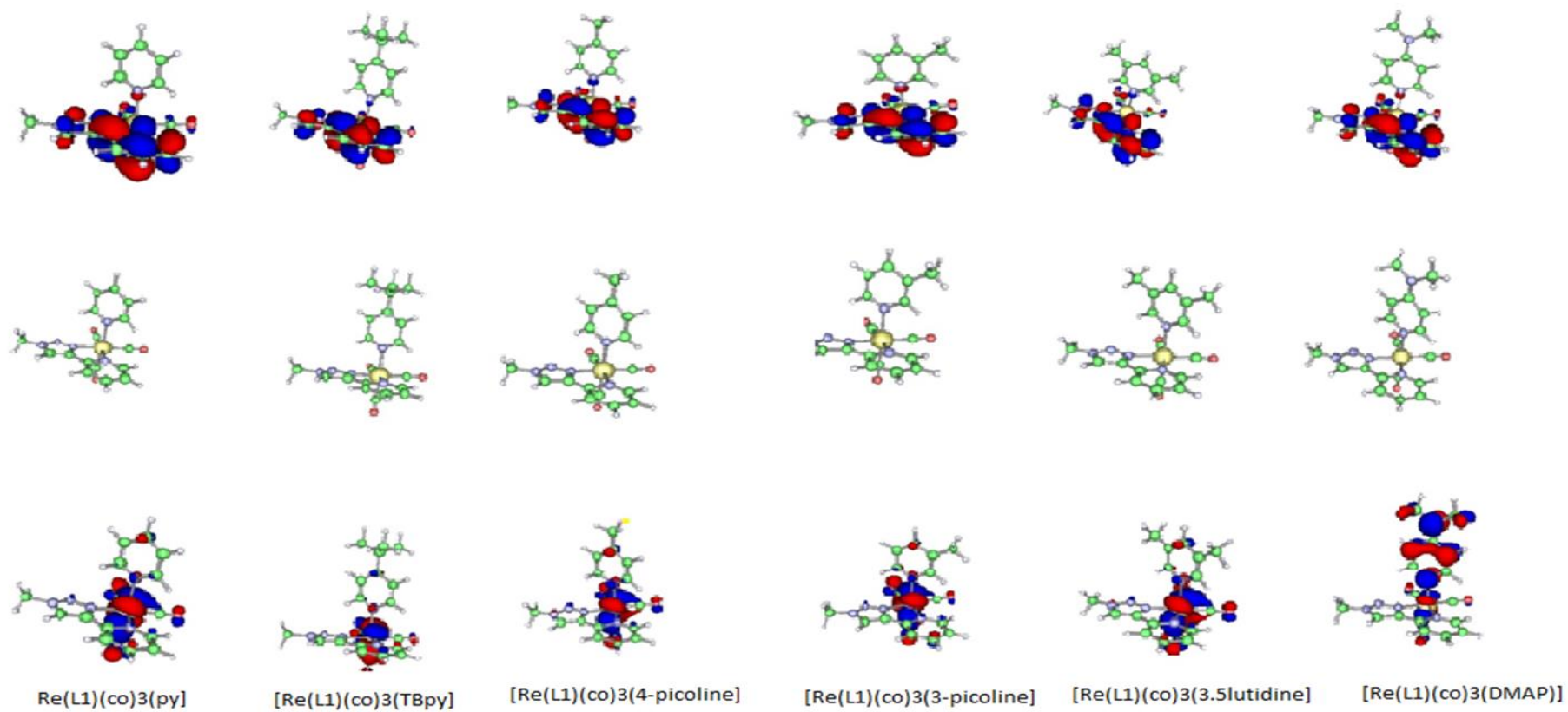
Figure 2-17 the optimized ground state geometries (middle), HOMO (bottom) and LUMO (top) orbital representations for complexes [Re(Bn-pytzs)(CO)$_3$(X)]$^+$.

Re(L1)(co)3(py)   [Re(L1)(co)3(TBpy]   [Re(L1)(co)3(4-picoline]   [Re(L1)(co)3(3-picoline]   [Re(L1)(co)3(3.5lutidine]   [Re(L1)(co)3(DMAP)]
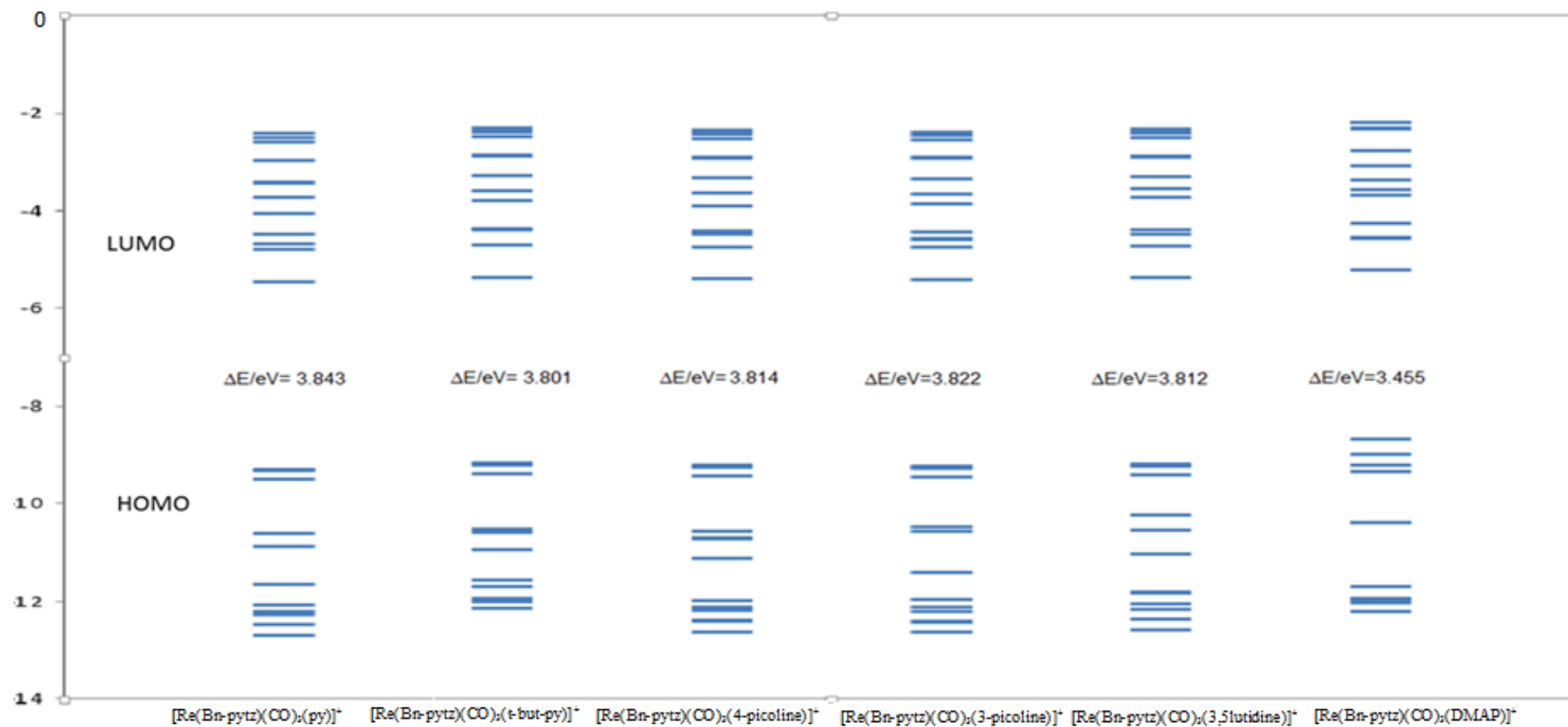
Figure 2-18 -Molecular orbital energy level diagram for the complexes [Re(Bn-pytz)(CO)$_3$(Xp)]$^+$.

2.5.2 Time dependent DFT (TDDFT) Calculations

To confirm the interpretation of the photophysical results, time-dependent density functional theory calculations were performed to determine the absorption spectra of the complexes. Figure 2.19 show comparison of calculated (vertical excitations) and experimental spectra for complexes [Re(Bn-pytz)(CO)$_3$(X)]. From the figure we can see that all complexes have the absorption bands appeared in the two obvious absorption bands in the simulated spectra are about the UV region at 255-265 nm which can be safely assigned to intraligand $\pi \rightarrow \pi^*$ transitions. Furthermore, all of the complexes presented here had absorption in the lower-energy region with bands around 340 nm. These transitions mainly originate from transition from HOMO to LUMO and are assigned to a metal-to-ligand charge transfer (MLCT) from dπ (Re) to π^* (Bn-pytz). We can see that energy is slightly over estimated in the calculation spectra comparing with the experimental spectra but are never the less in good agreement. As with experiment observation substituents on the pyridine ring have no a significant effect on the absorption spectra which means that these substituents have minimum electronic effect on the MLCT energy. However, for the DMAP complex we can see that the complex display an extra shoulder transition at 390 nm, which DFT predicts to be of MLCT/IL character.
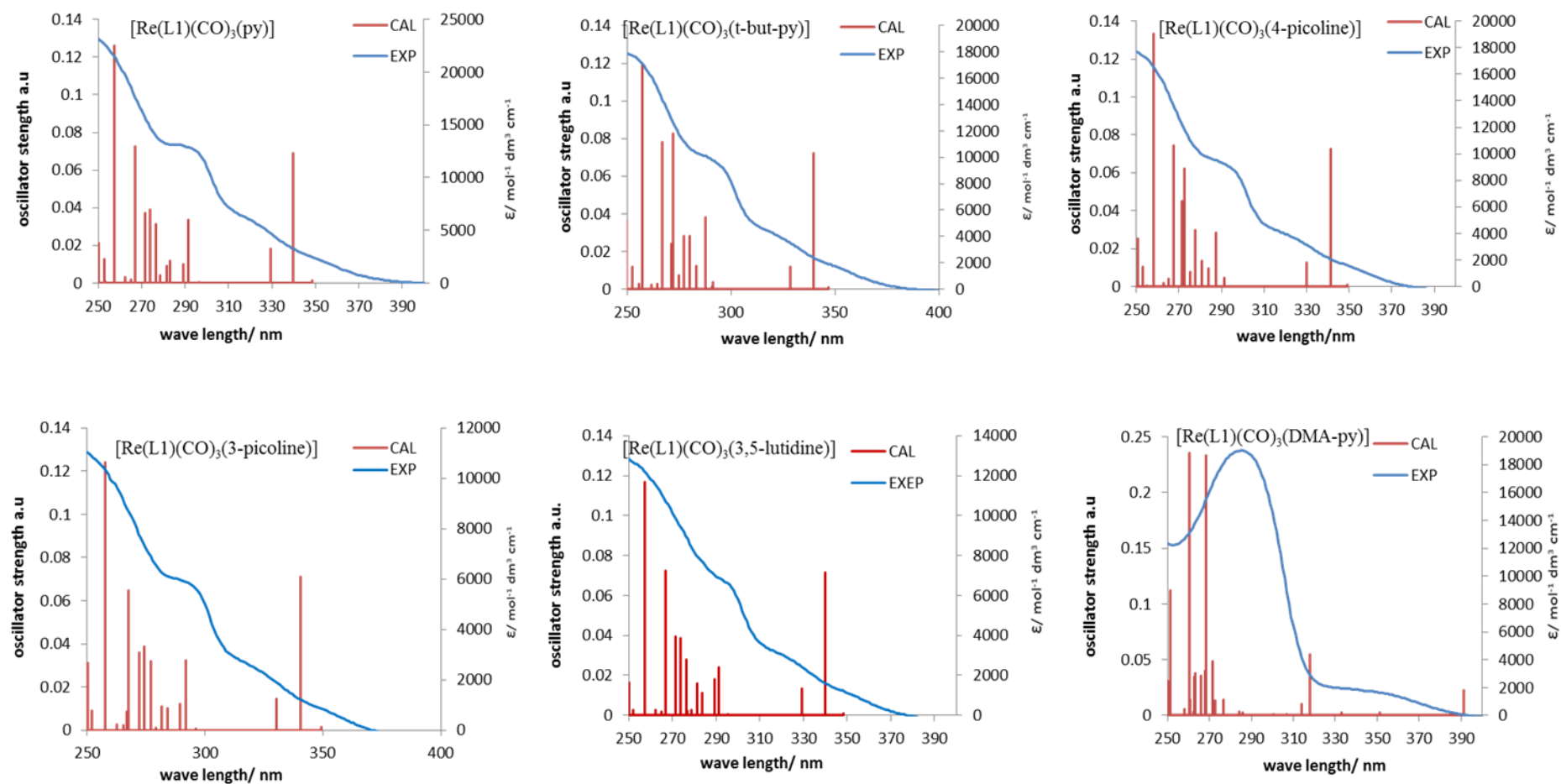
Figure 2-19 -The UV-Vis absorption spectra and electronic transitions calculated with the TDDFT/B3LYP method (bars) for [Re(L1)(CO)3(X)], L1= Bn-pytz

2.6 **Light-Emitting Electrochemical cells**

Two Complexes [Re(Bn-pytz)(CO)$_3$(py)](PF$_6$) and [Re(bpy)(CO)$_3$(py)](PF$_6$) were applied in LEEC devices by Dr. Antonio Pertegas Ojeda from University of Valencia, giving a promising results. [Re(Bn-pytz)(CO)$_3$(py)](PF$_6$) complex exhibt weak photoluminescence in the blue-green region with low photoluminescence quantum yield. As can be seen from the electrolumincence spectrum in Figure 2-20, the device's emission data is a good match to the photoluminescence emission observed in this work.
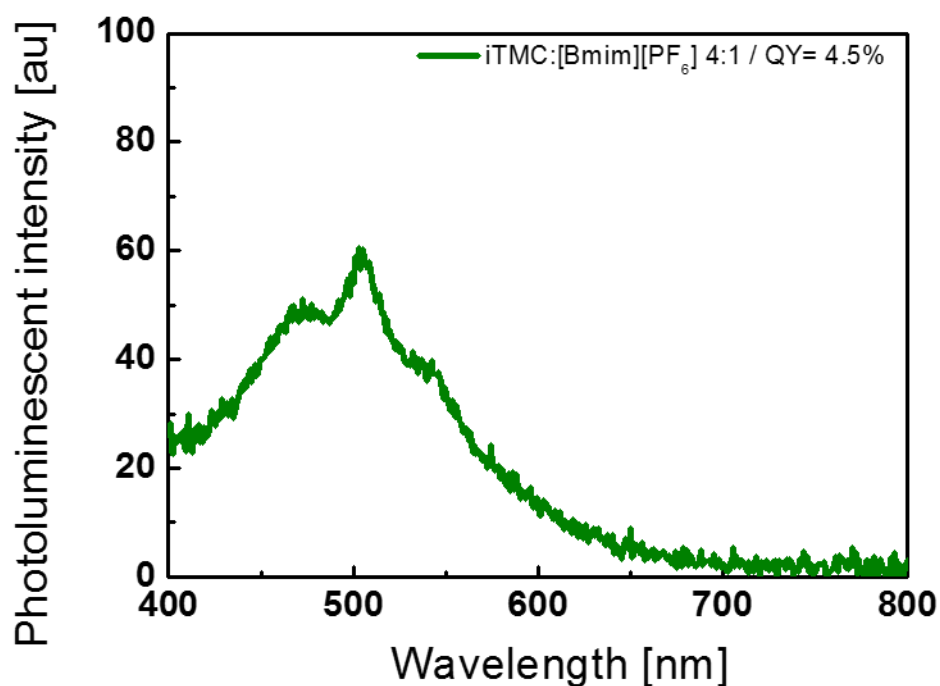
Figure 2-20 Photoluminescence (PL) Of complex [Re(Bn-pytz)(CO)$_3$(py)]$^+$. Excitation: 320 nm, [Bmim][PF$_6$] = 1-butyl-3-methylimidazolium hexafluorophosphate

The electroluminescence emission is red-shifted with respect to the photoluminescence emission (Figure 2-21). Similar effects have been observed for blue iridium emitters in LEECs.[195] The LEEC exhibits blue- green electroluminescence with emission maxima located at 500 nm.
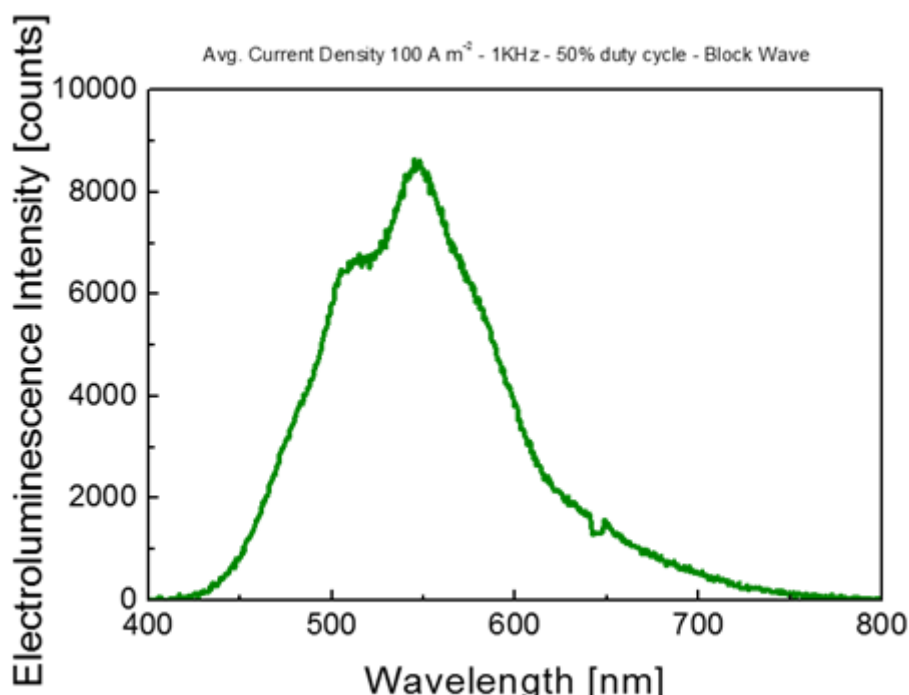
Figure 2-21 electrolumincence (EL) Of complex [Re(Bn-pytz)(CO)₃(py)].

The performance of the LEEC based on [Re(Bn-pytz)(CO)₃(py)](PF₆) showed better performance than [Re(bpy)(CO)₃(py)](PF₆), which was unexpected due to the lower photoluminescence quantum yield in thin film. While no light was emitted after >100 hours of operation with [Re(bpy)(CO)₃(py)](PF₆). Voltage drops versus time due to the formation of electric double layers at the electrode interface with [Re(Bn-pytz)(CO)₃(py)](PF₆) complex were obsarved. The voltage reaches a minimum at 6V, which is a high for "normal" LEECs (<3V) (Figure 2-22). This indicates a "high" energy barrier for electronic injection. Because the stability is poor, the luminance decay could be related with doping quenching as voltage

does not increase during the luminance decay. For this reason few examples of Re based LEECs have been reported. While no emission for LEEC based on [Re(bpy)(CO)$_3$(py)](PF$_6$) was observed, [Re(Bn-pytz)(CO)$_3$(py)](PF$_6$) complex showed weak photoluminescence.

LEC based on [Re(bpy)(CO)$_3$(py)][PF$_6$] complex

LEC based on [Re(L1)(CO)$_3$(py)][PF$_6$] complex
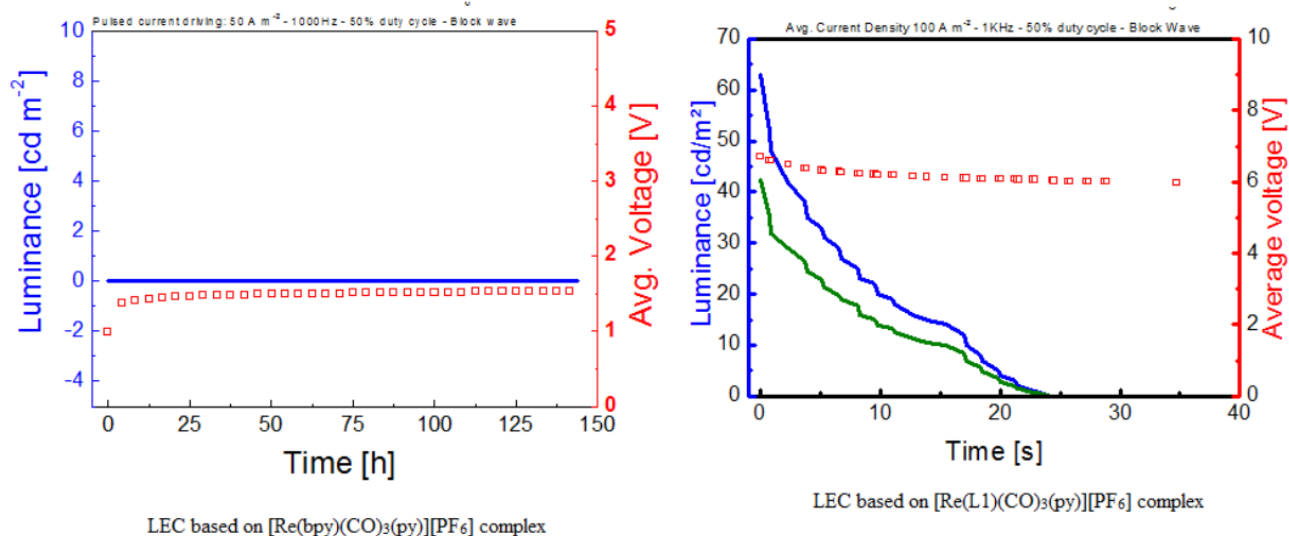
Figure 2-22 data of Light-emitting electrochemical cells based complex [Re(Bn-pytz)(CO)$_3$(py)].

2.7 **Conclusions:**

In this chapter, a series of tricarbonyl rhenium(I) complexes[Re(N^N)(CO)$_3$Cl], (N^N = 1-benzyl-4-(2-pyridyl)-1,2,3-triazole, 2,6-bis(1-phenyl-1H-1,2,3-triazol-4-yl)pyridine, 2,2′-bipyridyl and 1,10-phenanthroline) and [Re(CO)$_3$(Bn-pytz)(X)]PF$_6$ with different axial monodentate ligands X were successfully synthesized in good to excellent yields (70%-90%). A number of conclusions were reached concerning the photophysical properties of the emitting MLCT states of [Re(N^N)(CO)$_3$Cl] and how their properties compare to related [Re(N^N)(CO)$_3$(X-py)]$^+$ complexes; all the pytz complexes display ^{3}MLCT emission which is blue-shifted in electronic absorption and luminescence spectra of the resulting [Re(Bn-pytz)(CO)$_3$Cl] and [Re(btzpy)(CO)$_3$Cl] complexes comparing withe another [Re(N^N)(CO)$_3$Cl] indicated that Bn-pytz and btzpy have higher energy level of LUMO. From DFT calculations the HOMO of the complexes are localized on rhenium centre, while the LUMO are localized on N^N ligands. In the case of the DMAPcomplex, the HOMO also has py character but in general the emission proparties are not affected by the nature of the ligand X. One candidate complex along with a model bpy complex were applied in the manufacture of LEEC devices. Whilst these showed poor stability and performance, EL emission was observed for [Re(Bn-pytz)(CO)$_3$(py)]$^+$, which might be sutible for further devolpment as a LEEC phosphor.

Chapter 3: Synthesis, characterisation and cellular uptake studies of osmium (II) 4-(pyrid-2-yl)-1,2,3 triazole complexes

3.1 **Introduction**

The increase in the applications in numerous technological area of luminescent complexes depended on thier lifetime.[196] For example, in biological applications, d-block metal phosphorescent probes typically have two to three orders of magnitude longer in their emission lifetimes in comparison to fluorescent organic molecules.[48, 197, 198] Since the 1980s complexes of Os(II) in particular have been of significant interest, because of their advantageous photochemical and photophysical properties, and the complex electronic structures of their (MLCT) excited states,[199] $[Os(bpy)_3]^{2+}$, having been described in detail and compared and contrasted to its well-known Ru(II) analogue.[200-202] The osmium(II) complexes exhibit direct ^{3}MLCT optical absorption bands of average extinction coefficient associated to the high spin-orbit coupling constants for the osmium center [203-205]. The principle sustains efficient excitation at low energies that eliminate the possibility of cellular damage and negates the autofluorescent requirement and additional cost of time gated apparatus.[15, 206] The absorption and emission bands operating at wavelengths closer to the red in comparison to the common iridium(III) complexes facilitate the use of increased biologically transparent regions of the spectrum that sustain deeper penetration for excitation and imaging.[207] Osmium complexes are generally inert to ligand photo-substitution and are highly robust, but show a sensitivity of phosphorescence emission to the presence of oxygen in the system, resulting in quenching through changing of ground state $^3O_2$ to the reactive $^1O_2$. This supports their potential exploitation in the photodynamic therapy (PDT).[208] The combination of properties maintains the possibility for the development of unique dual mode theranostic agents.[209] A considerable number of reports have been issued detailing the photochemical and photophysical properties of triazole-based complexes of Ru(II), Re(I) and Ir(III).[96, 144, 210] In this chapter we explore the use of 1,2,3-triazole based ligands as bidentate donors and investigate the influence of these

ligands on the photophysical characteristics of a series of osmium(II) complexes prepared as their hexafluorophosphate and chloride salts. The water soluble chloride salts have been subjected to preliminary cellular uptake and luminescence imaging studies and the results are also reported.

3.2 Synthesis and characterisation

3.2.1 Synthesis of osmium(II) 4-(pyrid-2-yl)-1,2,3 triazole complexes

The complex $[Os(bpy)_2(Bn-pytz)](PF_6)_2$ was prepared by adaption of an established procedure for the synthesis of heteroleptic osmium(II) complexes.[204, 211] Briefly, $[Os(bpy)_2Cl_2]$ was heated under reflux conditions in ethylene glycol with one equivalent of the ligand Bn-pytz. Subsequent counter-ion metathesis with ammonium hexaflulorophosphate then enabled isolation of $[Os(bpy)_2(Bn-pytz)](PF_6)_2$ as a dark green solid. As the Bn-pytz ligand is not symmetrical the two bpy ligands give rise to two separate sets of resonances in the ^{1}H NMR spectrum of $[Os(bpy)_2(Bn-pytz)](PF_6)_2$ (Figure 3.1). The pyridyl triazole ligand exhibits a resonance for the triazole ring proton at δ 8.61, shifted by 0.34 ppm compared to the corresponding resonance for the free ligand at δ 8.27. Also, the methylene protons, which exhibits a singlet resonance in the free ligand at δ 5.60, are observed as a diastereotopic pair of roofed doublets centred at δ 5.49 due to the chirality of the complex.
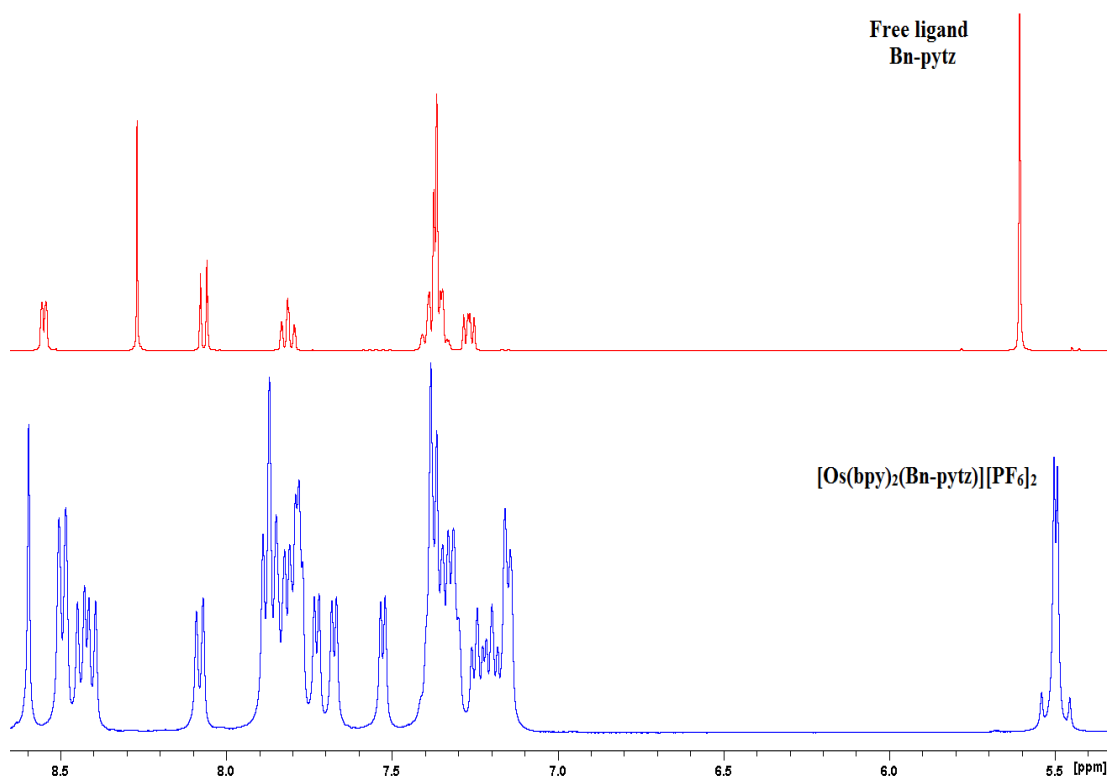
Figure 3-1- The ^{1}H-NMR spectra (400 MHz, CD$_3$CN) of [Os(bpy)$_2$(Bn-pytz)](PF$_6$)$_2$ and free ligand Bn-pytz .

The complex [Os(bpy)(Bn-pytz)$_2$](PF$_6$)$_2$ was prepared in a three-step procedure. Firstly osmium(III) chloride hydrate was allowed to react with 20 equivalents of (1,3-cyclohexadiene) in degassed ethanol at reflux to form [{Os(η^6-C$_6$H$_6$)Cl$_2$}$_2$]. This then underwent reaction with 2 equivalents of bpy in methanol to produce [Os(η^6-C$_6$H$_6$)(bpy)Cl]$^+$ which was isolated as its (PF$_6$) salt. This was then allowed to react with Bn-pytz in refluxing ethanol to yield the final product which was also isolated as the hexaflulorophosphate salt. Synthesis of Os(II) complexes through reaction with ligands often requires high temperatures in solvents like ethylene glycol (200 ^{O}C)[212] and dimethylformamide (150 ^{O}C).[213] Such high temperatures can not be used with all types of ligand, because some decompose at high tempreture. Via the [Os(η^6-C$_6$H$_6$)(bpy)Cl]$^+$ intermediate, the synthesis of Os(II) complexes can be achieved in the mild temperature (EOH-79 ^{o}C). This brings a wide ranging synthetic approach to heteroleptic osmium(II) complexes under relatively mild conditions.

102

$$cis,cis\text{-}[Os(bpy)(Bn\text{-}pytz)_2](PF_6)_2 \quad + \quad cis, trans\text{-}[Os(bpy)(Bn\text{-}pytz)_2](PF_6)_2 \quad + \quad trans, cis\text{-}[Os(bpy)(Bn\text{-}pytz)_2](PF_6)_2$$
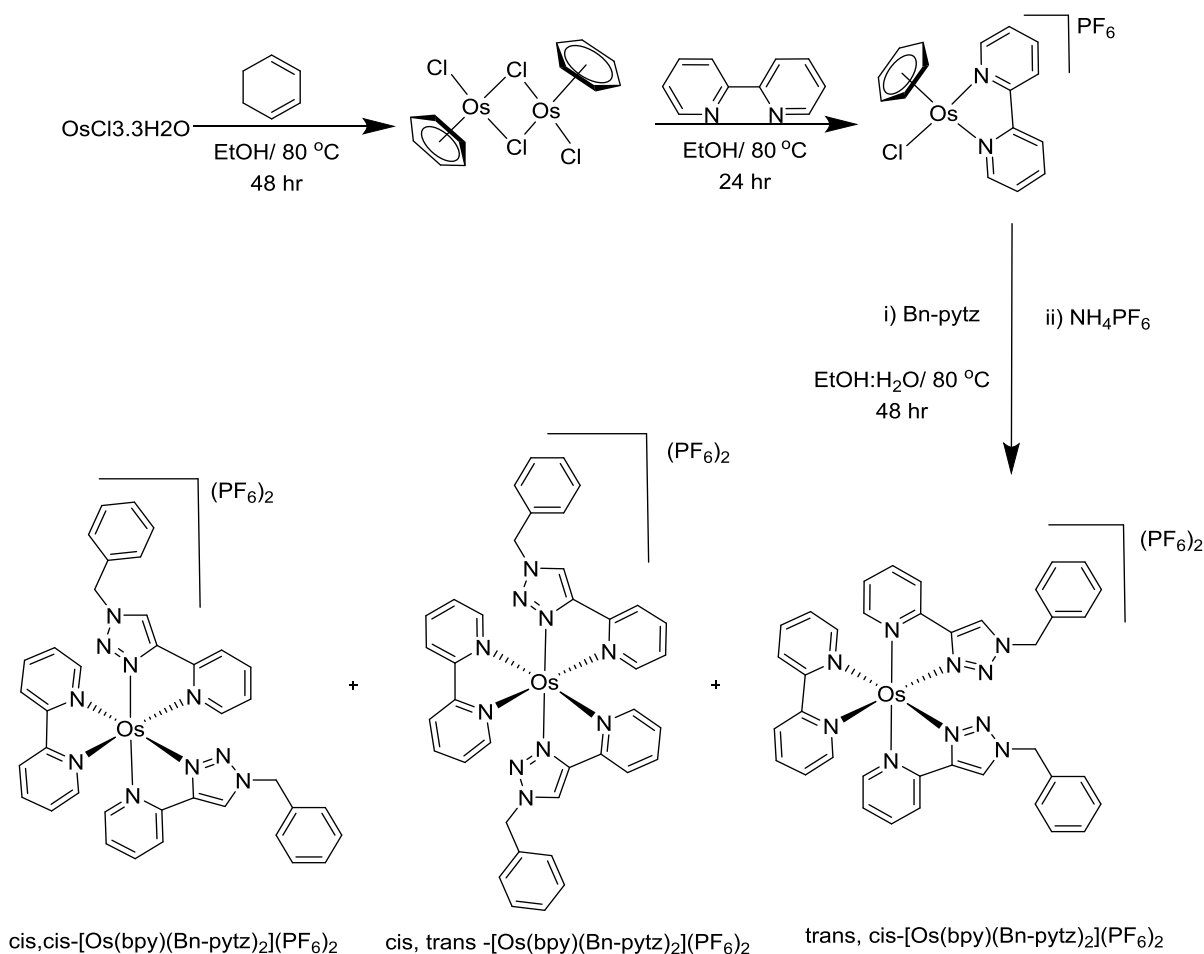
Scheme 3-1- Synthesis of [Os(bpy)(Bn-pytz)$_2$](PF$_6$)$_2$

Due to the asymmetry of the Bn-pytz ligand, the complex is produced as a mixture of three isomers, *cis, cis, cis, trans* and *trans, cis* dependent on the respective regiochemistry of the pyridyl and triazole moieties respectivly of the two Bn-pytz ligands (Scheme 3.1). In *cis, trans* and *trans, cis* isomers, the complexes are C$_2$ symmetric and should each show one singlet triazole resonance, while the *cis, cis* isomer is not symmetrical and then the two triazole resonance are unique and should show two singlets in its ^{1}H NMR spectrum. The complex isomers could not be seperated despite repeated efforts and four resonances are obtained from the ^{1}H NMR spectrum at δ 8.63, 8.62, 8.61 and 8.63 for the triazole ring protons of the regioisomers. In the *cis, trans* and *trans, cis* isomers, where the complexes are C$_2$ symmetric, the two pyridine rings in bpy ligands are equivalent and should show four set of NMR

resonance for each 2 protons in each isomer, while the *cis, cis* isomer the two pyridine rings in bpy ligands are magnetically inequivalent and should show 8 resonances with one for each proton. Because the complex isomers could not be separated and the bpy proton resonances are overlaping with the protons of py rings protons in Bn-pytz the NMR spectra of the complex is complicated. (Figure 3.2). Four multplet resonances are therefore obtained in the ^{1}H NMR spectrum in the ranges of δ 8.45-8.37, 8.1-8.05, 7.65-7.61 and 7.30-7.10, for the bpy protons. Similarly the benzylic methylene protons should show four singlets resonance, one singlet for each C_2 symmetric isomer (*cis, trans* and *trans, cis* isomers) and two singlets for the *cis, cis* isomer which is not symmetrical but this is complicated by the fact that they can appear diasterotopic as multplet resonances in the rang of δ 5.55-5.46. Due to the difficulty in separating the three isomers, the photophysical electrochemical data are henceforth presented for the mixture of the three isomers.
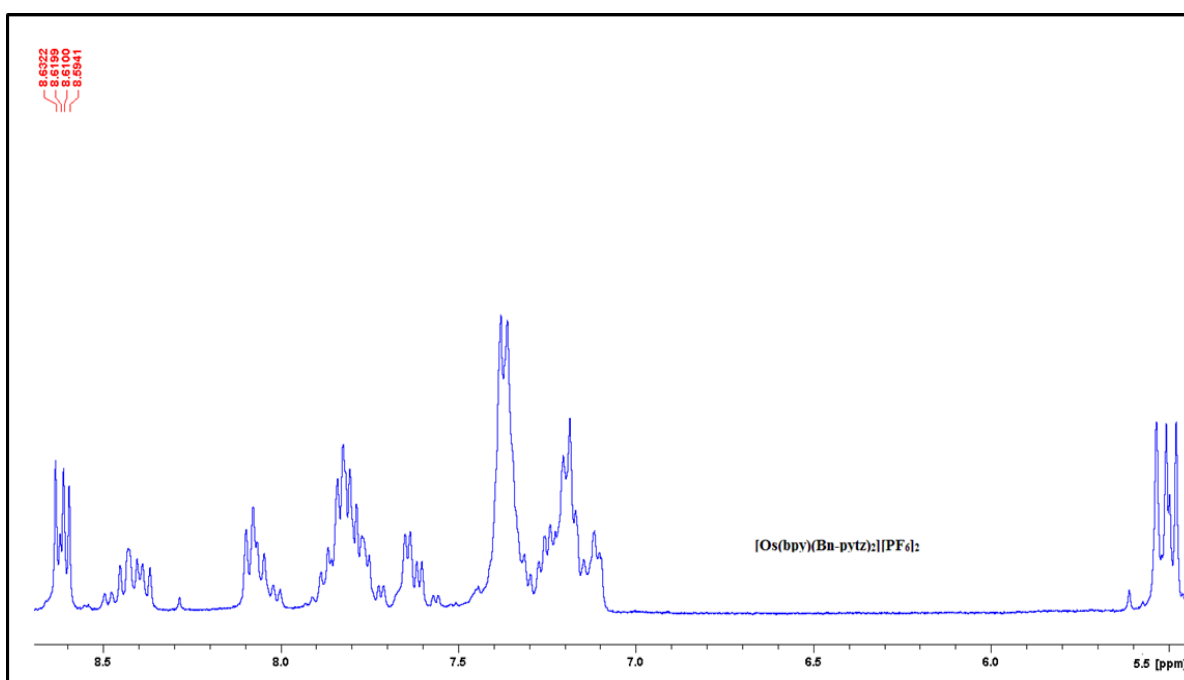
Figure 3-2- The ^{1}H-NMR spectra (400 MHz, CD$_3$CN) of mixture of isomers for [Os(bpy)(Bn-pytz)$_2$](PF$_6$)$_2$

The homoleptic complex [Os(Bn-pytz)$_3$](PF$_6$)$_2$ was prepared by reaction of [(NH$_4$)$_2$OsCl$_6$] with three equivalents of Bn-pytz in ethylene glycol under refluxing conditions followed by counter-ion metathesis. Due to the asymmetry of the Bn-pytz ligand the ^{1}H NMR spectrum of

the initial product understandably shows signals for both meridional and facial isomers of [Os(Bn-pytz)$_3$](PF$_6$)$_2$ in an approximate 1: 0.8 ratio (Scheme 3.2, Figure 3.3)
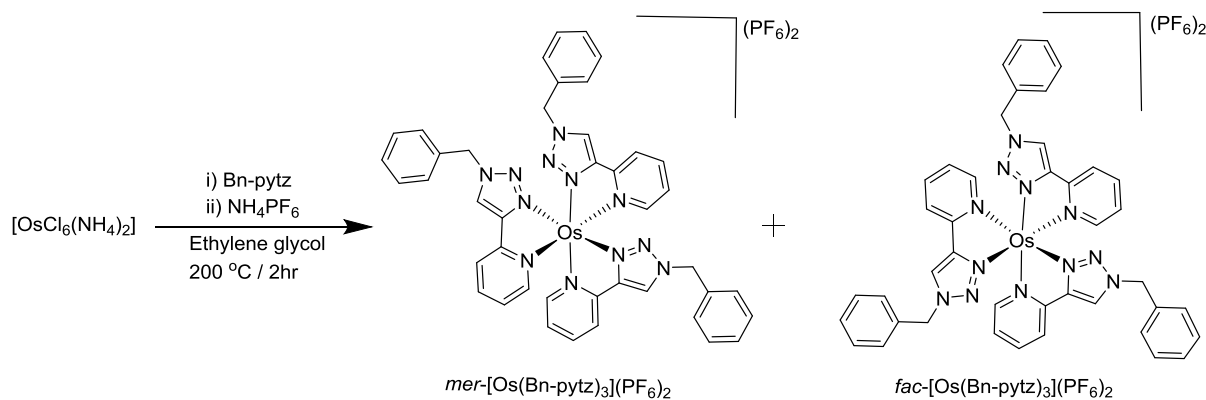
Scheme 3-2 Synthesis of [Os (Bn-pytz)$_3$](PF$_6$)$_2$

Separation of the two isomers again proved extremely difficult with both co-eluting in column chromatography with a wide range of solvent systems. Successful separation was possible but only on a small scale by preparative thin-layer chromatography yielding only very small quantities of each isomer, only enough to allow spectroscopic characterisation. Figure 3.3 shows the ^{1}H NMR for complex [Os(Bn-pytz)$_3$](PF$_6$)$_2$ as a mixture and the meridional and facial isomers. For *mer*-[Os(Bn-pytz)$_3$](PF$_6$)$_2$ where the three Bn-pytz ligands are magnetically unique and so three singlet resonances are observed at δ 8.63, 8.61 and 8.60 corresponding to the triazole ring protons. The ^{1}H NMR spectrum of *fac*-[Os(Bn-pytz)$_3$](PF$_6$)$_2$ is much simpler than that of its meridional isomer due to the C$_3$ symmetry of the cation. A singlet resonance is observed at δ 8.61 for the triazole ring proton along with a resonance at δ 5.50 for the benzylic methylene protons. These are accompanied by four multiplets deriving from resonance for the pyridine and benzylic phenyl rings (Figure 3.3).
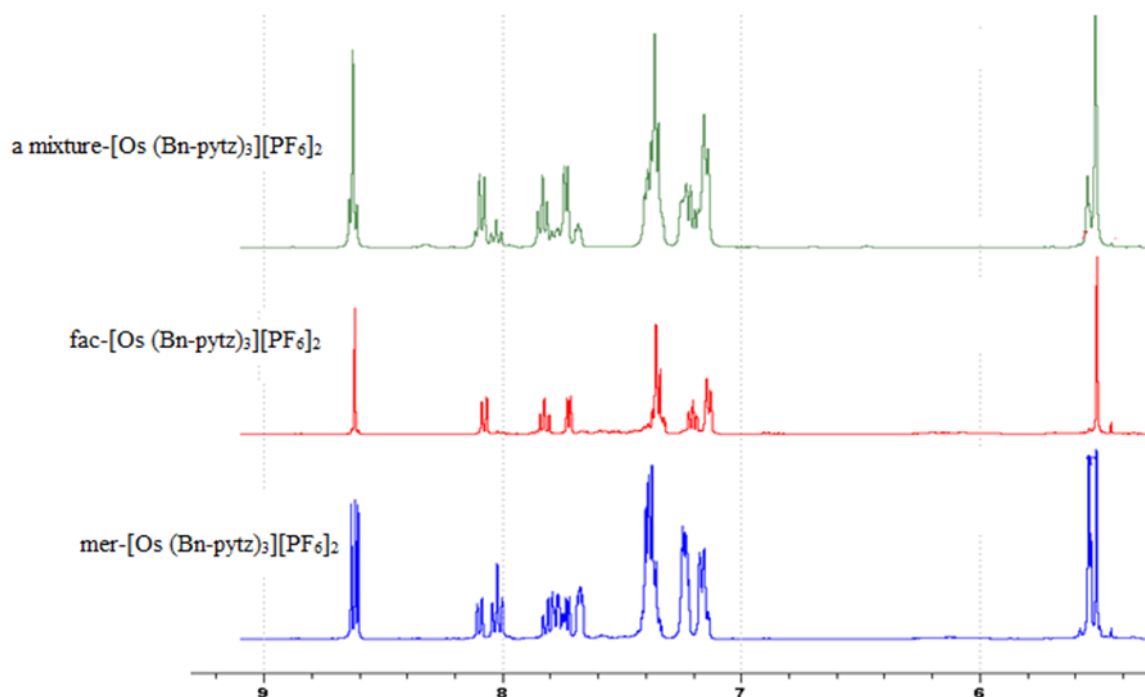
Figure 3-3- The 1H-NMR spectra (400 MHz, CD$_3$CN) of [Os (Bn-pytz)3](PF$_6$)$_2$ and the pure mer and fac isomers

From nOe correlation NMR spectroscopy of *mer*-[Os(Bn-pytz)$_3$](PF$_6$)$_2$ (Figure 3.4) the methylene protons of the benzyl substituent corresponding to each of the triazole ring protons were identified. The diastereotopic doublet at δ 5.51 shows correlation with the triazole at δ 8.60. The triazole protons in the same ligand which are appear at δ 8.61 and 8.63 correlate with the multiplet at δ 5.54 for those methylene protons.

106
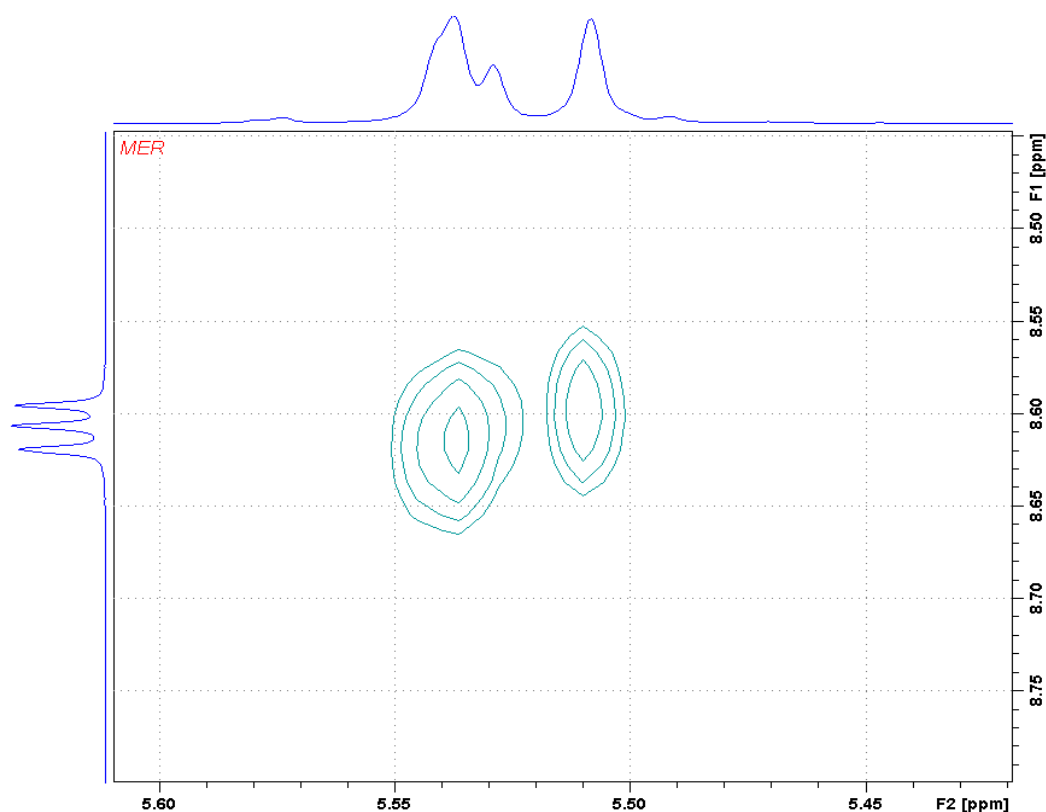
Figure 3-4- ^{1}H/^{1}H NOESY spectrum (400 MHz, (CD$_3$CN) of *mer*-[Os(Bn-pytz)$_3$](PF$_6$)$_2$

The chloride salts of complexes which are soluble in water are obtained by stirring the PF$_6^-$ salts in methanol with Amberlite IRA-400 (chloride form) anion-exchange resin. The resultant solutions were then filtered and evaporated, taken up into water and freeze dried. The successful counter ion metathesis and formation of chloride salts was confirmed by the complete absence of resonance for the PF$_6^-$ counerion in the ^{19}F and ^{31}P NMR spectra. The chloride salts were then characterized by ^{1}H-NMR, UV/vis absorption and emission spectroscopy.

3.3 **Electrochemical studies**

Cyclic voltammetry experiments were carried out on the complexes in order to characterise their electrochemical properties. Electrochemical data for the various complexes as obtained are summarized in Table 3.1. Figure 3.5 shows the cyclic voltammagrams of complexes in acetonitrile. For the homoleptic complex $[Os(Bn-pytz)_3]^{2+}$, this was recorded on the mixture of *fac* and *mer* isomers.

Table 3-1- electrochemical data for complexes in CH$_3$CN, 0.2 M [NBu$_4$][PF$_6$], 100 mVs^{-1}, at room temperature

No	Complex	Reduction $E_{1/2}$ V vs. Fc$^+$/Fc	Oxidation $E_{1/2}$ V vs. Fc$^+$/Fc
1	$[Os(bpy)_3](PF_6)_2$	-1.85(0.078)[a], -1.665(0.083)[a]	0.436(0.078)[a]
2	$[Os(bpy)_2(Bn-pytz)](PF_6)_2$	-1.93(0.094)[a], -1.72(0.083)[a]	0.441(0.075)[a]
3	$[Os(bpy)(Bn-pytz)_2](PF_6)_2$	-1.79(0.09)[a]	0.438(0.078)[a]
4	mix-$[Os(Bn-pytz)_3](PF_6)_2$	====== [b]	0.453(0.089)[a]

$E_{1/2}$ = (Epa+ Epc) /2, Epa and Epc are anodic and cathodic peak potentials respectively. a = reversible, b = reduction couples are outside the available electrochemical window. $\Delta EP^{a,c}$ = (Epa- Epc) are inparentheses

The observed couples are all reversible, where reversibility as used here implies that the separation between the anodic and cathodic peak potentials was less than 100 mV and no degradation products were observed on the following scan. The general behaviour is quite similar for all complexes. A cyclic voltammogram of all complexes gave the Os$^{3+/2+}$ metal-based redox processes with an $E_{1/2}$ around +0.44 V with little variation and the an indicates that HOMO is located on the metal center. $[Os(bpy)_3]^{2+}$ gave two one electron bipyridine ligand based reduction processes, with $E_{1/2}$ values of -1.66 V (bpy$^{0/1-}$), and -1.85 V (bpy$^{1-/2-}$) (the third reduction was not observed in the the solvent window). As more Bn-pytz ligands are incorporated, the bpy based reduction potantials are shifted to more negative potential. This is

due to Bn-pytz ligand not being as good a π acceptor leading to more back bonding to bpy. Because the Bn-pytz ligand has higher energy π^* orbital, the pytz-based reduction for the complex mix-[Os(Bn-pytz)$_3$](PF$_6$)$_2$ are not be seen which confirms that the reduction values noticed here belong to the bpy ligand This strongly suggests that any differences in the MLCT absorption and emission energies between the complexes (see later) are primarily due to differences in the energy of the ligand centred π^* orbitals.
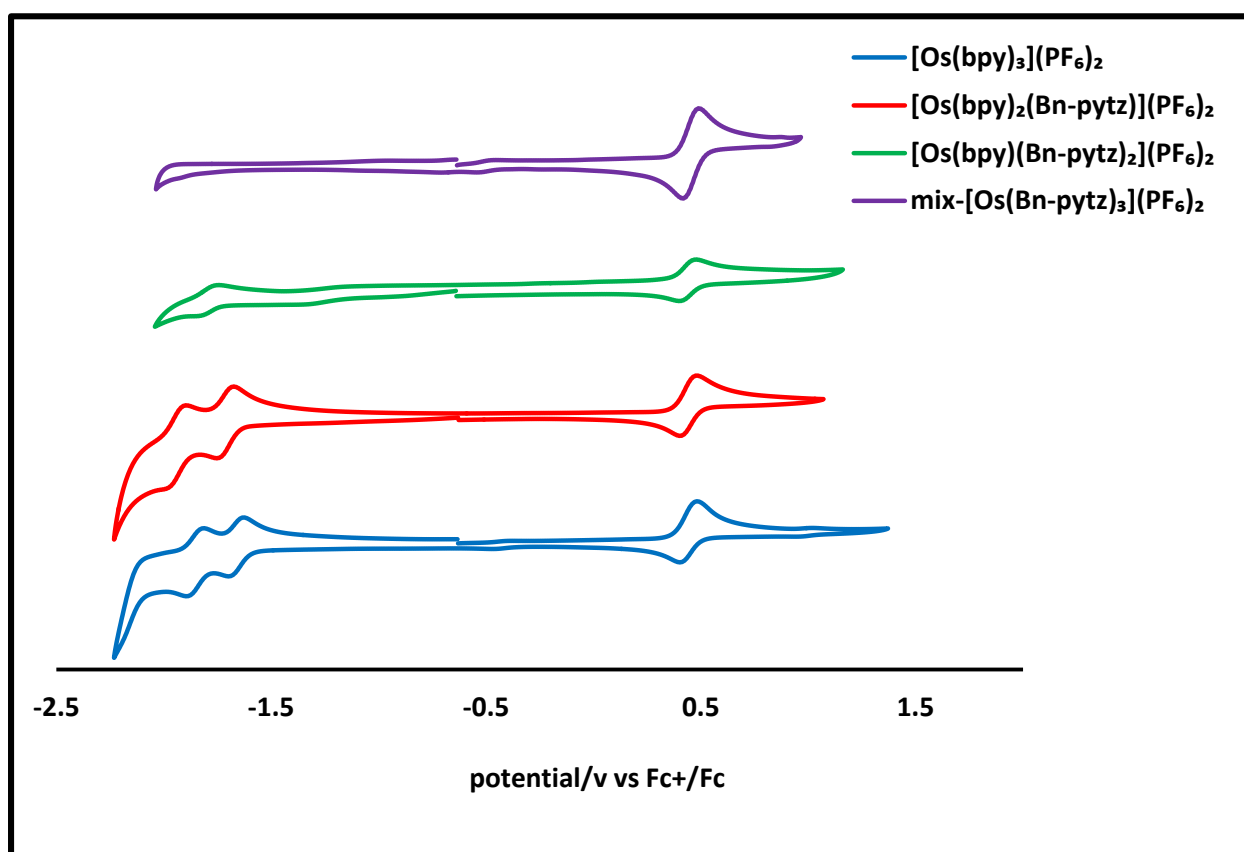
Figure 3-5- Cyclic voltammogram of complexe in CH$_3$CN /0.2 M NBu4PF$_6$; scan rate (v) = 100 mV s $^{-1}$. Potentials V are reported against ferrocene (Fc$^+$/Fc= 0.0 V)

3.4 **Photophysical studies**

Table 3.2 summarizes the UV-vis electronic absorption data for the complexes, UV-Vis absorption spectra of complexes in acetonitrile are shown in Figure 3.6.

Table 3-2- The UV-vis electronic absorption data for the complexes in aerated acetonitrile

Compound	λ / nm(ε/ dm^3.mol^{-1}cm^{-1})
[Os(bpy)$_3$)](PF$_6$)$_2$	246(19460), 255(16929), 290(62491), 331(7040), 372(7315), 392(6840), 437(8820), 487(8712), 667(1940)
[Os(bpy)$_2$(Bn-pytz)](PF$_6$)$_2$	240(19605), 279 (34054), 290(42108), 327(6179), 372 (8716), 356(6772), 386(7767), 421(6848), 468(7625)
[Os(bpy)(Bn-pytz)$_2$](PF$_6$)$_2$	237(20868), 274(29949), 288(20694), 380(7296), 459(4620)
mix-[Os(Bn-pytz)$_3$](PF$_6$])$_2$	235(30277), 273(51121), 308(7534), 373(11684), 402(10929), 484(3492), 530(2589)
mer-[Os(Bn-pytz)$_3$](PF$_6$])$_2$	235(28966), 273(50240), 308(6976), 373(11500), 402(10429), 484(3288), 530(2535)
fac-[Os(Bn-pytz)$_3$](PF$_6$)$_2$	235(27377), 273(48693), 308(6360), 373(10763), 402(10475), 484(3110), 530(2207)

The UV-vis absorption spectrum of [Os(bpy)$_2$(Bn-pytz)](PF$_6$)$_2$ in acetonitrile exhibits a sharp and intense band at 290 nm ascribed to singlet ligand-centered $\pi \rightarrow \pi^*$ transition centred on bpy ligands. [Os(bpy)$_3$)](PF$_6$)$_2$ also has the 290 nm transition which confirms that this absorption is bpy localised $\pi \rightarrow \pi^*$ transition. The intensity of this band is seen to decrease when bpy ligands are replaced with Bn-pytz until disappears for [Os(Bn-pytz)$_3$](PF$_6$)$_2$. This reduction in absorbance with increased Bn-pytz ligands is accompanied by the growth of an intense band at 280 nm reflective of Bn-pytz centered $\pi \rightarrow \pi^*$ transitions. In the visible region

the complexes exhibit panchromatic absorption with moderately intense absorption bands between 370 and 520 nm with absorptions of lower intensity at longer wavelength tailing off towards 700 nm. The more intense, higher energy bands in the visible are assigned to spin-allowed ^{1}MLCT transitions whereas the weaker and lower energy bands are assigned to spin-forbidden ^{3}MLCT transitions. The spin forbidden absorption populates the ^{3}MLCT state directly from the ground state and is readily apparent because of the large spin-orbital coupling effect that results from the heavy osmium atom.[214] Since the LUMO of the Bn-pytz ligand is significantly destabilised relative to that of bpy, the replacement of one of the bpy ligands by Bn-pytz leads to the shift of the ^{1,3}MLCT bands to higher energy. The LUMO of isomers of $[Os(Bn-pytz)_3](PF_6)_2$ (meridional, facial) are heavily destabilised relative to those of $[Os(bpy)(Bn-pytz)_2](PF_6)_2$, $[Os(bpy)_2(Bn-pytz)](PF_6)_2$ and $[Os(bpy)_3]^{2+}$. As a result, the blue shift is very large from the $[Os(bpy)(Bn-pytz)_2](PF_6)_2$ to $[Os(Bn-pytz)_3](PF_6)_2$, because the LUMO previously localised on the bpy ligands most now localise on Bn-pytz. These data are in agreement with the electrochemical data which indicate an increased HOMO-LUMO gap as the Bn-pytz content increases. From the Figure 3.6 we can note that the UV-Vis absorption spectra of the isomers of $[Os(Bn-pytz)_3](PF_6)_2$ complexes (meridional, facial) are largely indistinguishable from each other.
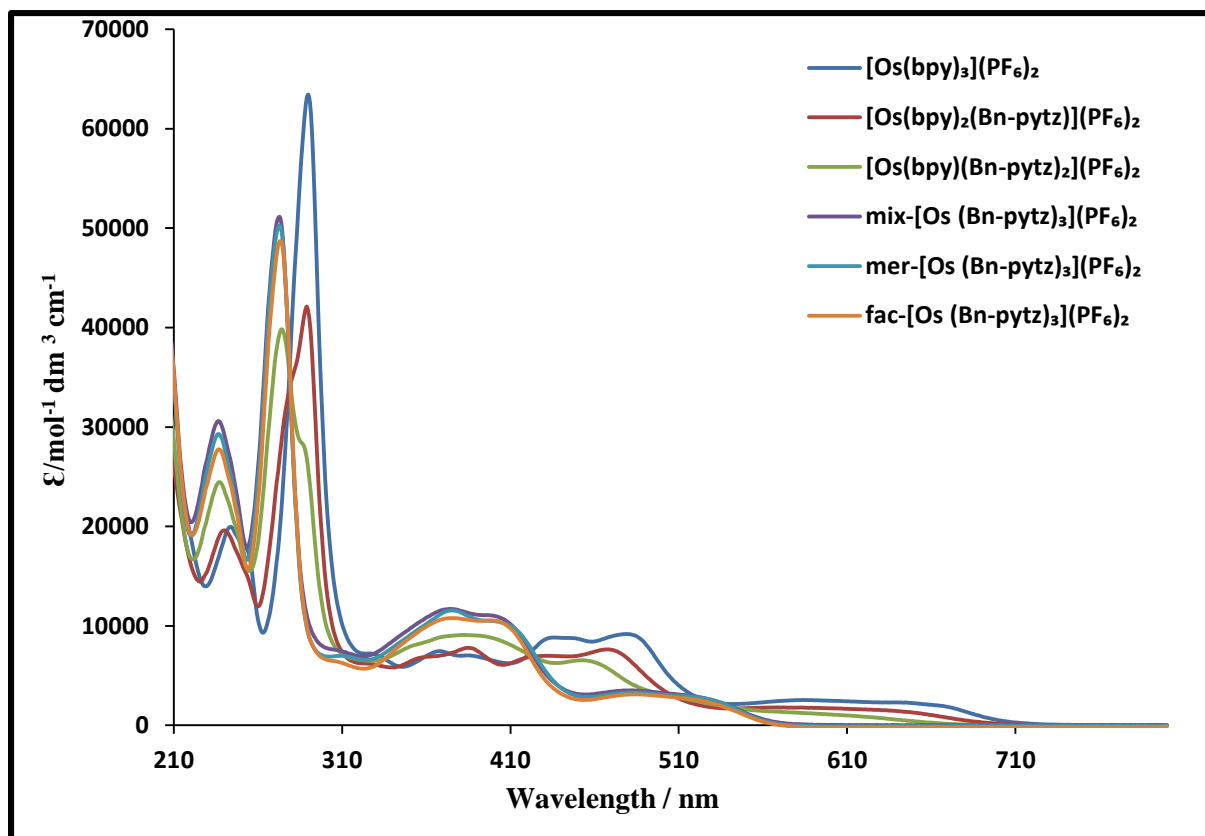
Figure 3-6- UV–visible absorption spectra of complexes in aeriated acetonitrile at 295 K.

All of the complexes exhibit broad featureless emission bands at room temperature which are assigned to emission from a ^{3}MLCT state (Figure 3.7). In the room temperature spectrum, the complex [Os(bpy)$_2$(Bn-pytz)](PF$_6$)$_2$ exhibits phosphorescence with a broad, featureless band in the red/near-infrared region of the spectrum (λ_{max} = 730 nm, Table 2). Because the pytz ligand is less π-accepting than bpy, then bpy recieves more back bonding, which leads to a higher LUMO energy. This results in the emission being slightly blue-shifted relative to that of [Os(bpy)$_3$]$^{2+}$ (λ_{max} = 737 nm).[215] Emission from [Os(bpy)(Bn-pytz)$_2$](PF$_6$)$_2$ (λ_{max} = 720 nm) is blue shifted even further. [Os(Bn-pytz)$_3$](PF$_6$)$_2$ exhibits a very big blue shift (λ_{max} = 615 nm) due to the LUMO being necessarily localised on Bn-pytz, which has a higher energy LUMO. Comparing the osmium complexes to the ruthenium(II) analogues [Ru(bpy)$_{3-n}$(pytz)$_n$](PF$_6$)$_2$, the ^{1}MLCT absorption and ^{3}MLCT emission bands (at 77 K) are also observed to blue-shift on increasing pytz content, howevere, ruthenium(II) complexes show little or no emission at

room temperature.[94] Increasing the pytz content leads to a quenching of emission presumably due to ^{3}MC states becoming more accessible and reduced ^{3}MLCT / ^{3}MC separation. Even at 77 K emission is not observed from the homoleptic complex $[Ru(pytz)_3](PF_6)_2$. Osmium complexes are emissive at room temperature with the emission being characterized by a broad featureless band attributed to an emissive ^{3}MLCT state. This is because the ligand-field splitting is much larger leading to destablsation of the ^{3}MC state which become thermally inaccessible.
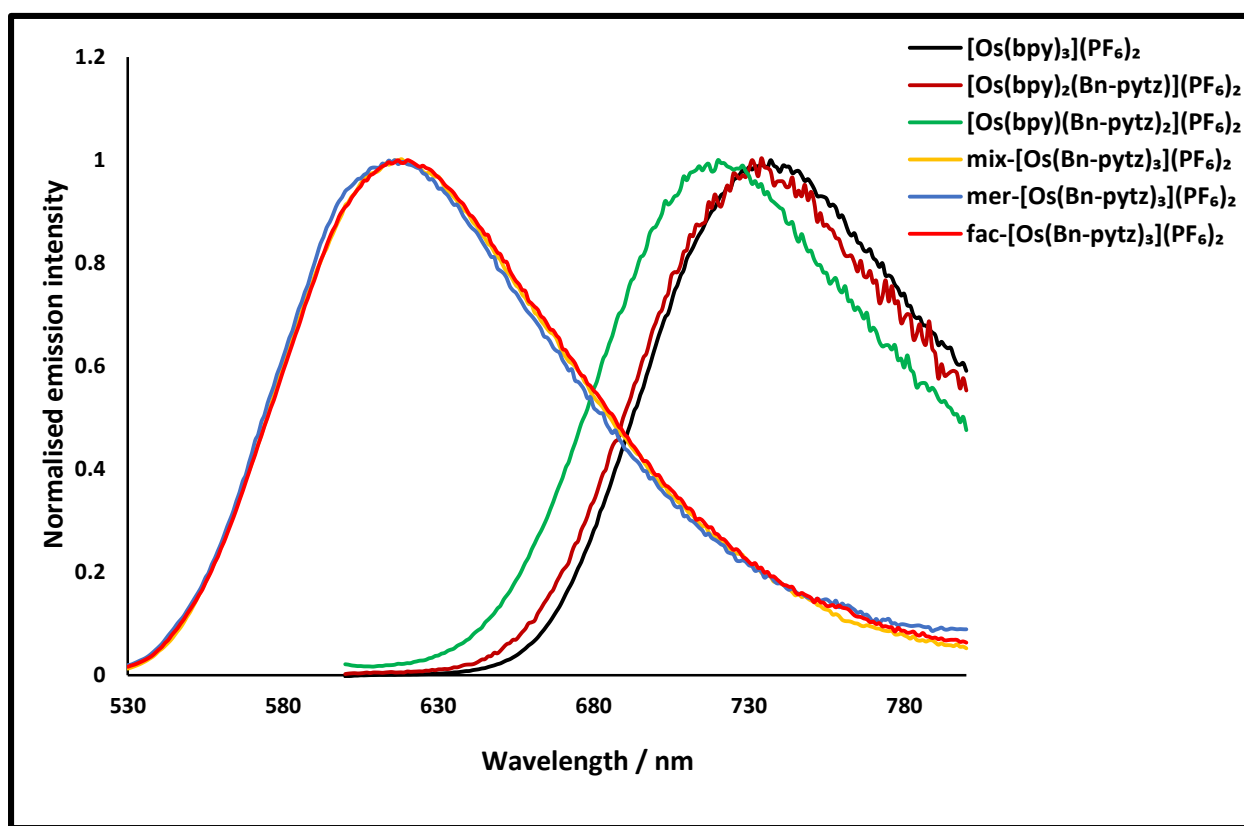
Figure 3-7- Emission spectra of the complexes in aerated acetonitrile at room temperature

Osmium complexes with btz ligand have been studied.[120] Increasing btz ligand content leads to a progressive blue-shift in the ^{1}MLCT and ^{3}MLCT-based absorptions compared to the absorption for $[Os(bpy)_3]^{2+}$. The shift in the MLCT bands is highly noticeable upon replacement of the final bpy by btz. Heteroleptic osmium(II) btz complexes $[Os(bpy)_2(btz)]^{2+}$

and $[Os(bpy)(btz)_2]^{2+}$ where the ligand containing two triazole rings display emission at 724 and 713 nm respectively this means that these complexes exhibit emission bands at higher energy than Bn-pytz complexes. The homoleptic complex $[Os(btz)_3]^{2+}$ appears to display extremely weak emission at room temperature, while the homoleptic $[Os(Bn-pytz)_3]^{2+}$ complex is emissive at room temperature 615 nm. This is because the Bn-pytz LUMO destablsation is not big enough for quenching of emission while the btz ligand has higher energy LUMO enough to quenched the emission.

The emission spectrum was also recorded in a 4:1 EtOH/MeOH glass matrix at 77 K. All complexes display structured emission bands with vibronic progressions relative to the emission spectrum at room temperature. Figure 3.8. The emission for all complexes undergo a rigdochromic blue-shift of approximately 35 nm. This is typical for metal-to-ligand charge transfer band emission, due to the frozen solvent molecules matrix where stabilization of the charge transfer states through relaxation of the geometry of the complex and solvent shell rearrangement cannot occur, and therefore the HOMO–LUMO gap is effectively increased. The photophysical data are summarized in Table 3.3. As with room temperature solution spectra increasing the number of Bn-pytz ligands leads to blue shifts in the emission with increasing in the lifetime and quantum yield ϕ. The bigest change is again obsarved for the complex $[Os(Bn-pytz)_3]^{2+}$. This data is consistent with the energy gap law.
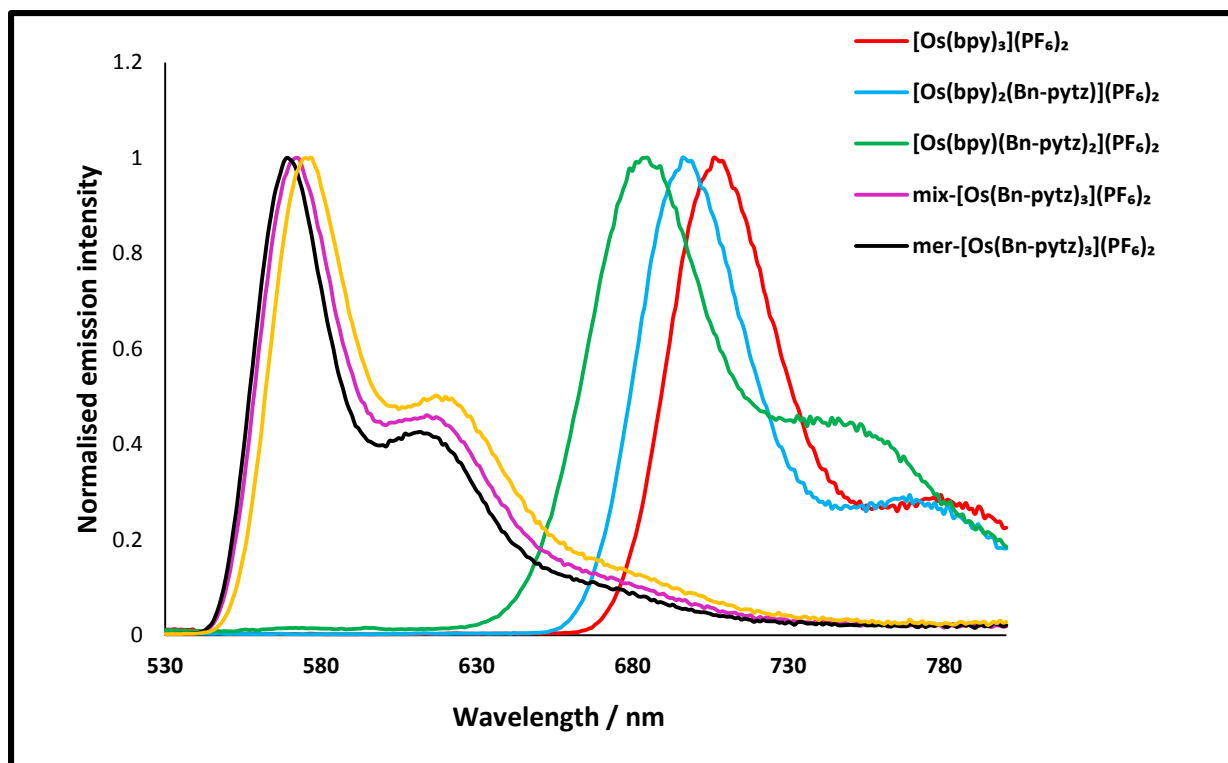
Figure 3-8- Emission spectra of the complexes in rigid matrix (4:1 EtOH/MeOH) at 77 K.

Table 3-3- Luminescence data and lifetime of the complexes at room temperature (acetonitrile) and 77 K (4:1 EtOH/MeOH glass matrix)

Compound	At room temperature			At 77 k
	λ_{max} (nm)	Ʈ ns	φ% In aerated MeCN*	λ max (nm)
$[Os(bpy)_3)](PF_6)_2$	737	37	0.56	702
$[Os(bpy)_2(Bn\text{-}pytz)](PF_6)_2$	730	43	0.54	698
$[Os(bpy)(Bn\text{-}pytz)_2](PF_6)_2$	721	53	0.59	683
mix-$[Os(Bn\text{-}pytz)_3](PF_6)_2$	615	52	1.35	574
mer-$[Os(Bn\text{-}pytz)_3](PF_6)_2$	615	50	1.27	574
fac-$[Os(Bn\text{-}pytz)_3](PF_6)_2$	615	50	1.59	576

* Relative to $[Ru(bpy)_3](PF6)2$φ= 0.018

Changing the counter-ion from PF_6 to chloride deos not effect significantly the photophysical properties of these complexes as we can note from Figures 3.9-3.10 which respectively are showing the UV-vis absorption spectra and the emission spectra of complexes with chloride counter-ions. The complexes are still emissive in water negligible changes in spectra are

observed in changing the solvent from acetonitrile to water. Because the water is more polar and increasing polarity of the solvent shifts π-π^* to higher energy, red shift was expected but the aqueous solution spectra here are near identical to those of the PF_6 salts in acetonitrile.

Table 3-4
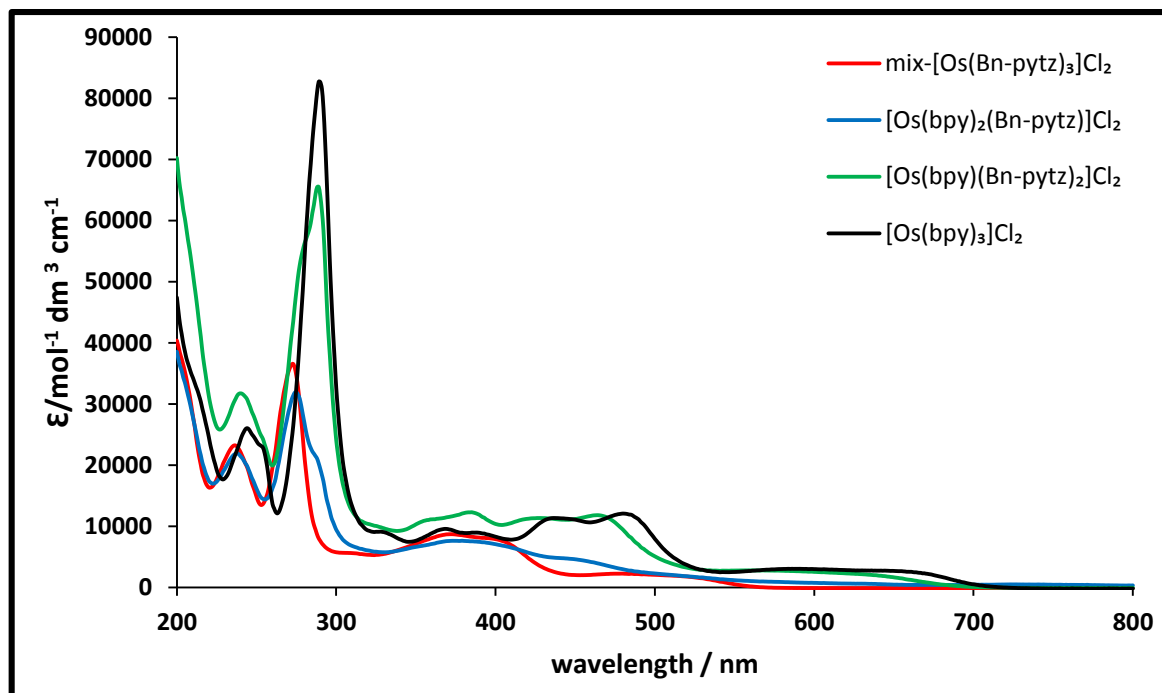
Figure 3-9- UV–visible absorption spectra of complexes with chloride counter-ion in water at 295 K.

Table 3-4 UV-vis absorption and luminescence data of the complexes with chloride counter-ion at room temperature in water

Compound	λ_{abs} / nm(ε/ dm^3.mol^{-1}cm^{-1})	λ_{em} (nm)
[Os(bpy)$_3$)]Cl$_2$	244(26057), 256(20703), 289(82743), 329(9133), 369(9553), 390(8938), 437(11362), 486(11912), 670(2321)	735
[Os(bpy)$_2$(Bn-pytz)]Cl$_2$	237(21907), 275 (31928), 289(20292), 331(5772), 357(6957), 373(7631), 468(3700)	729
[Os(bpy)(Bn-pytz)$_2$]Cl$_2$	239(31753), 274(46097), 289(65528), 383(12290), 464(11827)	719
mix-[Os (Bn-pytz)$_3$]Cl$_2$	235(23240), 273(36558), 309(5620), 372(8716), 403(7715), 484(2196), 529(15002)	624
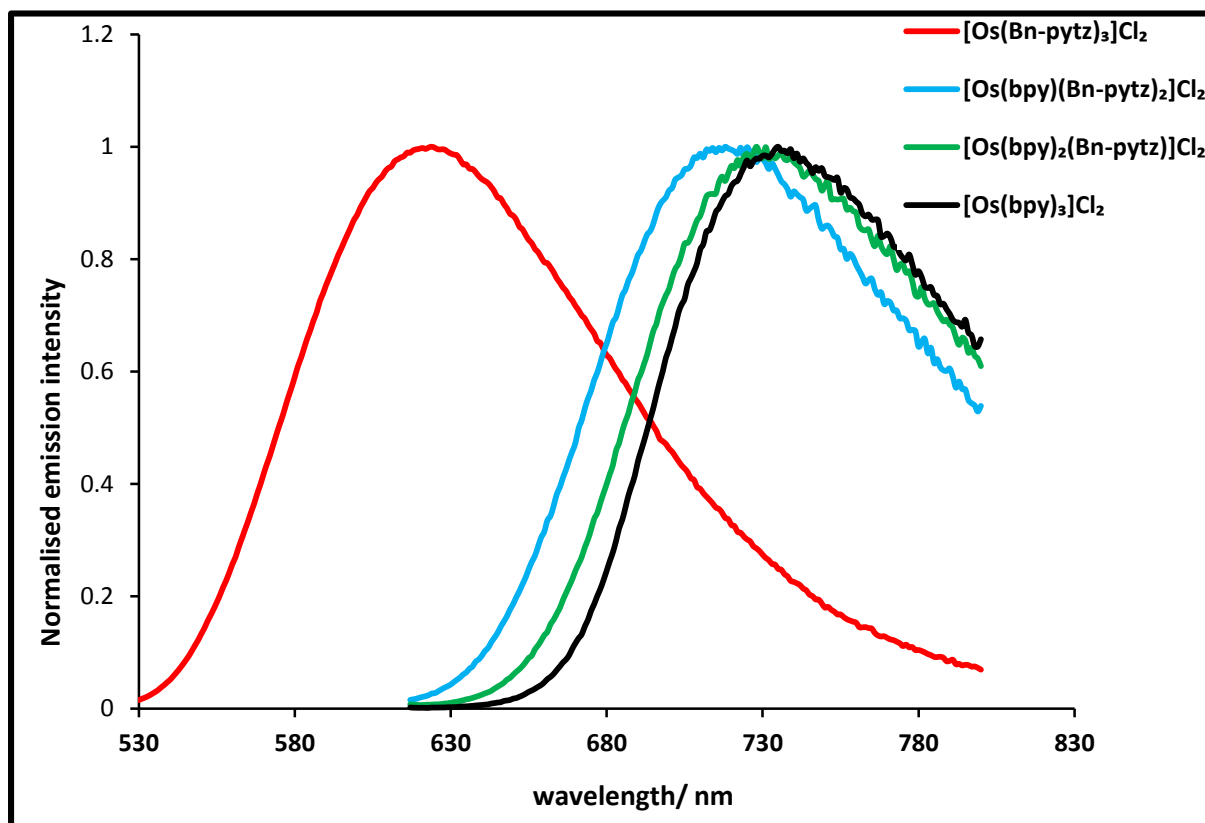
Figure 3-10- Emission spectra of the complexes with chloride counter-ion in water at 295 K

3.5 Luminescence Quenching by Oxygen

As oxygen is introduced to the complex, the lifetime and emission intensity decrease.[216] This is because the triplet ground state of O_2 ($^3O_2$) can quench the phosphorescence from the ^{3}MLCT state of the complex through triplet-triplet annilation (TTA)[217] when collision of these molecules occur. The quenching efficiency and consequently, the luminescence intensity or lifetime will be determined by the concentration of the ambient oxygen.[218] Thus, the lifetime and intensity of the luminescence is inversely proportional to the amount of oxygen present. This relationship can be quantified by the Stern-Volmer equation:

$$Io/I = 1 + Ksv[O_2]$$

117

Here I_o is the intensity (or lifetime) of the complex in an oxygen free environment, I is the measured intensity (or lifetime) at a given oxygen concentration (O_2), and K_{sv} is the derived Stern-Volmer constant that quantifies the relationship between the two variables. The changes in the emission spectra of the complexes are measured in acetonitrile. The intense phosphorescence was observed in the absence of oxygen, whereas increasing the oxygen concentration led to a decrease in the phosphorescence intensity. The responses of phosphorescence to molecular oxygen obeyed Stern–Volmer relationships. Generally, a more sensitive system will have a steeper slope and, as a result, a higher Ksv value. Table 3.5 summarise the emission life times of the complexes in the presence of different concentations of oxygen:

Table 3-5- Life time (ns) of the complexes in different concentation of oxygen in acetonitrile:

Compound	0 atm	0.21 atm	1.0 atm
$[Os(bpy)_3)](PF_6)_2$	1674	37	11
$[Os(bpy)_2(Bn\text{-}pytz)](PF_6)_2$	1726	41	16
$[Os(bpy)(Bn\text{-}pytz)_2](PF_6)_2$	1518	53	11
mix-$[Os(Bn\text{-}pytz)_3](PF_6)_2$	1809	56	14
mer-$[Os(Bn\text{-}pytz)_3](PF_6)_2$	1571	45	12
fac-$[Os(Bn\text{-}pytz)_3](PF_6)_2$	1384	29	11

Figure 3.11 shows the emission intensities at the different oxygen concentrations for the complexes. Generally, replacement of the bpy ligand by Bn-pytz gives more efficient quenching. This shows that $[Os(bn\text{-}pytz)_3]^{2+}$ is more potent at $^1O_2$ production than $[Os(bpy)_3]^{2+}$ complex and the other bpy containing complexes.
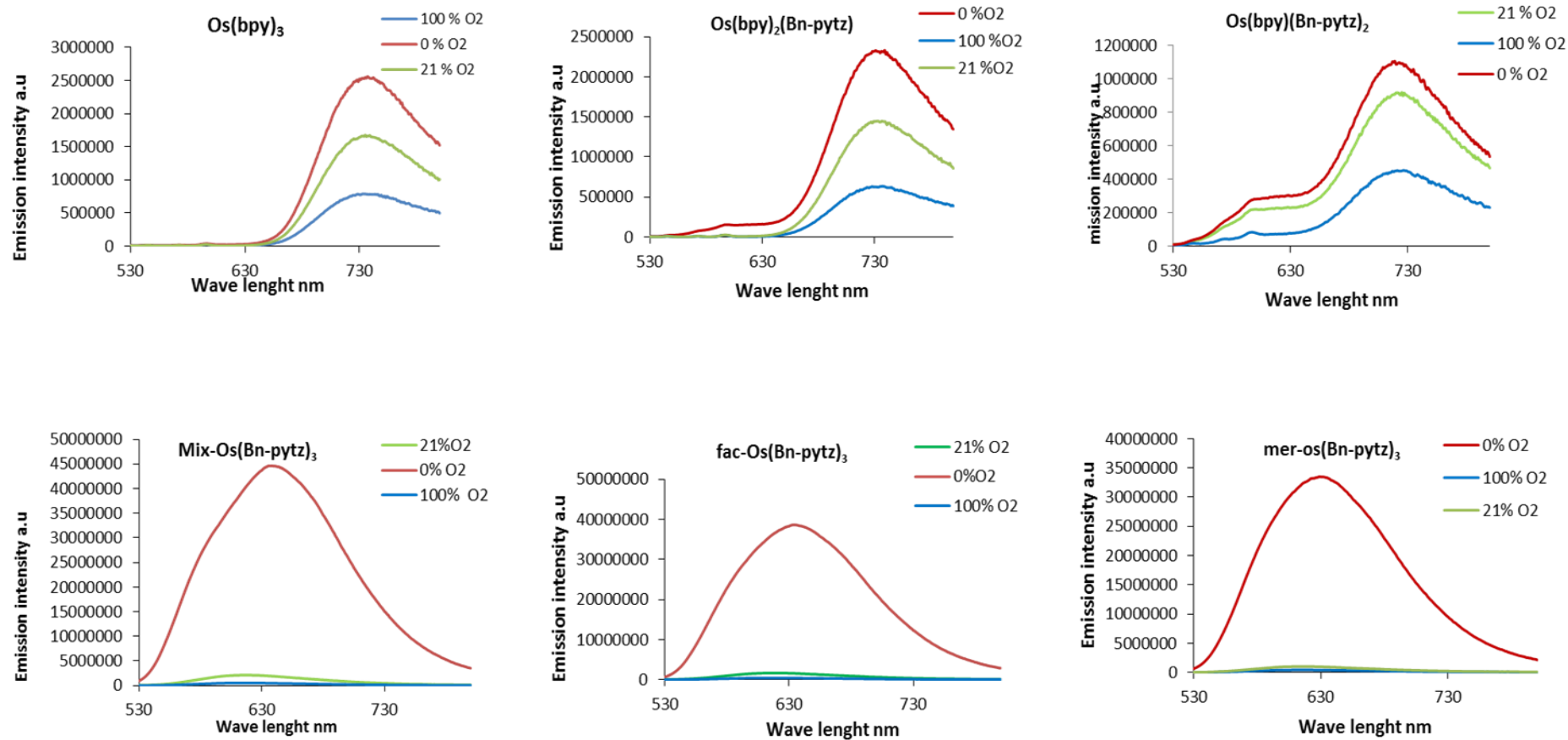
Figure 3-11 Emission response of complexes to varying [O$_2$] IN CH$_3$CN

The sensitivity of emission from the complexes to $[O_2]$ was determined through the Stern-Volmer quenching constant (Ksv). As shown in Figure 3.12, the oxygen concentration was proportionate to the ratio of the phosphorescent intensities I_0/I. As seen in Table 3.6, which show the Ksv values of the complexes, replacement of one of the bpy ligands by Bn-pytz leads to more $^3O_2$ quenching until the biggest $^3O_2$ quenching observed in $[Os(Bn-pytz)_3](PF_6)_2$ complex.

Table 3-6- Stern-Volmer quenching constant (Ksv) for the complexes

Compound	Ksv/atm^{-1} for the complexes as PF$_6$ salts	$^1O_2$ quantum yield % as Cl salts
$[Os(bpy)_3)]^{2+}$	2.2	
$[Os(bpy)_2(Bn-pytz)]^{2+}$	2.7	19
$[Os(bpy)(Bn-pytz)_2]^{2+}$	8.3	32
mix-$[Os(Bn-pytz)_3]^{2+}$	83	62
mer-$[Os(Bn-pytz)_3]^{2+}$	83	
fac-$[Os(Bn-pytz)_3]^{2+}$	89	
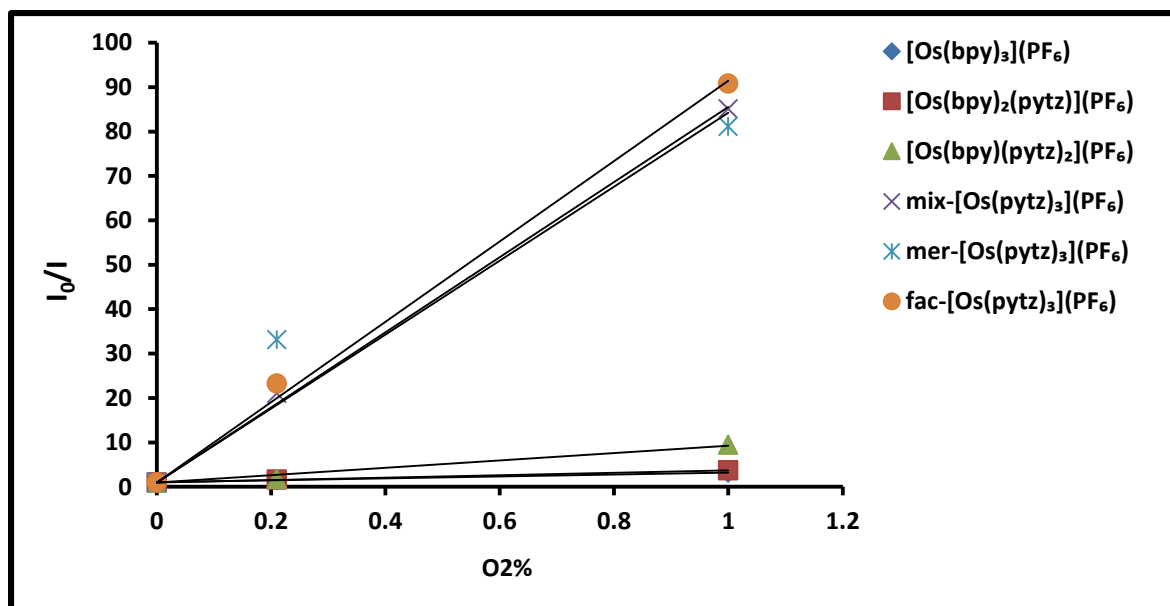
Figure 3-12- Ksv plot for all complexes

Generally, there is a significantly higher sensitivity to $[O_2]$ observed with $[Os(Bn-pytz)_3](PF_6)_2$ complexes ($Ksv = 88$ atm^{-1}) compared with other complexes and we can see that $[Os(bpy)(Bn-pytz)_2](PF_6)_2$ has higher $Ksv = 8.29$ atm^{-1} comparing with $[Os(bpy)_2(Bn-pytz)](PF_6)_2$ $Ksv = 2.69$ atm^{-1} which means that Bn-pytz complexes are more sensitive than bpy-containing complexes. Singlet oxygen quantum yields were determined by Luke K. McKenzie (University of Sheffield) for the chloride salts of complexes in acetonitrile, by massuring the near-IR luminescence from ($^1O_2$) relaxation. The ($^1O_2$) quantum yield data is in agreement with the Ksv data. High quantum yields of singlet oxygen 19% for $[Os(bpy)_2(Bn-pytz)]^{2+}$ and 32 % for $[Os(bpy)(Bn-pytz)_2]^{2+}$ are observed with the highest quantum yield of 62% observed for $[Os(Bn-pytz)_3]^{2+}$ in agreement with the quenching data for the hexafluorophosphate salts. This is because the Bn-pytz ligand has higher LUMO than bpy ligand and the so the triplet ground state of O_2 ($^3O_2$) can quench the phosphorescence of the (^3MLCT) of complex when collision of these molecules occurs increasing the quenching efficiency

3.6 Density functional theory (DFT) studies

In order to further understand the electronic transitions of the complexes and validate the interpretation of the electrochemical and photophysical results density functional theory (DFT) studies were undertaken. Calculations were preformed by Dr Nathan Patmore and the result presented and interpreted here.

3.6.1 Ground state properties:

Density functional theory (DFT) calculations were carried out to study the nature, localisation and relative energies of the frontier orbitals in addition to simulate the optical absorption spectra of the complexes. The calculations optimised the geometries of the ground states in acetonitrile by using PCM solvation model with the SDD effective core potential for osmium and 6-311G* basis sets for all other atoms. Here the density functional calculations indicate that for all the complexes in the singlet ground state the HOMO orbital is of approximately in the same energy which is in agreement with the obtained CV data. In all complexes the HOMO is predominantly of Os d_z^2 orbital character, (Figure 3.13). On the other hand, the LUMOs are essentially the π^* orbital of ligands. For the bpy-containing complexes the LUMO is localised on the bpy ligands, having π^* character. For the homoleptic complex $[Os(Bn-pytz)_3](PF_6)_2$ the LUMO is distributed over the three Bn-pytz ligands predominantly over pyridine rings. Progressing across the series the LUMO is destabilised (Table 3.7), resulting in an increased HOMO–LUMO gap as the bpy ligands are replaced by Bn-pytz with a big jump in energy observed for the LUMO and HOMO–LUMO gap for $[Os(Bn-pytz)_3](PF_6)_2$ in agreement with the experimental electrochemical data.

Table 3-7- Calculated HOMO and LUMO energies and HOMO-LUMO gap ΔE for $[Os(bpy)_{3-n}(Bn\text{-}pytz)n](PF_6)_2$ complexes (n =1, 2, 3)

Complex	HOMO /eV	LUMO /eV	ΔE/eV
$[Os(bpy)_2(Bn\text{-}pytz)](PF_6)_2$	-6.20	-2.67	3.53
cis-cis-$[Os(bpy)(Bn\text{-}pytz)_2](PF_6)_2$	-6.18	-2.57	3.61
cis-trans-$[Os(bpy)(Bn\text{-}pytz)_2](PF_6)_2$	-6.18	-2.53	3.65
trans-cis-$[Os(bpy)(Bn\text{-}pytz)_2](PF_6)_2$	-6.19	-2.60	3.59
mer-$[Os(Bn\text{-}pytz)_3](PF_6)_2$	-6.17	-2.22	3.95
fac-$[Os(Bn\text{-}pytz)_3](PF_6)_2$	-6.17	-2.21	3.96
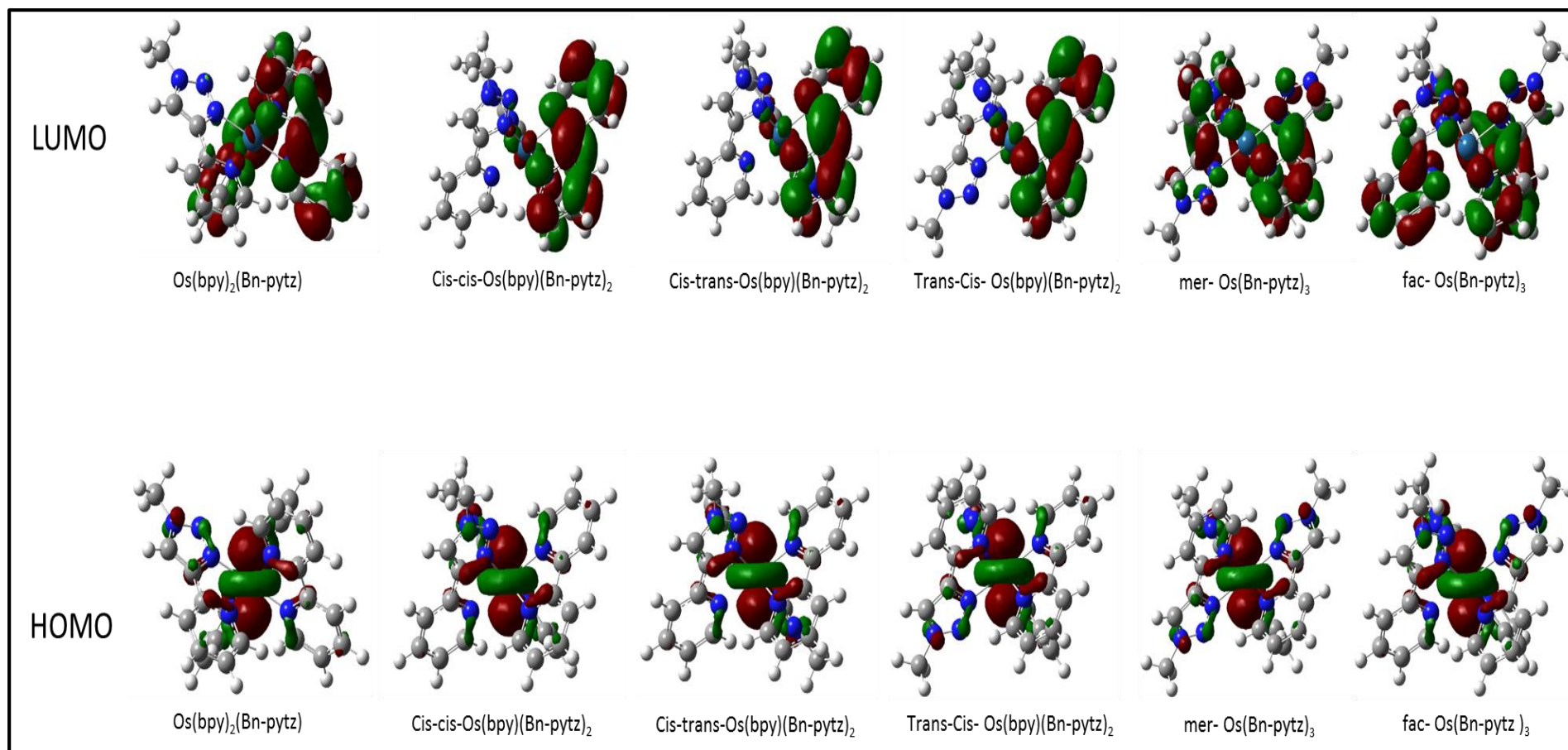
Figure 3-13: HOMO (bottom) and LUMO (top) orbital representations for complexes in the singlet ground-state in acetonitrile (PCM)
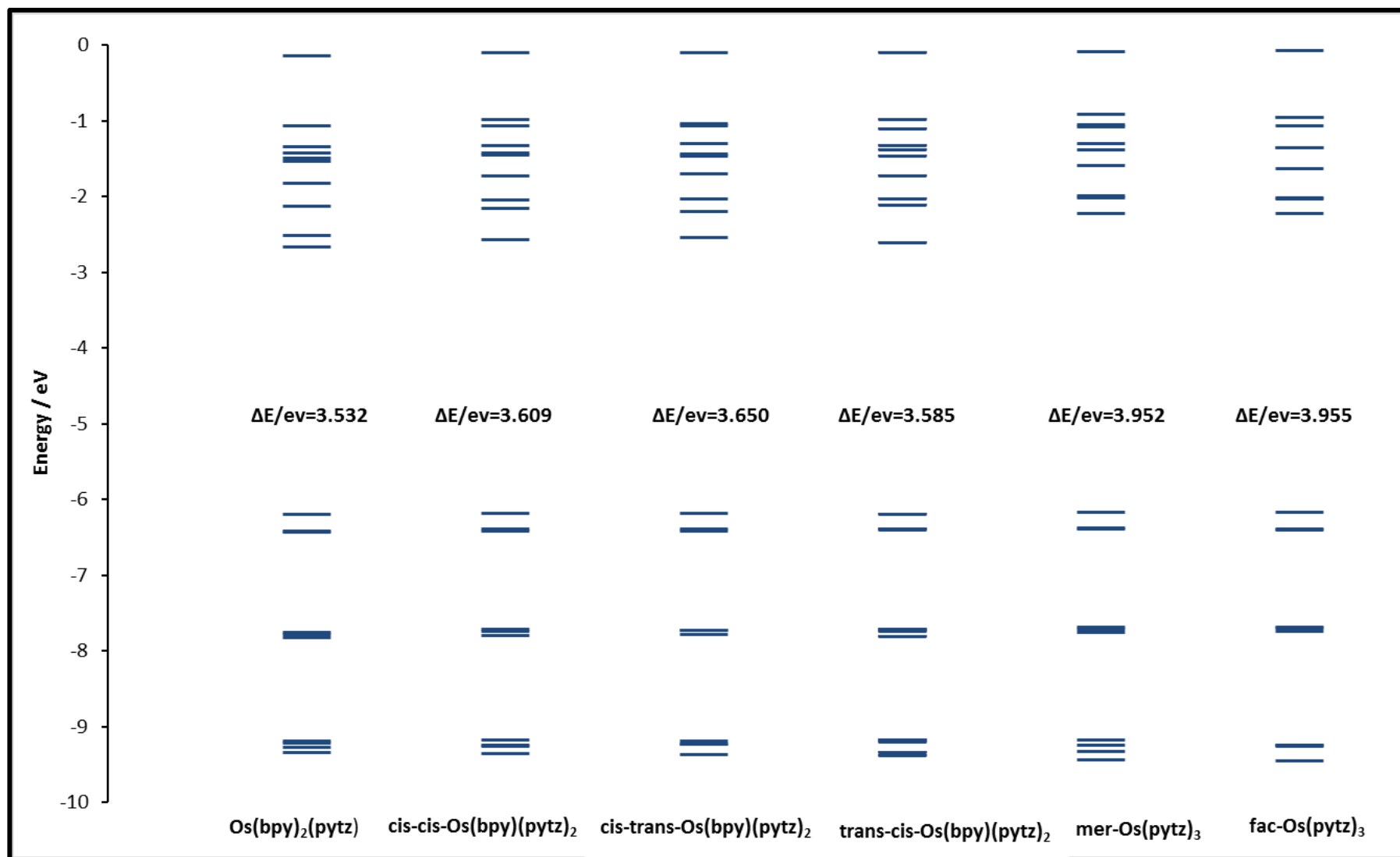
Figure 3-14: Molecular orbital energy level diagram of complexes (PCM, acetonitrile)

3.6.2 Time dependent DFT (TDDFT) Calculations

To confirm the interpretation of the photophysical results, time-dependent density functional theory calculations performed to determine the absorption spectra of the complexes. In general the calculated absorption spectra from time-dependent DFT calculations are in good agreement with experimental spectra. Figure 3.15 shows comparison of calculated vertical excitations and experimental spectra for complexes. In the UV region at 290 nm transitions can be safely assigned to intraligand $\pi \rightarrow \pi^*$ transitions. Furthermore, all of the complexes presented here had absorptions at the low-energy between 370 nm to 500 nm. These mainly originate from HOMO-2/HOMO to LUMO/LUMO+1 based transitions and are assigned to metal-to-ligand charge transfer from an Os d orbital to bpy-π^* for the bpy-containing complexes. For [Os(Bn-pytz)$_3$](PF$_6$)$_2$ the LUMO is predominantly distributed over the pyridine rings of the three pytz ligands and is destabilised by approximately 0.42 eV compare to that of [Os(bpy)$_2$(Bn-pytz)](PF$_6$)$_2$ complex indicative of the significantly higher energy LUMO of the pytz ligand compared to bpy. Consequently the lowest energy transisions are distablishied and blue shefted relative to [Os(bpy)$_2$(Bn-pytz)](PF$_6$)$_2$.
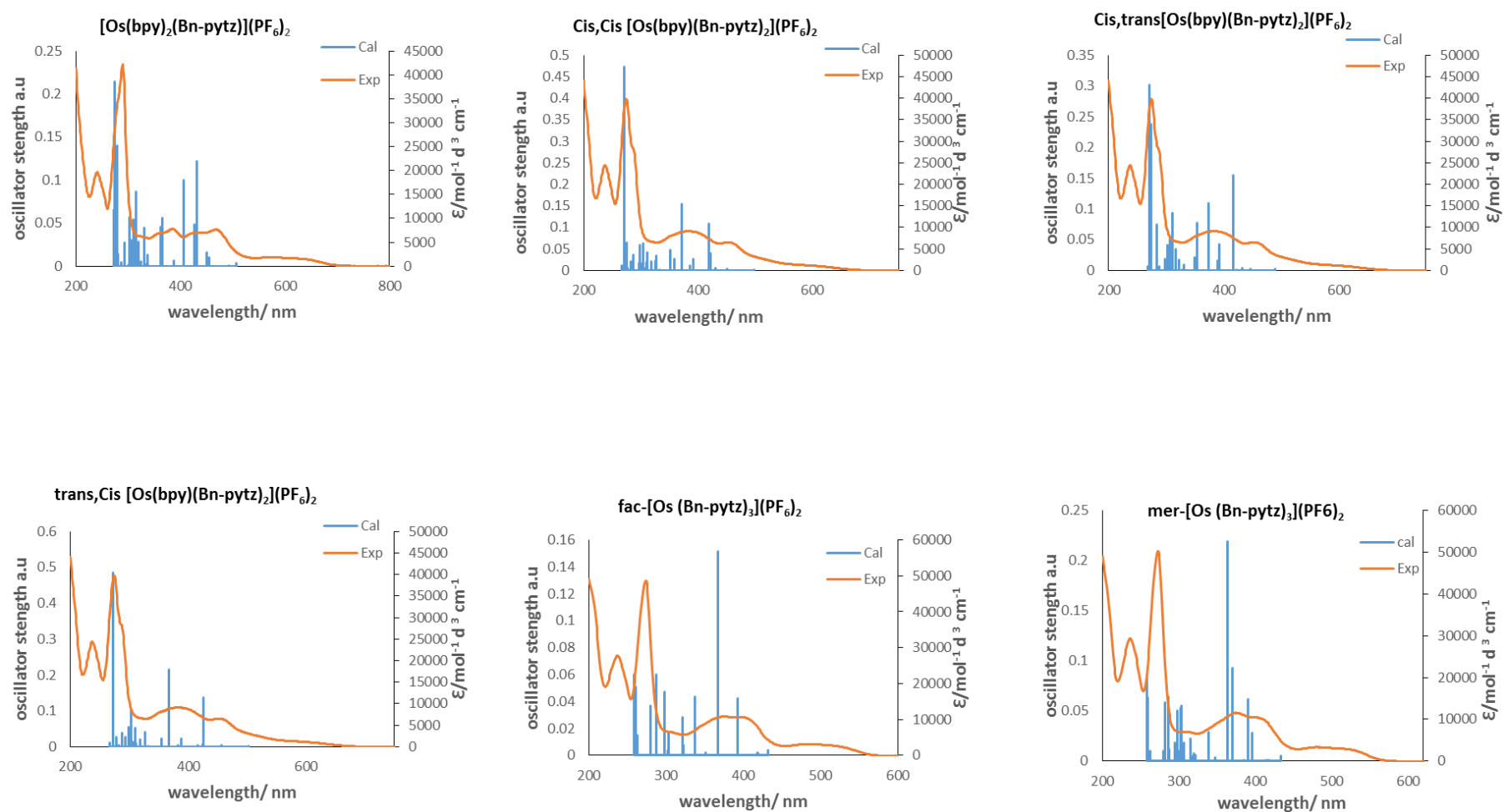
Figure 3-15 Calculated TDDFT optical absorption spectra for complexes overlaid with experimental UV-Visible absorption data in acetonitrile (PCM)

3.7   Cellular uptake and imaging microscopy studies

Based on the promising photophysical data described above, the water soluble chloride form of the complexes were subjected to preliminary cellular uptake and luminescence imaging microscopy studies in collaboration with Luke K. McKenzie, Dr Helen E. Bryant, and Professor Julia A. Weinstein at the University of Sheffield. The results from these studies show that complexes are successfully taken up by two cancer cell lines HeLa (human cervical cancer) and EJ (bladder carcinoma). Figure 3.16 shows the MTT assay results for dark toxicity of the complexes as well as preliminary PDT toxicity results. The results indicate that the complexes have relatively low dark toxicity in both cell lines, however, a relative cell survival of ~80 % is observed for $[Os(Bn-pytz)_3]^{2+}$ in the bladder carcinoma cell line at a relatively concentration of 100 µM.
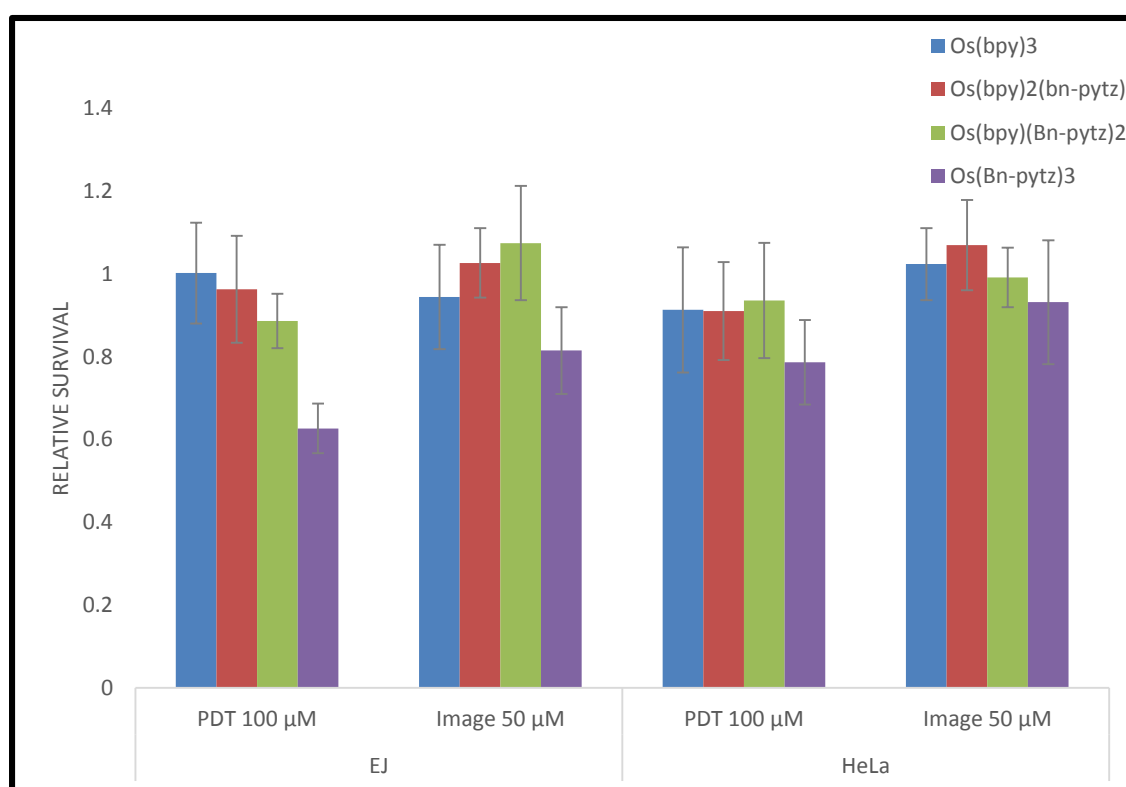
Figure 3-16 MTT assays and PDT toxicity and dark toxicity imaging samples for complexes **1** to **4** with EJ bladder carcinoma and HeLa cell lines.

Confocal imaging microscopy studies demonstrate that the two complexes $[Os(bpy)_3]^{2+}$ and $[Os(bpy)_2(Bn\text{-}pytz)]^{2+}$ did not go in cells at any appreciable degree. The complex $[Os(bpy)(Bn\text{-}pytz)_2]^{2+}$ does enter cells but $[Os(Bn\text{-}pytz)_3]^{2+}$ is the only one to go into cells to any appreciable degree, with the bright emission which can be seen by confocal microscopy. This could therefore explain the higher toxicity of the latter observed in the MTT assays. Confocal images for various incubations periods for $[Os(Bn\text{-}pytz)_3]^{2+}$ in both cell lines are presented in Figure 3-17. Colocalisation studies were hampered by overlap of the ^{3}MLCT/ ^{1}MLCT bands with those of Mito tracker dye used, but the complex $[Os(Bn\text{-}pytz)_3]^{2+}$ appears to localise at lysosomes, despite the high singlet oxygen quantum yields for these complexes, no significant photo-cytotoxicity is observed indicative that $[Os(Bn\text{-}pytz)_3]^{2+}$ is a poor PDT agent. This possibly stems from the envelopment of the complex within a biological molecular mating which excludes it from local O_2 thereby preventing $^1O_2$ generation. The complexes presented here therefore provide an excellent platform for the development of luminescent cellular imaging agents. This results indicate that the triazoles really help cell uptake and might be a good future design strategy. Beyond application in biological imaging, the complexes and modified derivatives may also offer probable applications as phosphors for deep-red/near-IR light emitting devices.[120]

Os(Bn-pytz)₃ 20 uM 6 hours excitation 543 emission 565-615

Os(Bn-pytz)₃ 10 uM 6 hours excitation 543 emission 565-615

Os(Bn-pytz)₃ 10 uM 24 hours excitation 543 emission 565-615
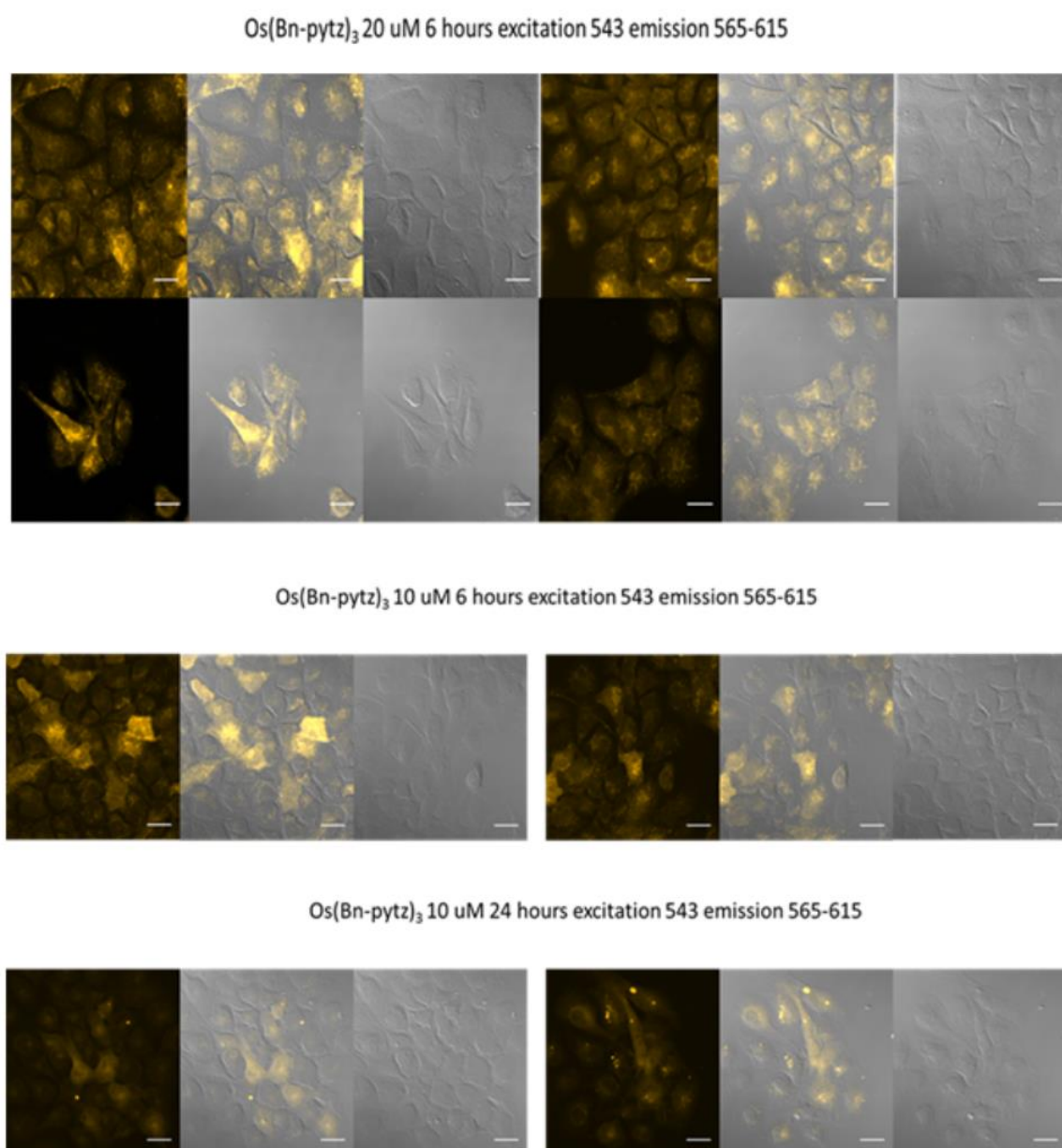
Figure 3-17- Confocal images of complex [Os(Bn-pytz)₃][Cl], following 4 h incubation Both cell lines HeLa (human cervical cancer) (left) and EJ (bladder carcinoma) (right) cells co-localised with central overlaid image, scale bars 20 µm.

Left hand pane = luminescence imaging. Right hand pane = bright field imaging. Middle pane = merger of these two.

130

3.8 **Conclusions:**

In this chapter, a series of heteroleptic osmium(II) Bn-pytz complexes [Os(bpy)$_2$(Bn-pytz)]$^{2+}$ and [Os(bpy)(Bn-pytz)$_2$]$^{2+}$and homoleptic osmium(II) complexes [Os(bpy)$_3$]$^{2+}$ and [Os(Bn-pytz)$_3$]$^{2+}$ were successfully synthesized in good to yields (60%-70%). The resulting osmium(II) complexes were characterized by ^{1}H and ^{13}C NMR spectroscopy, and mass spectroscopy HR-ESI-MS. The photophysical properties of these systems were investigated by UV-VIS, emission and lifetime spectrometry. All the complexes display ^{3}MLCT emission, that blue-shift as a result of replacing bpy with Bn-pytz. The blue-shift in electronic absorption and luminescence spectra of the resulting complexes indicative of the Bn-pytz ligands having a higher energy LUMO than bpy. In the presence of oxygen one of the complexes [Os(Bn-pytz)$_3$](PF$_6$)$_2$ was shown to display significant quenching of luminescence intensity, presenting the possibility of applying complexes based on [Os(bn-pytz)$_3$]$^{2+}$ as potential ^{1}O$_2$ sensitizers for photodynamic therapeutic applications. The increased celluler uptake of the complex [Os(Bn-pytz)$_3$]$^{2+}$, which is the only one to go into cells, localises at lysosomes, could be due to the increased the lipophilicity of the benzyl side chains; however, no PDT activity is observed. This result indicates that the triazoles help cellular uptake and they might be a good future design strategy. The use of CuAAC coupling reaction in the ligand preparation opens up various ways for tailored derivitisation and bioconjugation that would enable the optimisation of cellular uptake and a wider scope for organelle targeting within cells. I would like to thank Luke K. McKenzie, Dr Helen E. Bryant, and Professor Julia A. Weinstein University of Sheffield, for the collaborative biological studies reported in this chapter.

Chapter 4: Synthesis, characterisation and cellular system of a osmium (II) 2,6-bis(1-phenyl-1H-1,2,3-triazol-4-yl)pyridine, (btzpy) complex

4.1 **Introduction**

Photodynamic Therapy (PDT)

Photodynamic therapy (PDT) is a technique that uses light to activate an otherwise nontoxic drug, often referred to as a photosensitizer (PS), generally in the presence of oxygen.[219] PDT involves irradiation of a tissue-bound photosensitizer which goes to its triplet excited state and generates, upon energy transfer to oxygen, the cytotoxic singlet oxygen ($^1O_2$) resulting in cell necrosis.[220] This techniques advantage over other available therapies comes from its inherent ability to induce highly localized cytotoxicity in the targeted tissues when light activated. In terms of definition, photosensitizers are light-sensitive compounds which are able to absorb light-specific wavelengths (chromophores) and convert it into useful energy leading to the formation of singlet oxygen, which produces peroxidative reactions that can cause cell damage and death.[221] Consequently, unwanted cells can be effectively removed while incurring little to no damage on the surrounding tissue. It is generally accepted that a good photodynamic therapy PS should: (i) be known composition, chemically pure, with good stabilization, (ii) be collected preferentially and kept by target tumor tissue, (iii) be cytotoxic only upon photoactivation, and have minimal toxicity in the dark, (iv) have high quantum yield of $^1O_2$ and (v) have high absorbance and high molar extinction coefficient, particularly in the red and near IR spectral regions (600–800 nm). This last property is related with light penetration into the tissues, which is associated with the wavelength; for example, the light depth penetration at $\lambda = 500 - 600$ nm is about 4 mm, while in the range 600-800 nm it is about 8 mm.[222] Over the last 40 years, transition metal-based coordination compounds have been investigated for their therapeutic properties in several fields of medicine. Among others, a major advantage of metal-based drugs over the more common organic therapeutic agents is the ease at which changes in the chemical and physical properties of the drug can be brought about by modifying ligands in the

coordination sphere.[51] In recent years, transition metal-based drugs have played a particularly important role in the clinical treatment of cancer.[223, 224] many complexes exhibit luminescent emission which presents the potential for use as imaging agents, since phosphorescence is longer-lived than the autofluorescence from biological organic compounds.[15] While direct population of the low-lying ^{3}MLCT state is spin-forbidden and rarely observed in metal complexes.[225] These spin-forbidden transitions are more common in osmium complexes due to an increase in spin orbit coupling.[205, 206, 226] Consequently, Os(II) complexes often exhibit absorbance well into the red and occasionally, near-IR region.[227] All of these combined properties present considerable opportunities for the development of unique dual-mode theranostic agents. This chapter will explore the use of the 2,6-bis(1-phenyl-1,2,3-triazol-4-yl)pyridine (ptzpy) ligand as a tridentate donor ligand to investigate the influence of (N^N^N) ligands on photophysical characteristics of an osmium(II) complex compared with terpy derivatives. We report the synthesis of the orange-emissive bis(terdentate) osmium(II) complex [Os(btzpy)$_2$]$^{2+}$ as its hexafluorophosphate and chloride salts. The water soluble chloride salt of the osmium(II) complex was subject to preliminary cellular uptake and luminescence imaging studies and the data were also reported. The results in this chapter have been published.[228]

4.2 **Synthesis and characterisation**

4.2.1 **Synthesis of Ligand**

The synthesis of the btzpy ligand is discussed in Chapter 2

4.2.1.1 Synthesis of **4'-(p-tolyl)-2,2':6',2''-terpyridine**

The ligand 4'-(p-tolyl)-2,2':6',2''-terpyridine was synthesized as follow.[229] At room temperature, the reaction of 2-acetylpyridine and 4-methylbenzaldheyde was performed in ethanol under basic reaction conditions to afford a white solid (Scheme 4.1). The off-white solid was collected by filtration and washed with ice-cold EtOH. Recrystallisation from EtOH afforded a white crystalline solid. The ^{1}H NMR spectra was in agreement with a literature data.[229]
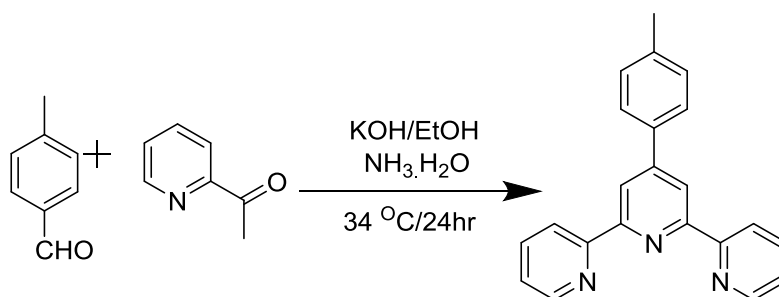
Scheme 4-1 - Synthesis of 4'-(p-tolyl)-2,2':6',2''-terpyridine

The tridenate ligands 4'-(p-tolyl)-2,2':6',2''-terpyridine was fully characterised by ^{1}H and ^{13}C NMR spectroscopy and mass spectrometry. The ^{1}H NMR spectrum of 4'-(p-tolyl)-2,2':6',2''-terpyridine (Figure 4.1) shows pyridyl protons in the range of δ 8.74-7.26. The proton signals were fully assigned by using ^{1}H-^{1}H correlation (COSY) spectroscopy the methyl group gives a singlet resonance at δ 2.42 of the methyl protons (Figure 4.2) The ESI mass spectrum of 4'-(p-tolyl)-2,2':6',2''-terpyridine shows a peak at m/z = 323.1428 assignable to the species (M^{2+}).
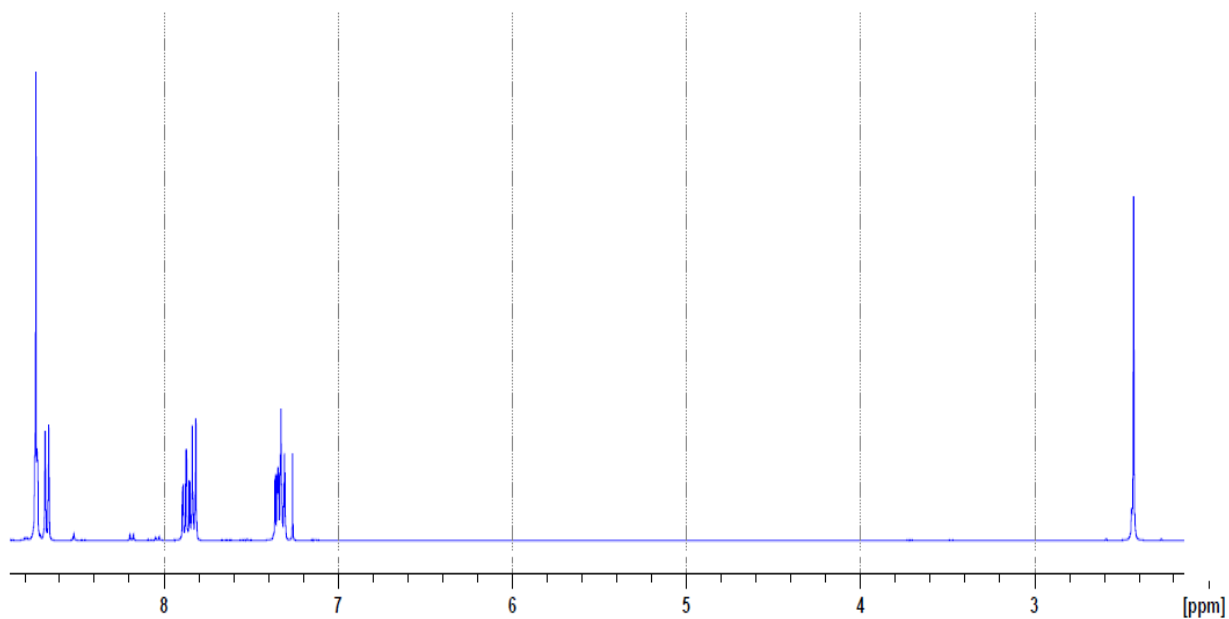
Figure 4-1- The ^{1}H-NMR spectrum (400 MHz, CDCl$_3$) of free ligand 4'-(p-tolyl)-2,2':6',2"-terpyridine
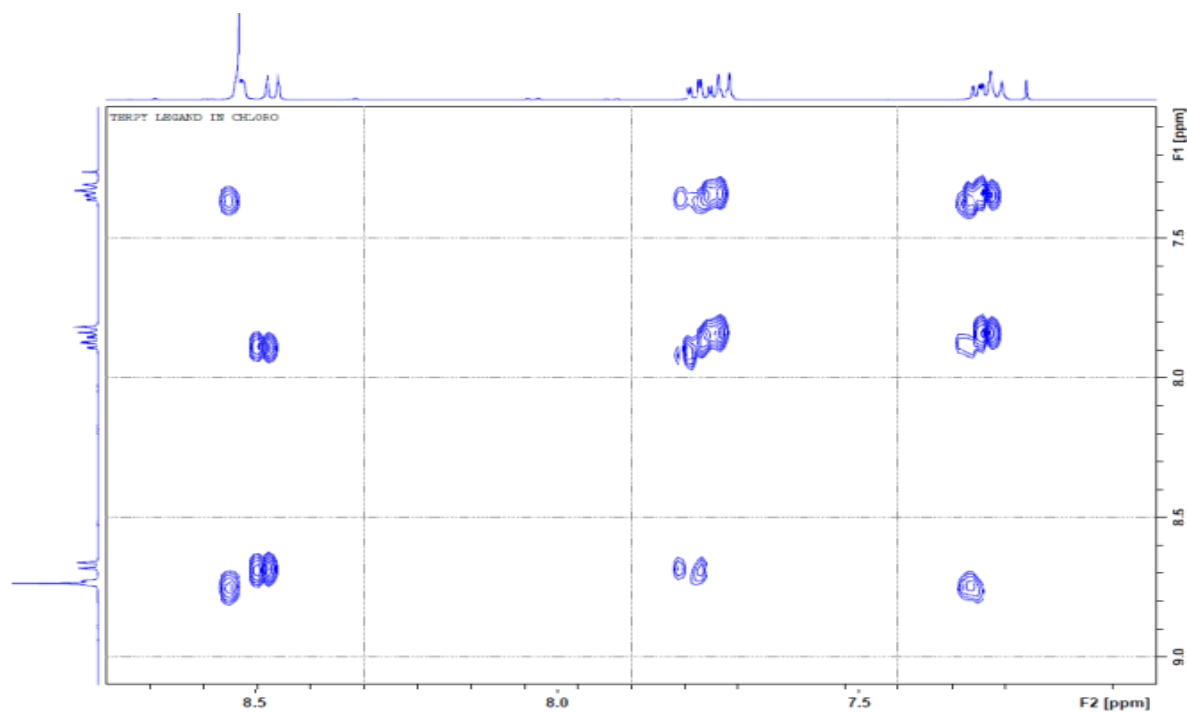
Figure 4-2- The ^{1}H-^{1}H COSY spectrum (400 MHz, CDCl$_3$) of free ligand 4'-(p-tolyl)-2,2':6',2"-terpyridine

4.2.2 Synthesis of osmium (II) complexes

4.2.2.1 Synthesis of [Os(toltpy)₂](PF₆)₂

The complex [Os(toltpy)$_2$](PF$_6$)$_2$ was prepared by reaction of (NH$_4$)$_2$[OsCl$_6$] with two equivalents of 4'-(p-tolyl)-2,2':6',2''-terpyridine in ethylene glycol under refluxing conditions followed by counter-ion metathesis and was isolated in the solid state as its hexafluorophosphate salt.
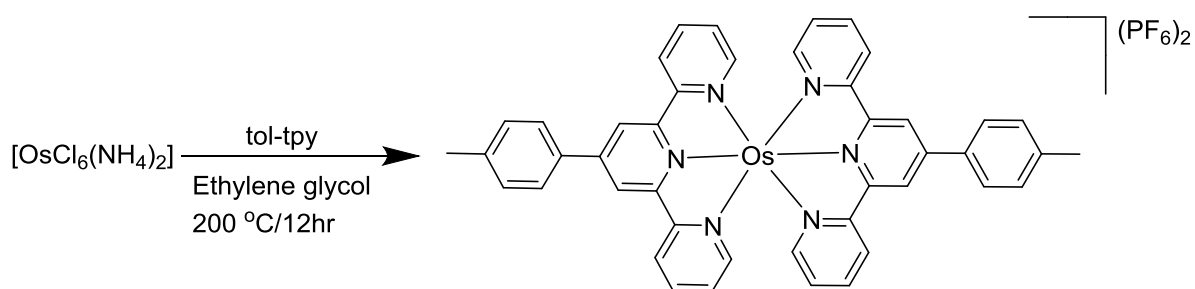
Scheme 4-2 Synthesis of [Os(toltpy)$_2$](PF$_6$)$_2$

Due to the symmetry of the (toltpy) ligands the ^{1}H NMR spectrum of the product (Figure 4.3) shows 7 aromatic signals in the range of δ 9.01-7.10 The spectrum is completed by one singlet at δ 2.57 coresponding to the methyl protons The ESI mass spectrum of the complex shows a peak at m/z = 419.1238 assignable to the species M^{2+}.
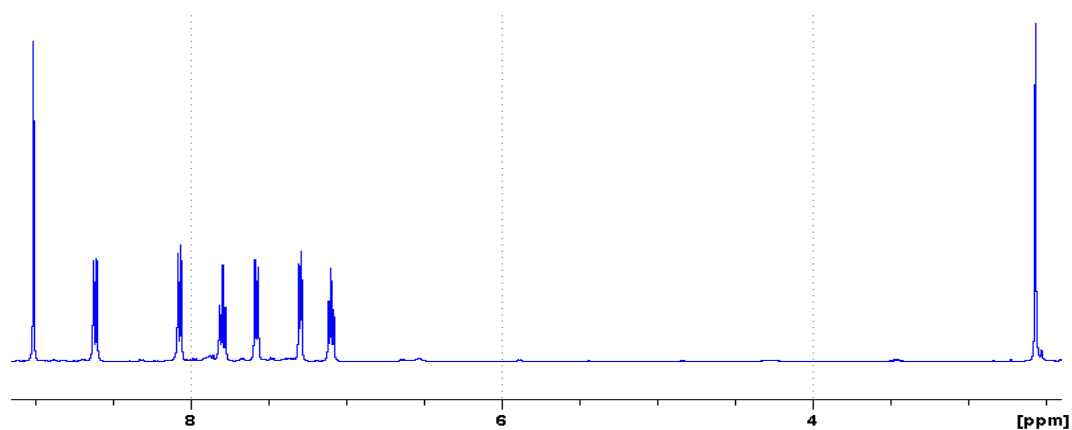
Figure 4-3- The ^{1}H-NMR spectrum (400 MHz, CD₃CN) of [Os(toltpy)$_2$](PF$_6$)$_2$

4.2.2.2 Synthesis of [Os(btzpy)₂](PF6)₂

The complex $[Os(btzpy)_2](PF_6)_2$ was prepared by reaction of $(NH_4)_2[OsCl_6]$ with two equivalents of ligand btzpy in ethylene glycol under refluxing conditions followed by counter-ion metathesis. The complex was isolated in the solid state as its hexafluorophosphate salt then redissolved in acetonitrile. The acetonitrile solution was cooled in the fridge overnight and filtered and the filtrate recrystallized on addition of diethyl ether to remove unwanted ligand.
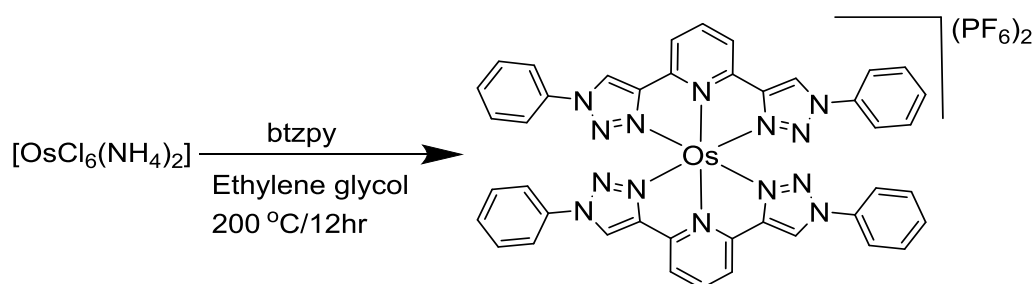
Scheme 4-3 Synthesis of $[Os(btzpy)_2](PF_6)_2$

Due to the a symmetry of the btzpy ligands the ^1H NMR spectrum (Figure 4.4) of the product shows one singlet resonance at δ 9.13 for the triazole ring protons which is shifted by 0.86 ppm relative to the corresponding resonance for the free ligand (δ 8.97). The ESI mass spectrum of the complex shows a peak at *m/z*= 461.1192 assignable to the species $[Os(btzpy)_2]^{2+}$.

138
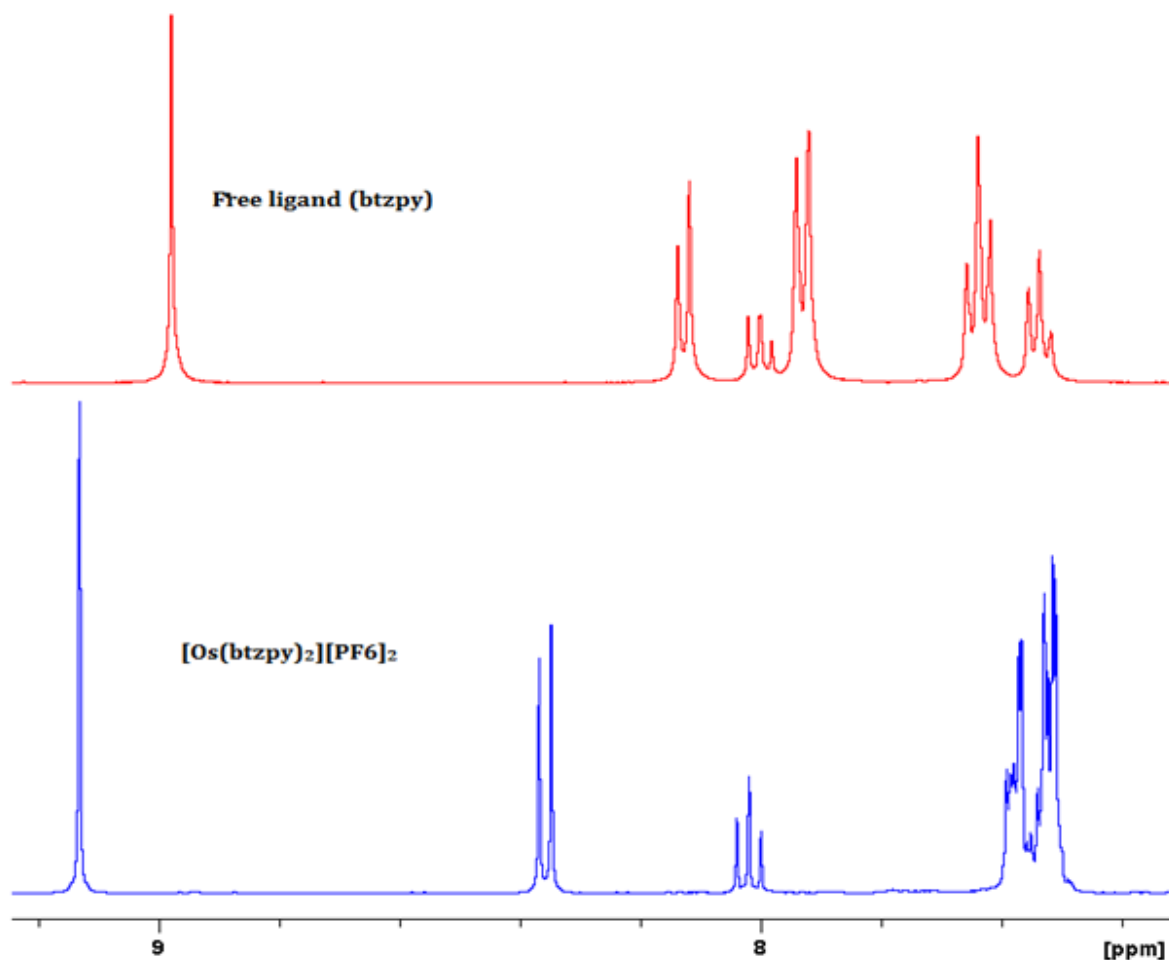
Figure 4-4-The ^{1}H-NMR spectra (400 MHz, CD$_3$CN) for free ligand btzpy and [Os(btzpy)$_2$](PF$_6$)$_2$

The chloride salt of the [Os(btzpy)$_2$]$^{2+}$complex which is soluble in water is obtained by stirring the PF$_6^-$ salt in methanol with Amberlite IRA-400 (chloride form) anion-exchange resin. The resultant solution was then filtered and evaporated, taken up into water and freeze dried. The successful counter ion metathesis and formation of chloride salt was confirmed by the complete absence of resonance for the PF$_6^-$ anion in its ^{19}F and ^{31}P NMR spectra. The chloride salt was then characterized by ^{1}H-NMR, UV/vis absorption and emission spectroscopy.

4.3 Electrochemical Properties of complexes

The electrochemical properties of the complexes have been investigated by cyclic voltammetry. The measurements were performed using acetonitrile distilled over calcium

hydride with 0.2 M [NBu$_4$][PF$_6$] as supporting electrolyte at room temperature. Ferrocene was added at the end of each experiment as an internal reference, and all redox potentials are quoted vs. the ferrocene-ferrocenium couple (Fc / Fc $^+$ = 0.0 V). The measurements were carried out in the region from +1.5 to -2.0V with a scan rate of 100 mVs^{-1}. Electrochemical data for the various complexes as obtained by cyclic voltammetry are summarized in Table 4-1.

Table 4-1: Electrochemical data for the complexes in CH$_3$CN, 0.2 M [NBu$_4$] [PF$_6$], 100 mVs^{-1}, at room temperature

No	Complex	Reduction $_{E1/2}$ V vs. Fc$^+$/Fc	Oxidation E$_{pa}$ V vs. Fc$^+$/Fc
1	[Os(toltpy)$_2$](PF$_6$)$_2$	-1.87(0.086)[a], -1.605(0.075)[a]	0.487(0.1)[a]
2	[Os(btzpy)$_2$](PF$_6$)$_2$	===========[b]	0.633(0.1)[a]

E1/2= (Epa+ Epc)/ 2, Epc are anodic and cathodic peak potentials respectively. a = reversible.b = reduction coples are outside the available electrochemical window.

For complexes [Os(toltpy)$_2$](PF$_6$)$_2$ and [Os(btzpy)$_2$](PF$_6$)$_2$ the observed couples were all reversible. Figure 4.5 shows the cyclic voltammagrams of the complexes. The cyclic voltammograms of two complexes gave the Os$^{3+/2+}$ metal-based redox processes, which for the [Os(btzpy)$_2$]$^{2+}$ complex appears at +0.64 V (E$_{ox}$ vs Fc/Fc$^+$ = 0.0 V). This is close to that exhibited by the known model complex [Os(toltpy)$_2$](PF$_6$)$_2$ (E$_{ox}$ = +0.49 V) and other related osmium(II) complexes.[230, 231] Replacing (toltpy) with (btzpy) ligand caused changes to the reduction potantials which are significantly more to negative. Unlike in the CV trace for [Os(toltpy)$_2$]$^{2+}$, no ligand-based reductions are observed within the available electrochemical window (−2.0 to +1.5 V) for [Os(btzpy)$_2$]$^{2+}$, which is indicative of the higher energy lowest unoccupied molecular orbital localized on the btzpy ligand compared to that for the [Os(toltpy)$_2$]$^{2+}$. The latter complex gave two one electron terpyridine ligand based reduction

processes with $E_{1/2}$ values of -1.60 (mtpy$^{0/1-}$) and -1.87 (mtpy$^{1-/2-}$). This LUMO destabilisation is consistent with previously reported data of [Ru(toltpy)$_2$]$^{2+}$ versus the ruthenium(II) analogue [Ru(tpy)$_2$]$^{2+}$ (tpy = 2,2, :6 ,2,,-terpyridine based ligand).[232, 233] This strongly suggests that terpyridine is better acceptor than triazole and differences in the MLCT absorption and emission energies between the complexes are primarily due to differences in the energy of the π* level.
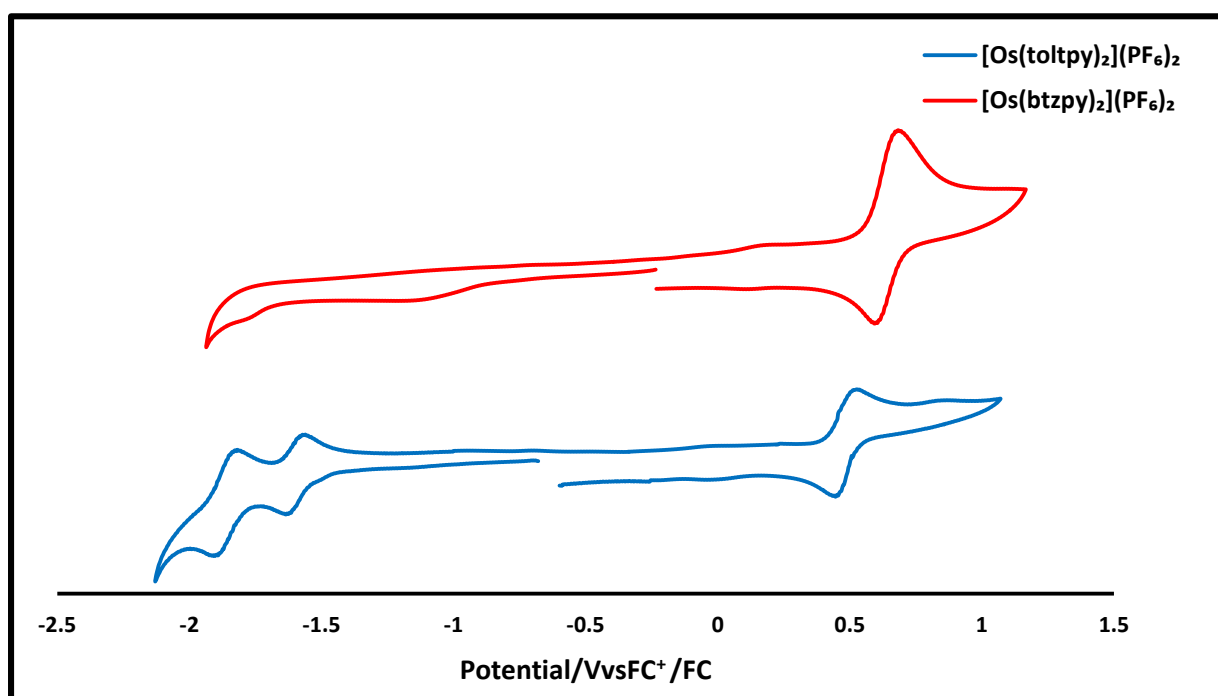
Figure 4-5- Cyclic voltammogram of complexes in CH$_3$CN /0.2 M NBu$_4$PF$_6$; scan rate (v) = 100 mV s^{-1}. Potentials V are reported against ferrocene (Fc$^+$/Fc = 0.0 V)

4.4 **Photophysical studies**

Table 4.2 summarizes the UV-vis electronic absorption data for the complexes, UV-Vis absorption spectra of the complexes, in MeCN are shown in Figure 4.6.

Table 4-2: The UV-VIS electronic absorption data for the complexes

Compound	λ / nm(ε/mol^{-1}dm^{3}cm^{-1})
[Os(toltpy)$_2$](PF$_6$)$_2$	286(48000), 314(54300), 406(7520), 491(19250), 645(4600), 669(5070),
[Os(btzpy)$_2$](PF$_6$)$_2$	288(49015), 297(68480), 337(13475), 382(19470), 434(5700), 526(3025)

The UV-vis absorption spectrum of [Os(toltpy)$_2$](PF$_6$)$_2$ in acetonitrile exhibits two intense bands at 286 nm and 314 nm ascribed to the ligand-centered (^{1}LC) $\pi \rightarrow \pi^*$ transitions. [Os(btzpy)$_2$](PF$_6$)$_2$ also has two intense bands at 239 nm and 297 nm and a shoulder at 285 nm similarly ascribed to the ligand-centred (^{1}LC) $\pi \rightarrow \pi^*$ transitions. Both complexes exhibit an intense absorption band in the visible region at 490 and 386 nm respectively assignable to the ^{1}MLCT d $\rightarrow \pi^*$ transitions, and a broad and weaker band at 668 nm for [Os(toltpy)$_2$](PF$_6$)$_2$ and 530 nm for [Os(btzpy)$_2$](PF$_6$)$_2$. These weaker and lower energy bands are assigned to spin-forbidden ^{3}MLCT transitions. The spin forbidden absorption populates the ^{3}MLCT directly from the ground state because of the large spin-orbital coupling that results from the heavy osmium atom.[214] Since the LUMO of the btzpy ligand is significantly destabilised relative to that of toltpy, the replacement of the ligands leads to shift of MLCT bands to the higher energy. This is analogous to the behavior observed with bidentate ligands when changing bpy in [Os(bpy)$_3$](PF$_6$)$_2$ to Bn-pytz in [Os(Bn-pytz)$_3$](PF$_6$) in Chapter 3.
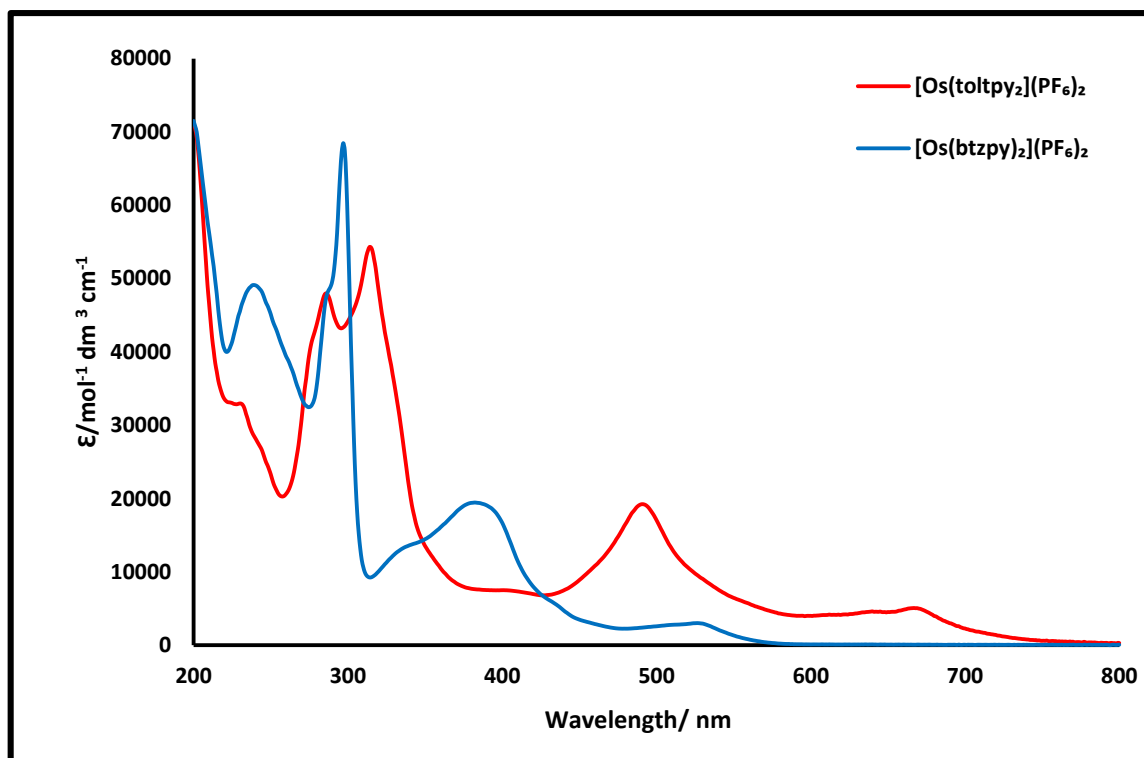
Figure 4-6- UV–visible absorption spectra of complexes in aerated acetonitrile at 295 K.

The photophysical emission data are summarized in Table 4-3. Both of the complexes exhibit a broad featureless emission band at room temperature in aerated solvent which is assigned to emission from a ^{3}MLCT state (Figure 4.7). For $[Os(btzpy)_2]^{2+}$ this band appears in the orange region of the spectrum ($\lambda_{max} = 595$ nm, Table 4-3) and is significantly blue-shifted relative to that of $[Os(toltpy)_2]^{2+}$ which is located in the red/near-infrared region of the spectrum ($\lambda_{max} = 738$ nm). [215]
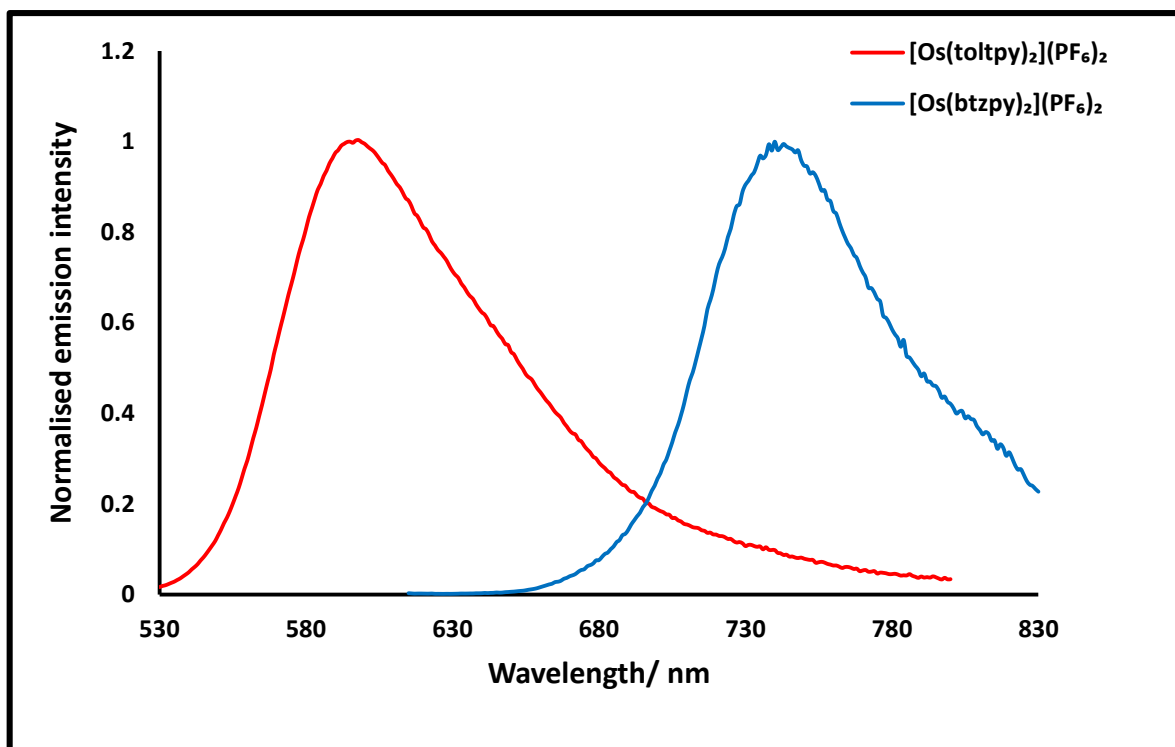
Figure 4-7- Emission spectra of the complexes in in aerated acetonitrile at room temperature

The emission spectrum was also recorded at 77 K in a 4:1 EtOH / MeOH glass matrix and shows structured emission bands. Due to rigidochromic effects, the position of the bands is blue-shifted by approximately 20-30 nm compared with the spectra recorded at room temperature. These observations are typical for metal-to-ligand charge transfer (MLCT) based emissions. Since the solvent molecules are frozen at 77 K and any stabilization of the charge transfer transitions involving the rearrangement of solvent and geometry relaxation for the complex can not occur and therefore the HOMO–LUMO gap is effectively increased. (Figure 4.8).

Table 4-3: photoluminescence data and lifetime for the complexes in aerated acetonitrile at room temperature and 77 K

Compound	At room temperature		At 77 K	ϕ^* %
	λ max (nm)	τ (ns)	λ max (nm)	
[Os(toltpy)$_2$](PF$_6$)$_2$	738	72	718,795	3.2
[Os(btzpy)$_2$](PF$_6$)$_2$	595	66	564,606	9.3

* **Relative to [Ru(bpy)₃](PF₆)₂ Φ= 0.018 in air**
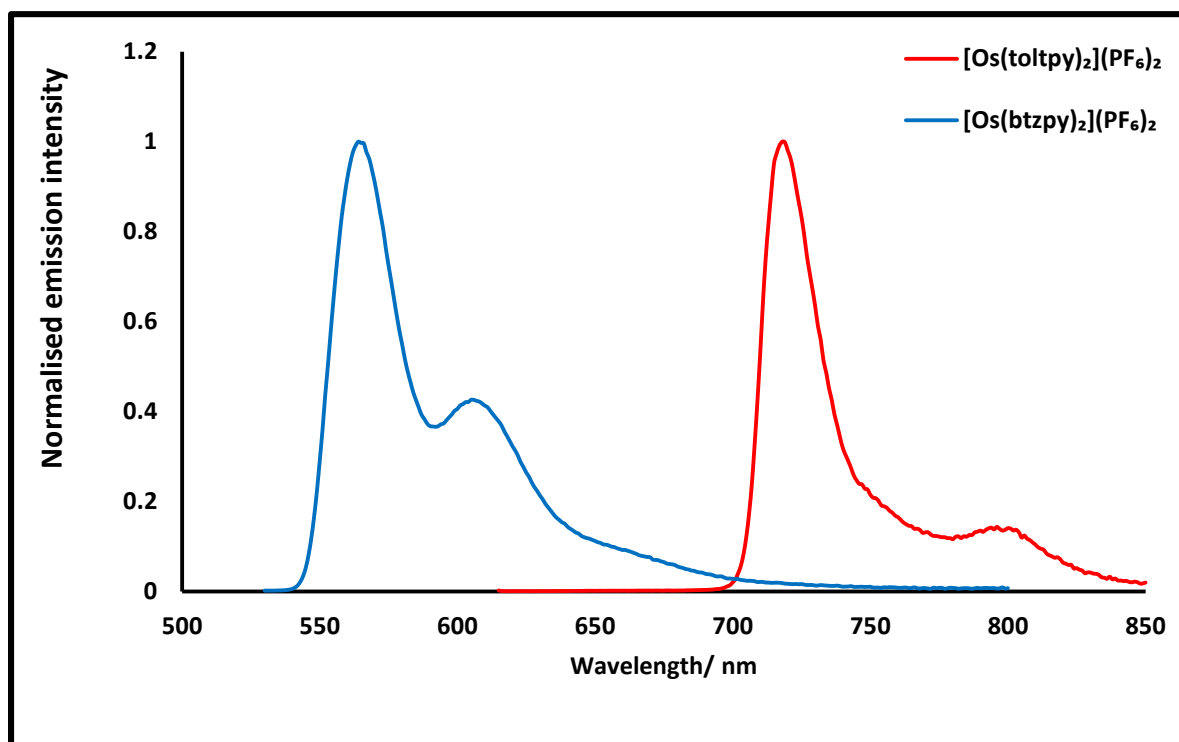
Figure 4-8- Emission spectra of the complexes in rigid matrix (4:1 EtOH/MeOH) at 77 K.

Changing the PF_6^- counter-ion to chloride appears to have no significant effect on the photophysical properties of these complexes as we can note from Figures 4.9-4.10 which respectively are show the visible absorption spectrum and the emission spectrum of the complexes as the chloride salts in water. The complexes are still emissive in water and the change in spectra is negligible when the solvent is changed from acetonitrile to water.

145
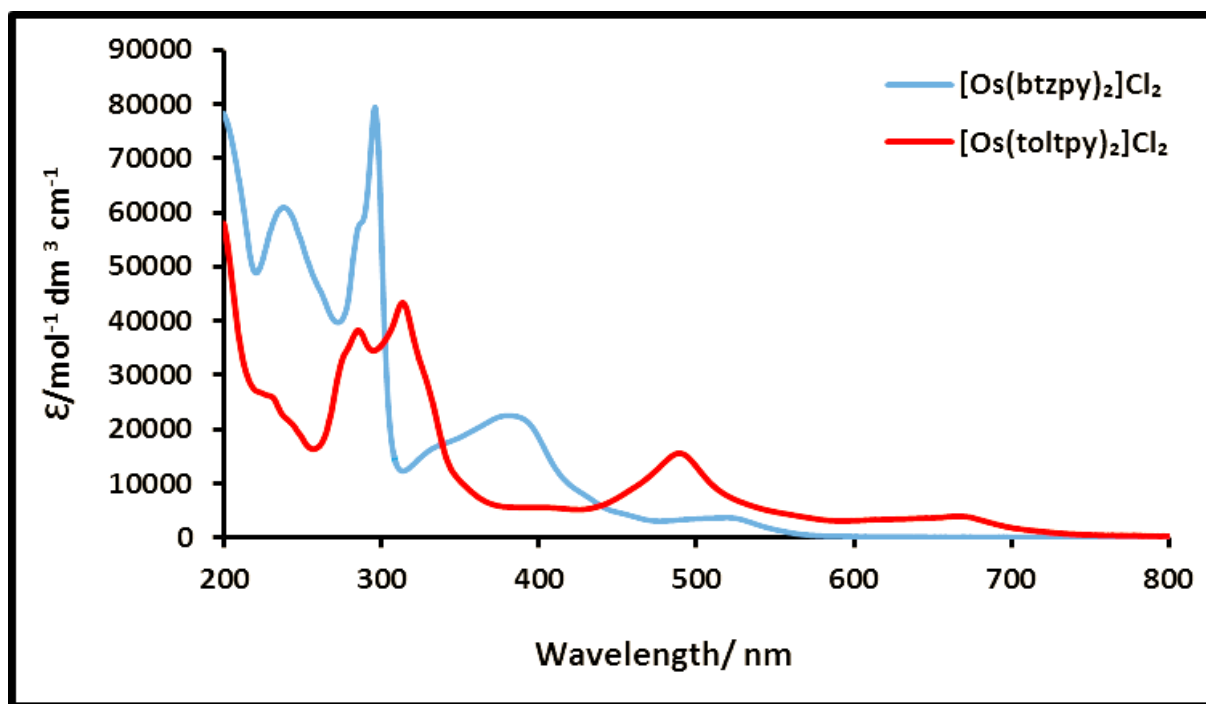
Figure 4-9-UV–visible absorption spectra of complexes as their chloride salts in water at 295 K.
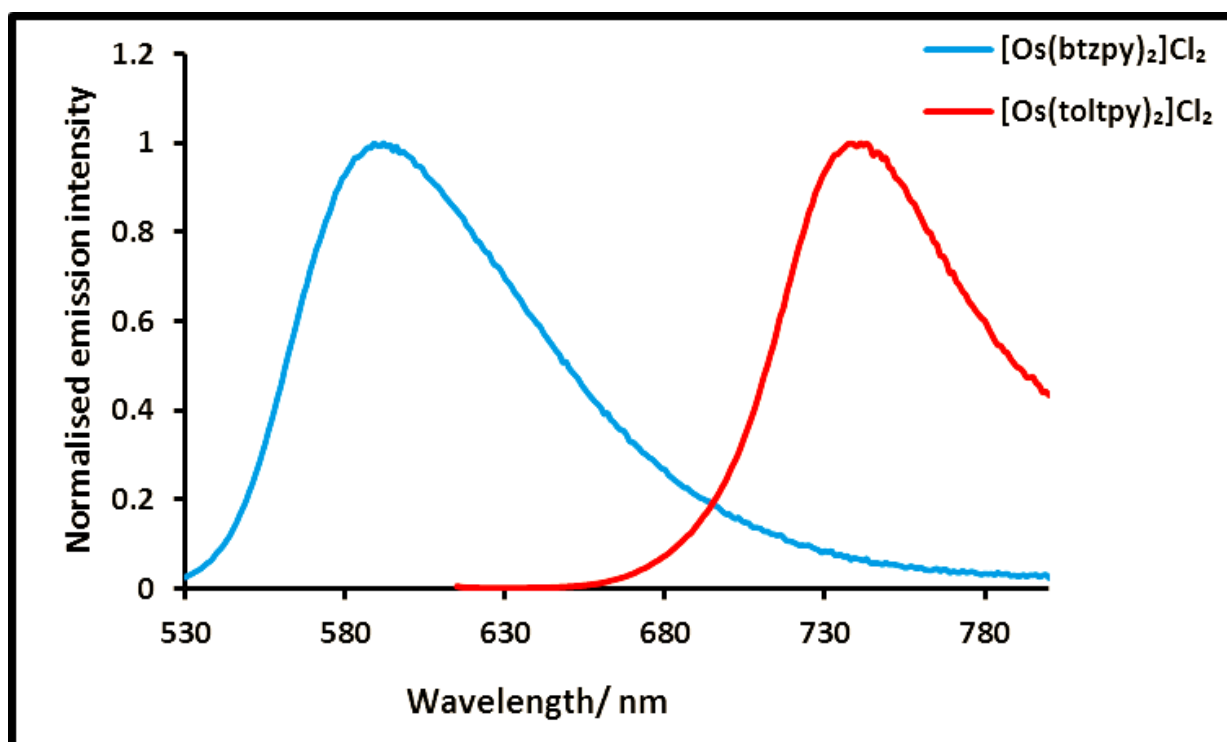
Figure 4-10- Emission spectra of the complexes as their chloride salts in water

4.5 **Luminescence Quenching by Oxygen**

Table 4-4 illustrates the life time of the complexes in the presence of different ratios of oxygen: Emission intensity from the $[Os(btzpy)_2]^{2+}$ complex is dramatically affected by the presence of oxygen (Figure 4.11). When recorded in air and compared to deaerated conditions, the emission intensity is quenched by approximately 43-fold. The responses of phosphorescence to molecular oxygen approximately obeyed Stern–Volmer relationships. As shown in Figure 4-11. This sensitivity to the presence of oxygen confirms the ^{3}MLCT character of the emissive state.[202] This significant quenching of emission by oxygen and the long lifetime of emission in deaerated solution thus presents the possibility of employing complexes based on $[Os(btzpy)_2]^{2+}$ as a potential $^1O_2$ sensitizer for photodynamic therapeutic applications.

Table 4-4: Life time (ns) of the complexes at different concentation of oxygen in acetonitrile:

compound	0 atm	0.21 atm	1.0 atm
$[Os(toltpy)_2](PF_6)_2$	339	72	22
$[Os(btzpy)_2](PF_6)_2$	937	66	12
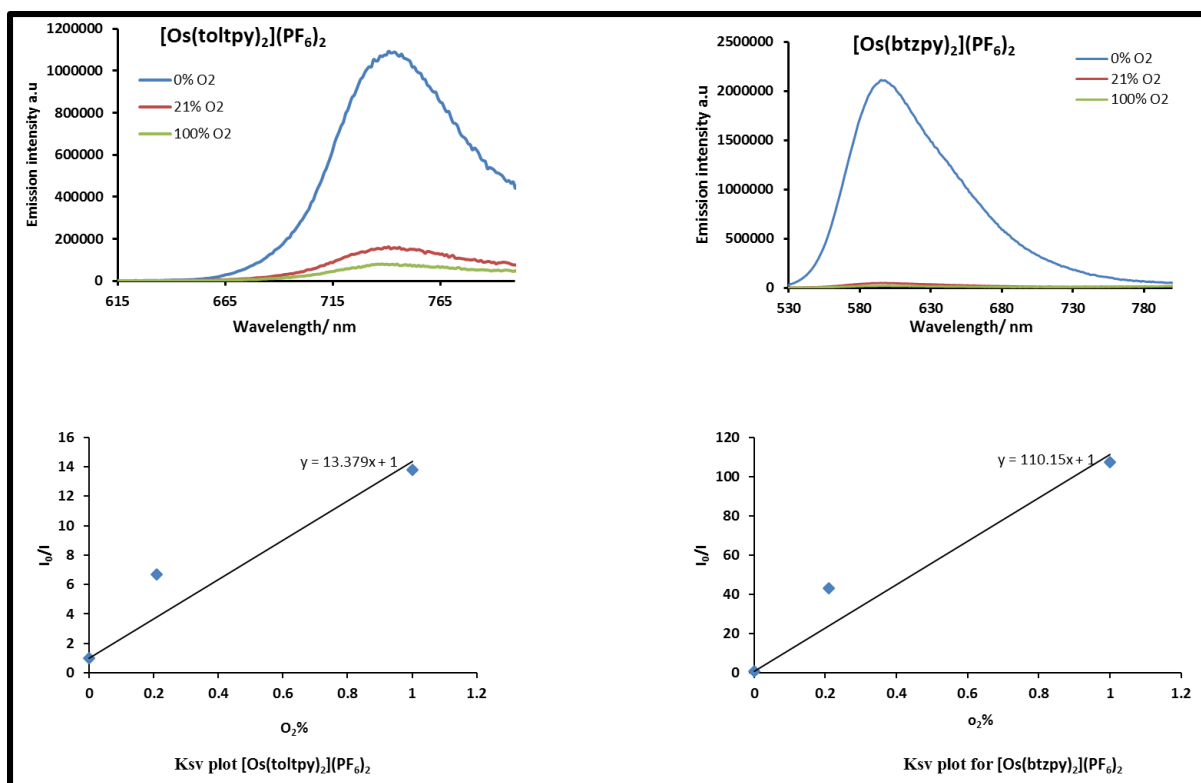
Figure 4-11- Emission response of complexes to varying $[O_2]$

Generally, as seen in Table 4-5, replacement of the (toltpy) ligand by (btzpy) gives more quenching efficiency. This means that $[Os(btzpy)_2]^{2+}$ is more potent for $^1O_2$ production than $[Os(toltpy)_2]^{2+}$ complexes indicated by the 10-fold increase in the K_{sv} cinstant for the complex.

Table 4-5: Ksv for complexes as hexafluorophosphate salt and quantum yield for $[Os(btzpy)_2]^{2+}$ complex as chloride salts

Compound	K_{sv} for PF_6^- form	$^1O_2$ quantum yield% for Cl^- form
$[Os(toltpy)_2]^{2+}$	13	
$[Os(btzpy)_2]^{2+}$	110	57

The singlet oxygen $^1O_2$ quantum yield was measured in collaboration with Luke K. McKenzie at University of Sheffield and is appreciably high and 57%.

4.6   **Density functional theory (DFT) studies**

In order to further understand the electronic transitions of the complex $[Os(btzpy)_2]^{2+}$ and validate the interpretation of the electrochemical and photophysical results density functional theory (DFT) studies were undertaken by Professor Paul Elliott and the result presented and discussed here.

4.6.1   **Ground state properties:**

Density functional theory (DFT) calculations were used to study the nature, localisation and relative energies of the frontier orbitals of complex $[Os(btzpy)_2]^{2+}$ and in addition to simulate the optical absorption spectrum. The geometry was obtained in the gas phase with the phenyl substituent replaced by methyl to reduce the computational cost. The data show that with a small contribution from the π-systems of the four triazole rings, the HOMO is localized primarily on the osmium(II) centre as expected (Figure 4.12 a). The LUMO is localised on one of the btzpy ligands, mainly on the central pyridine ring and with a minimal contribution from the triazole rings (Figure 4.12 b) but also a small metallic d-orbital contribution. In agreement with the experimental electrochemical data. The HOMO of $[Os(btzpy)_2]^{2+}$ is slightly stabilized (-10.63 eV) relative to that of $[Os(toltpy)_2]^{2+}$ (-10.35 eV). On the other hand the LUMO of $[Os(btzpy)_2]^{2+}$ (-6.95 eV) is significantly destabilized relative to that of $[Os(toltpy)_2]^{2+}$ (-7.32 eV) due to the presence of the electron rich triazole moieties and due to the smaller π-system associated with the btzpy ligand compared to toltpy. This results in a larger HOMO–LUMO gap for $[Os(btzpy)_2]^{2+}$ of 3.68 eV compared to that for $[Os(toltpy)_2]^{2+}$ (3.03 eV) reflecting the significantly blue shifted absorption and emission data (Table 4.6).

Table 4-6: Selected calculated energies of the HOMO and LUMO orbitals and the HOMO–LUMO gap ΔE of complexes

Complex	HOMO E/eV	LUMO E/eV	ΔE/eV
$[Os(toltpy)_2]^{2+}$	-10.35	-7.32	3.03
$[Os(btzpy)_2]^{2+}$	-10.63	-6.95	3.68
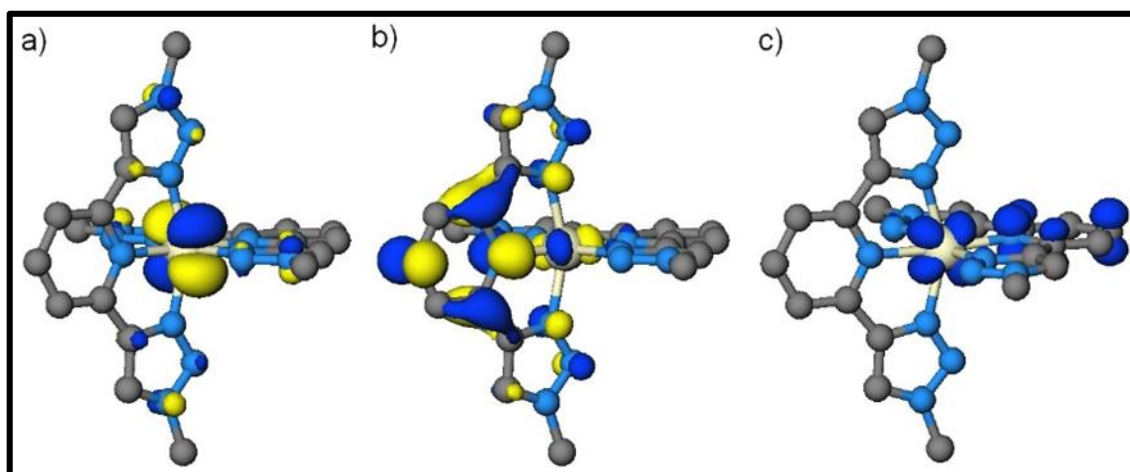
Figure 4-12- Plots of the HOMO (a) and LUMO (b) for the ground state and the spin density for the T1 state of $[Os(btzpy)_2]^{2+}$

4.6.2 Time dependent DFT (TDDFT) Calculations

To confirm the interpretation of the photophysical results, time-dependent density functional theory calculations were performed to determine the absorption spectrum of the complex $[Os(btzpy)_2]^{2+}$. The lowest energy 30 singlet state vertical excitations at the ground state geometry along with the lowest energy 10 spin-forbidden triplet excitations for complex $[Os(btzpy)_2]^{2+}$ were calculated . The data agree well with the experimental spectra but with a slight overestimation of the energies of transitions compared to bands in the UV-visible absorption spectrum. Figure 4.13 shows the comparison of calculated vertical excitations and experimental spectrum for the complex. From the Figure we can see that the two strongest simulated transition in the same places as the strongest bands in the experiments about the UV

region at 290 nm which can be safely assigned to intraligand $\pi \to \pi^*$ transitions. The S_{27} state which is primarily of HOMO-4 $\to$ LUMO ^{1}LC in character is calculated to have an energy of 4.53 eV (274 nm). The S_1 state which is primarily HOMO $\to$ LUMO ^{1}MLCT in character, calculated to have an energy of 2.74 eV (452 nm). The first transition of significant intensity (S_7, 374 nm) is consists of a HOMO $\to$ LUMO+2 transition and is similarly of ^{1}MLCT character confirming our experimental assignment of the band in this region of the UV-visible absorption spectrum. In agreement with the assignment of the lesser intensity absorptions between 450 and 550 nm as arising from spin-forbidden direct ^{3}MLCT transitions, the T_1 state is calculated to appear at 512 nm (2.42 eV) and is of mixed HOMO-2 $\to$ LUMO+1 and HOMO-1 $\to$ LUMO character. The optimization of the lowest lying triplet state of $[Os(btzpy)_2]^{2+}$ starting from the optimized ground state geometry is calculated to lie 2.40 eV the ground state. The spin density was plotted and is illustrated in Figure 4.12 c. It shows that the ^{3}MLCT character of this T_1 state is confirmed by unpaired electron density on both the metal and one of the btzpy ligands. Curiously, unlike in the case of $[Os(toltpy)_2]^{2+}$, the T_1 state of $[Os(btzpy)_2]^{2+}$ undergoes a puckering like distortion of the btzpy ligand in which the unpaired electron density is localized. Such distortions have been observed, however, in theoretical calculations of the T_1 states of $[Os(terpy)_2]^{2+}$[234] and bis(tridentate) ruthenium(II) cyclometalated complexes.[235]
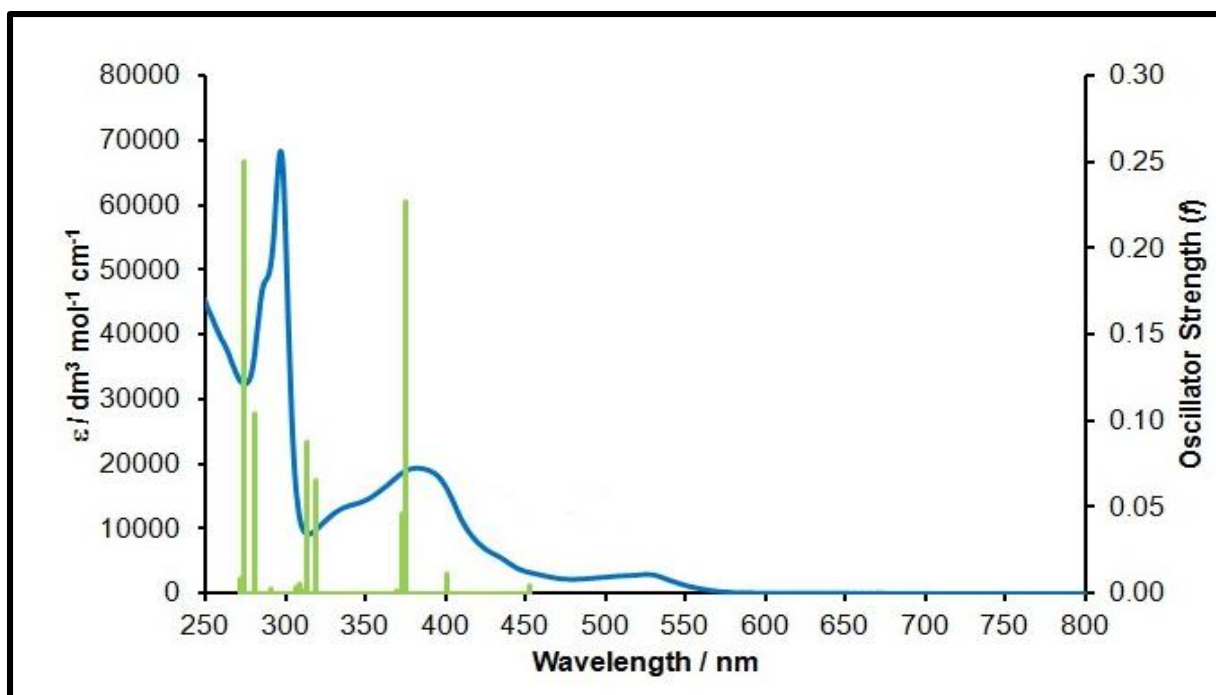
Figure 4-13- Calculated TDDFT optical absorption spectra for complexes overlaid with experimental UV-Visible absorption data in acetonitrile solution

4.7   Cellular uptake and imaging microscopy studies

Based on the encouraging photophysical data reported above, the water soluble chloride form of the complex $[Os(btzpy)_2]^{2+}$ was subjected to preliminary cellular uptake and luminescence imaging microscopy studies in collaboration with Luke K. McKenzie, Dr Helen E. Bryant, and Professor Julia A. Weinstein from the University of Sheffield. The results from these studies reveal that the complex is successfully taken up by two cancer cell lines, HeLa (cervical cancer) and U2OS (osteosarcoma) and shows mitochondrial localization. Following a short incubation time of 4 h and at concentrations as low as 1 µM colocalisation with the mitochondrial stain MitoView 633 with the bright emission was seen by confocal microscopy (Figure 4.14). Pearson's correlation coefficients of r = 0.7 and 0.85 for U2OS and HeLa cells respectively.
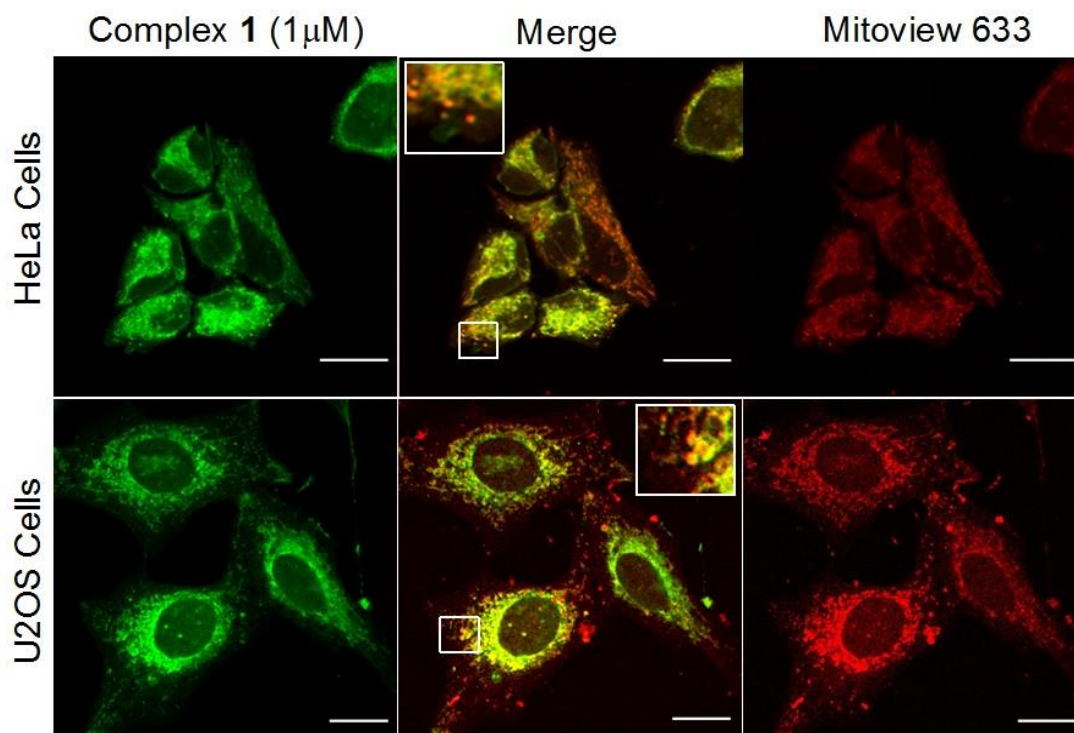
Figure 4-14 Confocal images of complex [Os(btzpy)$_2$] Cl$_2$ (green) following 4 h incubation in HeLa and U2OS cells co-localised with Mitoview 633 (red) with central overlaid image, scale bars 20 µm.[228]

Figure 4.15 shows the MTT assay results for dark toxicity of the complex as well as preliminary PDT toxicity results. The results indicate that the complex at a concentration effective for luminescence imaging microscopy the complex is non-cytotoxic, giving support to potential application as a PDT cellular imaging agent. Unfortunately, preliminary PDT studies revealed no significant photo-toxicity. This is again possibly due to the envelopment of the complex and exclusion for interaction with molecular oxygen.

153
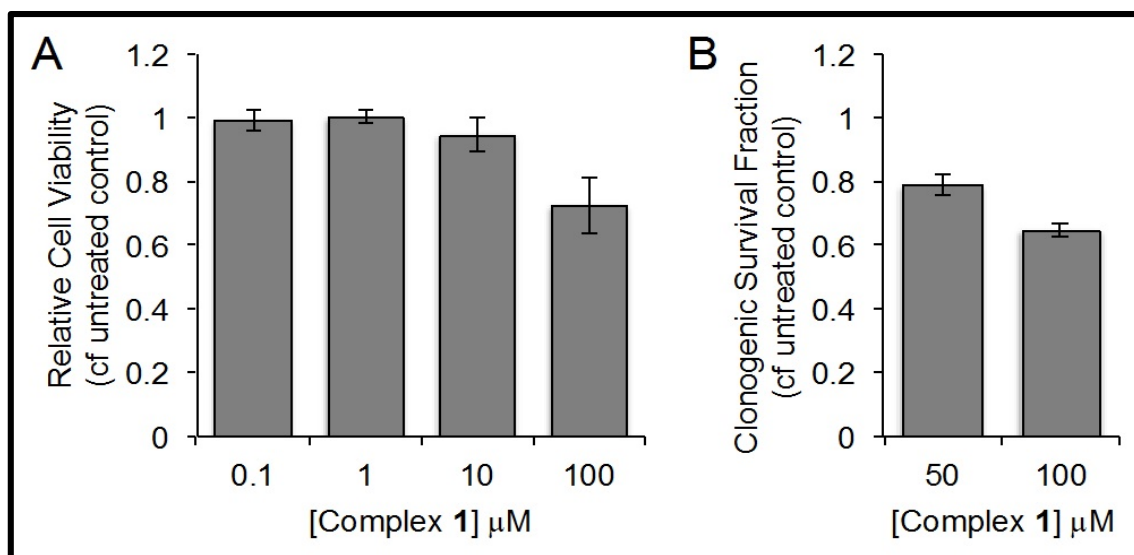
Figure 4-15 (A) MTT and (B) Clonogenic survival assays following incubation of HeLa cells with increasing concentrations of complex, [Os(btzpy)$_2$][Cl]$_2$ in the dark. In each case, mean and standard deviation of at least 3 independent repeats.[228]

4.8 Conclusions:

 In this chapter, two homoleptic osmium(II) complexes [Os(toltpy)$_2$]$^{2+}$, [Os(btzpy)$_2$]$^{2+}$ as tridentate osmium(II) complexes were successfully synthesized in good yields (60%-70%). The resulting osmium(II) complexes were characterized by ^{1}H and ^{13}C NMR spectroscopy, and mass spectroscopy HR-ESI-MS. The photophysical, properties of these systems were investigated by UV-vis, emission and their emissive lifetimes. A number of conclusions were reached concerning the photophysical properties of the emitting MLCT state of the complexes and how their properties compare to each other. The complexes are emissive at room temperature in air in the orange to red region of the visible spectrum. Triazole moities are destabilising compared with pyridines with respect to the energy of the LUMO resulting in higher energy MLCT state. The triazole complex also shows are increase sensitivity to O$_2$. The novel luminescent osmium(II) triazole-based complex [Os(btzpy)$_2$]$^{2+}$ was shown to exhibit significant quenching of luminescence intensity in aerated acetonitrile solution compared to degassed solution and has a high quantum yield for singlet oxygen sensitization as its chloride

salt, indicating potential applications in photodynamic therapy. The complex was also investigated in cancer cells by luminescence imaging microscopy. The results from these studies reveal that the complex is successfully taken up by two cancer cell lines with a high degree of mitochondrial localization and low dark toxicity. Inclusion of the triazole donor leads to increase in the quantum yield of emission, lifetime, sensitivity to oxygen and cellular uptake. Utilization the Cu(I)-catalysed-cycloaddition (the CuAAC reaction) coupling to synthesise the triazole based ligands opens up various ways to prepare many kinds of transition metal complexes which can use in specific application based on photochemical, electrochemical and photophysical properties of these complexes. The triazole based complex described in this chapter gives a good example of the complexes that can be worked on for development in order to improve the photophysical properties to get the preferable complex which can be used as luminescence imaging/singlet oxygen sensitisation photodynamic theranostic complex. I would like to thank Luke K. McKenzie, Dr Helen E. Bryant, and Professor Julia A. Weinstein from the University of Sheffield.

Chapter 5: Dinuclear supramolecular complexes using triazole based bridging ligand

5.1 **Introduction**

The design and synthesis of metallosupramolcular and multicomponent molecular systems have attracted a great deal of recent attention, largely due to their potential as the basis of novel functional materials. The synthesis of metallosupramolcular materials has depended on the preparation of bridging ligands with multiple coordination sites into which can then be integrated into metal centers. In recent years a lot of bridging ligands have been used, especially those containing pyridine-type coordinating units which are either directly connected or separated by a set of spacers. Rigid spacers are much preferred than non-rigid bridging ligands for energy and electron transfer applications, as the geometry (metal-to-metal distance) of the system is better defined. However, while scientists have an abundance of diverse of bridging ligands available to use in the metallosupramolecular field, either a large number of those ligands are expensive and time-consuming in their preparation via many steps, or under specific conditions and some of them to produced bridging ligands in limits that allow minimal incorporation of interesting functional groups.[157] Fundamentally, it is advantageous to have new methodologies to prepare bridging ligands, which are high yielding, easy, and versatile. Also to be able to use preformed components, coupling them together under moderate reaction conditions in as few steps as possible. Such processes would require a coupling reaction that is highly efficient and high yielding, for this, functional groups are required which can be easily inserted into the periphery of the metal complex components. Cu(I)-catalysed-cycloaddition (the CuAAC reaction) possesses the immense ability for this case because it has moderate reaction conditions. A few reports have appeared on the CuAAC modification of transition metal complexes as bridging ligands multiple coordination sites. A number of groups are reported "click" ligands[158-160] in the formation of coordination polymers. Generally, triazole ligands act as donors in ligand exchange reactions, just like imidazole and pyridine-based

ligands. The metal complexes developed through triazole ligand systems have unique photophysical properties, which attracts attention in coordination chemistry, as does their analogues (bpy and tpy).[137, 236] There are several synthetic strategies available for the development of triazole complexes which use triazole as bridging ligand to allow for the study of specific photochemical, electrochemical and photophysical properties.[237, 238] When synthesizing dinuclear compounds, transition metal complexes (for example, ruthenium, osmium, and iridium) can be used as building blocks where triazole ligands act as bridges. The synthesis of dinuclear transition metal complexes have been demonstrated with ease, but the product exhibit weak metal-to-ligand interaction, which makes it difficult to study the intrinsic properties of both the metal and the ligand in the complex, but strong enough to allow for the study of the overall characteristics of the complex.[83, 239-241] However, a triazole linker can be used to develop di- and trinuclear complexes and organometallic complexes. Crowley and co-workers used 1, 4-bis-({4-(pyrid-2-yl)-1, 2, 3-triazol-1-yl}methyl) benzene as bridging ligand in Co[242] and Fe metal complex systems. The cobalt complex was tested for antimicrobial activity while the iron complex was tested for it's the antifungal activity. Both complexes were not active against either strain of bacteria for cobalt complex and no antifungal activity against the yeast for the iron complex. They suggest that a high charge of the $[Co_2(Lpytrz)_3]^{6+}$ cylinders prevented them from crossing the bacterial cell membranes, rendering the compounds biologically inactive. Also, the poor stability of the "click" complexes in the presence of DMSO and the amino acid histidine found in the biological test media caused decomposition of the Fe(II) "click complex in the yeast S. cerevisiae media. The same group applied 1, 4-bis-({4-(pyrid-2-yl)-1, 2, 3-triazol-1-yl}methyl) benzene ligand to synthesis ruthenium(II) helicate complex.[243] Compared to similar iron complexes, the more kinetically inert ruthenium(II) system proved stable when exposed to DMSO solution of the common biological ligand histidine. The ruthenium(II) helicate complex was tested for antimicrobial activity in vitro

against both Gram negative (Escherichia coli) and Gram positive (Staphylococcus aureus) microorganisms. The Ru(II) helicate complex revealed antimicrobial activity but the minimum inhibitory concentrations. This chapter presents complexes using the bis-({4-(pyrid-2-yl)-1, 2, 3-triazol-1-yl}methyl)benzene as the bridging ligand in metal complexes of Os, Ru, and Ir. and later characterize their photophysical as well as chemical properties.

5.2 Synthesis and characterisation

5.2.1 Synthesis of 1,4-bis-{4-(pyrid-2-yl)-1,2,3-triazol-1-yl methyl}benzene = L4

The ligand 1,4-bis-{4-(pyrid-2-yl)-1,2,3-triazol-1-yl methyl}benzene (L4) was prepared in a two step/one-pot synthesis, starting from the corresponding halide and acetylene starting materials. The azide was prepared *in situ* from its corresponding bis(bromomethyl) substituted benzene analogue by nucleophilic substitution with a slight excess of NaN_3 in DMSO at room temperature for 2 hours. Upon completion of the substitution reaction, two equivelnts of 2-ethynylpyridine was added to the reaction vessel along with catalytic quantity of $CuSO_4$ and excess sodium ascorbate along with an equivalent of 2,6-lutidine per acetylene. The compound **L4** was purified by re-crystallisation from dichloromethane and hexane and isolated in good yields.
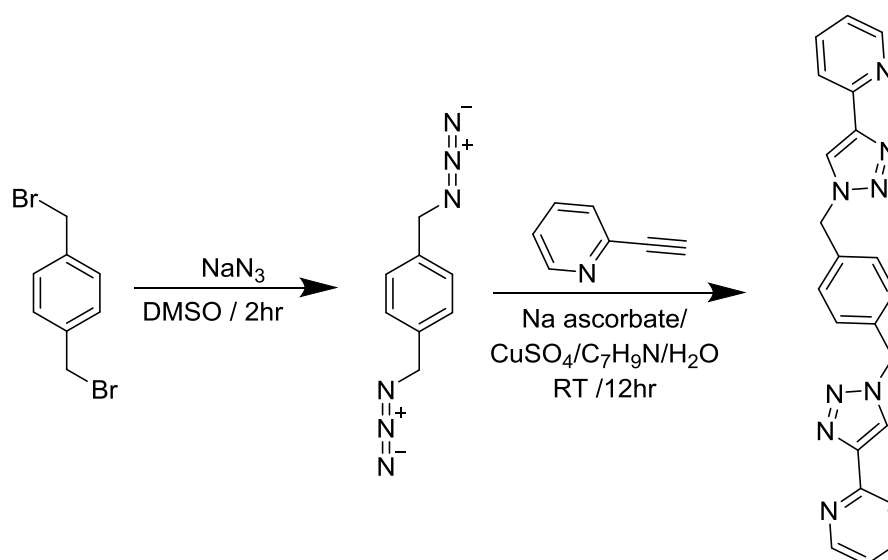
Scheme 5-1 One-pot synthesis of ligand 1,4-bis-{4-(pyrid-2-yl)-1,2,3-triazol-1-ylmethyl}benzene = L4

Ditopic ligand **L4** was fully characterised by ^{1}H and ^{13}C NMR spectroscopy. The symmetrical nature of the bis-triazole ligand results in a simple set of resonances in the ^{1}H NMR spectrum. A characteristic singlet resonance arising from the triazole protons TRZ (Figures 5.1, 5.2) is observed at δ 8.66, and is clearly distinguishable as with other triazole signals as there is no coupling to any other protons evident in the COSY spectrum.
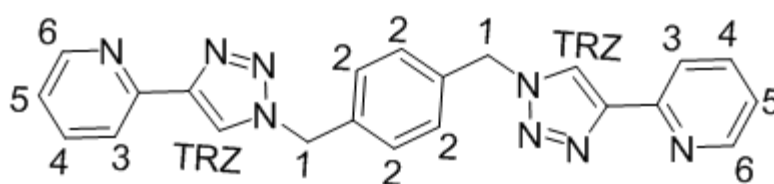
Figure 5-1 - Number of protons of triazole Ligand 1,4-bis-{4-(pyrid-2-yl)-1,2,3-triazol-1-ylmethyl}benzene = L4

160
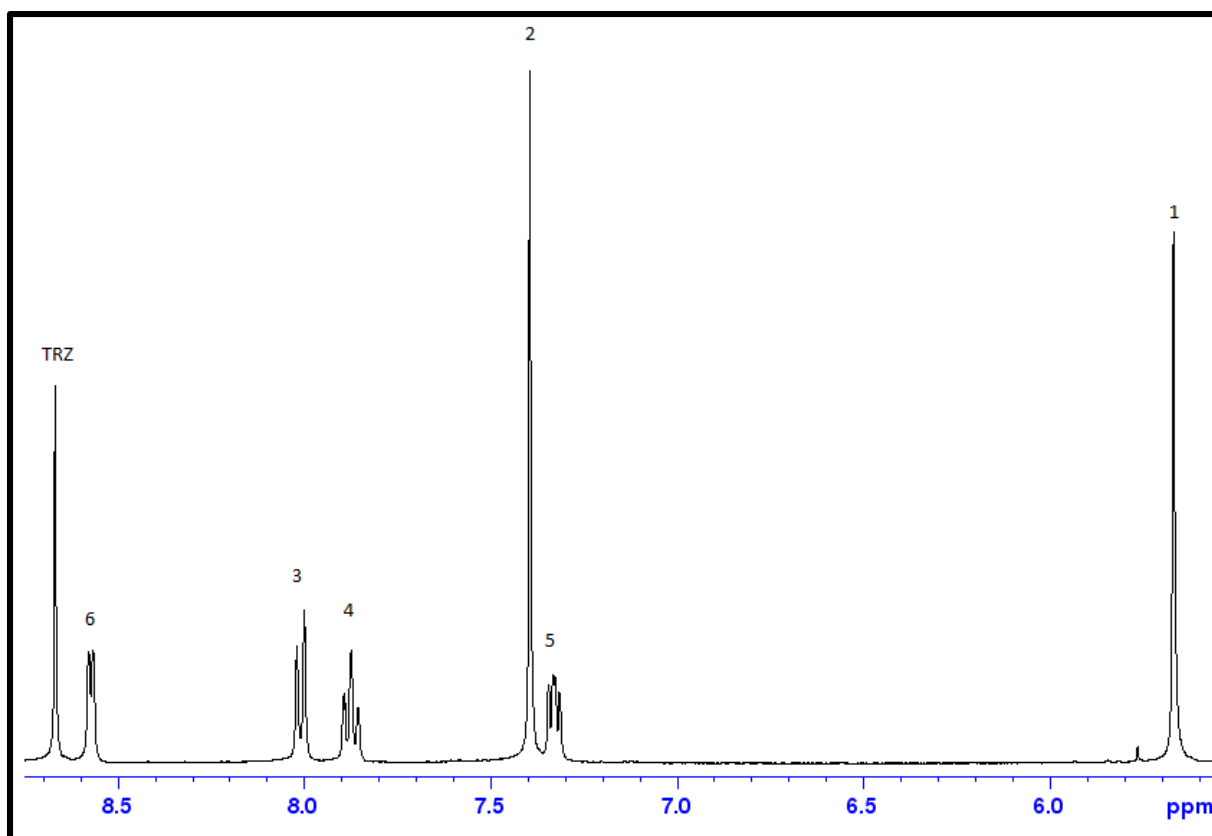
Figure 5-2 1H NMR (400MHz) spectrum of free ligand L4 in d6 DMSO

This signal shows nOe interactions in its two dimensional NOESY correlation spectra with the methylene protons of the benzyl substituent (1) which appears as a singlet resonance at δ 5.66. From the COSY spectrum the proton next to N in pyridyl ring (6) is the most down field which appears as a doublet resonances at δ 8.57. This proton displays COSY correlation with the signal which appears at δ 7.32 (5). Proton 5 also displays strong COSY correlations with the signals appearing at δ 7.76 (4) and (6) also displays weak COSY correlation with (4) due to long range coupling with (4). Pyridyl ring signal appears as a doublet resonances at δ 8.10 (3). The L4 regio chemistry confirmed by two dimensional NOESY correlation spectra which show nOe interactions between the triazole protons (trz) and protons 1 and 3. This confirms the 1,4-disubstitution regio chemistry of the triazole rings in the product. All the spacer phenyl protons (2) appear as singlet resonance at δ 7.39 (Figure 5.3)
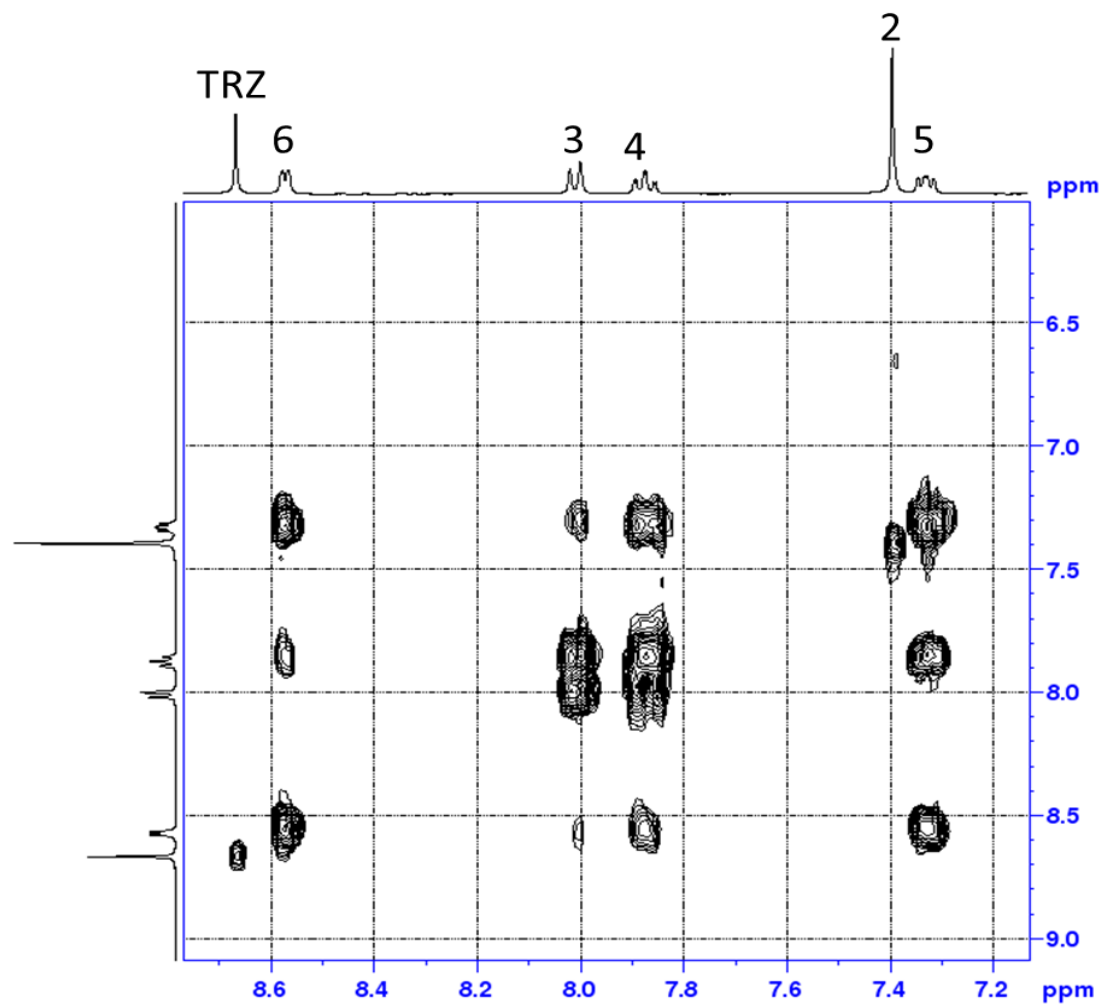
Figure 5-3 2D H-H COSY NMR spectrum of free ligand *1,4-bis-{4-(pyrid-2-yl)-1,2,3-triazol-1-ylmethyl}benzene = L4*

In d6 DMSO

5.2.2 Synthesis and Characterisation of Dinuclear complexes

5.2.2.1 Synthesis and Characterisation of Dinuclear Iridium Complexes

Iridium complexes [Ir(ppy)$_2$-L4](PF$_6$) and [Ir(ppy)$_2$-L4-Ir(ppy)$_2$](PF$_6$)$_2$ were prepared by refluxing two equivalents of L4 (to prepare [Ir(ppy)$_2$-L4-](PF$_6$)), (Scheme 5-2) or one equivalent of L4 (to prepare [Ir(ppy)$_2$-L4-Ir(ppy)$_2$](PF$_6$)$_2$), (Scheme 5-3) with one equivalent of [{Ir(ppy)$_2$Cl}$_2$] and NaPF$_6$ in mixture of methanol and chloroform under nitrogen for 24 hr. Because of the poor solubility of 1,4-bis-{4-(pyrid-2-yl)-1,2,3-triazol-1-ylmethyl}benzene in acetonitrile, the crude product was redissolved in acetonitrile kept in fridge for 24 hr and filtered to remove unwanted ligand. The solvent was then removed after filtration and the complex recrystallised from dichloromethane and hexane.
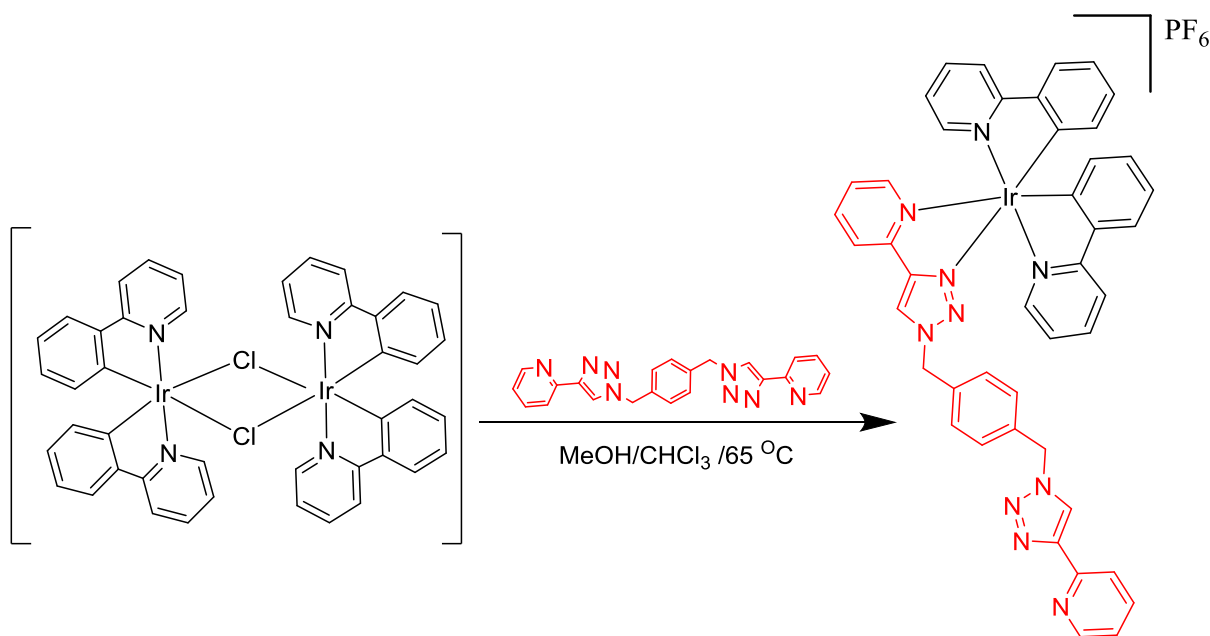
Scheme 5-2 - Synthesis of [Ir(ppy)$_2$-L4](PF$_6$)
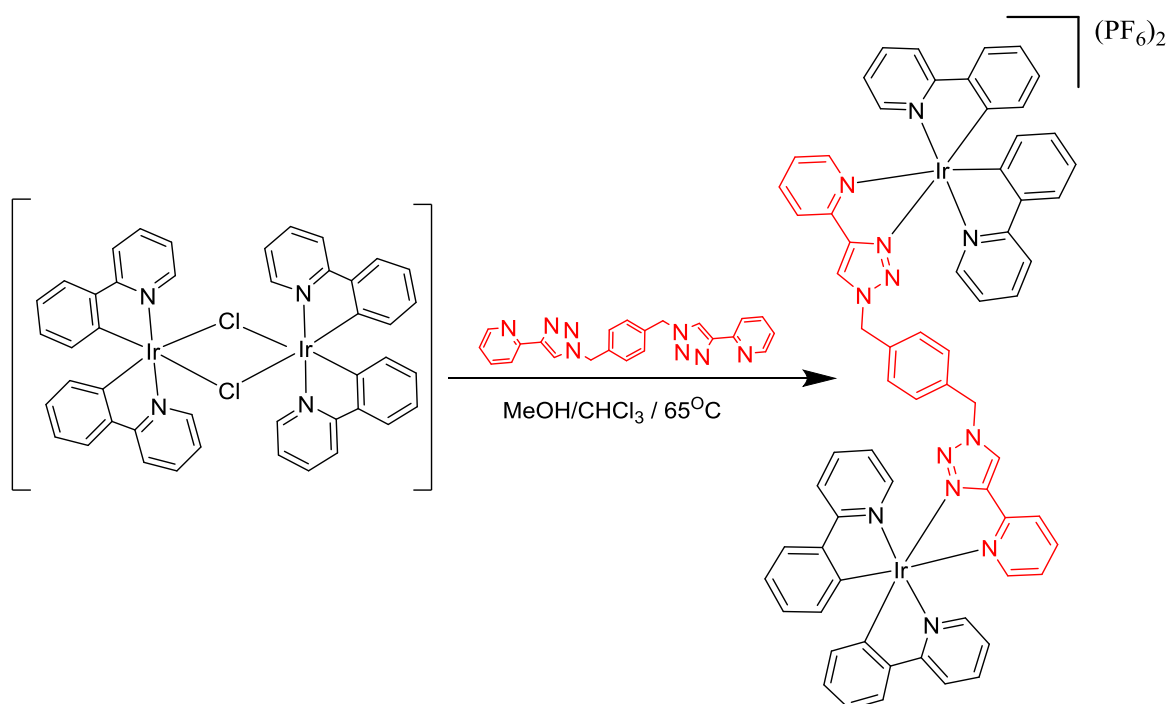
Scheme 5-3 -Synthesis of [Ir(ppy)$_2$-L4-Ir(ppy)$_2$](PF$_6$)$_2$

Both complexes were fully characterised by ^{1}H and ^{13}C NMR spectroscopy. Due to the symmetry of the L4 ligand in [Ir(ppy)$_2$-L4-Ir(ppy)$_2$](PF$_6$) complex, two diasteroisomers pairs are possible to produced: the ΔΔ /ΛΛ and ΔΛ / ΛΔ. For the ΔΔ and ΛΛ isomers, the triazole rings protons are equivalent, showing one peak in^{1}H NMR spectrum, while they show two peaks in ΔΛ isomer, due to the triazoles being magnetically inequivalent. Three singlet resonances are expected to be observed from the ^{1}H NMR spectrum corresponding to the triazole protons from three isomers, however, it is likely the difference in chemical shift is small meaning that some of the resonances overlap, for this reason the ^{1}H NMR spectrum is complicated. The ^{1}H NMR spectrum (Figure 5-4) of the product shows two singlet resonances at δ 8.66 and δ 8.65 for the triazole ring protons which are shifted by 0.11 ppm relative to the corresponding resonance for the free ligand (δ 8.55). For [Ir(ppy)$_2$-L4](PF$_6$) the triazole rings protons show two singlets, one at δ 8.64 which is corresponds to the coordinated side and

second at δ 8.54 which is corresponds to the free side. The methylene protons appear as a singlet at δ 5.59 for all 4 protons for [Ir(ppy)$_2$-L4-Ir(ppy)$_2$](PF$_6$)$_2$, while the same protons show two doublets at δ 5.60 and δ 5.57 for [Ir(ppy)$_2$-L4](PF$_6$). The ESI mass spectrum of the [Ir(ppy)$_2$-L4](PF$_6$) complex shows a peak at m/z = 895.25890 assignable to the species [M]$^+$, while the ESI mass spectrum of the [Ir(ppy)$_2$-L4-Ir(ppy)$_2$](PF$_6$)$_2$ complex shows a peak at m/z = 698.17640 assignable to the species M^{2+}.
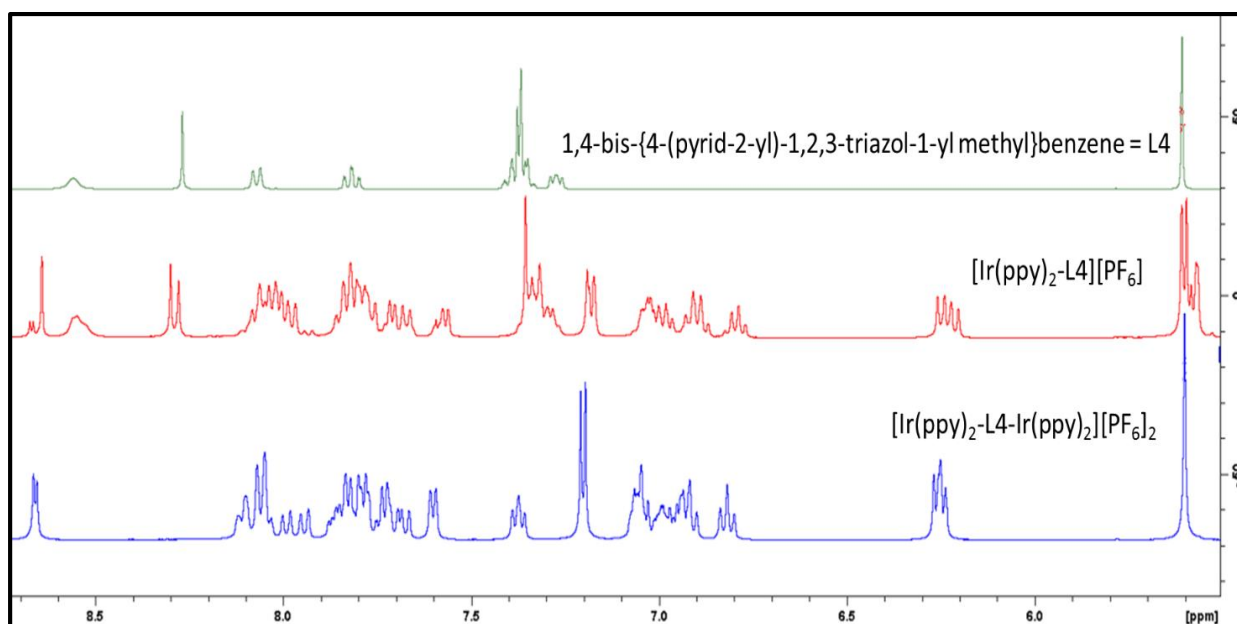
Figure 5-4 The ^{1}H-NMR spectra (400 MHz, CD$_3$CN) for L4 free ligand and [Ir(ppy)$_2$-L4]$^+$, [Ir(ppy)$_2$-L4-Ir(ppy)$_2$]$^{2+}$ complexes

5.2.2.2 Synthesis and Characterisation of Dinuclear Ruthenium complexes

Ruthenium complexes [Ru(bpy)$_2$-L4](PF$_6$)$_2$ and [Ru(bpy)$_2$-L4-Ru(bpy)$_2$](PF$_6$)$_4$ were prepared by heating at reflux, [Ru(bpy)$_2$Cl$_2$] with one equivalent of L4 to prepare [Ru(bpy)$_2$-L4](PF$_6$)$_2$ (Scheme 5-4) or half an equivalent of L4 to prepare [Ru(bpy)$_2$-L4-Ru(bpy)$_2$](PF$_6$)$_4$ (Scheme 5-5) in ethanol in the dark under nitrogen for 24 hr. The complexes were isolated as their hexafluorophosphate salts.
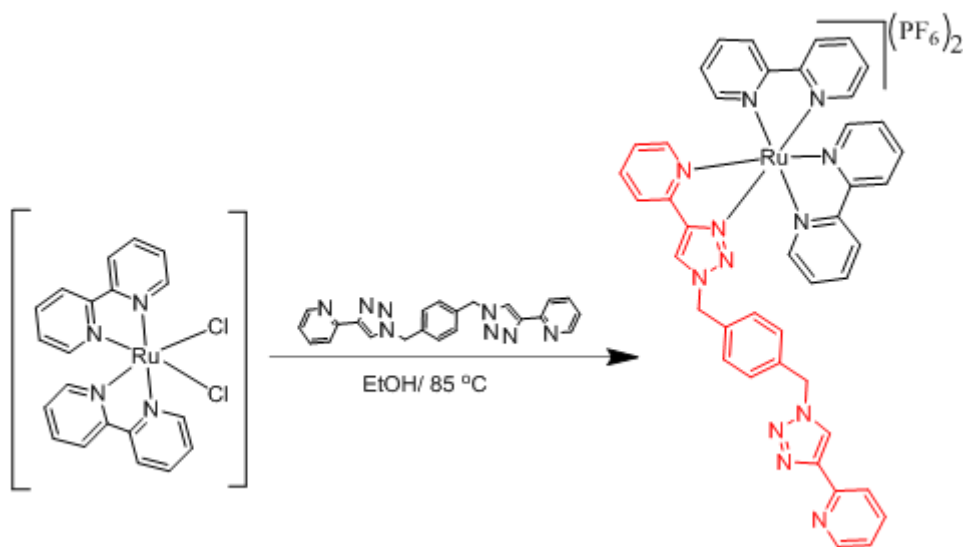
Scheme 5-4 - Synthesis of [Ru(bpy)$_2$-L4](PF$_6$)$_2$
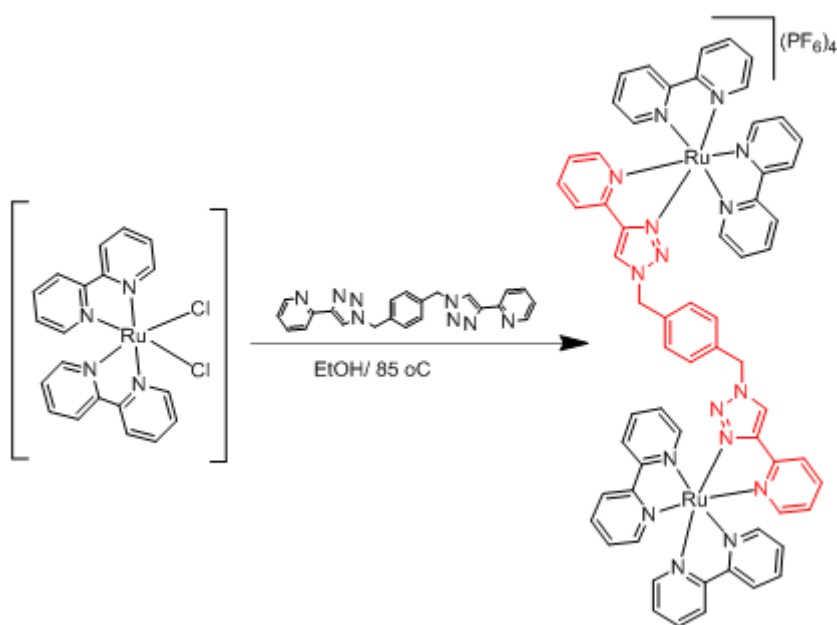
Scheme 5-5 Synthesis of [Ru(bpy)$_2$-L4- Ru(bpy)$_2$](PF$_6$)$_4$

Both complexes were fully characterised by ^{1}H and ^{13}C NMR spectroscopy. Two diasteroisomer pairs are prducsed (ΔΔ/ ΛΛ and ΔΛ/ ΛΔ). Due to the symmetry of the L4 ligand in [Ru(bpy)$_2$-L4-Ru(bpy)$_2$](PF$_6$)$_4$ complex, three singlet resonances are expected to be observed from the ^{1}H NMR spectrum corresponding to the triazole protons from three isomers,

however, it is likely the difference in chemical shift is small meaning that some of the resonances overlap and the ^{1}H NMR spectrum is complicated. The ^{1}H NMR spectrum (Figure 5-5) of the product shows two singlet resonances at δ 8.69 and δ 8.68 for the triazole rings protons which are shifted by 0.14 ppm relative to the corresponding resonance for the free ligand (δ 8.55). For [Ru(bpy)$_2$-L4](PF$_6$)$_2$ the triazole rings protons show two singlets, first one at δ 8.63 which is corresponds to the coordinated side and second one at δ 8.56 ppm which is corresponded to the free side. Even methylene protons show singlet at δ 5.53 for all 4 protons in [Ru(bpy)$_2$-L4-Ru(bpy)$_2$](PF$_6$)$_4$ complex, while the same protons show one singlet at δ 5.62 and one doublet at δ 5.51 for [Ru(bpy)$_2$-L4](PF$_6$)$_2$. Relative to the corresponding resonances for the free ligand we can see the appearance of bpy protons in both complexes in ranges of δ 7.79–7.55 and δ 8.49–8.34. The ESI mass spectrum of the [Ru(bpy)$_2$-L4](PF$_6$)$_2$ complex shows a peak at m/z = 404.10300 assignable to the species M^{2+}, while the ESI mass spectrum of the [Ru(bpy)$_2$-L4-Ru(bpy)$_2$](PF$_6$)$_4$ complex shows a peak at m/z = 305.56216 assignable to the species M^{4+}.
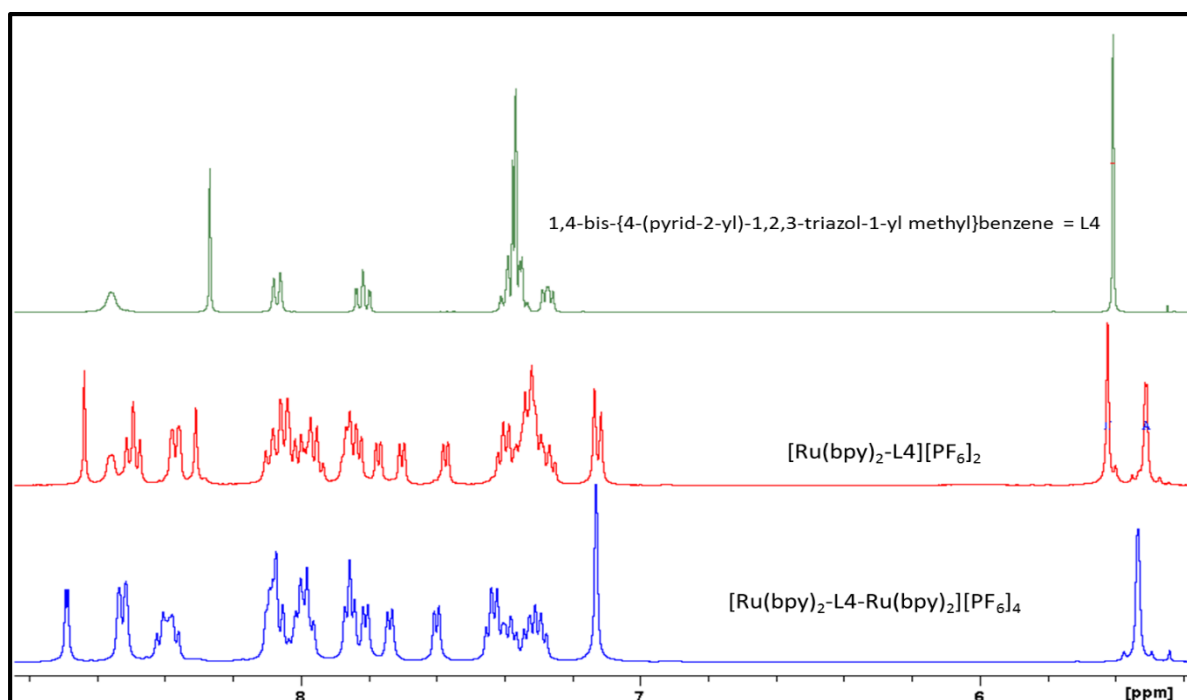
Figure 5-5 The 1H-NMR spectra (400 MHz, CD3CN) for L4 free ligand and [Ru(bpy)$_2$-L4]$^{2+}$, [Ru(bpy)$_2$-L4-Ru(bpy)$_2$]$^{4+}$complexes

5.2.2.3 Synthesis and Characterisation of HetroDinuclear Iridium-Ruthenium complex

$[Ru(bpy)_2\text{-}L4\text{-}Ir(ppy)_2](PF_6)_3$ was prepared by reacting $[\{Ir(ppy)_2Cl\}_2]$ with two equivalents $[Ru(bpy)_2\text{-}L4]^{2+}$ and $NaPF_6$ in of mixture of methanol and chloroform under nitrogen for 24 hr in dark. The orange precipitate was collected by filtration. The complex was isolated as the hexafluorophosphate salt (Scheme 5-6).
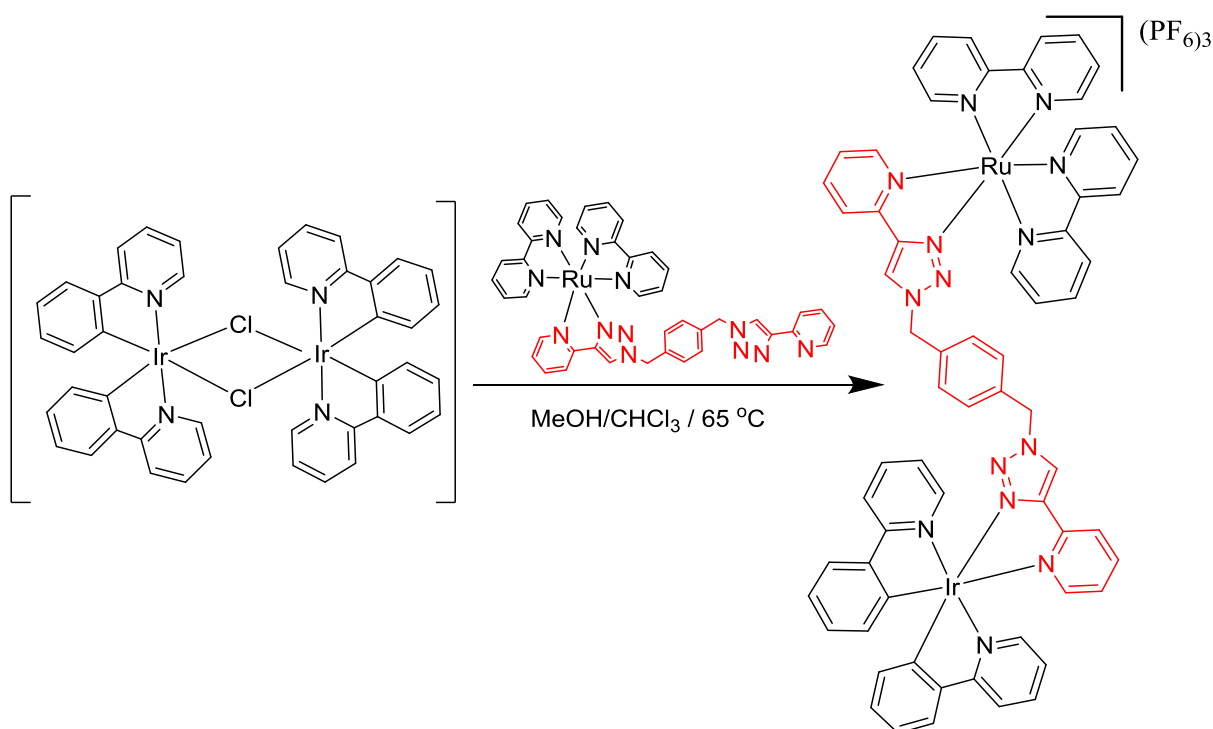
Scheme 5-6- Synthesis of $[Ru(bpy)_2\text{-}L4\text{-}Ir(ppy)_2](PF_6)_3$

The complex was fully characterised by ^1H and ^{13}C NMR spectroscopy. Due to the asymmetry of the $[Ru(bpy)_2\text{-}L4\text{-}Ir(ppy)_2](PF_6)_3$ complex, the ^1H NMR spectrum of the product shows one singlet at δ 8.69 and another one at δ 8.52 for the triazole rings protons. The methylene protons show two resonances at δ 5.61 and δ 5.54. The ESI mass spectrum of the complex shows a peak at $m/z = 436.43335$ assignable to the species M^{3+}.

5.2.2.4 Synthesis and Characterisation of Dinuclear osmium complexes

Osmium dinuclear complexes [{Os(bpy)$_2$}$_2$L4](PF$_6$)$_4$ and [{Os(Bn-pytz)$_2$}$_2$L4](PF$_6$)$_4$ were prepared by reaction of L4 with two equivalents of Os(bpy)$_2$Cl$_2$ for [{Os(bpy)$_2$}$_2$L4]$^{4+}$ (Scheme 5-7) or [Os(Bn-pytz)$_2$Cl$_2$] for [{Os(Bn-pytz)$_2$}$_2$L4]$^{4+}$ (Scheme 5-8) and AgPF$_6$ in ethylene glycol under refluxing conditions under nitrogen for 24 hr. The resulting solution was allowed to cool to room temperature and the precipitate was separated by vacuum filtration and washed with cold water and diethyl ether. The mixture then redissolved in acetonitrile and kept in fridge for 24 hrs, filtered through celite to remove AgCl. The product was then recrystallization from dichloromethane and hexane.
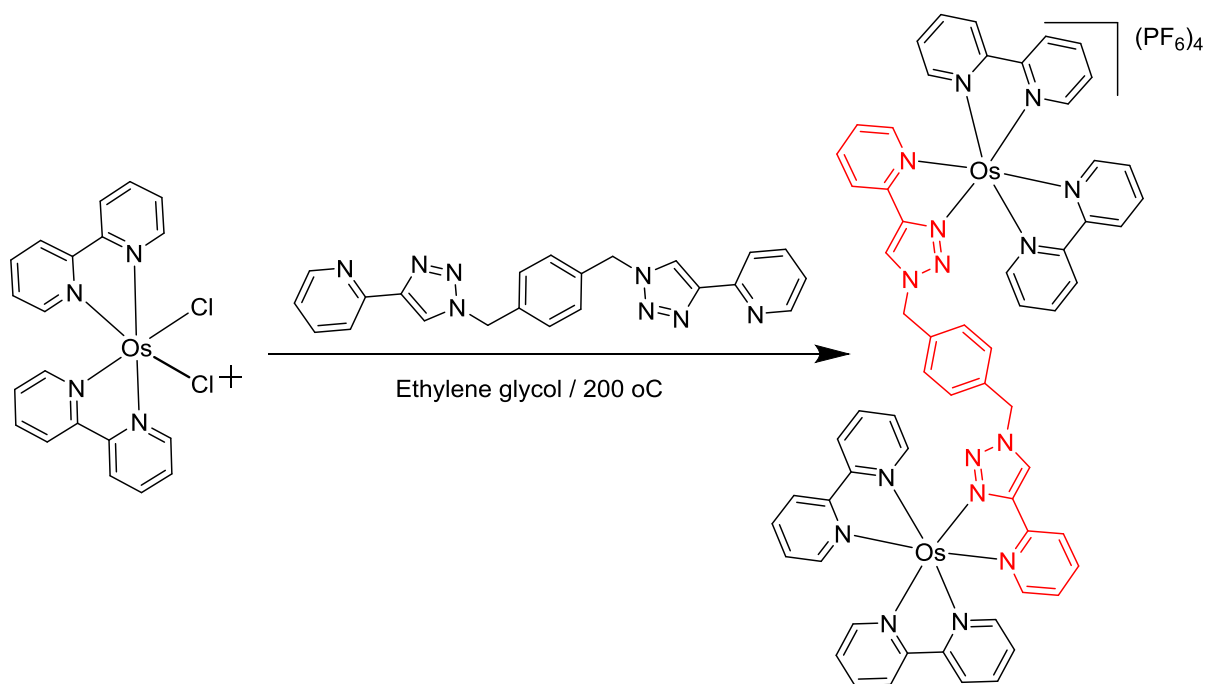
Scheme 5-7 -Synthesis of [Os(bpy)$_2$-L4- Os(bpy)$_2$](PF$_6$)$_4$

169
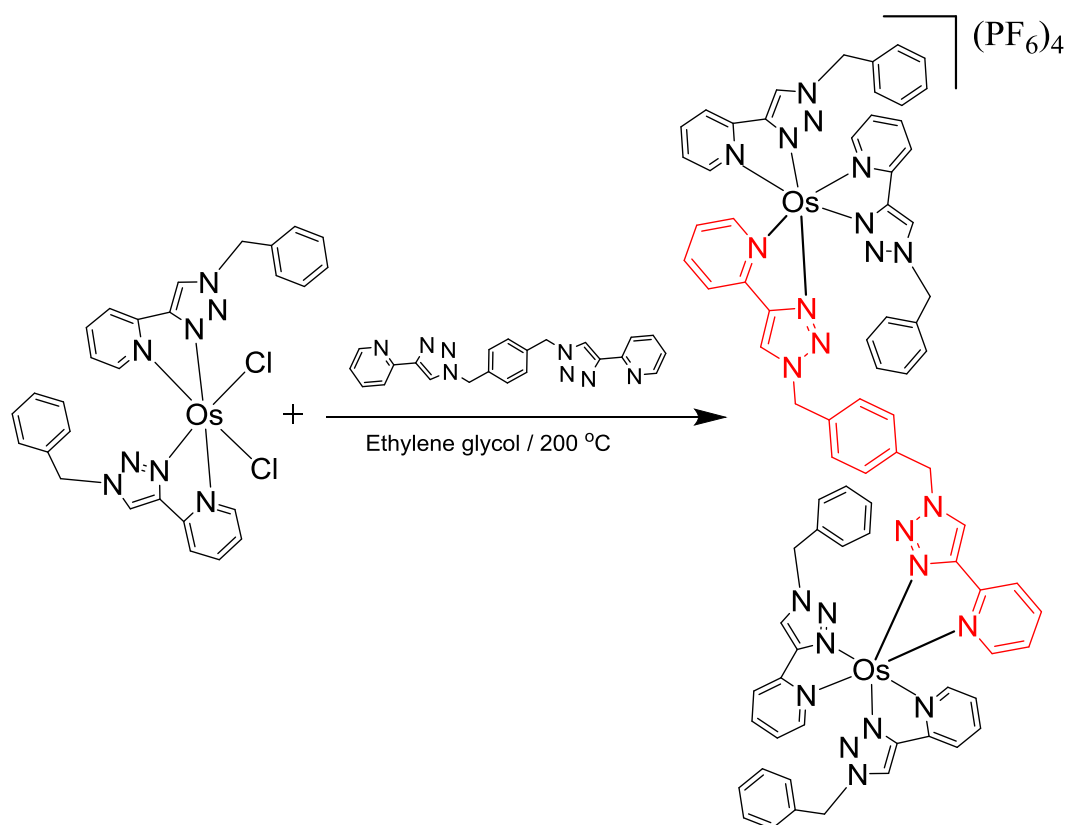
Scheme 5-8 Synthesis of [Os(Bn-pytz)₂- L4- Os(Bn-pytz)₂](PF₆)₄

Both complexes were fully characterised by ^{1}H and ^{13}C NMR spectroscopy. Due to the symmetry of the L4 ligand in both complexs, the ^{1}H NMR spectrum for [Os(bpy)₂-L4-Os(bpy)₂](PF₆)₄ shows two singlet resonances, one at δ 8.65 and a second at δ 8.64 for the triazole rings protons. For [Os(Bn-pytz)₂-L4-Os(Bn-pytz)₂](PF₆)₄, There are possibility to produce *fac* or *mer-* like isomers for each side of the complex, for the *mer* isomer the complex is produced as a mixture of three isomers, *fac / fac, fac / mer* and *mer / mer* dependent on the respective regiochemistry of the pyridyl and triazole moieties respectivly of the two Bn-pytz ligands. Two diasteroisomeric combination of each are also possible (ΔΔ/ ΛΛ/ and ΔΛ/ ΛΔ) which lead to large number of isomers. The ^{1}H NMR spectrum is complicated for this reason. The triazole rings protons show one multiplet at range of δ 8.64- 8.55 which is corresponded to the all six protons. The methylene protons show one doublet at δ 5.60 for [Os(bpy)₂ -L4-Os(bpy)₂](PF₆)₄ complex and one multiplet at range of δ 5.54- 5.47 for [Os(Bn-pytz)₂-L4-

170

Os(Bn-pytz)$_2$](PF$_6$)$_4$ complex, (Figure 5-6). The ESI mass spectrum of the [Os(bpy)$_2$ -L4-Os(bpy)$_2$](PF$_6$)$_4$ complex shows a peak at m/z = 350.0953 assignable to the species M^{4+}, while the ESI mass spectrum of the for [Os(Bn-pytz)$_2$-L4-Os(Bn-pytz)$_2$](PF$_6$)$_4$ complex shows a peak at *m/z* = 430.1275 assignable to the species M^{4+}.
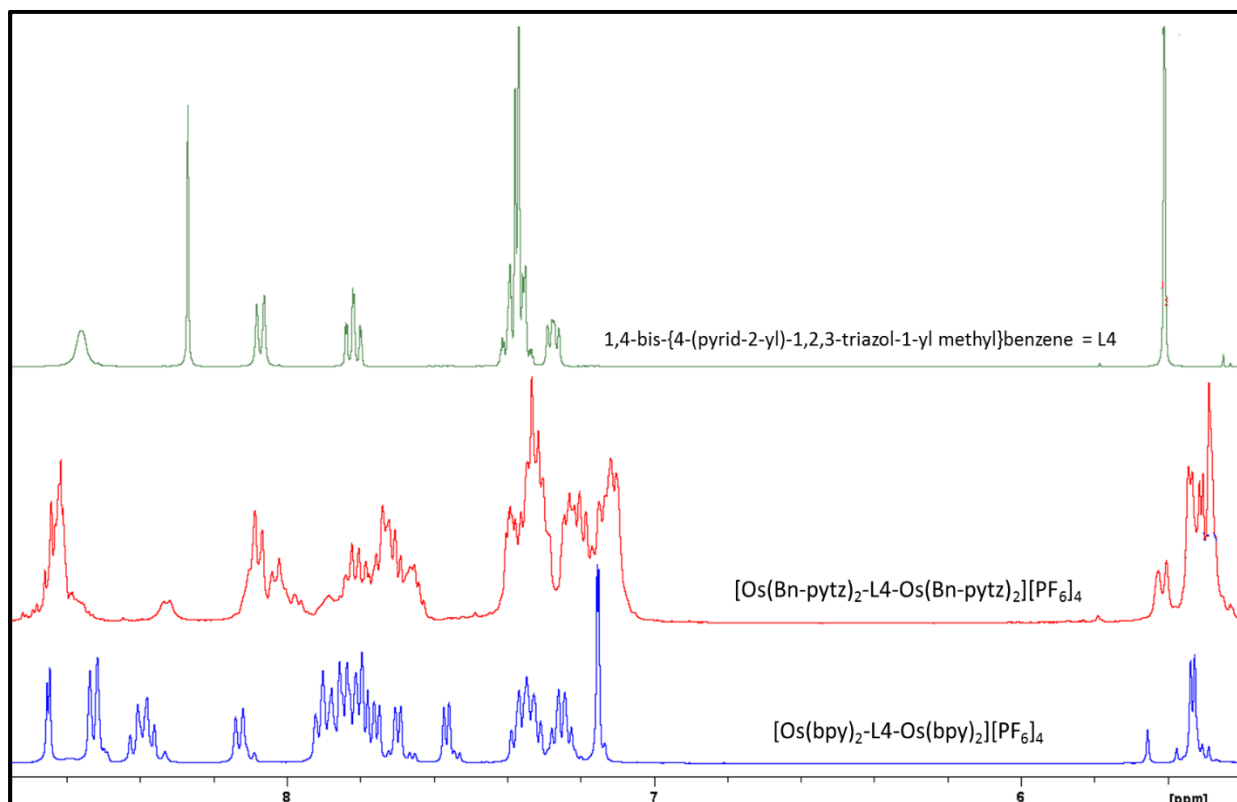
Figure 5-6 The 1H-NMR spectra (400 MHz, CD$_3$CN) for L4 free ligand and [Os(bpy)2-L4-Os(bpy)$_2$]$^{4+}$, [Os(Bn-pytz)$_2$- L4-Os(Bn-pytz)$_2$]$^{4+}$ complexes

5.3 **Electrochemical Properties of Complexes**

Electrochemical data for the various complexes as obtained by cyclic voltammetry are summarized in Table 5.1.

Table 5-1: Electrochemical data for the complexes in CH_3CN, 0.2 M [NBu$_4$] [PF$_6$], 100 mVs^{-1}, at room temperature

Complex	Reduction $E_{1/2}$ V vs. Fc/Fc$^+$	Oxidation E_{pa} V vs. Fc/Fc$^+$
[Ir(ppy)$_2$-L4](PF$_6$)	-2.18	0.94
[Ir(ppy)$_2$-L4-Ir(ppy)$_2$](PF$_6$)$_2$	-2.16	0.93
[Ru(bpy)$_2$-L4](PF$_6$)$_2$	-1.978(0.084)[a],-1.767(0.061)[a]	0.9(0.07)[a]
[Ru(bpy)$_2$-L4- Ru(bpy)$_2$](PF$_6$)$_4$	-1.94(0.085)[a], -1.76(0.08)[a]	0.92(0.09)[a]
[Ru(bpy)$_2$-L4 -Ir(ppy)$_2$](PF$_6$)$_3$	-2.17, -1.96(0.07)[a], 1.76(0.06)[a]	0.94
[Os(bpy)$_2$-L4-Os(bpy)$_2$](PF$_6$)$_4$	-1.9(0.09)$_a$, -1.7(0.08)[a]	0.44(0.073)[a]
[Os(Bn-pytz)$_2$-L4-Os(Bn-pytz)$_2$](PF$_6$)$_4$	============[b]	0.458(0.078)[a]

E1/2= (Epa+ Epc)/ 2, Epc are anodic and cathodic peak potentials respectively. a = reversible.b = reduction coples are outside the available electrochemical window.

Figure 5.7 shows the Cyclic voltammagram of complexes [Ir(ppy)$_2$-L4](PF$_6$) and [Ir(ppy)$_2$-L4-Ir(ppy)$_2$](PF$_6$)$_2$ in acetonitrile. For iridium complexes [Ir(ppy)$_2$-L4](PF$_6$) and [Ir(ppy)$_2$-L4-Ir(ppy)$_2$](PF$_6$)$_2$ the observed couples were irreversible for [Ir(ppy)$_2$-L4-Ir(ppy)$_2$](PF$_6$)$_2$ and quasi-reversible for [Ir(ppy)$_2$-L4](PF$_6$). Oxidation process for the two complexes gave the Ir$^{3+/4+}$ metal-based redox processes with an $E_{1/2}$ = + 0.94V for [Ir(ppy)$_2$-L4](PF$_6$) and + 0.93 V for [Ir(ppy)$_2$-L4-Ir(ppy)$_2$](PF$_6$)$_2$. The complex [Ir(ppy)$_2$-L4](PF$_6$) gave irreversible one

electron ppy ligand based reduction process, at -2.17 V (ppy$^{0/1-}$), and [Ir(ppy)$_2$-L4-Ir(ppy)$_2$](PF$_6$)$_2$ gave one electron ppy ligand based reduction process, at -2.16 (ppy$^{0/1-}$).
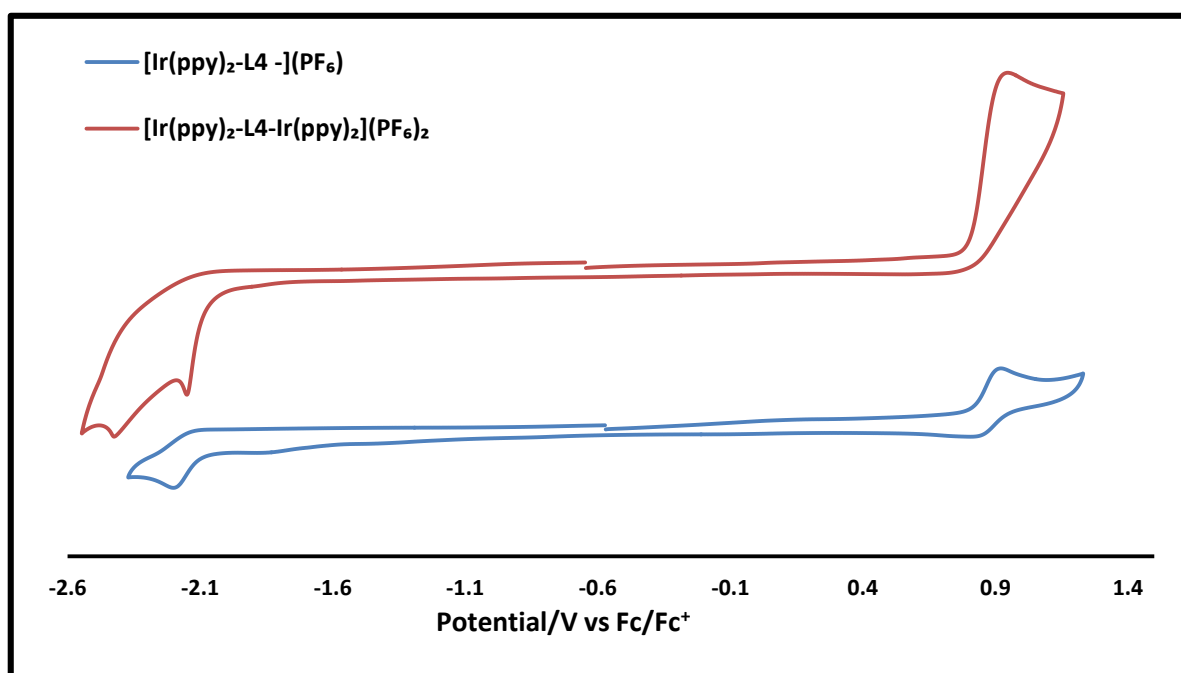
Figure 5-7 Cyclic voltammogram of iridium complexes in CH$_3$CN /0.2 M NBu$_4$PF$_6$; scan rate (v) = 100 mV s $^{-1}$. Potentials are reported against ferrocene (Fc/Fc $^+$ = 0.0 V)

For the ruthenium(II) complexes [Ru(bpy)$_2$-L4](PF$_6$)$_2$ and [Ru(bpy)$_2$-L4-Ru(bpy)$_2$](PF$_6$)$_4$. The observed couples were all reversible (Figure 5.8). Oxidation process for the two complexes gave Ru$^{3+/2+}$ metal-based redox couples with an E$_{1/2}$ = $+ 0.90$ V for [Ru(bpy)$_2$-L4](PF$_6$)$_2$ and $+$ 0.92 V for [Ru(bpy)$_2$-L4-Ru(bpy)$_2$](PF$_6$)$_4$. The complex [Ru(bpy)$_2$-L4](PF$_6$)$_2$ gave two one electron bipyridine ligand based reduction processes, with $E_{1/2}$ values of -1.77 (bpy$^{0/1-}$), and -1.98 (bpy$^{1-/2-}$). [Ru(bpy)$_2$-L4-Ru(bpy)$_2$](PF$_6$)$_4$ appeared to give two simultaneous one electron bipyridine ligand based reduction processes, on both sides with $E_{1/2}$ values of -1.76 (bpy$^{0/1-}$), and -1.94 (bpy$^{1-/2-}$). From the Figure, due to the reduction occur in the same potential as [Ru(bpy)$_2$-L4](PF$_6$)$_{2,}$ complex [Ru(bpy)$_2$-L4-Ru(bpy)$_2$](PF$_6$)$_4$ gave two simultaneous one electron reductions which mean that the electronic communication through the bridge ligand is poor.
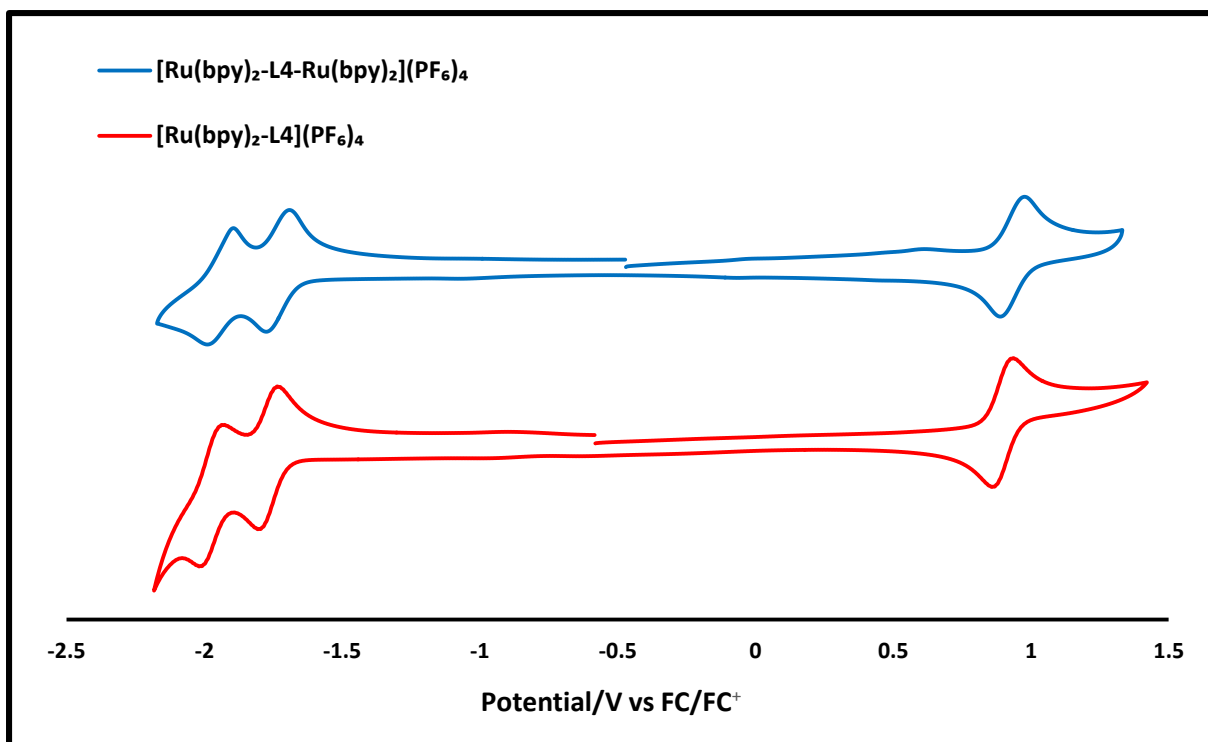
Figure 5-8- Cyclic voltammogram of ruthenium complexes in CH$_3$CN /0.2 M NBu$_4$PF$_6$; scan rate (v) = 100 mV s^{-1} . Potentials V are reported against ferrocene (Fc/Fc $^+$ = 0.0 V)

Figure 5.9 shows the cyclic voltammagram of complex [Ru(bpy)$_2$-L4-Ir(ppy)$_2$](PF$_6$)$_3$ in acetonitrile. A cyclic voltammogram of complex [Ru(bpy)$_2$-L4-Ir(ppy)$_2$](PF$_6$)$_3$ gave the metal-based redox processes with an E$_{1/2}$ = +0.94 which was assigned to a Ir$^{3+/4+}$ pattern due to similarity to[Ir(ppy)$_2$-L4](PF$_6$) and [Ir(ppy)$_2$-L4-Ir(ppy)$_2$](PF$_6$)$_4$ cyclic voltammograms. The complex gave two electron ligand based reduction processes, with $E_{1/2}$ values of −1.76 V (bpy$^{0/1-}$), and −1.96 V (bpy$^{1-/2-}$).

174

$[Ru(bpy)_2\text{-}L4\text{-}Ir(ppy)_2](PF_6)_3$

Potential/V vs FC/FC+
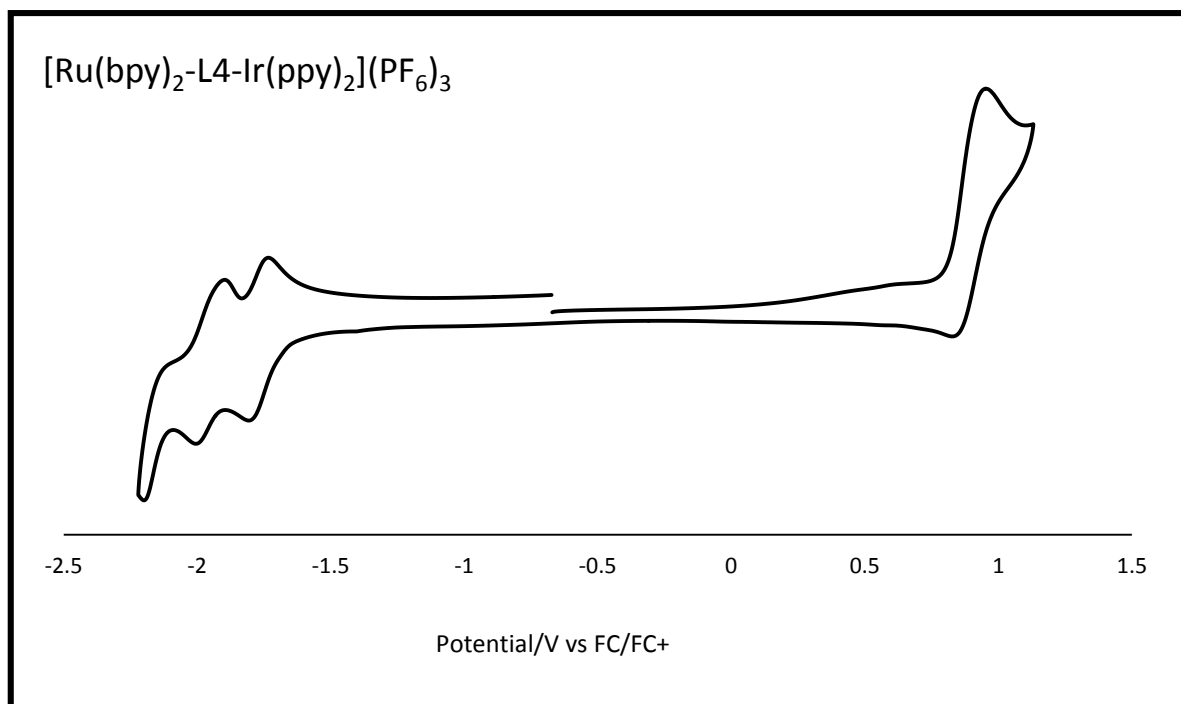
Figure 5-9- Cyclic voltammogram of ruthenium- iridium complex in CH₃CN /0.2 M NBu₄PF₆; scan rate (v) = 100 mV s⁻¹. Potentials V are reported against ferrocene (Fc/Fc⁺ = 0.0 V)

Figure 5.10 shows the cyclic voltammagram of complexes $[Os(bpy)_2\text{-}L4\text{-}Os(bpy)_2](PF_6)_4$ and $[Os(Bn\text{-}pytz)_2\text{-}L4\text{-}Os(Bn\text{-}pytz)_2](PF_6)_4$ in acetonitrile. For osmium complexes $[Os(bpy)_2\text{-}L4\text{-}Os(bpy)_2](PF_6)_4$ and $[Os(Bn\text{-}pytz)_2\text{-}L4\text{-}Os(Bn\text{-}pytz)_2](PF_6)_4$ the observed couples were all reversible. A cyclic voltammogram for each complex gave the $Os^{3+/2+}$ metal-based redox processes with an $E_{1/2} = +0.44$ V for $[Os(bpy)_2\text{-}L4\text{-}Os(bpy)_2](PF_6)_4$ and $+0.458$ V for $[Os(Bn\text{-}pytz)_2\text{-}L4\text{-}Os(Bn\text{-}pytz)_2](PF_6)_4$. The complex $[Os(bpy)_2\text{-}L4\text{-}Os(bpy)_2](PF_6)_4$ gave two one electron bipyridine ligand based reduction processes, with $E_{1/2}$ values of -1.7 V (bpy$^{0/1-}$), and -1.9 V (bpy$^{1-/2-}$). Replacing Bn-pytz with bpy ligand caused the changing in reduction values to more negative values such that the ligand reduction process cannot be seen in the available electrochemical window for $[Os(Bn\text{-}pytz)_2\text{-}L4\text{-}Os(Bn\text{-}pytz)_2](PF_6)_4$.

175
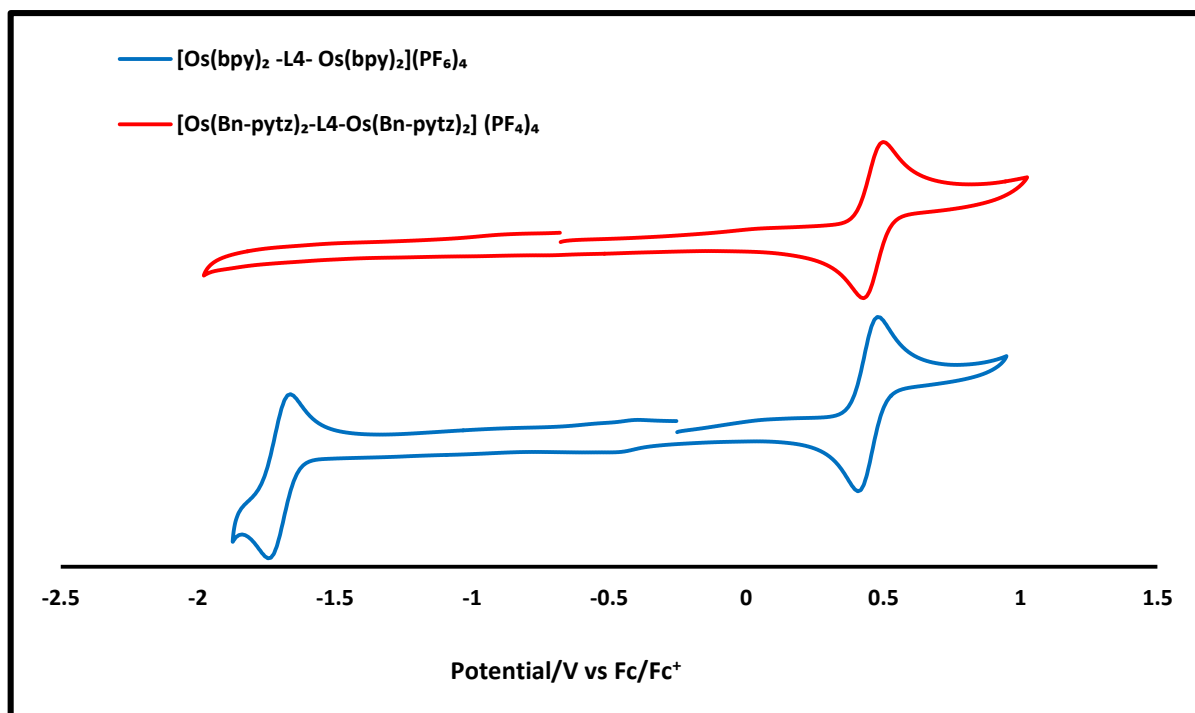
Figure 5-10- Cyclic voltammogram of osmium complexes in CH$_3$CN /0.2 M NBu$_4$PF$_6$; scan rate (v) = 100 mV s^{-1}. Potentials V are reported against ferrocene (Fc/Fc$^+$ = 0.0 V)

The cyclic voltammograms for the dinuclear complexes where the complexes are coordinated in both domains again shows a similar shape, with only 1 oxidation peak potential and typically reduction peaks potential of the bidentate donor ligand complexes.[120, 121, 244] This indicates that both of the complex centres present are oxidised and reduced simultaneously and do not form an intermediate mixed valence species. It was hoped that two redox waves would be observed, indicative of the formation of a mixed valence in [Os(Bn-pytz)$_2$-L4-Os(Bn-pytz)$_2$](PF$_6$)$_4$, [Os(bpy)$_2$-L4-Os(bpy)$_2$](PF$_6$)$_4$ and [Ru(bpy)$_2$-L4-Ru(bpy)$_2$](PF$_6$)$_4$ complexes as an intermediate for which near infrared intervalence charge transfer transition might have been expected. Generaly no or at least very little communication between the two metal centers is observed electrochemically. This behaviour may be useful in the applications where the two chromophores are required to act independently.

5.4 **Photophysical studies**

Table 5.2 summarizes the UV-vis electronic absorption data for the all complexes.

Table 5-2: UV-vis Absorption data, for the complexes in aerated acetonitrile

Compound	λ / nm(ε/mol^{-1}dm^{3}cm^{-1})
[Ir(ppy)$_2$-L4](PF$_6$)	249(42045), 268(31815), 272(32205), 287(20920), 314(9317), 379(3215), 411(1995)
[Ir(ppy)$_2$-L4-Ir(ppy)$_2$](PF$_6$)$_2$	252(84730), 268(73230), 380(8325), 411(5255)
[Ru(bpy)$_2$-L4](PF$_6$)$_2$	241(2850), 276(37850), 289(41550), 345(4348), 369(4502), 408(6150), 441(6430)
[Ru(bpy)$_2$-L4-Ru(bpy)$_2$](PF$_6$)$_4$	242(27575), 253(22179), 276(50932), 289(56882), 345(6217), 371(6592), 411(9373), 440(9601)
[Ru(bpy)$_2$-L4-Ir(ppy)$_2$](PF$_6$)$_3$	250(83428), 268(84235), 273(88342), 288(86725), 372(12337), 408(13158), 445(9915)
[Os(bpy)$_2$-L4-Os(bpy)$_2$](PF$_6$)$_4$	240(72385), 278(123185), 289(143355), 326(21755), 362(23755), 385(26250), 425(23535), 466(25610), 559(6140)
[Os(Bn-pytz)$_2$-L4-Os(Bn-pytz)$_2$](PF$_6$)$_4$	236(47150), 276(67280), 307(10390), 374(15005), 392(14000), 406(13460), 484(4625), 525(3820)

The UV-vis absorption spectrum of the iridium complexes [Ir(ppy)$_2$-L4](PF$_6$) and [Ir(ppy)$_2$-L4-Ir(ppy)$_2$](PF$_6$)$_2$ were recorded and show absorption features similar to those reported for other Ir(ppy)$_2$ containing complexes[121] with typical strong $\pi \rightarrow \pi^*$ transitions in the UV region localized on the ppy and the bridging ligands at approximately 250 - 268 nm and weaker metal-to-ligand charge transfer bands ^{1}MLCT (d$_\pi \rightarrow \pi^*$) at lower energies between 350 and 430 nm (Figure 5.11). From the figure it can be seen that the absorbance for the dinuclear [Ir(ppy)$_2$-L4-Ir(ppy)$_2$](PF$_6$)$_2$ complex is about twice that for [Ir(ppy)$_2$-L4](PF$_6$) as would be expected due to the presence of two Ir-based chromophores in the complex. The UV-vis absorption spectrum of the iridium complexes [Ir(ppy)$_2$-L4](PF$_6$) and [Ir(ppy)$_2$-L4-Ir(ppy)$_2$](PF$_6$)$_2$ are also in agreement with the UV-vis absorption data for complex [Ir(ppy)$_2$(pytz)]$^+$.[111]
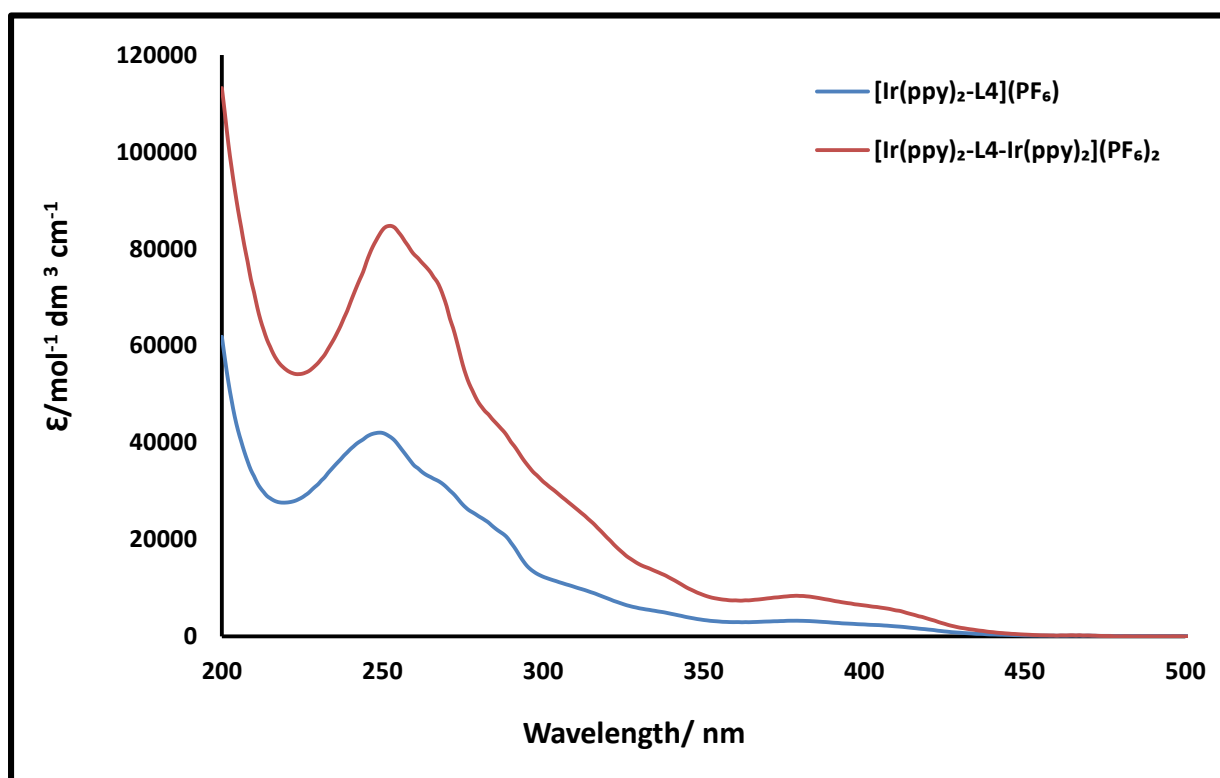
Figure 5-11 UV-vis absorption spectra of iridium complexes in acetonitrile

For ruthenium complexes [Ru(bpy)$_2$-L4](PF$_6$)$_2$ and [Ru(bpy)$_2$-L4-Ru(bpy)$_2$](PF$_6$)$_4$ in acetonitrile, the dominant absorption bands in the lower wavelength region at 240-285 nm assigned as intraligand $\pi \rightarrow \pi^*$ transitions. The low energy broad bands in the near UV region approximately 340-450 nm are attributed to ^{1}MLCT (d $\rightarrow \pi^*$) transitions. UV-visible absorption spectra of the complex [Ru(bpy)$_2$-L4-Ir(ppy)$_2$](PF$_6$)$_3$ shows absorption features in the lower region at 240-285 nm assigned as intraligand $\pi \rightarrow \pi^*$ transitions. The low energy broad bands in the near UV region approximately 370-450 nm are attributed to the metal to ligand charge transfer ^{1}MLCT (d $\rightarrow \pi^*$) transitions. Due to the presence of ruthenium in the the MLCT band of complex [Ru(bpy)$_2$-L4-Ir(ppy)$_2$](PF$_6$)$_3$, absorbance is further into red when compared to those of the iridium complexes [Ir(ppy)$_2$-L4](PF$_6$) and [Ir(ppy)$_2$-L4-Ir(ppy)$_2$](PF$_6$)$_2$, as well as, the difference in the ligands which containing (ppy and bpy) led to the appearance of two intense bands in the UV region 250 -290 localized on the both ligands ppy and bpy. It is easy to note from the UV-vis absorption spectrum (Figure 5.12) that the intensity of bands are stronger in the complexes which contains two metal centers [Ir(ppy)$_2$-L4-Ir(ppy)$_2$](PF$_6$)$_2$ for iridium complexes, [Ru(bpy)$_2$-L4-Ru(bpy)$_2$](PF$_6$)$_4$ for ruthenium complexes comparing with the complexes which contains one metal center [Ir(ppy)$_2$-L4](PF$_6$) for iridium complexes, and [Ru(bpy)$_2$-L4](PF$_6$)$_2$ for ruthenium complexes. Comparing data in Table 1 and Figures 5.11 with Figure 5.12 it can be noted that the complex [Ru(bpy)$_2$-L4-Ir(ppy)$_2$](PF$_6$)$_3$ has two intense bands in the UV region 268 -289 nm which are assigned to intraligand (IL) $\pi \rightarrow \pi^*$ transitions localized on ppy ligand for 268 nm and localized on bpy for 289 nm, and weaker metal-to-ligand charge transfer bands between 350 nm and 400 nm which are assigned to Ir ^{1}MLCT (d$_\pi \rightarrow \pi^*$) and the the intensity of bands between 370 nm and 450 nm which are assigned to Ru ^{1}MLCT (d$_\pi \rightarrow \pi^*$). The UV-vis absorption spectrum of [Ru(bpy)$_2$-L4-Ir(ppy)$_2$](PF$_6$)$_3$ is approxmintely the sum of those for [Ir(ppy)$_2$-L4](PF$_6$) and [Ru(bpy)$_2$-L4](PF$_6$)$_2$. (Figure 5.12).
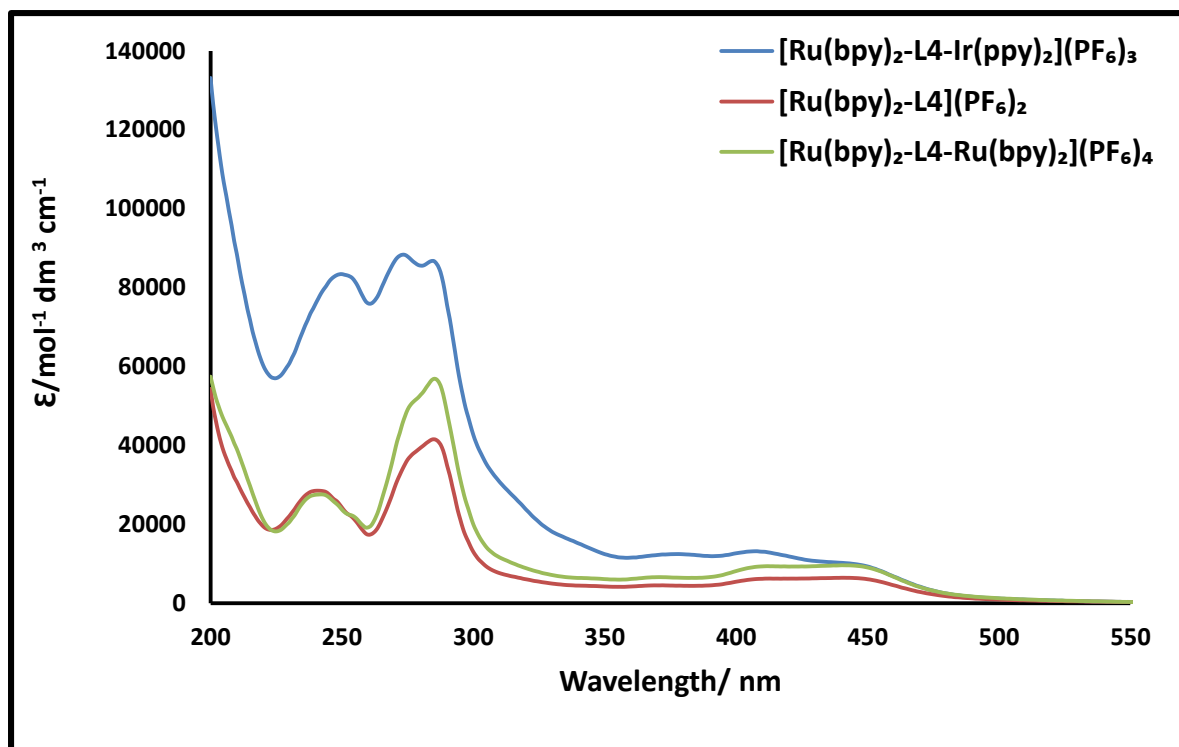
Figure 5-12 - UV-vis absorption spectra of ruthenium complexes and Iridium- Ruthenium complex in acetonitrile

The UV-vis absorption spectrum of osmium complexes [Os(bpy)₂-L4-Os(bpy)₂](PF₆)₄ and [Os(Bn-pytz)₂-L4-Os(Bn-pytz)₂](PF₆)₄ were also recorded in acetonitrile (Figure 5.13). [Os(Bn-pytz)₂-L4-Os(Bn-pytz)₂](PF₆)₄ exhibits two intense bands. The first (276 nm), is ascribed to the pytz and L4 ligands-centered ^{1}LC $\pi \to \pi^*$ transitions. The complex exhibits second intense absorption band in the visible region between 366- 410 nm assignable to the ^{1}MLCT (d $\to \pi^*$) transitions, from the Os metal center to π^* pytz (both bridging and exial ligands), and a broad and weak band at 530 nm. This weaker and lower energy band is assigned to direct spin-forbidden ^{3}MLCT transitions. [Os(bpy)₂-L4-Os(bpy)₂](PF₆)₄, has intense on band at (289 nm) with a shoulder at 278 nm. From Figure 5.13 it can be seen that the intense bands in the UV region in [Os(bpy)₂-L4-Os(bpy)₂](PF₆)₄ 289 nm localized on the bpy ligands, assigned as intraligand $\pi \to \pi^*$ transitions, which are appeared in the Ru complexes,[245] while the shoulder at 278 nm is assigned as intraligand $\pi \to \pi^*$ transitions localized on the pytz from the bridging ligand. [Os(bpy)₂-L4-Os(bpy)₂](PF₆)₄, also has a second intense absorption band

180

in the visible region between 370- 410 nm assignable to the ^{1}MLCT $(d \rightarrow \pi^{*)}$ transitions, from Os metal center to π^* of L4. This band extends to 475 nm. Compared to [Os(Bn-pytz)$_2$-L4-Os(Bn-pytz)$_2$](PF$_6$)$_4$, assignable to the ^{1}MLCT $(d \rightarrow \pi^*)$ transitions, from Os metal center to bpy π^*. The UV-vis absorption spectrum of [Os(bpy)$_2$-L4-Os(bpy)$_2$](PF$_6$)$_4$ has a broad and weak band at 650 nm, which is assigned to direct spin-forbidden ^{3}MLCT transitions. For both complexes, the spin forbidden ^{3}MLCT band is reasonably intense because of the large spin-orbital coupling that results from the heavy osmium atom.
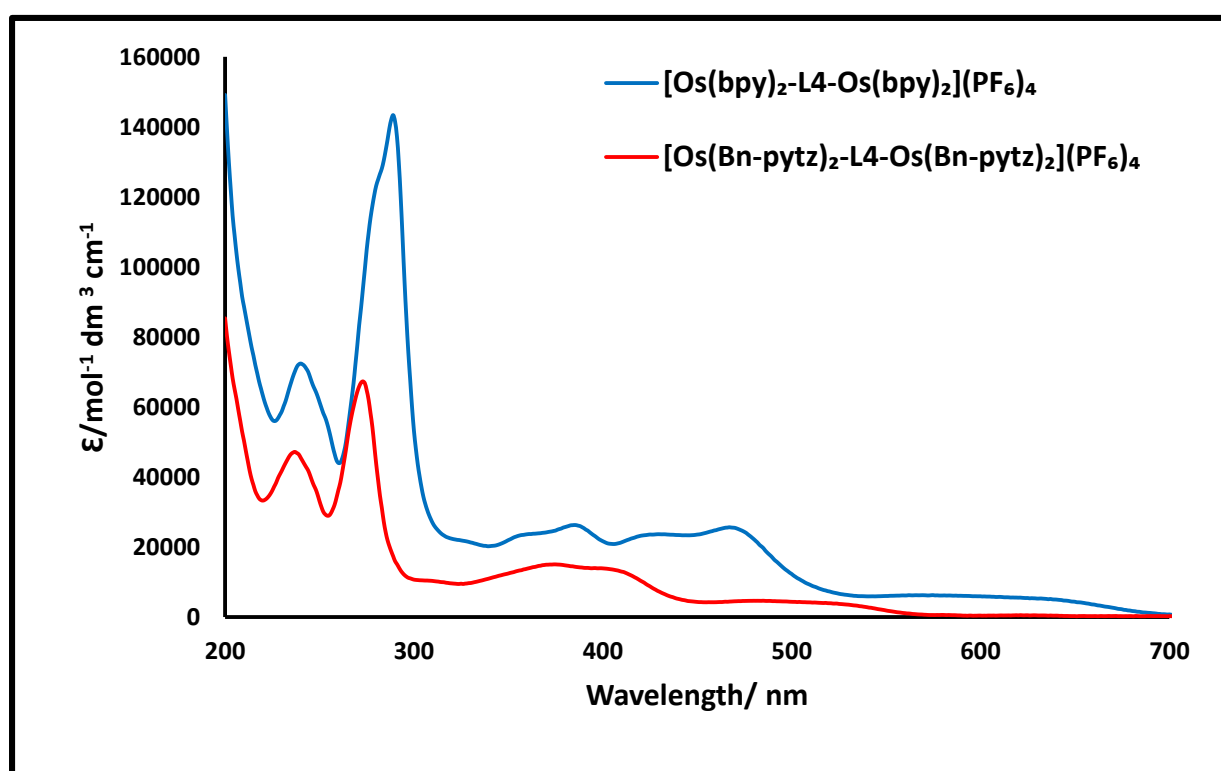
Figure 5-13 - UV-vis absorption spectra of osmium complexes in acetonitrile

Complexes $[Ru(bpy)_2\text{-L4}](PF_6)_2$ and $[Ru(bpy)_2\text{-L4-Ru(bpy)}_2](PF_6)_4$, exhibit a broad featureless emission bands at room temperature in acetonitrile, which we assigned to emission from ^3MLCT states (Figure 5.14). In the room temperature spectra, both complexes exhibit emission bands in the orange region of the spectrum ($\lambda_{max} = 615$ nm, Table 2). Compared with $[Ru(bpy)_2(bn\text{-pytz})]^{2+}$ which was found to be very weakly emissive in CH_2Cl_2 at room tempreture (quantum yield = 0.001),[246] $[Ru(bpy)_2\text{-L4}](PF_6)_2$ and $[Ru(bpy)_2\text{-L4-Ru(bpy)}_2](PF_6)_4$ approximately exhibit the same emission bands with small quantum yield, which are 0.068 and 0.066 respectively.
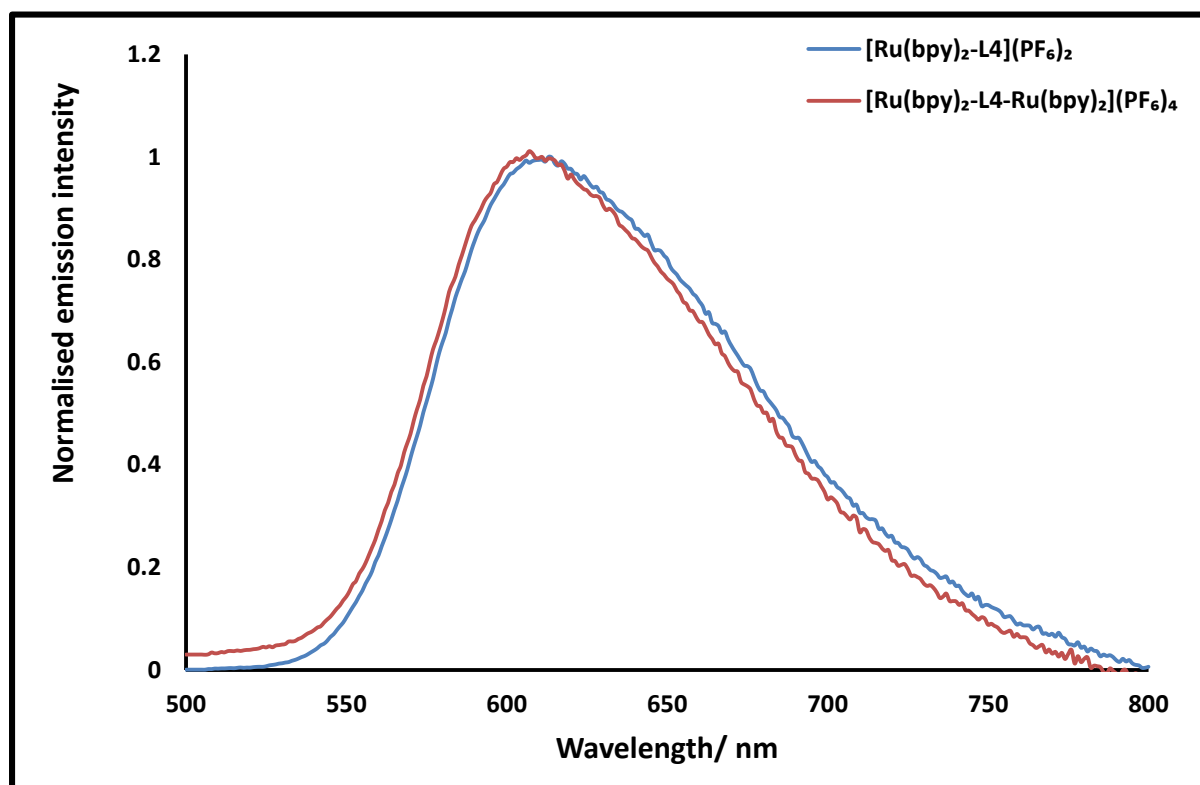
Figure 5-14 Room-temperature emission of complexes $[Ru(bpy)_2\text{-L4}](PF_6)_2$, $[Ru(bpy)_2\text{-L4-Ru(bpy)}_2](PF_6)_4$, in aerated acetonitrile

The complex $[Os(Bn\text{-}pytz)_2\text{-}L4\text{-}Os(Bn\text{-}pytz)_2](PF_6)_4$ exhibits an emission band in the orange region of the spectrum ($\lambda_{max} = 615$ nm, Table 2 and Figure 5-15). These emission bands are in very similar position to those of $[Os(Bn\text{-}pytz)_3](PF_6)_2$ (Chapter 3). Due to the much higher energy of the pytz π^* orbitals compared to bpy, the emission of $[Os(Bn\text{-}pytz)_2\text{-}L4\text{-}Os(Bn\text{-}pytz)_2](PF_6)_4$ is significantly blue-shifted relative to that of $[Os(bpy)_2\text{-}L4\text{-}Os(bpy)_2](PF_6)_4$ which emits in the deep red/near IR ($\lambda_{max} = 730$ nm) and has similar emission properties to those of $[Os(bpy)_2(Bn\text{-}pytz)](PF_6)_2$.
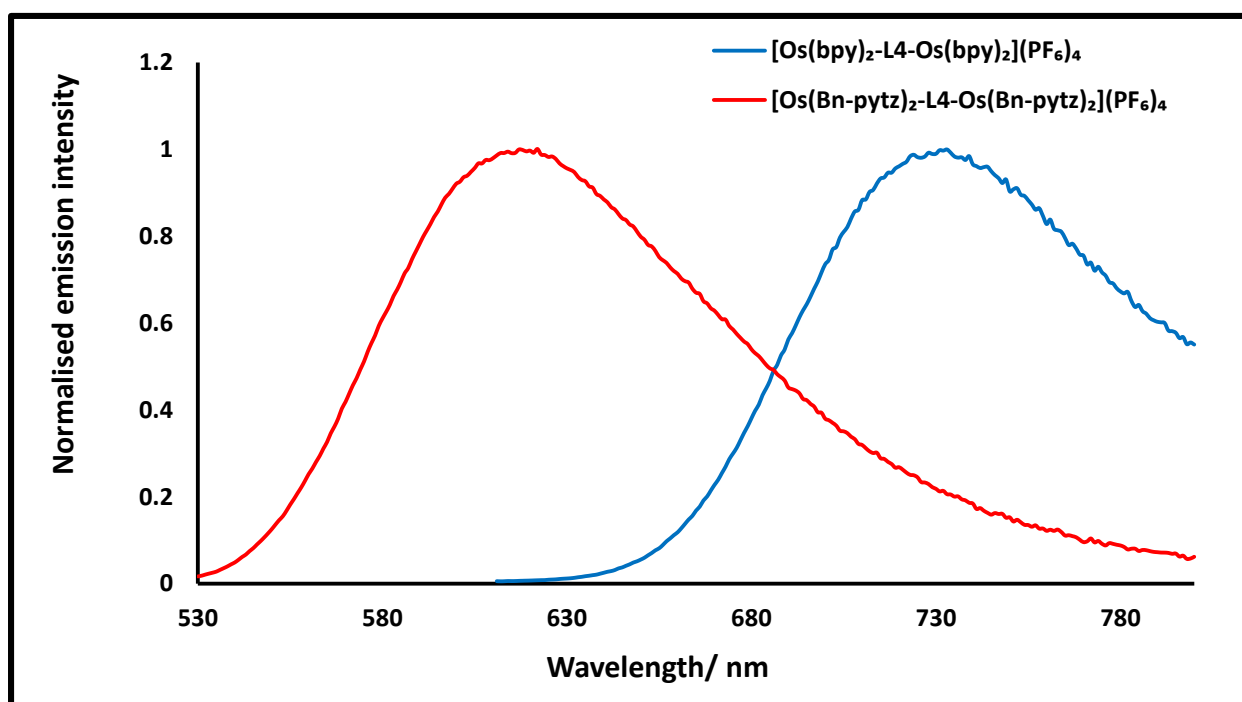
Figure 5-15 Room-temperature emission of complexes $[Os(Bn\text{-}pytz)_2\text{-}L4\text{-}Os(Bn\text{-}pytz)_2](PF_6)_4$, $[Os(bpy)_2\text{-}L4\text{-}Os(bpy)_2](PF_6)_4$, in aerated acetonitrile

Comparing the complexes which are reported here and related bidentate complexes $[Os(bpy)_2\text{-}L4\text{-}Os(bpy)_2](PF_6)_4$ to $[Os(bpy)_3]^{2+}$,[228] $[Os(Bn\text{-}pytz)_2\text{-}L4\text{-}Os(Bn\text{-}pytz)_2](PF_6)_4$ to $[Os(Bn\text{-}pytz)_3]^{2+}$ (Chapter 3), and $[Ru(bpy)_2\text{-}L4](PF_6)_2$ and $[Ru(bpy)_2\text{-}L4\text{-}Ru(bpy)_2](PF_6)_4$ to $[Ru(bpy)_2(Bn\text{-}pytz)]^{2+}$ $[Ru(bpy)_3]^{2+}$,[247] it is noted that there is no a significant difference in emission properties. This means that the ligand 1,4-bis-{4-(pyridi-2-yl)-1,2,3-triazol-1-yl}methylbenzene as bridging ligand has a negligable electronic effect on the MLCT

energy. This is confermed by electrochemistry investigation where the oxidation and reduction are in the same region for both compleces. The emission spectra of the iridium complexes [Ir(ppy)$_2$-L4](PF$_6$) and [Ir(ppy)$_2$-L4-Ir(ppy)$_2$](PF$_6$)$_2$ were also recorded in acetonitrile. The compounds display structured emission bands, often indicative of the presence of a large amount of ligand-centred character in the emissive excited states. These are indeed a mixture of ^{3}MLCT and ^{3}ILCT character with similar vibrational features to those reported for other [Ir(ppy)$_2$]$^{+/0}$ based complexes (λ max = 474, 503 nm).[105] There is no a significant difference or change in emission when comparing the complexes [Ir(ppy)$_2$-L4](PF$_6$) and [Ir(ppy)$_2$-L4-Ir(ppy)$_2$](PF$_6$)$_2$ to [Ir(ppy)$_2$(bn-pytz)]$^{2+}$.[121] The heterodinuclear complex [Ru(bpy)$_2$-L4-Ir(ppy)$_2$](PF$_6$)$_3$ shows emission features similar to those observed in the spectra for both [Ru(bpy)$_2$-L4](PF$_6$)$_2$ and [Ir(ppy)$_2$-L4](PF$_6$) (λ max = 474, 503 and 615 nm) and this shows dual emission. Figure 5-16. While the quantum yield of [Ir(ppy)$_2$(pytz)]$^+$ is 21%[144] and < 0. 1% for [Ru(bpy)$_2$(pytz)]$^{2+}$,[246] the quantum yield of [Ru(bpy)$_2$-L4-Ir(ppy)$_2$]$^{3+}$ is 0.33 % . What is noteworthy is that emission for iridium and ruthenium based chromophors in the complex are observed to be of the similar intensity which indicates that the quantum yield of the Ir chromophore in [Ru(bpy)$_2$-L4-Ir(ppy)$_2$](PF$_6$)$_3$ is a lot less than the quantum yield for [Ir(ppy)$_2$(pytz)]$^+$. It therefore appears that partial photo induced energy transfer from the Ir chromophore to the Ru chromophore occurs, which means that Ir is partially sensitising emission from the Ru chromophore.
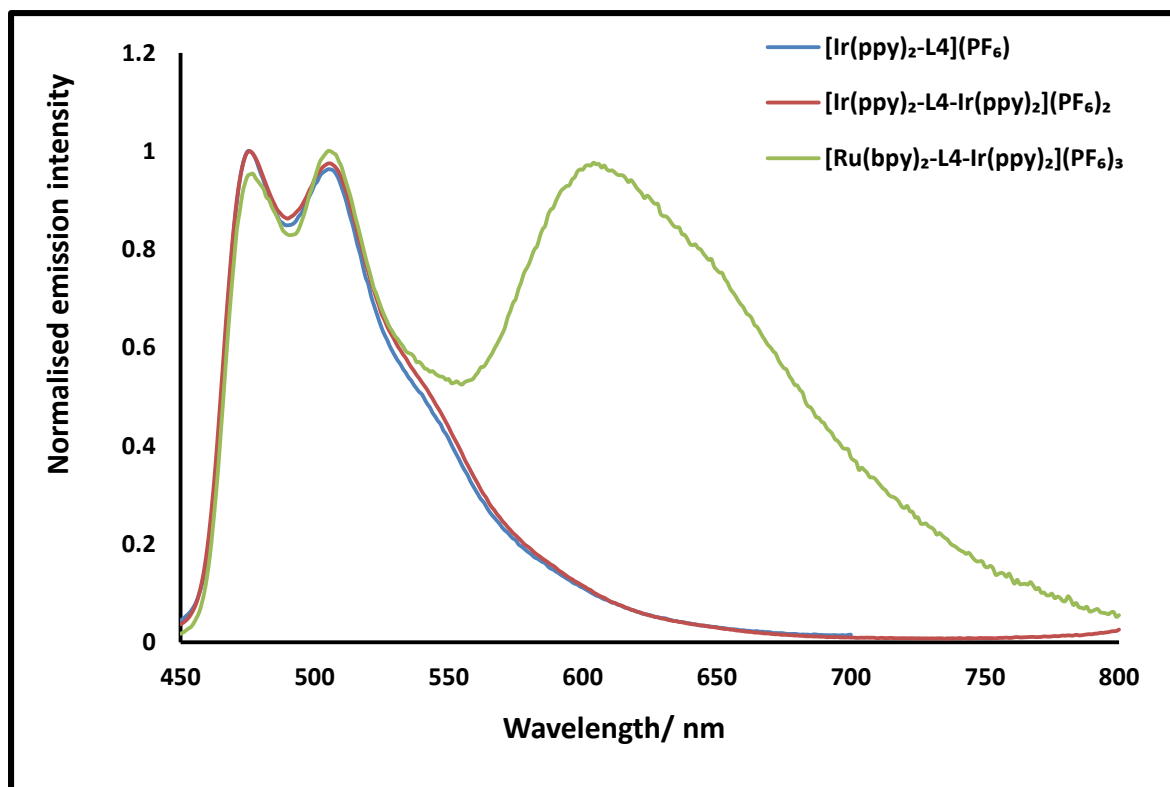
Figure 5-16 Room-temperature emission of complexes [Ir(ppy)$_2$-L4](PF$_6$), [Ir(ppy)$_2$-L4-Ir(ppy)$_2$](PF$_6$)$_2$ and [Ru(bpy)$_2$-L4-Ir(ppy)$_2$](PF$_6$)$_3$ in aerated acetonitrile

The potential of energy transfer across the bridging ligand results in broadened emission and hence open up the possibility of making white light emitters. Commission Internationale De L'Eclairage (CIE) 1931 chromaticity coordinates were determined to establish the perceived colour of the complexes [Ir(ppy)$_2$-L4-Ir(ppy)$_2$](PF$_6$)$_2$, [Ru(bpy)$_2$-L4-Ru(bpy)$_2$](PF$_6$)$_4$ and [Ru(bpy)$_2$-L4-Ir(ppy)$_2$](PF$_6$)$_3$ using photoluminescence spectral data in acetonitrile at room temperature. The calculated values of x and y are displayed in Table 5.3. From the (CIE) diagram (Figure 5.17) we can see that there is a straight line through color coordnate of the three complexes as would be expected if the emission spectrum of the hetero dinuclear complex was essentially a linear combination of contribution for the Ir and Ru chromophores. The coordinates for heteronuclear complex [Ru(bpy)$_2$-L4-Ir(ppy)$_2$](PF$_6$)$_3$ appears in yellow/white.
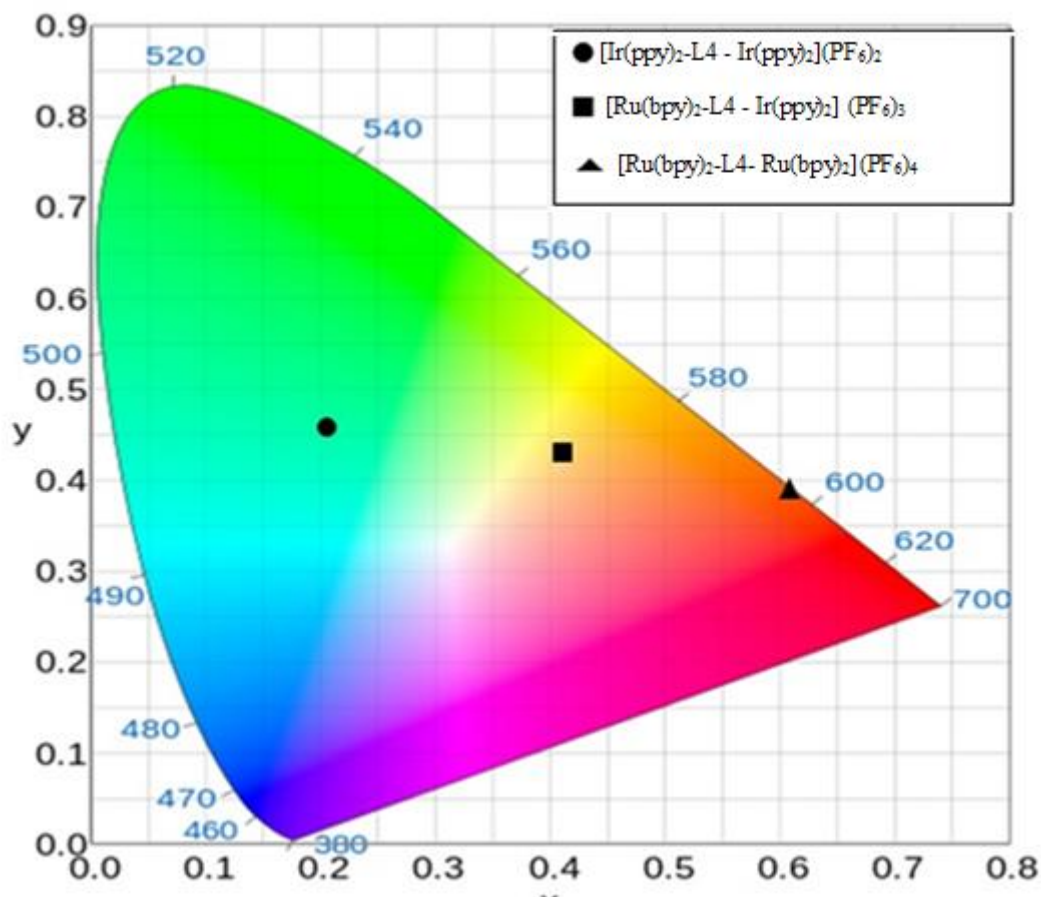
Figure 5-17 Color space chromaticity CIE diagram of the complexes[Ir(ppy)$_2$-L4 - Ir(ppy)$_2$] (PF$_6$)$_2$,[Ru(bpy)$_2$-L4- Ru(bpy)$_2$] (PF$_6$)$_4$ and [Ru(bpy)$_2$-L4 - Ir(ppy)$_2$](PF$_6$)$_3$

Table 5-3: The calculated values of *x* and *y* for complexes [Ir(ppy)$_2$-L4-Ir(ppy)$_2$](PF$_6$)$_2$, [Ru(bpy)$_2$-L4-Ru(bpy)$_2$](PF$_6$)$_4$ and [Ru(bpy)$_2$-L4-Ir(ppy)$_2$](PF$_6$)$_3$.

complex	X	Y	Colour
[Ir(ppy)$_2$-L4-Ir(ppy)$_2$](PF$_6$)$_2$	0.206	0.458	Turquoise
[Ru(bpy)$_2$-L4-Ru(bpy)$_2$](PF$_6$)$_4$	0.608	0.391	Orange
[Ru(bpy)$_2$-L4-Ir(ppy)$_2$](PF$_6$)$_3$	0.410	0.430	Yellow/white

The emission spectra of the complexes were also recorded at 77 K in rigid (4:1 EtOH/MeOH glass matrix). From Figures 5.18 – 5-21 it can be seen that on lowering the temperature to 77 K, the emission undergoes a rigdochromic blue-shift of between 30-40 nm for all complexes. For all complexes such behaviour is again typical for metal-to-ligand charge transfer (MLCT) emissions, at 77 K. Also we can note that all complexes show vibronic progressions in emission spectra which are typical of mononuclear analogues already known[109] (Chapter 3). The photophysical data are summarized in Table 5.4.

Table 5-4: Photoluminescence data and lifetime for the complexes in aerated acetonitrile at room temperature and 77 K (4:1 EtOH/MeOH glass matrix

Compound	At room temperature		At 77 k
	λ max(nm	ʈ ns	λ max (nm)
[Ir(ppy)$_2$-L4](PF$_6$)	475, 503	63	468,503
[Ir(ppy)$_2$-L4-Ir(ppy)$_2$](PF$_6$)$_2$	475, 503	65	468, 503
[Ru(bpy)$_2$-L4](PF$_6$)$_2$	615	6(75%), 14(25%),	568
[Ru(bpy)$_2$-L4-Ru(bpy)$_2$](PF$_6$)$_4$	615	7(75%), 16(25%)	568
[Ru(bpy)$_2$-L4-Ir(ppy)$_2$](PF$_6$)$_3$	475, 506, 615	5(40%), 42(60%)	468, 503, 568
[Os(bpy)$_2$-L4-Os(bpy)$_2$](PF$_6$)$_4$	732	49	700
[Os(Bn-pytz)$_2$-L4-Os(Bn-pytz)$_2$](PF$_6$)$_4$	617	60	570

The emission spectra of the complexes [Os(Bn-pytz)$_2$-L4-Os(Bn-pytz)$_2$](PF$_6$)$_4$ and [Os(bpy)$_2$-L4-Os(bpy)$_2$](PF$_6$)$_4$ were recorded at 77 K in rigid (4:1 EtOH/MeOH glass matrix), Figure 5-18. [Os(Bn-pytz)$_2$-L4-Os(Bn-pytz)$_2$](PF$_6$)$_4$ complex exhibits emission features similar to those observed in [Os(bn-pytz)$_3$]$^{2+}$ (Chapter 3) and [Os(btzpy)$_2$]$^{2+}$ (Chapter 4) complexes, while [Os(bpy)$_2$-L4-Os(bpy)$_2$](PF$_6$)$_4$ complex displys the same features of the complex [Os(bpy)$_2$(bn-pytz)]$^{2+}$ in the same conditions (Chapter 3).
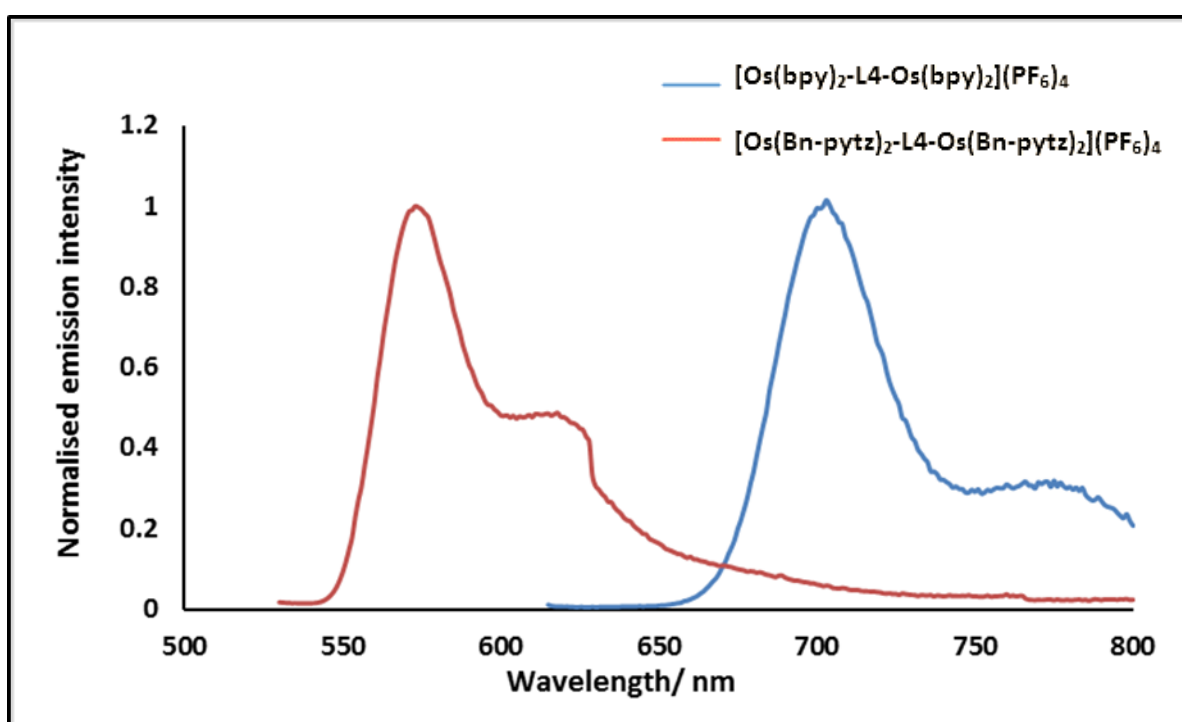
Figure 5-18 Emission spectra of the complexes [Os(bpy)$_2$-L4-Os(bpy)$_2$](PF$_6$)$_4$ and [Os(Bn-pytz)$_2$-L4-Os(Bn-pytz)$_2$](PF$_6$)$_4$ in rigid matrix at 77 K.

The emission spectra in the low-temperature experiments become well-structured for the iridium complexes [Ir(ppy)$_2$-L4](PF$_6$) and [Ir(ppy)$_2$-L4-Ir(ppy)$_2$](PF$_6$)$_2$. Figure 5-19, the complexes have spectra that nearly overlap in peak position and relative peak intensities. As expected the complexes disply the same features of the complexes [Ir(ppy)$_2$(bn-pytz)]$^{2+}$.[144]
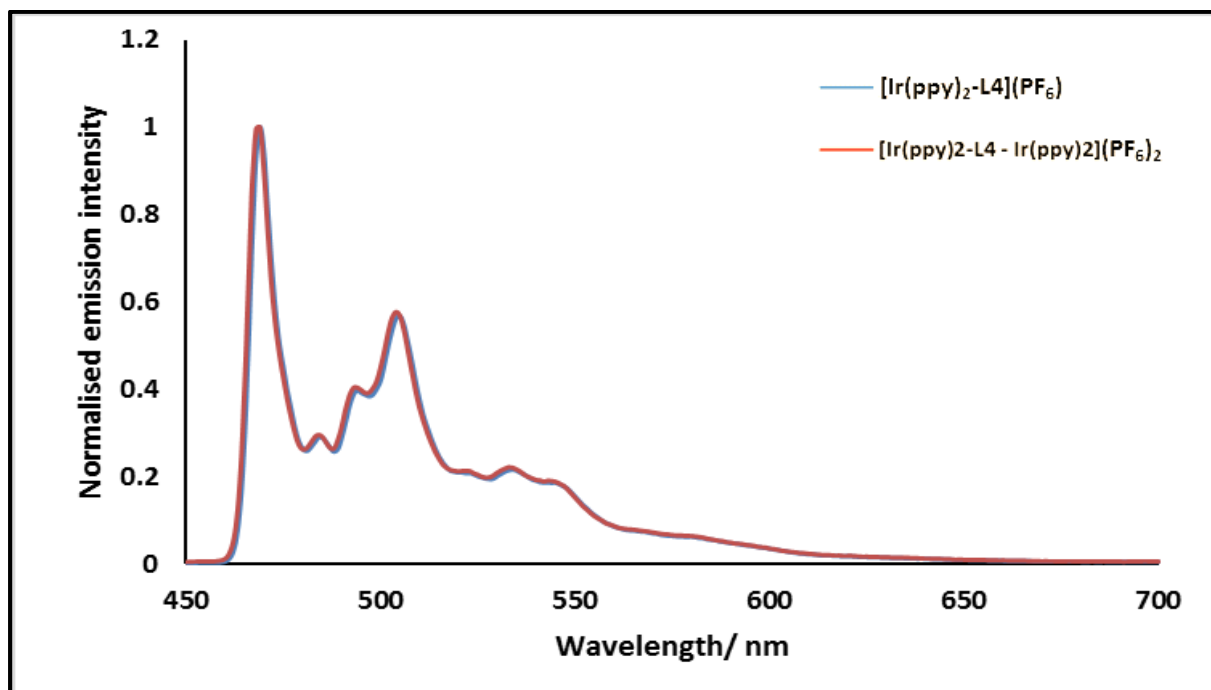
Figure 5-19 Emission spectra of the complexes [Ir(ppy)$_2$-L4](PF$_6$) and [Ir(ppy)$_2$-L4-Ir(ppy)$_2$](PF$_6$)$_2$ in rigid matrix at 77 K.

Figure 5.20 shows the emission spectra of the [Ru(bpy)$_2$-L4](PF$_6$)$_2$ and [Ru(bpy)$_2$-L4-Ru(bpy)$_2$](PF$_6$)$_4$ complexes at 77 K in rigid 4:1 EtOH/MeOH glass matrices. Again comparing with the spectra at room temperature (Figure 5-14), the emission spectra in the low-temperature experiments become well-structured. The complexes have spectra that closely overlap in peak position and relative peak intensities. As expected the complexes disply the same features of the complexes [Ru(bpy)$_2$(bn-pytz)]$^{2+}$.[94]
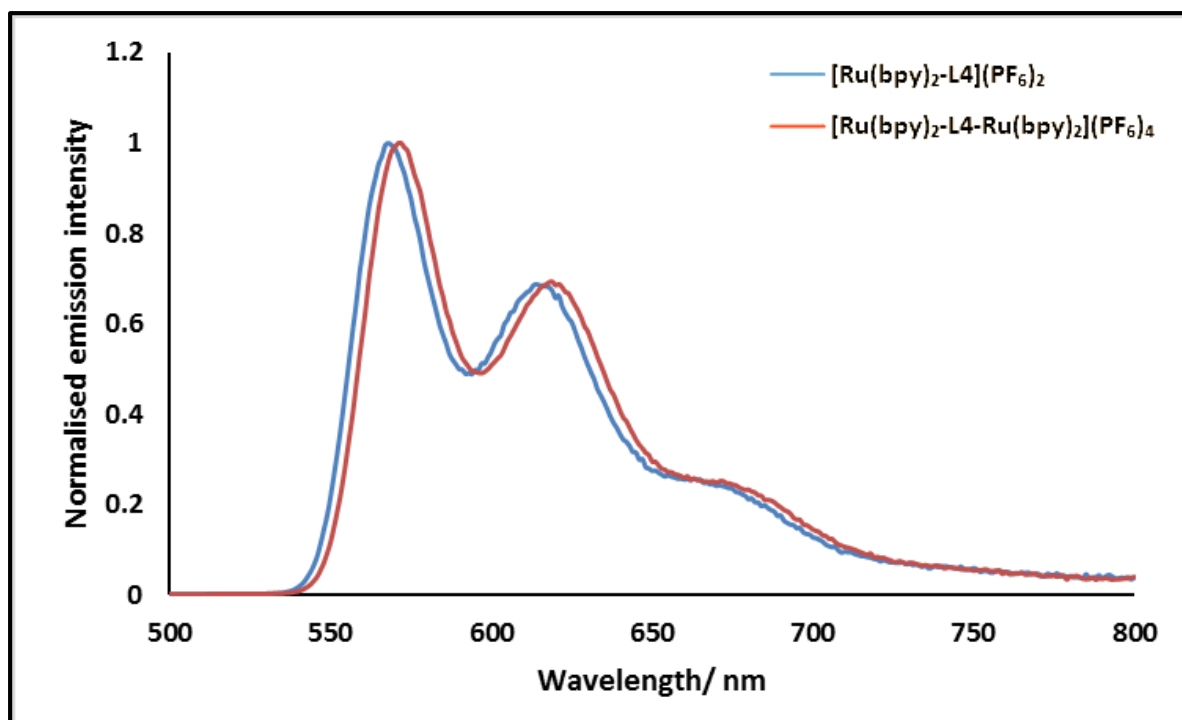
Figure 5-20 Emission spectra of the complexes [Ru(bpy)$_2$-L4](PF$_6$)$_2$ and [Ru(bpy)$_2$-L4-Ru(bpy)$_2$](PF$_6$)$_4$ in rigid matrix at 77 K.

[Ru(bpy)$_2$-L4-Ir(ppy)$_2$](PF$_6$)$_3$ at 77 K in rigid (4:1 EtOH/MeOH glass matrix Figure 5-21. shows emission features similar to those observed in the both spectra for [Ru(bpy)$_2$-L4](PF$_6$)$_2$ and [Ir(ppy)$_2$-L4](PF$_6$)complexes in the same conditions (λ max = 468, 503 and 568 nm). Figure 5-22. There again appears to be partial energy transfer from the Ir chromophore to the Ru chromophore, which means again that the Ir is sensitising emission from the Ru chromophore. Here, however, the intensity of emission for the Ru centre is of slightly greater intensity than that for Ir.
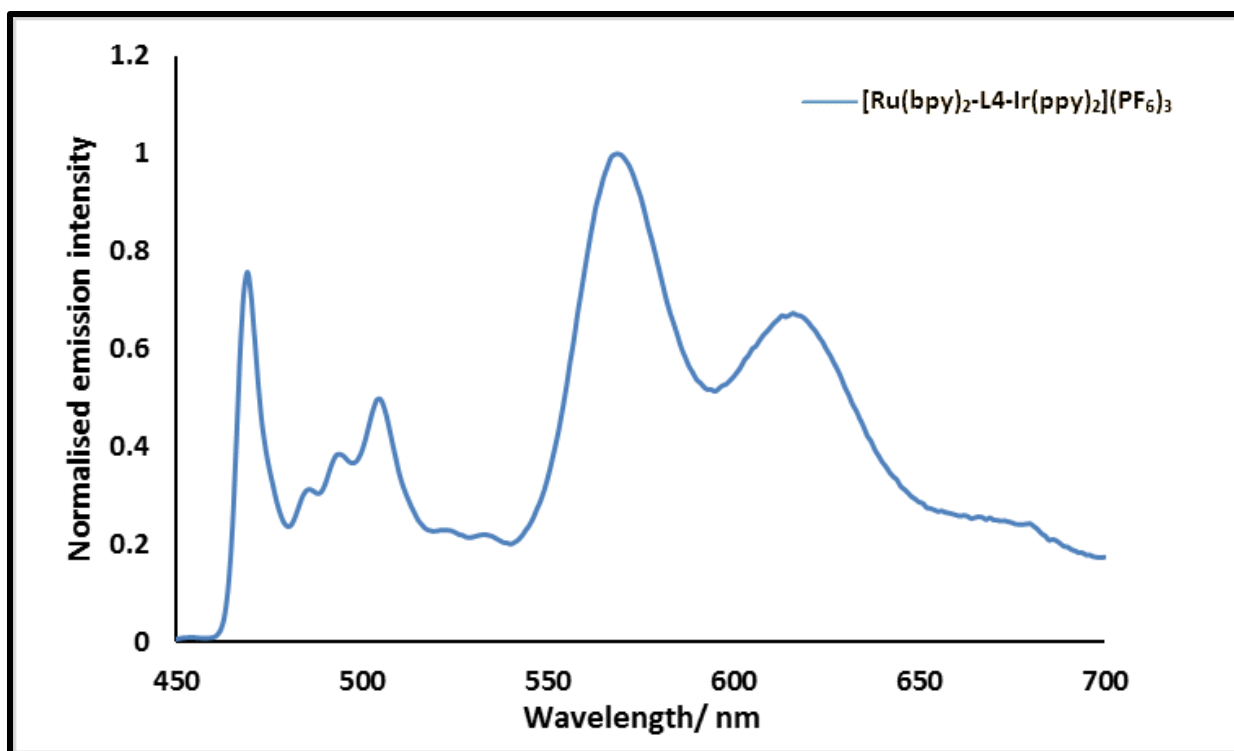
Figure 5-21 Emission spectra of the complex [Ru(bpy)$_2$-L4-Ir(ppy)$_2$](PF$_6$)$_3$ in rigid matrix at 77 K.
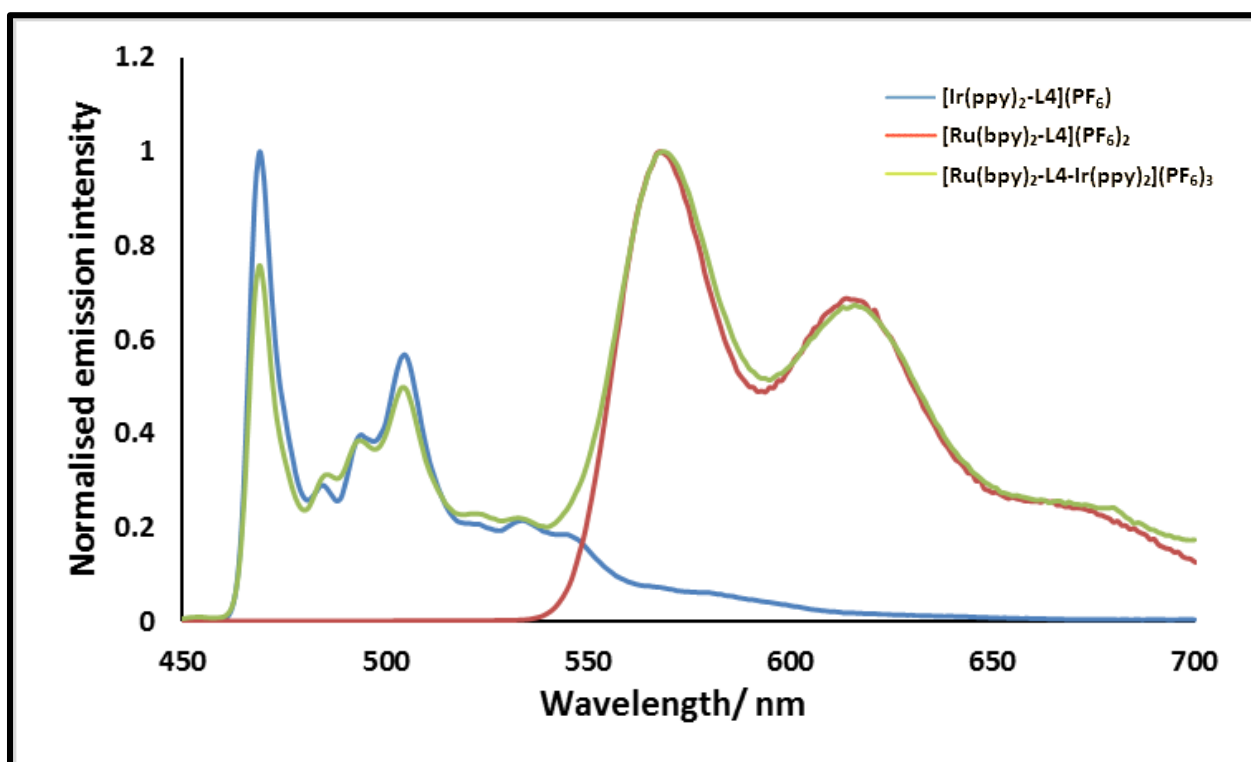
Figure 5-22 Emission spectra of the complexes [Ir(ppy)$_2$-L4](PF$_6$), Ru(bpy)$_2$-L4](PF$_6$)$_2$ and [Ru(bpy)$_2$-L4-Ir(ppy)$_2$](PF$_6$)$_3$ in rigid matrix at 77 K.

5.5 Conclusion

In conclusion homodinuclear complexes $[Ir(ppy)_2\text{-}L4\text{-}Ir(ppy)_2](PF_6)_2$, $[Ru(bpy)_2\text{-}L4\text{-}Ru(bpy)_2](PF_6)_4$, $[Os(bpy)_2\text{-}L4\text{-}Os(bpy)_2](PF_6)_4$ and $[Os(Bn\text{-}pytz)_2\text{-}L4\text{-}Os(Bn\text{-}pytz)_2](PF_6)_4$ and the heterodinuclear complex $[Ru(bpy)_2\text{-}L4\text{-}Ir(ppy)_2](PF_6)_3$ have been successfully prepared and characterised . From the photophysical and electrochemical studies it was shown that the dinuclear species exhibit additive luminescent intensities when compared to their mono-nuclear analogue complexes. There is little evidence of ground state communication between the metal centres across the triazole based bridging ligand. However, there appears to be some excited state energy transfer between Ir and Ru chromophores in the heterodinuclear complex. It becomes clear, therefore, that the auxiliary ligands coordinated to the metal center play a significant role in the photophysical properties of these complexes which mean photophysical properties of these complexes could be improved by controlling the auxiliary ligands coordinated to the metal center. For the reported complex $[Ru(bpy)_2\text{-}L4\text{-}Ir(ppy)_2](PF_6)_3$, dual emission resulted in near white light emission; this might be achevible through modification of the Ir chromophore to blue shift the emission but also through modification of the bridging ligand in order to tune the rates of energy transfer between chromophore and thus the relative contribution from Ir and Ru chromophores in the overall emission.

Chapter 6: General conclusions and outlook

6.1 **General conclusion**

The original goal of the research presented in this thesis was to study the photophysics of 1,2,3-triazole-based luminescent complexes and explore their potential applications, for example, in biological imaging. In the attempt to meet the criteria put forth above, research was directed toward complexes containing previously under-developed ligands containing 1,2,3-triazole moieties. This group of ligands was chosen in part for its ease of synthesis. The copper-catalyzed azide-alkyne cycloaddition being one of the most versatile click reactions allows isolation of pure products simply through filtering or other simple extraction methods not requiring recrystallisation or chromatography.[96] In this work, different types of 1,2,3-triazole ligands were synthesized including 2-(1-benzyl-1H-1,2,3-triazol-4-yl)pyridine as a bidentate ligand, 2,6-bis(1-phenyl-1H-1,2,3-triazol-4-yl)pyridine as a tridentate ligand and 1,4-bis((4-(pyridin-2-yl)-1H-1,2,3-triazol-1-yl)methyl)benzene which was applied as a bridging ligand, Through this work it is demonstrated that the CuAAC reaction can be utilized as an excellent tool for the preparation of new chelating ligands incorporating either one or multiple binding sites starting from benzyl azide and reacting them with 2-ethynylpyridine.

This work began with an investigation of rhenium tricarbonyl complexes which shows that 1,4- disubstituted-1,2,3-triazole ligands can act as bidentate N^N donor ligands. The blue-shift in electronic absorption and luminescence spectra of the resulting [Re(Bn-pytz)(CO)$_3$Cl] compound indicated that Bn-pytz behaves like a bipyridine imitative with strongly electron-donating substituents. Even though Bn-pytz ligand is a poor π-acceptor, EL emission was observed from [Re(Bn-pytz)(CO)$_3$(py)]$^+$. Absorption and emission spectra are broad and featureless. The HOMO localized on (Re), while the LUMO localized on (N^N). These results indicate that changing the diimine ligand to 1,4- disubstituted-1,2,3-triazole effects the LUMO of complex, and MLCT energy. The effect of changing an axial ligand was found to be minimal

194

with respect to the absorption spectra and emission maxima. The [Re(Bn-pytz)(CO)$_3$(py)]$^+$ complex was applied in LEEC devices. Even with poor stability, the performance of the LEEC based on [Re(Bn-pytz)(CO)$_3$(py)](PF$_6$) showed better performance than [Re(bpy)(CO)$_3$(py)](PF$_6$).

1,4-disubstituted-1,2,3-triazole ligands were also applied as bidentate N^N donor ligands to prepare osmium(II) complexes. A series of heteroleptic osmium(II) triazole-containing complexes [Os(bpy)$_2$(Bn-pytz)]$^{2+}$, [Os(bpy)(Bn-pytz)$_2$]$^{2+}$ and homoleptic osmium(II) complexes [Os(bpy)$_3$]$^{2+}$ and [Os(Bn-pytz)$_3$]$^{2+}$ as their hexafluorophosphate and chloride salts were prepared and characterised. Successful separation of the two isomers of [Os(Bn-pytz)$_3$](PF$_6$)$_2$ was possible but only on a small scale. All the complexes display ^{3}MLCT emission in the orange to red region, blue-shifted as a result of replacing bpy with Bn-pytz. In the presence of oxygen, the complex [Os(Bn-pytz)$_3$]$^{2+}$ was shown to exhibit significant quenching of luminescence intensity. The water soluble chloride salts were subjected to preliminary cellular uptake and luminescence imaging studies. [Os(Bn-pytz)$_3$]$^{2+}$ is the only one of complexes that goes into cells and localises at lysosomes, but no PDT activity is observed, despite having a high ^{1}O$_2$ quantum yield.

Based on promising results with [Os(Bn-pytz)$_3$]$^{2+}$, the 2,6-bis(1-phenyl-1,2,3-triazol-4-yl)pyridine) ligand was used as a tridentate donor ligand to prepare the orange-emissive bis(tridentate) osmium(II) complex [Os(btzpy)$_2$]$^{2+}$ as its hexafluorophosphate and chloride salts. The photophysical properties of these systems was investigated. The complexes are emissive at room temperature in air in the orange to red region of the visible spectrum. In the presence of oxygen, the novel luminescent osmium(II) triazole-based complex, [Os(btzpy)$_2$]$^{2+}$ was shown to exhibit significant quenching of luminescence intensity and a high quantum yield for singlet oxygen sensitization as its chloride salt. The water soluble chloride form of the complex was subjected to preliminary cellular uptake and luminescence imaging microscopy

studies. The results from these studies showed [Os(Bn-pytz)₃]²⁺ complex is successfully taken up by two cancer cell lines with a high degree of mitochondrial localization and low dark toxicity.[228] Complexes based on this type of ligand are good candidates for development of cellular imaging agents.

The CuAAC reaction was used to prepare 1,4-bis-({4-(pyrid-2-yl)-1,2,3-triazol-1-yl}methyl) benzene as the bridging ligand in metal homodinuclear complexes of Os(II), Ru(II), and Ir(III) and a heterodinuclear Ir and Ru complex. Photophysical and electrochemical studies were carried out. The results of these studies showed that the dinuclear species exhibit greater luminescent intensities than mono-nuclear model complexes. The potential energy transfer and dual emission for the hetrodinuclear iridium- ruthenium complex results in near-white light emission. The products might find useful applications in LEECs and other artificial lighting technologies.

6.2 Future work

The work presented in this thesis has the potential to be extended further:

Osmium triazole complexes, which present an excellent platform for the development of novel theranostic agents for anticancer activity by shifting both absorption and emission in the red region by using more nitrogen withdrawing triazole ligand for example; pyrimidine and pyrazine:
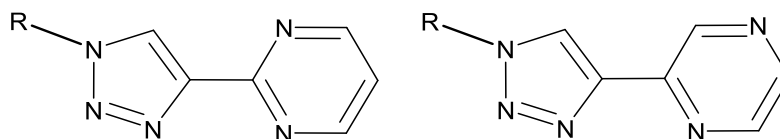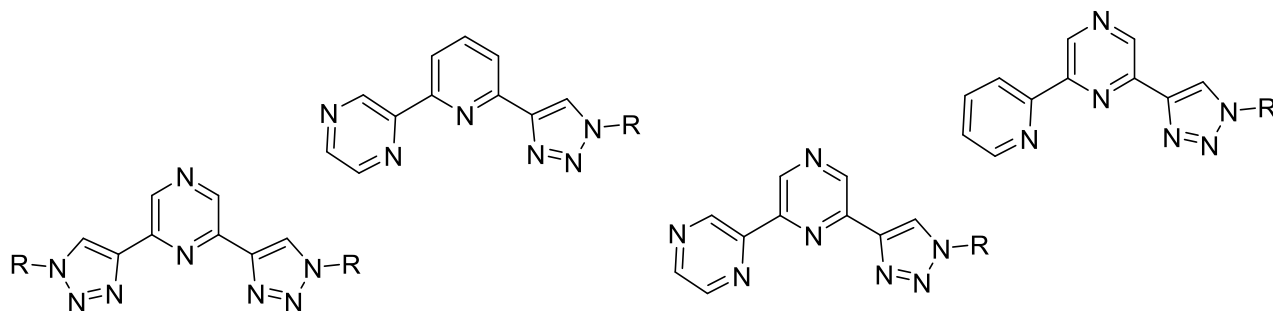
Pyrimidine and pyrazine have a lower LUMO than pyridine. This is expected to result in a red shift of the emission and absorption into the more useful window, red light goes through the biological tissue, which is more useful for cell imaging and also, gives greater depth of light penetration for single oxygen sensitisation. The study in this work indicates that maintaning localization of the excited state on the triazole containing ligand is important for the high $^3O_2$ quenching to $^1O_2$ with a high quantum yield of $^1O_2$. The kind of nitrogen withdrawing ring will give the ability to control the photophysical and electrochemical properties of complexes by controlling of the HOMO− LUMO gap and the number of triazole rings leads to control of the sensitivity of the complex to oxygen. Some of the possible applications of mixed metal complexes include:

Mixed Ru/Re complexes for the photocatalysis of CO_2 reduction. Rhenium chromophore was shown to be effective photocatalysts for CO_2 reduction with a high level of catalytic stability.[248] While the ruthenium chromophore will act as photosensitizer part.
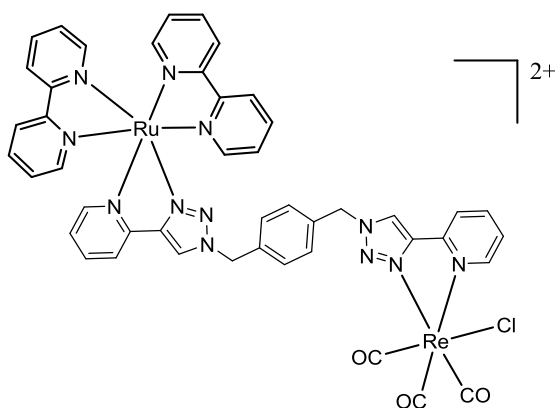
Mixed Os/Ir complexes could be envisaged and have potential applications in water oxidation photocatalysis and CO_2 reduction. This heteronuclear complex is expected to give dual emission resulting in near white light emission. Both chromophores showed good catalytic water oxidation activity.[249, 250] Water soluble chloride salts of these complexes could be envisaged and subjected to preliminary cellular uptake and luminescence imaging microscopy studies.
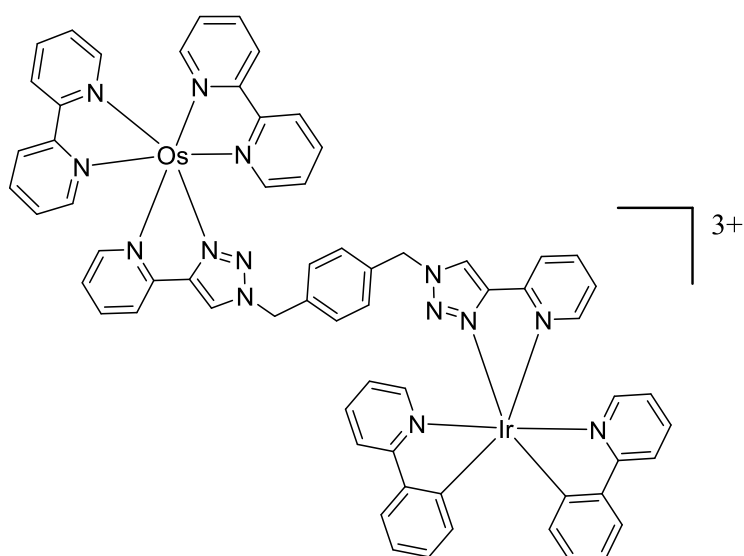
The photophysical and electrochemical properties of dinuclear transition metal complexes [Ru(bpy)$_2$-L4-Ir(ppy)$_2$](PF$_6$)$_3$ and related complexes can be improved and controlled by controlling the auxiliary ligands coordinated to the metal center which play a significant role in the photophysical properties of these complexes. For example: using (difppy = 2-(2,4-

difluorophenyl)pyridine) as a chromophore ligand instead of ppy leads to an increase in the HOMO− LUMO gap, which make the Ir emitter more blue rather than a greenish emitter. This will take the line connecting the CIE coordinates of the complex closer to the white region, which may give the dinuclear transition metal complexes ability to emit white light and therefore maybe suitable for use in white light emiting LEC applications. As well we can also explore adapting the nature of the bridging ligand
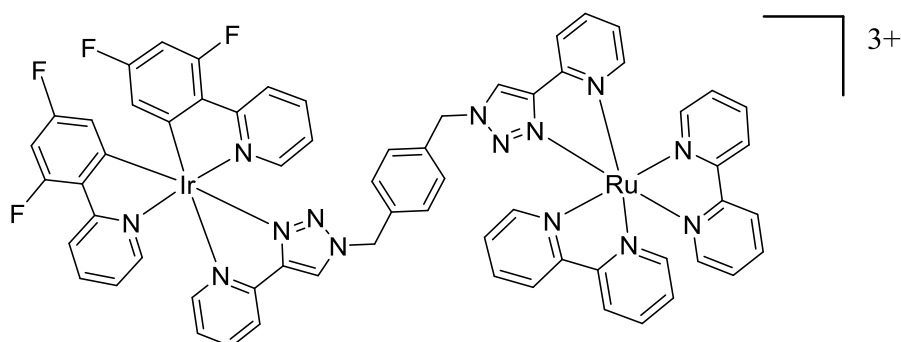
We can also control the photophysical and electrochemical properties of complexes by using CuAAC reactions for ligand design and as supramolecular linkers to modify the design. For example, we might prepare a shorter linker ligand to improve the electron communication in the complex. The spacer of the linker ligand effects the photophysical and properties of the complex. Removing the saturated ethyl group makes the metal centres closer to each other and thus increases the electron communication.
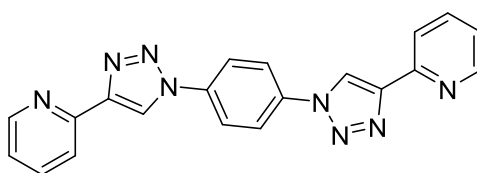
We can also control the regiochemistry of the substituents of the central benzene ring of the ligand to vary the rate of energy transfer through varying the distance between the metal cente, which give ability to prepare complexes even with more than two metal centres
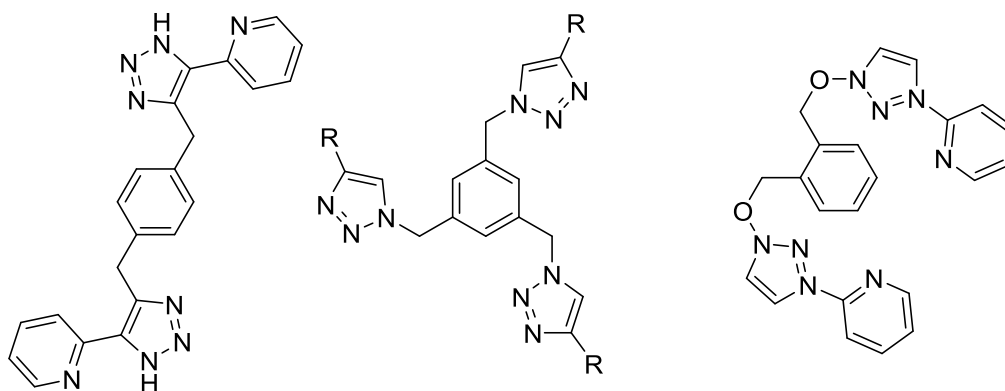
This provides a new opportunity for the synthesis and application of novel luminescent iridium complexes, for example, in electrochemiluminescent devices (LECs) with highly improved efficiency. The water soluble chloride form of these complexes could be subjected to luminescent imaging microscopy studies.

Chapter 7: EXPERIMENTAL

7.1 General methods

Ammonium hexachloroosmate(IV) was purchased from Alfa Aesar whilst all other reagents and solvents were purchased from Sigma-Aldrich or Acros Organics and used as supplied. [Re(bpy)(CO)$_3$Cl],[185] [Re(bpy)(CO)$_3$(Py)][PF$_6$],[185] [Ru(bpy)$_2$Cl$_2$][251] and [Ir(ppy)$_2$Cl]$_2$[252] were all prepared according to literature procedures. NMR spectra were recorded on a Bruker Ascend 400 MHz spectrometer, with all chemical shifts being quoted in ppm referenced relative to the residual solvent signal (MeCN, $\delta = 1.94$, CDCl$_3$ $\delta = 7.26$, DMSO $\delta = 2.5$). High resolution mass spectrometry was performed on an Agilent 6210 TOF instrument with a dual ESI source. UV-visible absorption spectra were recorded on an Agilent Cary 60 spectrophotometer whilst emission spectra were recorded on a Fluoromax-4 spectrophotometer (aerated and degassed in acetonitrile and data at 77 K in ethanol: methanol 4:1). Lifetime measurements were recorded by time-correlated single-photon counting using an Edinburgh instruments Mini-Tau spectrometer.

7.2 Electrochemistry:

The autolab PGSTAT100N potentiostat alongside NOVA electrochemical program was used to record the cyclic voltammograms. Dry acetonitrile saturated with nitrogen was used to prepare analyte solutions. All measurements were made at room temperature under a stream of dry nitrogen at scan rates between 20 and 500 mVs^{-1}. NBu$_4$PF$_6$ acted as a supporting electrolyte, with a solution concentration of 0.2 mol dm^{-3}. A platinum disc was the working electrode, while the counter electrode was a platinum wire. The reference electrode was Ag/AgCl. Finally, Ferrocene was used as an internal reference, with all potentials reported against the Fc$^+$/Fc couple.

7.3 Ligand Synthesis:

7.3.1 Synthesis of benzyl azide

Benzyl azide may cause an explosion, as many other azides, so it is advisable to use extreme caution during purification and handling. Pure compound can be stored in dark and cold, and even then, shelf-life is only weeks.
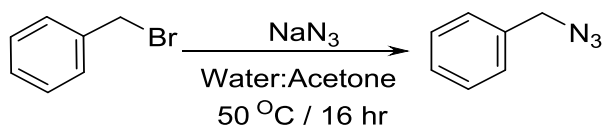
Benzyl bromide (12.0 ml, 101 mmol, 1.0 eq.) was dissolved in water and acetone (1:4 v/v) (120 ml). Sodium azide (10 g, 154 mmol, 1.5 eq.) was added and the reaction was stirred overnight at 50 °C. After evaporating acetone, water (75 ml) was added slowly before extracting the product into diethyl ether (3 × 150 ml). The combined diethyl ether layers were washed with brine (1 × 150 ml), dried over magnesium sulphate and the solvent removed to leave colourless oil. Yield = 10.5 g, 74 mmol, 75%. ^{1}H NMR (400 MHz, CDCl$_3$): δ: 7.42-7.32 (m, 5H), 4.35 (s, 2H). ^{13}C NMR (101 MHz, CDCl$_3$) δ: 135.4, 128.9, 128.3, 128.2, 54.82. IR solution (cm^{-1}) C-$_{N=N=N}$: 2090 s.

7.3.2 Synthesis of 1-benzyl-4-(2-pyridyl)-1,2,3-triazole (Bn-pytz):[96]

203
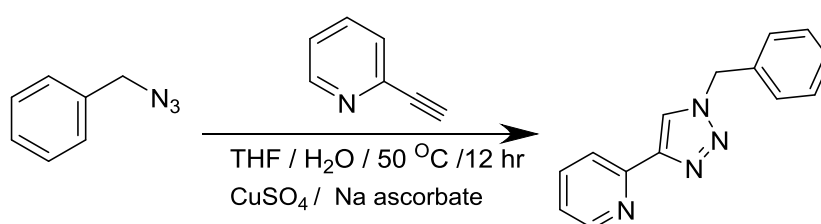
Benzyl azide (2.32 g, 17 mmol) and 2-ethynylpyridine (1.676 g, 17 mmol) were dissolved in a mixture of THF and water (1:1 v/v) (120 ml). To the solution was added 1 M sodium ascorbate (aq) (3.2 ml) and 7.5 wt% $CuSO_4$ (aq) (5.2 ml). The mixture was stirred at 50 ^{O}C overnight. After the mixture had cooled down. THF was evaporated under reduced pressure. The resulting precipitate of the Cu complex was decomposed by addition of small portions of aqueous ammonia. The aqueous phase was extracted with $CHCl_3$, washed with water, saturated $NaHCO_3$ (aq) and brine. After drying over Na_2SO_4, the solvent was removed under reduced pressure. The crude product was purified by column chromatography (SiO_2, 2% MeOH, 98% DCM) to give a white solid (2.95 g). Yield 82%.^{1}H NMR (400 MHz, CD_3CN): δ: 8.55 (d, J = 4.5 Hz, 1H), 8.26 (s, 1H), 8.11 (dt, J =1.0 , 8.0 Hz, 1H), 7.76 (tt, J = 1.1, 7.5 Hz, 1H), 7.41– 7.30 (m, 5H), 7.28-7.24 (m, 1H), 5.60 (s, 2H). ^{13}C NMR (101 MHz, CD_3CN): δ: 150.1, 149.3, 147.9, 135.6, 135.5, 128.6, 128.0, 127.6, 122.3, 119.2, 117.0, and 53.3. ESI HRMS: m/z calculated for ($C_{14}H_{13}N_4$) m/z = 237.1135 (M+H)$^+$, found m/z = 237.1129 [M+H]$^+$. ESI HRMS: m/z calculated for ($C_{14}H_{12}N_4Na$) m/z = 259.0954 [M+Na]$^+$ found m/z = 259.0950 [M+Na] $^+$.

7.3.3 Synthesis of 4'-(*p*-tolyl)-2,2':6',2''-terpyridine = tol-terpy[229]
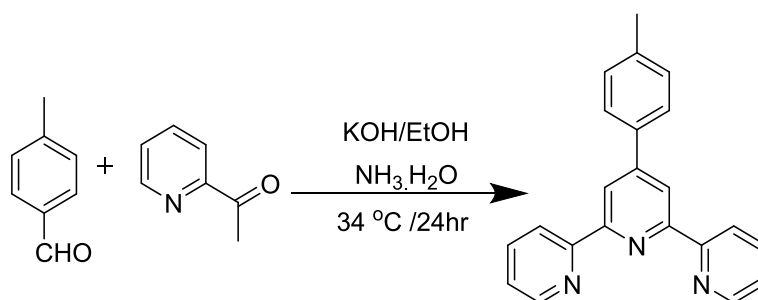
The ligand 4'-(*p*-tolyl)-2,2':6',2''-terpyridine = tol-terpy was synthesized as follows:[229] 2-Acetylpyridine (4.84 g, 40 mmol) and 4-methylbenzaldehyde (2.40 g, 20 mmol) were added into EtOH (100 mL). KOH pellets (3.08 g, 85%, 46 mmol) and NH_3 (60 mL, 30%) were then added to the solution. The solution was stirred at 34 °C for 24 hrs. The mixture was cooled to

room temperature and then the off-white solid was collected by filtration and washed with ice-cold EtOH (10 mL). Recrystallization from EtOH. Yield = 4.2 g, 13.0 mmol, 65%. ^{1}H NMR (400 MHz, CDCl$_3$) δ: 8.74-8.72 (m, 4H); 8.67 (d, J = 7.9 Hz, 2H); 7.87 (td, J = 1.8, 7.7 Hz, 2H); 7.83 (d, J = 8.1 Hz, 2H); 7.36-7.31 (m, 4H); 2.42 (s, 3H); ^{13}C NMR (101 MHz, CDCl$_3$) δ: 156.4, 155.9, 150.2, 149.1, 139.1, 136.85, 135.5, 129.7, 127.2, 123.8, 121.4, 118.6, 21.3. ESI HRMS calculated for (C$_{22}$H$_{17}$N$_3$) m/z = 323.1422, found m/z = 323.1430 [M]$^+$.

7.3.4 Synthesis of 2,6-bis(trimethylsilylethynyl)pyridine
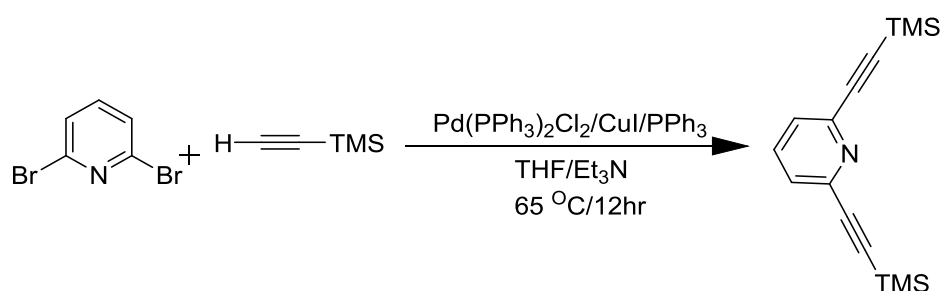
2,6-Dibromopyridine (2.4 g, 10 mmol), dichlorobis(triphenylphosphine)palladium(II) (561 mg, 0.8 mmol), copper(I) iodide (285 mg, 1.5 mmol), triphenylphosphine (210 mg, 0.8 mmol) and triethylamine (5 ml) were dissolved in a mixture of dry THF (20 ml) and trimethylsilylacetylene (2.8 ml, 20 mmol) and heated at reflux under nitrogen overnight. The solvent was removed under reduced pressure, then the crude product was purified by column chromatography (SiO$_2$, (2:1) Hexane: DCM) to give a white solid. Yield = 2.25 g, 90%. ^{1}H NMR (400 MHz, CDCl$_3$) δ: 7.70 (t, J = 7.8 Hz, 1H); 7.41 (d, J = 7.8 Hz, 2H); 0.25 (s, 18H); ^{13}C NMR (101 MHz, CDCl$_3$) δ: 142.89, 137.2, 126.7, 103.21, 94.4, and 0.96). ESI HRMS calculated for (C$_{15}$H$_{21}$NSi$_2$) m/z = 272.1285, found m/z =272.1287 [M]$^+$.

7.3.5 Synthesis of 2,6-bis(1-phenyl-1H-1,2,3-triazol-4-yl)pyridine, btzpy:[88]
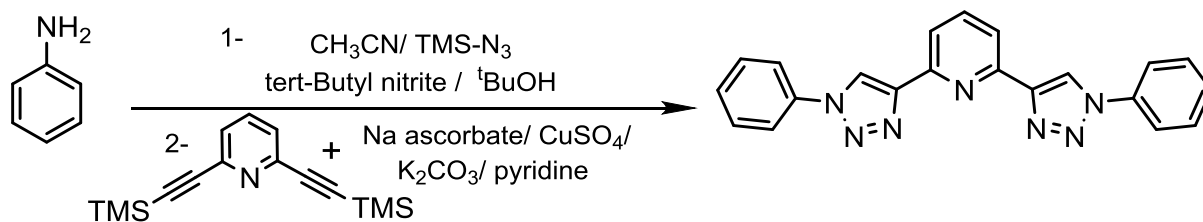
In a 500 ml round-bottomed flask equipped with a magnetic stirrer, acetonitrile (100 ml) and aniline (1.82 g, 20 mmol) were added. The mixture was stirred in an ice bath then tert butyl nitrite (1.5 g, 20 mmol) and trimethylsilylazide (2.3 g, 20 mmol) were added. The mixture was warmed up to room temperature and stirred for 2 hrs. To the solution were added 1 M sodium ascorbate (aq) (10 ml) and 7.5 wt% $CuSO_4$ (aq) (10 ml), 1 M potassium carbonate (10 ml) (aq), 100 ml of H_2O, pyridine (10 ml), tert-butanol (10 ml) and 2,6-bis(trimethylsilyl)pyridine (2 g, 7.4 mmol). The mixture was stirred overnight at room tempreture. Acetonitrile was removed under reduced pressure. The resulting precipitate of the Cu complex was decomposed by addition of small portions of aqueous ammonia. The product was extracted into $CHCl_3$, washed with aqueous ammonia, water and brine. After drying over Na_2SO_4, the solvent was removed under reduced pressure. The crude product was purified by column chromatography (SiO_2, 5% Ethyl acetate, 95% DCM) to give the btzpy ligand (3.15 g, 8.2 mmol). Yield 91%. ^{1}H NMR (400 MHz, CD_3CN) δ: 8.97 (s, 2H); 8.13 (d, $J = 7.7$ Hz, 2H); 7.99 (t, $J = 8.2$ Hz, 1H); 7.93 (d, $J = 7.8$ Hz, 4H); 7.63 (t, $J = 7.6$ Hz, 4H); 7.53 (t, $J = 7.5$ Hz, 2H); ^{13}C NMR (101 MHz, CD_3CN) δ: 149.99, 138.28,137.3, 129.91, 128.97, 121.27, 120.50, 118.88, 117.33. ESI HRMS calculated for ($C_{21}H_{15}N_7Na$) $m/z = 388.1281$, found $m/z = 388.1285$ [M+Na]$^+$.

7.3.6 Synthesis of 1, 4-bis-({4-(pyrid-2-yl)-1, 2, 3-triazol-1-yl}methyl) benzene

=L
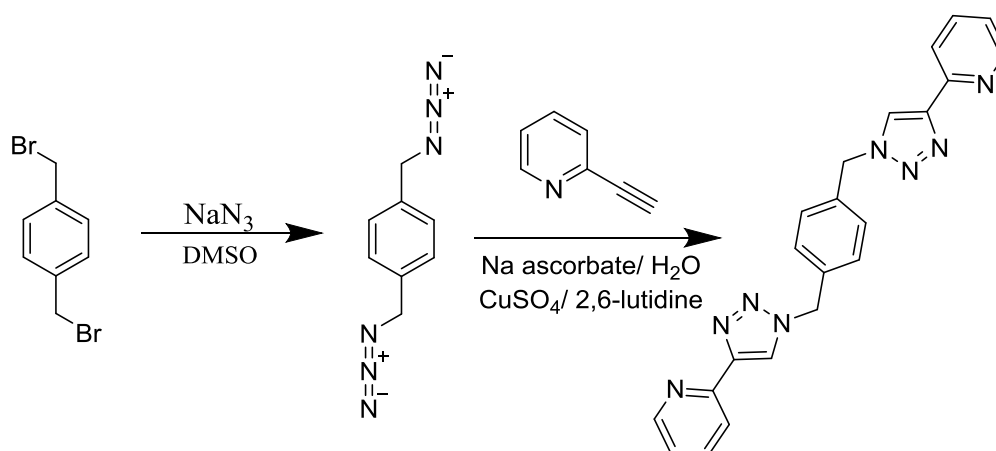
1,4-Dibromomethylbenzene (2 g, 7.6 mmol) and sodium azide (1.00 g, 15.35 mmol) were combined in dimethyl sulfoxide (20 mL). The mixture was stirred at room temperature for two hours. Then to the reaction mixture was added water (15 ml), 2-ethynylpyridine (3.4 g, 31 mmol), $CuSO_4$ (1M aqueous solution 5 ml), sodium ascorbate (1M aqueous solution 5 ml) and 2,6-lutidine (2.4 mL, 31 mmol). The mixture was stirred at room temperature overnight. The resulting precipitate of the Cu complex was decomposed by addition of small portions of aqueous ammonia. The remaining solids were filtered and washed with water (50 mL) and dilute ammonia (50 mL) and the product was recrystallised from dichloromethane and hexane to yield a white solid. (Yield = 3.6 g, 88 %) ^{1}H NMR (400 MHz, $(CD_3)_2SO$) δ: 8.66 (s, 2H); 8.57 (d, J = 4.3 Hz, 2H); 8.01 (d, J = 7.9 Hz, 2H); 7.87 (td, J =1.6, 7.6 Hz, 2H); 7.39 (s, 4H); 7.34-7.31 (m, 2H); 5.66 (s, 4H); ^{13}C NMR (101 MHz, $(CD_3)_2SO$) δ: 150.33, 150.07, 147.95, 137.66, 136.42, 128.93, 123.91, 123.47, 119.87, 53.09. ^{1}H NMR (400 MHz, CDCl$_3$) δ: 8.52 (s, 2H); 8.16 (d, J = 7.6 Hz, 2H); 8.04 (s, 2H); 7.76 (t, J = 7.4 Hz, 2H); 7.34 (s, 4H); 7.20 (s, 2H); 5.58 (s, 4H); ^{13}C NMR (101 MHz, CDCl$_3$) δ: 150.2, 149.4, 148.9, 136.9, 135.3, 129.03, 122.9, 121.94, 120.3, 53.9. ESI HRMS calculated for ($C_{22}H_{18}N_8$) m/z = 394.16544, found m/z = 394.16550 [M]$^{+}$.

7.4 Synthesis of rhenium complexes

7.4.1 Preparation of the rhenium complexes [Re(N^N)(CO)₃Cl]
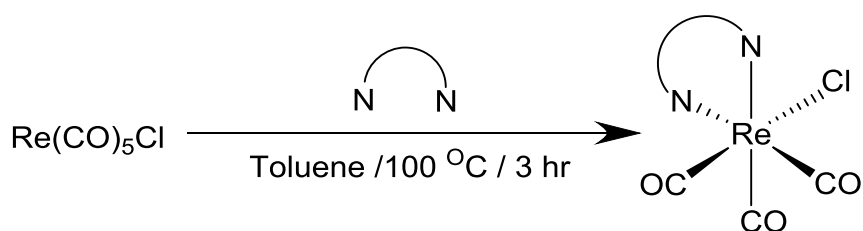
The rhenium complexes were prepared from pentacarbonylchlororhenium (I) [Re(CO)₅Cl] by the following general procedure: [Re(CO)₅Cl] one equivalent and the diimine (L) one equivalent (L= 2,2′-Bipyridyl, 1,10-Phenanthroline and 1-Benzyl-4-(2-pyridyl)-1,2,3-triazole in toluene were heated at 100 ^{O}C for 3 hr. After the solution cooled to room tempreture, the precipitate was collected, washed with diethyl ether and dried in *vacuo.* Yields were typicaly 80-90%. Thin-layer chromatography on silica gel plates and NMR were used to test for purity.

7.4.1.1 Synthesis of [Re(CO)₃(btzpy)Cl]
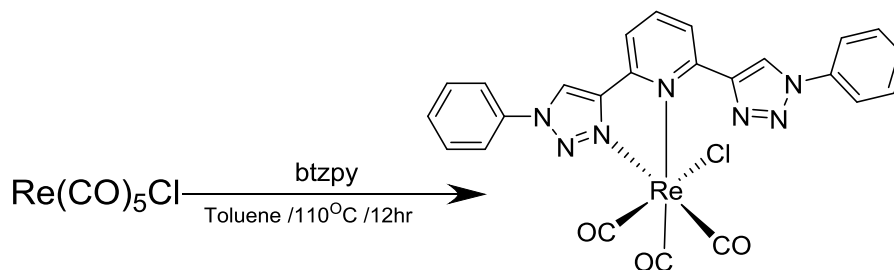
The rhenium complex was prepared from pentacarbonylchlororhenium(I) [Re(CO)₅Cl] by the general procedure,[191] a typical experiment: [Re(CO)₅Cl] (200 mg, 0.55 mmol) and 2,6-bis(1-phenyl-1H-1,2,3-triazol-4-yl)pyridine, (btzpy) (205 mg, 0.55 mmol) in toluene (20 mL) were heated overnight under reflux. The resulting mixture was allowed to cool to room temperature, and then the precipitate was collected by filtration, washed with diethyl ether and dried in *vacuo*. The crude product was purified by column chromatography (SiO₂, THF) to give a light yellow powder. Yield = 175 mg, 87 %. ^{1}H NMR (400 MHz, (CD₃)₂SO) δ : 10.0 (s, 1H); 9.32 (s, 1H); 8.52-8.44 (m, 2H); 8.06 (d, J = 7.04 Hz, 2H); 7.97 (d, J = 6.8 Hz, 3H); 7.76-7.69 (m,

5H); 7.59 (d, J = 6.4 Hz, 1H); ^{13}C NMR (101 MHz, (CD$_3$)$_2$SO) δ: 153.2, 150.4, 150.2, 148.1, 141.4, 136.9, 135.9, 131.0, 130.8, 130.6, 129.7, 128.0, 125.4, 124.9, 123.1, 121.4, 121.0. ESI HRMS calculated for (C$_{24}$H$_{15}$N$_7$ClRe) m/z = 694.0347, found m/z = 694.0364 [M+Na]$^+$.

7.4.2   Synthesis of [Re(N^N)(CO)$_3$(X)](PF$_6$)

[Re(L)(CO)$_3$(bpy)]$^+$ can be synthesized using different techniques. The first technique (method A) involves the treatment of [Re(L)(CO)$_3$Cl)] with AgPF$_6$. AgPF$_6$ and [Re(L)(CO)$_3$Cl)] are dissolved in dichloromethane and stirred in the dark for 12 hours at room temperature. One equivalent of Py (X) is then added to the solution and stirred for 48 hours in darkness. This solution is then filtered through celite and the filtrate thereafter dried through evaporation under reduced pressure[98] The obtained residue is then re-crystallized from DCM and diethyl ether to generate the product required. Another method (method B) involves producing [Re(N^N)(CO)$_3$(CH$_3$CN)](PF$_6$) through modifying the method reported[185] whereby [Re(N^N)(CO)$_3$Cl] as well as one equivalent of silver hexafluorophosphate AgPF$_6$ are dissolved into acetonitrile under an atmosphere of nitrogen which is heated to 85°C in darkness for twelve hours. After cooling, the solution is filtered through celite and then the filtrate is dried through evaporation under reduced pressure. The obtained residue is re-crystallized from acetonitrile and diethyl ether hence [Re(bpy)(CO)$_3$(CH$_3$CN](PF$_6$) is obtained. Afterwards, rhenium complex [Re(N^N)(CO)$_3$(CH$_3$CN)](PF$_6$), (one equivalent) is reacted with (X) (X = pyridine, 4-tert-butylpyridine, 4-methlypyridine, 3-methylpyridine, 4-dimethylaminopyridine, 3,5-dimethylpyridine) (six equivalents) in tetrahydrofuran (THF) under a nitrogen atmosphere at 65°C overnight. After cooling, hexane is added gradually to precipitate the product.

7.4.3 [Re(bipy)(CO)₃(py)](PF₆)
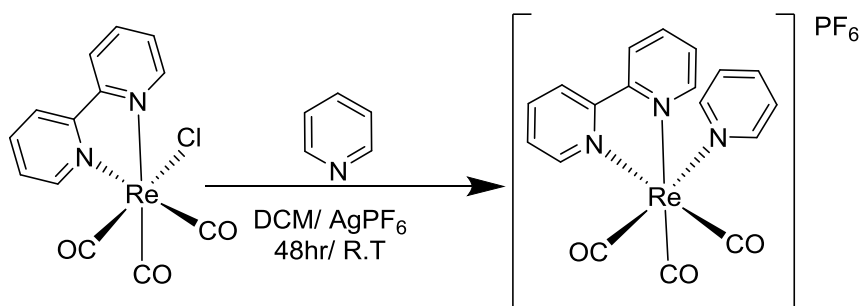
According to (method A): 2,2′-Bipyridyl (bpy) (216 mg, 1.383 mmol) was used to prepare the rhenium complex [Re(bpy)(CO)₃Cl]. In the second step 278 mg of [Re(bipy)(CO)₃Cl] was used to prepare [Re(bpy)(CO)₃(py)][PF₆]. The crude product was purified by column chromatography (SiO₂, 2% MeOH, 98% DCM) to give a yellow powder Yield 74%. ^{1}H NMR (400 MHz, CD₃CN): δ: 9.21 (d, J = 5.4 Hz, 2H), 8.36 (d, J = 8.0 Hz, 2H), 8.29- 8.22 (m, 4H), 7.85 (t, J = 7.5 Hz, 1H), 7.78 (t, J = 6.4 Hz, 2H), 7.29 (t, J = 6.7 Hz, 2H). ^{13}C NMR (101 MHz, CD₃CN) δ: 155.4, 153.5, 151.6, 140.8, 139.6, 128.5, 126.4, 124.4. ESI HRMS calculated for (C₁₈H₁₃N₃O₃Re) m/z = 504.0481, found m/z = 504.0468 [M]$^+$.

7.4.4 [Re(1,10-phenanthroline)(CO)₃(py)](PF₆)
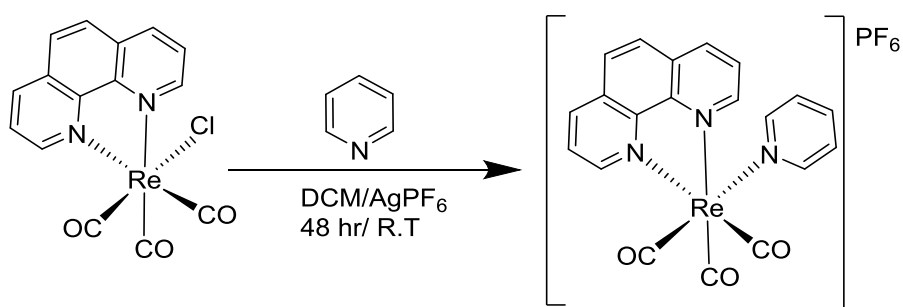
According to method A. In the first step 1,10-phenanthroline (249 mg, 1.383 mmol) was used to prepare the rhenium complex [Re(1,10-phenanthroline)(CO)₃Cl], then (318 mg) of [Re(1,10-phenanthroline)(CO)₃Cl] complex was used in the second step of this reaction to prepare [Re(1,10-phenanthroline)(CO)₃(py)](PF₆). The crude product was purified by column

chromatography (SiO$_2$, 2% MeOH, 98% DCM) to give a yellow powder Yield 72%. ^{1}H NMR (400 MHz, CD$_3$CN): δ : 9.60 (dd, J = 1.0, 5.3 Hz, 2H), 8.84 (dd, J = 1.1 , 8.3 Hz, 2H), 8.27 (d, J = 5.0 Hz, 2H), 8.16 (s, 2H), 8.13-8.09 (m, 2H), 7.74 (t, J = 7.8 Hz, 1H)7.19 (t, J = 6.6 Hz, 2H), ^{13}C NMR (101 MHz, CD$_3$CN) δ : 154.2, 151.5, 146.2, 140.0, 139.5, 130.9, 127.8, 126.8, 126.2.   ESI HRMS calculated for (C$_{20}$H$_{13}$N$_3$O$_3$Re) m/z = 528.0481, found m/z = 528.0469 [M]$^+$.

7.4.5 Preparation of [Re(btz)(CO)$_3$Cl]
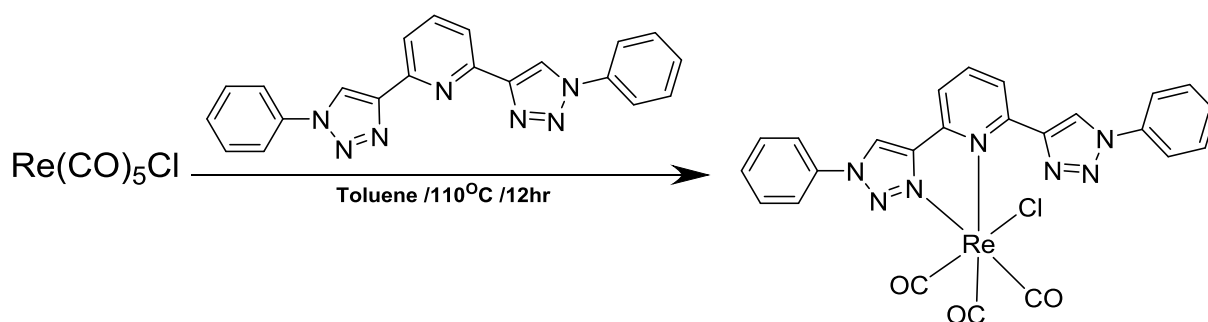
The Rhenium complex were prepared from pentacarbonylchlororhenium(I) [Re(CO)$_5$Cl] by the general procedure[191] a typical experiment: [Re(CO)$_5$Cl] (200 mg, 0.55 mmol) and 2,6-bis(1-phenyl-1H-1,2,3-triazol-4-yl)pyridine, (ph-tripy) L3 (205 mg, 0.55 mmol) in toluene (20 mL) were heated overnight under reflux. The resulting mixture was allowed to cool to room temperature, and then the precipitate was collected, by filtration, washed with diethyl ether and dried in vacuo. The crude product was purified by column chromatography (SiO2, THF) to give a light yellow powder Yields = 175mg, 87%. ^{1}H NMR (400 MHz, (CD$_3$)$_2$SO) δ: 10.0 (s, 1H); 9.32 (s, 1H); 8.52-8.44 (m, 2H); 8.01 (dd, J = 7.04 , 36.2Hz, 5H); 7.76-7.69 (m, 5H); 7.59 (d, J = 6.4 Hz, 1H); ^{13}C NMR (101 MHz, (CD$_3$)$_2$SO) δ: 153.2, 150.4, 150.2, 148.1, 141.4, 136.9, 135.9, 131.1, 130.8, 130.6, 129.7, 128.0, 125.4, 124.9, 123.1, 121.4, 12,. ESI HRMS calculated for (C$_{24}$H$_{15}$N$_7$O$_3$ClRe) m/z = 694.0347, found m/z = 694.0364 [M+Na]$^+$.

7.4.6 Preparation of [Re(Bn-pytz)(CO)₃Cl]
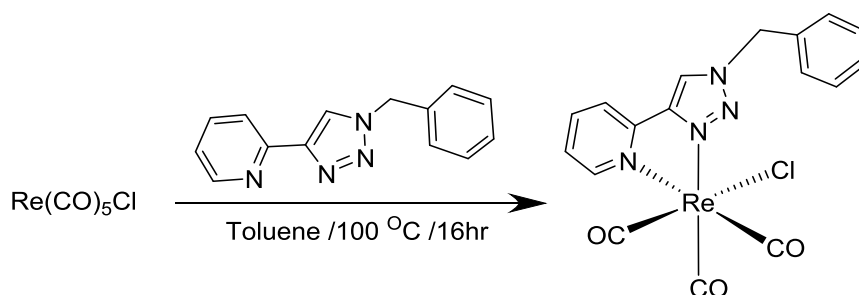
The rhenium complexes were prepared from pentacarbonylchlororhenium(I) [Re(CO)₅Cl] by the general procedure:[191] [Re(CO)₅Cl] (2.78 g, 0.516 mmol) and the substituted pytz (1-benzyl-4-(2-pyridyl)-1,2,3-triazole) compound (2.04 g, 0.516 mmol) in toluene (60 ml) were heated overnight at 100 °C. After the cooling to room temperature, the resulting precipitate was collected, washed with diethyl ether and dried in *vacuo.* Yields were typical 80% - 90%. Thin-layer chromatography on silica gel plates and NMR were used to test for purity. ¹H NMR (400 MHz, CD₃CN): δ: 8.95 (d, *J* = 5.6 Hz, 1H), 8.57 (s, 1H), 8.11 (td, *J* = 1.6 , 7.8 Hz, 1H), 8 (d, *J* = 8.1 Hz, 1H), 7.53-7.49 (m, 1H), 7.48-7.42 (m, 5H), 5.74 (s, 2H). ¹³C NMR (101 MHz, CD₃CN): δ: 153.9, 150.0, 149.8, 141.2, 134.6, 130.2, 130.2, 129.7, 127.1, 125.9, 123.5, and 56.4. ESI HRMS calculated for (C₁₇H₁₂Cl N₄O₃Re) *m/z* = 505.0434, found *m/z* = 505.0427 [M]⁺.

7.4.7 Preparation of [Re(Bn-pytz)(CO)₃(CH₃CN)](PF₆)
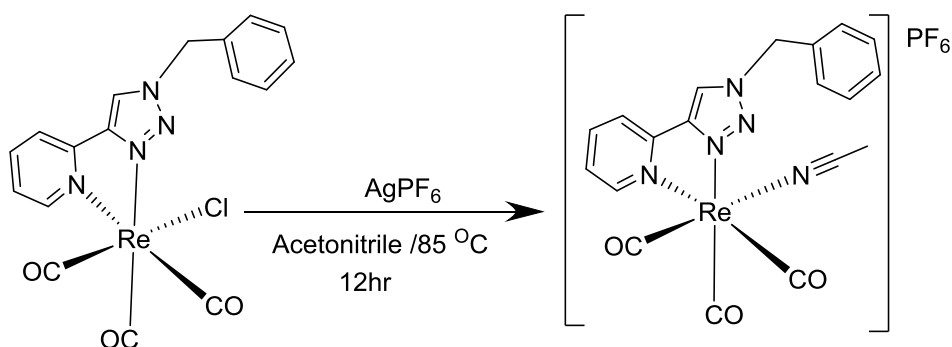
[Re(Bn-pytz)(CO)$_3$(CH$_3$CN)](PF$_6$) was prepared by a modification of the method reported:[185] 560 mg (1.03 mmol, 1 equiv) of [Re(Bn-pytz)(CO)$_3$Cl] and silver hexafluorophosphate (AgPF$_6$) (270 mg, 1.06 mmol, 1.03 equiv) were dissolved in 150 ml of acetonitrile under a nitrogen atmosphere and heated at 85 ^{O}C in the dark for 12 h. After the solution had cooled to room temperature, the solution was then filtered through celite and the filtrate was then dried by evaporation under reduced pressure. The resulting residue was re-crystallised from DCM and hexane [Re(Bn-pyta)(CO)$_3$(CH$_3$CN)](PF$_6$) was obtained as bright yellow-green powder. The crude product was purified by column chromatography (SiO$_2$, 2% MeOH , 98% DCM).^{1}H NMR (400 MHz, CDC$_3$N): δ : 8.96 (d, J = 5.4 Hz, 1H), 8.65 (s, 1H), 8.21 (t, J = 7.6 Hz, 1H), 8.07 (d, J = 7.3 Hz, 1H), 7.60 (t, J = 6.3 Hz, 1H), 7.47 (s, 5H), 5.76 (s, 2H).^{13}C NMR (101 MHz, CD$_3$CN) δ: 153.8, 149.4, 149.1, 141.0, 133.0, 129.0, 128.9, 128.50, 126.5, 125.3, 122.7, 122.2, 55.4. ESI HRMS calculated for [C$_{19}$H$_{15}$N$_5$O$_3$Re]$^+$ m/z = 546.0694, found m/z = 546.0704[M]$^+$.

7.4.8 Synthesis of [Re(Bn-pytz)(CO)$_3$(py)](PF$_6$)
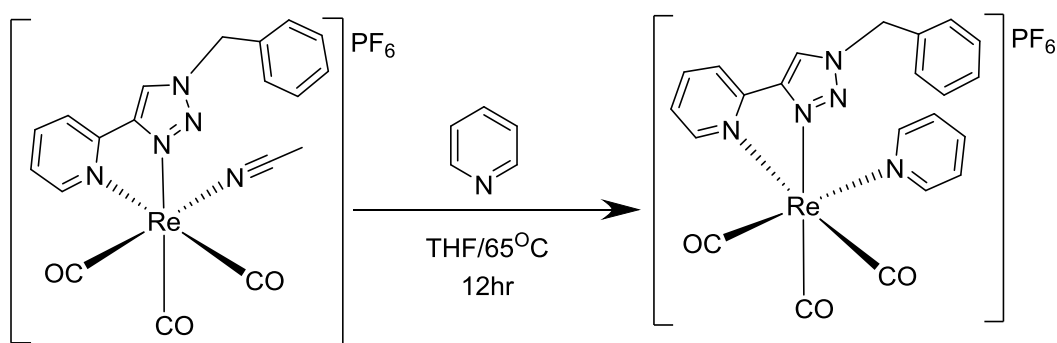
According to method B. Pyridine (py) (280 µl, 3.47 mmol) used in this reaction. The crude product was purified by column chromatography (SiO$_2$, 2% MeOH, 98% DCM) to give a yellow powder Yield 74%. ^{1}H NMR (400 MHz, CD$_3$CN): δ : 9.17 (d, J = 5.4 Hz, 1H), 8.53 (s, 1H), 8.26 (d, J = 5.2 Hz, 2H), 8.17 (t, J = 7.7 Hz, 1H), 7.92 (d, J = 8.2 Hz, 1H), 7.85 (t, J

= 7.4 Hz, 1H), 7.66 (t, J = 6.5 Hz, 1H), 7.46 (s, 5H), 7.29 (t, J = 6.5 Hz, 2H), 5.78 (d, J = 3.7

Hz, 2H). ^{13}C NMR (101 MHz, CD$_3$CN) δ: 153.6, 151.8, 149.2, 148.8, 141.1, 139.5, 133.2,

129.0, 128.9, 128.4, 127.1, 126.3, 125.6, 123.0, 55.6.   ESI HRMS calculated for

[C$_{22}$H$_{17}$N$_5$O$_3$Re]$^+$ m/z = 584.0861, found m/z = 584.0855 [M]$^+$.

7.4.9   Synthesis of [Re(Bn-pytz)(CO)$_3$(^{t}butpy)](PF$_6$)
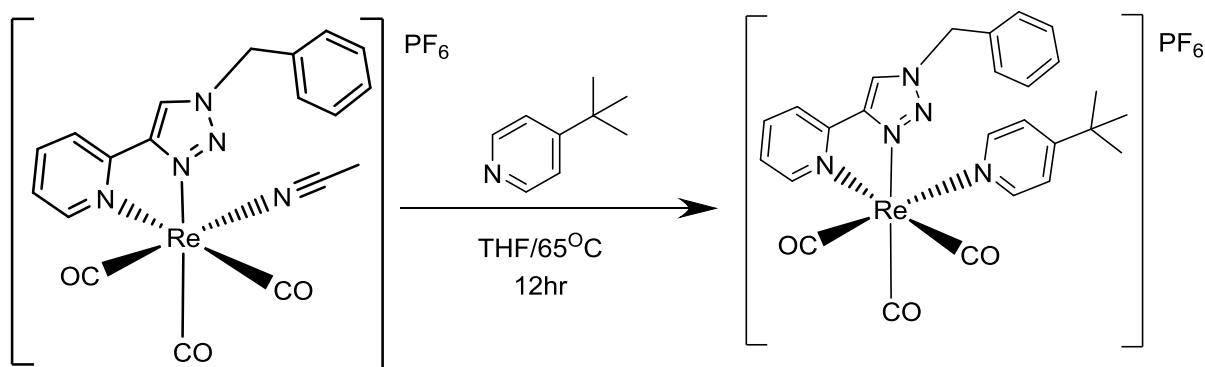
According to method B. 4-tert-butylpyridine (^{t}butpy) (508 µl, 3.47 mmol) used in this reaction.

The crude product was purified by column chromatography (SiO$_2$, 2% MeOH, 98% DCM) to

give a yellow powder Yield 72%. ^{1}H NMR (400 MHz, CD$_3$CN): δ : 9.17 (d, J = 5.7 Hz, 1H),

8.55 (s, 1H), 8.18 (td, J = 1.3, 7.9 Hz, 1H), 8.11 (dd, J = 1.3 , 4.94 Hz, 2H), 7.94 (d, J = 7.9

Hz, 1H), 7.68-7.64 (m, 1H), 7.46 (s, 5H), 7.25 (dd, J = 1.6 , 5.2 Hz, 2H), 5.78 (d, J = 6.6 Hz,

2H), 1.19 (s, 9H).^{13}C NMR (101 MHz, CD$_3$CN) δ : 164.2, 153.6, 151.2, 149.3, 148.8, 141.1,

133.2, 129.0, 128.9, 128.4, 127.1, 125.6, 123.3, 122.9, 55.6, 34.6, 28.8. ESI HRMS calculated

for [C$_{26}$H$_{28}$N$_5$O$_3$Re]$^+$ m/z = 640.1481, found m/z = 640.1472 [M]$^+$.

7.4.10 Synthesis of [Re(Bn-pytz)(CO)₃(4-Picoline)](PF₆)
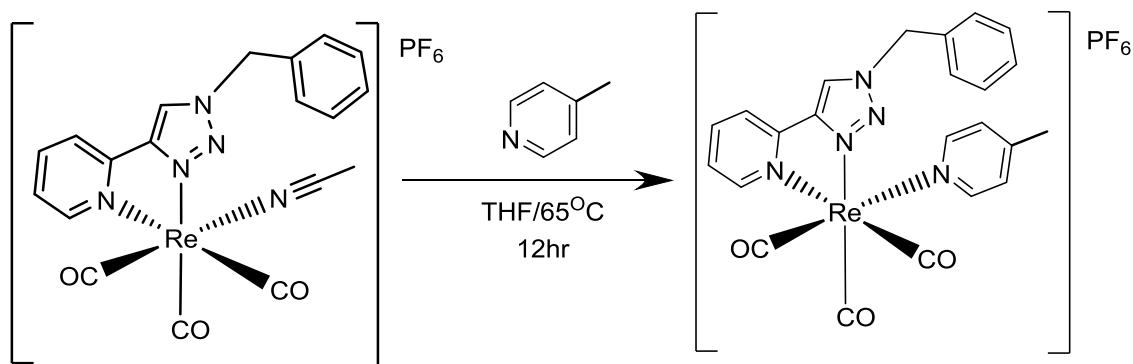
According to method B. 4-methylpyridine (4-picoline) (377 µl, 3.47 mmol) used in this reaction. The crude product was purified by column chromatography (SiO$_2$, 2% MeOH, 98% DCM) to give a yellow powder Yield 75%. ^{1}HNMR (400 MHz, CD$_3$CN): δ : 9.15 (d, J = 5.3 Hz, 1H), 8.53 (s, 1H), 8.17 (td, J = 1.3, 7.87 Hz, 1H), 8.07 (d, J = 6.4 Hz, 2H), 7.92 (d, J = 8.1 Hz, 1H), 7.65 (t, J = 6.6 Hz, 1H), 7.45 (d, J = 4.3 Hz, 5H), 7.10 (d, J = 6.1Hz, 2H), 5.78 (d, J = 3.8 Hz, 2H), 2.28 (s, 3H). ^{13}C NMR (101 MHz, CD$_3$CN) δ: 153.6, 152.3, 151.0, 149.2, 148.8, 141.1, 133.2, 129.0, 128.9, 128.4, 127.1, 126.9, 125.6, 122.9, 118.0, 55.6, 19.8. ESI HRMS calculated for [C$_{23}$H$_{19}$N$_5$O$_3$Re]$^+$ m/z = 598.1012, found m/z = 598.1011[M]$^+$.

7.4.11 Synthesis of [Re(Bn-pytz)(CO)₃(3-Picoline)](PF₆)
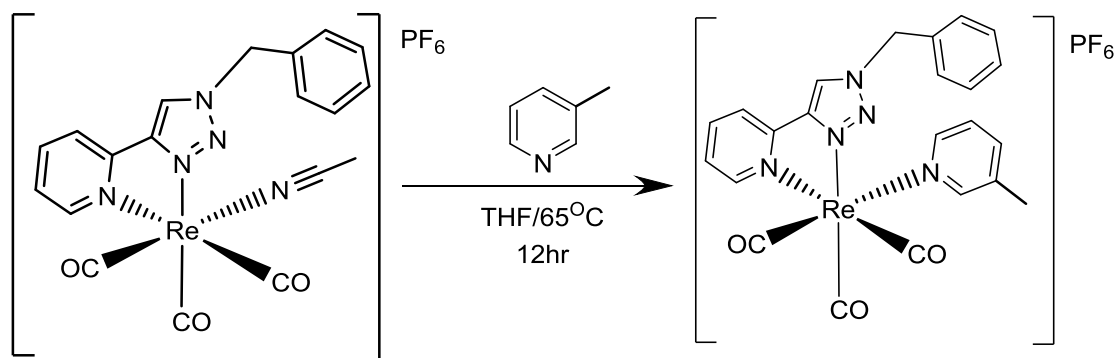
According to method B. 3-methylpyridine (3-picoline) (377 µl, 3.47 mmol) used in this reaction. The crude product was purified by column chromatography (SiO$_2$, 2% MeOH, 98% DCM) to give a yellow powder Yield 75%. ^{1}H NMR (400 MHz, CD$_3$CN): δ : 9.18 (d, J = 5.2 Hz, 1H), 8.55 (s, 1H), 8.17 (t, J = 7.6 Hz, 1H), 8.06 (s, 2H), 7.93 (d, J = 8.1 Hz, 1H), 7.65 (s, 2H), 7.46 (s, 5H), 7.16 (t, J = 6.7 Hz, 1H), 5.78 (d, J = 5.9 Hz, 2H), 2.12 (s, 3H). ^{13}C NMR (101 MHz, CD$_3$CN) δ: 153.9, 151.9, 149.2, 141.5, 140.3, 129.3, 129.3, 128.7, 127.4, 125.9, 123.2, 55.9, 17.3. ESI HRMS calculated for [C$_{23}$H$_{19}$N$_5$O$_3$Re]$^+$ m/z = 598.1012, found m/z = 598.1011[M]$^+$.

7.4.12 Synthesis of [Re(Bn-pytz)(CO)$_3$(3,5-Lutidine)](PF$_6$)
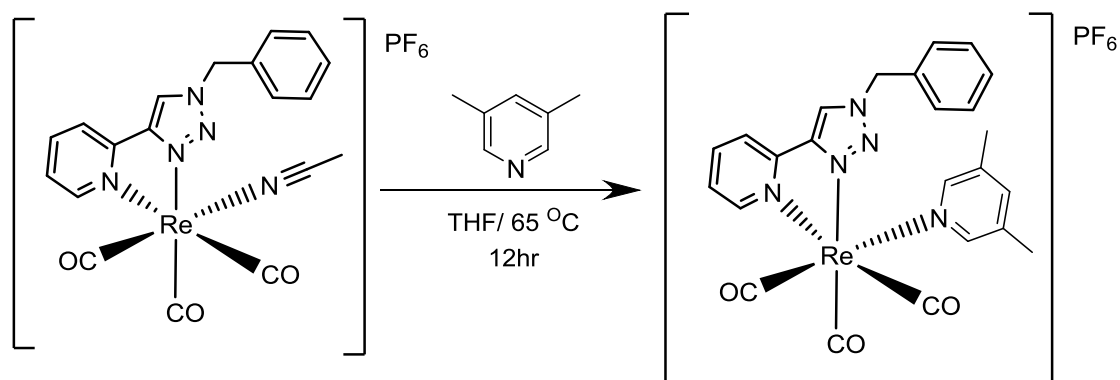
According to method B. 3,5-dimethylpyridine (3,5-Lutidine) (350 µl, 3.47 mmol) used in this reaction. The crude product was purified by column chromatography (SiO$_2$, 2% MeOH, 98% DCM) to give a yellow powder Yield 75%. ^{1}H NMR (400 MHz, CD$_3$CN): δ : 9.19 (d, J = 5.4 Hz, 1H), 8.58 (s, 1H), 8.17 (t, J = 7.7 Hz, 1H), 7.93 (d, J = 8.1 Hz, 1H), 7.87 (s, 2H) 7.65 (t, J = 6.6 Hz, 1H), 7.46 (s, 6H), 5.78 (d, J = 10.5 Hz, 2H), 2.07 (s, 6H). ^{13}C NMR (101 MHz, CD$_3$CN) δ : 153.68, 149.2, 148.8, 141.1, 136.2, 133.3, 129.0, 129.0, 128.4, 127.1, 125.6, 122.8, 55.6, 16.7. ESI HRMS calculated for [C$_{23}$H$_{19}$N$_5$O$_3$Re]$^+$ m/z = 612.1168, found m/z = 612.1162 [M]$^+$.

7.4.13 Synthesis of [Re(Bn-pytz)(CO)$_3$(DMAP)](PF$_6$)
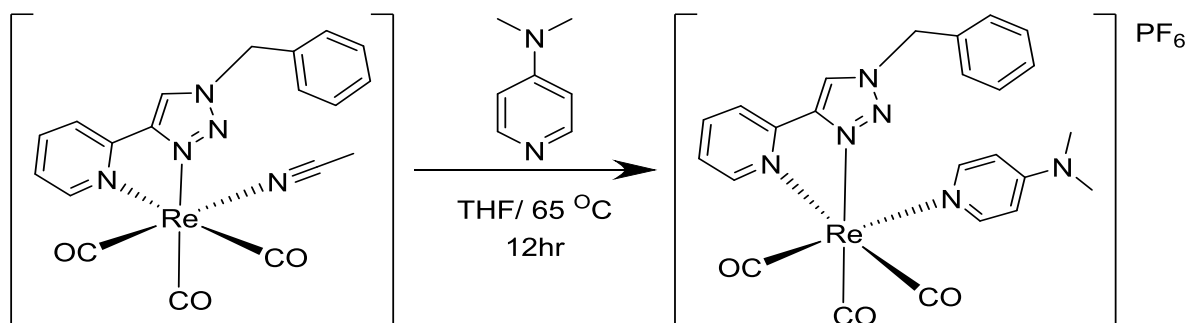
According to method B. 4-dimethylaminopyridine (DMAP) (424 mg, 3.47 mmol) used in this reaction. The crude product was purified by column chromatography (SiO$_2$, 2% MeOH, 98% DCM) to give a yellow powder Yield 75%. ^{1}H NMR (400 MHz, CD$_3$CN): δ : 9.12 (d, J = 5.6 Hz, 1H), 8.54 (s, 1H), 8.15 (td, J = 1.2 , 8.9 Hz, 1H), 7.92 (d, J = 8.0 Hz, 1H), 7.63 (d, J = 6.4 Hz, 1H), 7.59 (d, J = 7.3 Hz, 2H), 7.45 (s, 6H), 6.27 (d, J = 7.30 Hz, 2H), 5.77 (d, J = 11.0 Hz, 2H), 2.89 (s, 6H). ^{13}C NMR (101 MHz, CD$_3$CN) δ: 153.7, 151.9, 149.9, 148.3, 129.3, 129.2, 128.9, 128.4, 125.9, 107.6, 55.9, 38.2. ESI HRMS calculated for [C$_{24}$H$_{22}$N$_6$O$_3$Re]$^+$ m/z = 627.1277, found m/z = 627.1285 [M]$^+$.

7.5 Synthesis of osmium complexes

7.5.1 Synthesis of osmium complexes with bidentate ligands

7.5.1.1 Synthesis of [Os(bpy)₃](PF₆)₂
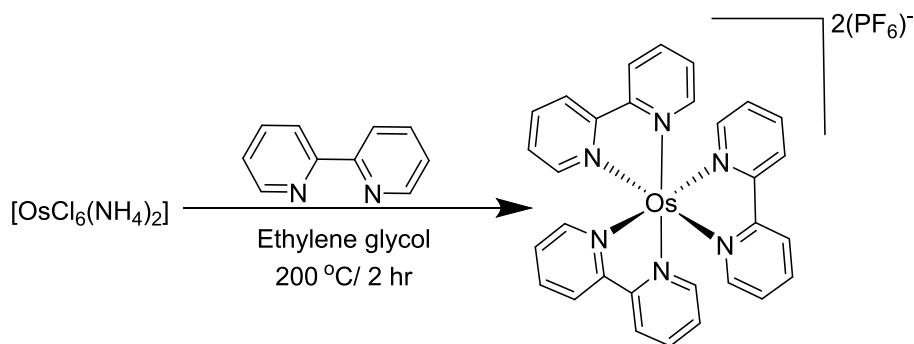
Ammonium hexachloroosmate [(NH$_4$)$_2$OsCl$_6$] (150 mg, 0.341 mmol) and (bpy) (218 mg, 1.4 mmol) were dissolved in ethylene glycol (20 ml) and refluxed under nitrogen for 2hrs. The resulting solution was allowed to cool to room temperature, then NH$_4$PF$_6$ (230 mg, 1.4 mmol) was added to the solution and stirred for 45 min. The dark green precipitate was separated by vacuum filtration and washed with cold water and diethyl ether. The product was dissolved in acetonitrile and filtered through a celite pad then the filtrate recrystallized from acetone and diethyl ether to give a dark green powder. Yield = 270 mg, 80%. ^{1}H NMR (400 MHz, CD$_3$CN) δ: 8.48 (d, J = 8.04 Hz, 6H); 7.86 (t, J = 7.68 Hz, 6H); 7.64 (d, J = 5.36 Hz, 6H); 7.30 (t, J = 6.44 Hz, 6H); ^{13}C NMR (101 MHz, CD$_3$CN) δ: 158.6, 150.5, 136.8, 127.7, and 124.1. ESI HRMS calculated for (C$_{30}$H$_{24}$N$_6$Os) m/z = 330.0833, found m/z = 330.0843 [M]$^{2+}$.

7.5.1.2 Synthesis of [Os(bpy)₂(Bn-pytz)](PF₆)₂[253]
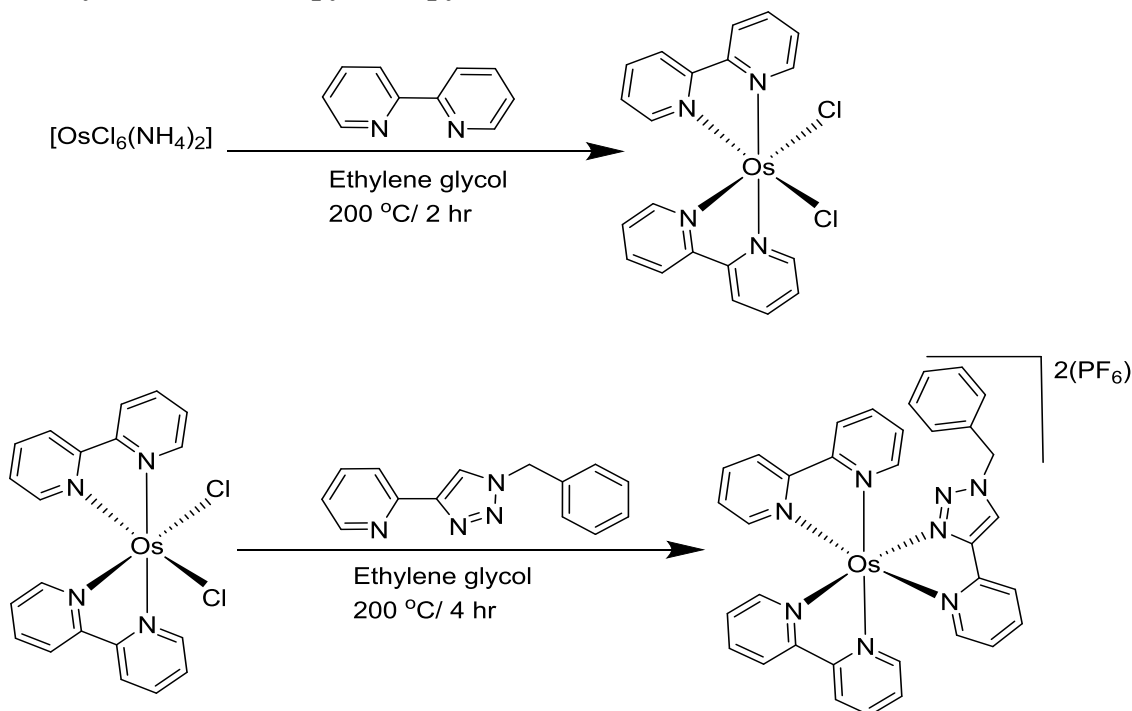
The complex [Os(bpy)$_2$(pytz)](PF$_6$)$_2$ was prepared through a two-step procedure. Firstly,[254] ammonium hexachloroosmate [(NH$_4$)$_2$OsCl$_6$] (150 mg, 0.341 mmol) and bpy (108 mg, 0.69 mmol) were dissolved in ethylene glycol (20 ml) and refluxed under nitrogen for 2hr. The resulting solution was allowed to cool to room temperature, then a 1M aqueous solution of Na$_2$S$_2$O$_3$ was added slowly (over 20 min). The solution was cooled in an ice bath for 1hr. The darkish precipitate [Os(bpy)$_2$Cl$_2$] was separated by vacuum filtration and washed with cold water and diethyl ether and used in further reactions without purification. [Os(bpy)$_2$Cl$_2$] (125 mg, 0.218 mmol) and (pytz) (52 mg. 0.218 mmol) were dissolved in ethylene glycol (50 ml) and refluxed under nitrogen for 4hr. The resulting solution was allowed to cool to room temperature, then NH$_4$PF$_6$ (123 mg, 0.75 mmol) was added to the solution and stirred for 45 min. The dark green precipitate was separated by vacuum filtration and washed with cold water and diethyl ether. The product was dissolved in MeCN and filtered through a celite pad, then the filtrate recrystallized from DCM and hexane to give a dark green powder. Yield = 100 mg, 61%. ^{1}H NMR (400 MHz, CD$_3$CN) δ: 8.59 (s, 1H); 8.49 (d, J = 8.2 Hz, 2H); 8.45-8.39 (m,

2H); 8.08 (d, *J* = 8.0 Hz, 1H); 7.88-7.82 (m, 4H); 7.8-7.76 (m, 3H); 7.72 (d, *J* = 5.6 Hz, 1H);

7.67 (d, *J* = 5.7 Hz, 1H); 7.52 (d, *J* = 5.7 Hz, 1H); 7.39-7.29 (m, 6H); 7.26-7.13 (m, 4H); 5.49

(d, *J* = 4.5 Hz, 2H); ^{13}C NMR (101 MHz, CD$_3$CN) δ: 159.0, 151.1, 151.0 150.9, 150.6, 150.6,

148.9, 137.3, 136.7, 136.6, 136.6, 133.3, 128.8, 128.7, 127.9, 127.7, 127.6, 127.5, 126.9, 126.0,

125.8, 124.1, 124.1, 123.7, 123.3, 122.2, 62.8, 55.1. ESI HRMS calculated for (C$_{34}$H$_{28}$N$_8$Os)

m/z = 370.1020, found *m/z* = 370.1027 [M]$^{2+}$.

7.5.1.3 Synthesis of [Os(bpy)(Bn-pytz)$_2$](PF$_6$)$_2$
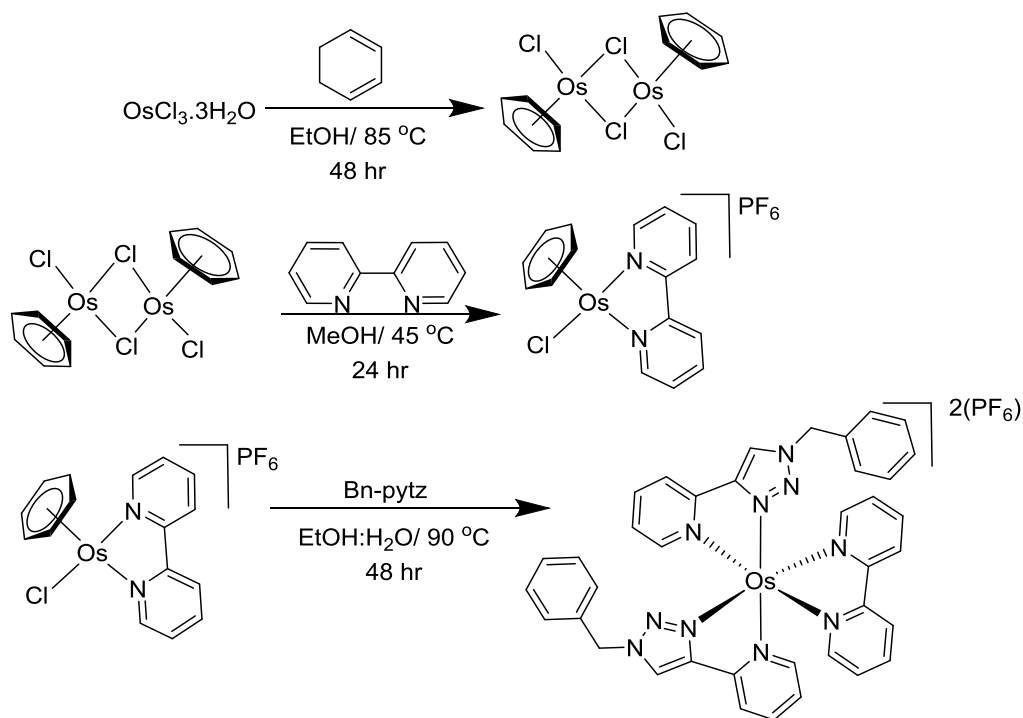
The complex [Os(bpy)(pytz)$_2$](PF$_6$)$_2$ was prepared in a three-step procedure.[255] Firstly, osmium

(III) chloride hydrate OsCl$_3$·3H$_2$O (150 mg, 0.429 mmol) and 1,3-cyclohexadiene (690 mg,

8.58 mmol) were dissolved in degassed ethanol (50 ml) and refluxed under nitrogen for 48 hrs.

The resulting solution was allowed to cool to room temperature and cooled in the fridge for

2hrs, then the green precipitate was separated by vacuum filtration and washed with ethanol

and diethyl ether (<10 ml). The resulting dimer (230 mg, 0.338 mmol) and bpy (106 mg, 0.676

mmol) were dissolved in methanol (50 ml) and heated at 45 °C under nitrogen for 24 hrs. The

resulting solution was allowed to cool to room temperature and filtered through a celite pad, then NH$_4$PF$_6$ (275 mg, 1.69 mmol) was added to the filtrate and stirred for 45 min. The yellow precipitate was separated by vacuum filtration and washed with cold water and diethyl ether. The resulting [Os(η^6-C$_6$H$_6$)(bpy)Cl](PF$_6$) (400 mg, 0.66 mmol) was dissolved in ethanol: water (3:1 v/v) (40 ml) with (pytz) (410 mg, 1.73 mmol) and refluxed under nitrogen for 48 hr. The resulting solution was allowed to cool to room temperature, then NH$_4$PF$_6$ (230 mg, 1.4 mmol) was added to the solution and stirred for 45 min and filtered. The solvent was removed and the solid recrystallized from DCM and hexane. The crude product was purified by column chromatography (SiO$_2$, 2% MeOH, 98% DCM) to give a dark green powder. Yield = 246 mg, 30%. ^{1}H NMR (400 MHz, CD$_3$CN) δ: 8.63-8.59 (m, 2H); 8.45-8.37 (m, 2H); 8.10-8.05 (m, 2H); 7.89-7.76 (m, 6H); 7.65-7.61 (m, 2H); 7.41-7.32 (m, 6H); 7.30-7.10 (m, 8H); 5.55-5.46 (m, 4H); ^{13}C NMR (101 MHz, CD$_3$CN) δ: 159.6, 152.2, 151.2, 150.9, 150.7, 149.3, 137.1, 136.5, 133.2, 128.8, 128.7, 128.0, 127.9, 127.5, 126.7, 126.0, 125.8, 123.0, 122.2, 55.2. ESI HRMS calculated for (C$_{38}$H$_{32}$N$_{10}$Os) m/z = 410.1208, found m/z = 410.1209 [M]$^{2+}$.

7.5.1.4 Synthesis of mer- and fac-[Os(Bn-pytz)₃](PF₆)₂[256]
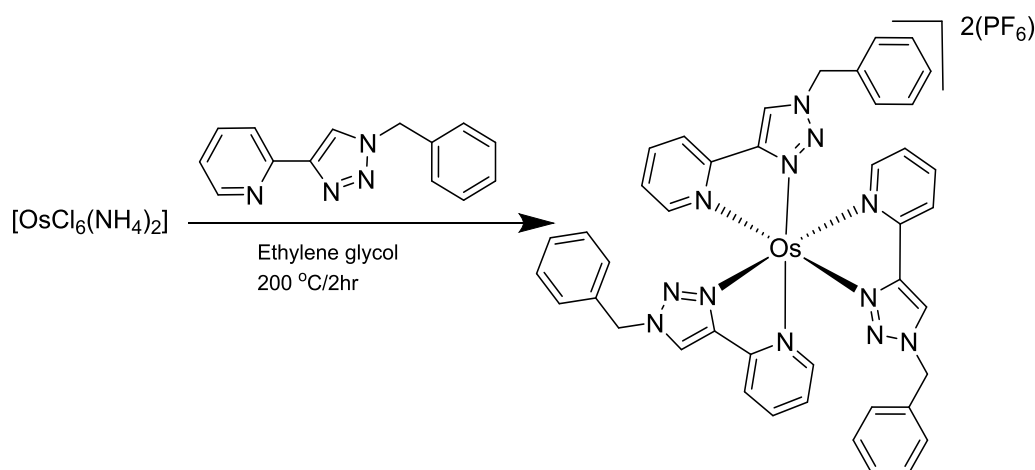
Ammonium hexachloroosmate [(NH$_4$)$_2$OsCl$_6$] (150 mg, 0.341 mmol) and pytz (330 mg, 1.4 mmol) were dissolved in ethylene glycol (20 ml) and refluxed under nitrogen for 2hrs. The resulting solution was allowed to cool to room temperature, then NH$_4$PF$_6$ (230 mg, 1.4 mmol)

was added and stirred for 45 min. The dark orange precipitate was separated by vacuum filtration and washed with cold water and diethyl ether. The product was dissolved in acetone and filtered through a celite pad then the filtrate recrystallized through adding of diethyl ether to give a dark orange powder. Yield = 185 mg, 61% (the product is a mixture of two isomers of [Os(pytz)$_3$](PF$_6$)$_2$, meridional and facial isomers in an approximate 1: 0.8 ratio as estimated by ^{1}H NMR. ^{1}H NMR (400 MHz, CD$_3$CN) δ: 8.62 (t, J = 5.9 Hz, 3H); 8.08 (d, J = 7.8 Hz, 2H); 8.02 (t, J = 8.2 Hz, 1H); 7.83 (t, J = 7.2 Hz, 2H); 7.79-7.76 (m, 1H); 7.73 (d, J = 5.7 Hz, 2H); 7.68 (t, J = 4.5 Hz, 1H); 7.4-7.32 (m, 9H); 7.25-7.14 (m, 9H); 5.54 (s, 2H); 5.53 (s, 4H); ^{13}C NMR (101 MHz, CD$_3$CN) δ: 152.8, 152.6, 151.7, 151.3, 151.2, 151.1, 149.7, 149.4, 149.2, 137.1, 136.9, 136.9, 133.7, 133.3, 128.8, 128.7, 128.6, 128.0, 128.0, 127.5, 125.9, 125.8, 125.7, 125.5, 125.2, 125.1, 124.9, 122.1, 121.8, 121.4, 121.3, 55.2, 55.2, 55.01, 53.3. ESI HRMS calculated for (C$_{42}$H$_{36}$N$_{12}$Os) m/z = 450.1395, found m/z = 450.1406 [M]$^{2+}$.

7.5.2   Separation of meridional and facial - [Os(Bn-pytz)$_3$](PF$_6$)$_2$

Separation of the two meridional and facial isomers of [Os(pytz)$_3$](PF$_6$)$_2$ proved extremely difficult with both co-eluting in column chromatography with a wide range of solvent systems. Successful separation was possible on a small scale by preparative thin-layer chromatography (Gradient: DCM then 20:80 acetone/ DCM) which resulted in the separation of the mer and fac isomers. This procedure yielded are only very small quantities of each isomer, enough to allow spectroscopic characterisation.

7.5.2.1 Meridional -[Os(Bn-pytz)$_3$](PF$_6$)$_2$
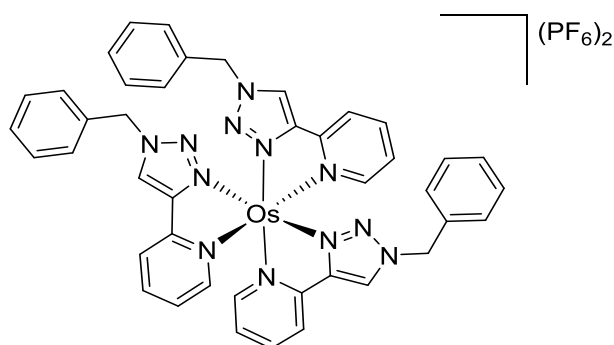
¹H NMR (400 MHz, CD₃CN) δ: 8.61 (t, *J* = 6.6 Hz, 3H); 8.09 (d, *J* = 7.8 Hz, 1H); 8.02 (t, *J* = 7.9 Hz, 2H); 7.83-7.74 (m, 3H); 7.73 (d, *J* = 5.7 Hz, 1H); 7.67 (t, *J* = 4.5 Hz, 2H); 7.41-7.34 (m, 9H); 7.25-7.22 (m, 5H); 7.17-7.13 (m, 4H); 5.54-5.53 (m, 4H); 5.51 (s, 2H); ¹³C NMR (101 MHz, CD₃CN) δ: 153.0, 152.9, 152.6, 151.7, 151.3, 151.2, 149.7, 149.3, 136.9, 136.9, 133.7, 133.3, 133.3, 128.8, 128.8, 128.7, 128.6, 128.0, 128.0, 127.5, 125.9, 125.8, 125.5, 125.1, 124.9, 122.1, 121.4, 121.3, 55.2, 55.2, 55.0. ESI HRMS calculated for (C₄₂H₃₆N₁₂Os) *m/z* = 450.1395, found *m/z* = 450.1368 [M]²⁺.

7.5.2.2 Facial -[Os(Bn-pytz)₃](PF₆)₂
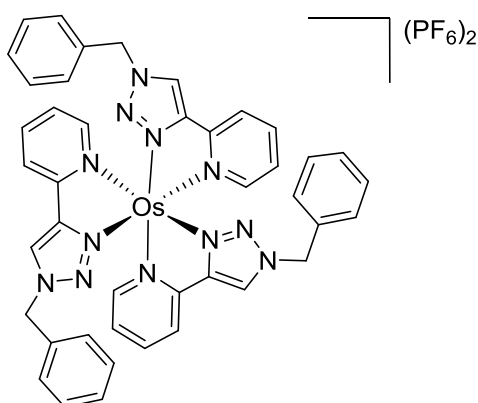
¹H NMR (400 MHz, CD₃CN) δ: 8.61 (s, 1H); 8.07 (d, *J* = 7.9 Hz, 1H); 7.82 (td, *J* =1.2, 7.8 Hz, 1H); 7.72 (d, *J* = 5.6 Hz, 1H); 7.37-7.32 (m, 3H); 7.19 (t, *J* = 6.9 Hz, 1H); 7.13 (dd, *J* = 1.3, 7.6 Hz, 2H); 5.50 (s, 2H); ¹³C NMR (101 MHz, CD₃CN) δ:152.8, 151.1, 149.4, 137.1, 136.9,

133.7, 128.8, 128.6, 127.6, 125.7, 125.2, 121.9, 117.0, 55.0. ESI HRMS calculated for

($C_{42}H_{36}N_{12}Os$) m/z = 450.1395, found m/z = 450.1381 $[M]^{2+}$.

7.5.3 Metathesis of PF$_6$ counter ions to chloride salts

The relevant Os complex as its hexafluorophosphate salt (100 mg) together with 2.5 weight

equivalents of Amberlite IRA-400 chloride-form ion exchange resin (250 mg) were stirred in

MeOH (25 ml) at room temperature in the dark for 24 hr. The resin was removed by filtration

and the filtrate evaporated to dryness. The residue was re-dissolved in the minimum volume of

H_2O (< 10 ml) with subsequent freeze drying afforded the relevant chloride salts as powders.

Successful counter-ion metathesis was confirmed by the complete absence of resonances in ^{31}P

and ^{19}F NMR spectra.

7.5.3.1 Synthesis of [Os(bpy)$_3$]Cl$_2$

^1H NMR (400 MHz, CD$_3$CN) δ: 8.61 (d, J = 8.2 Hz, 6H); 7.86 (t, J = 7.4 Hz, 6H); 7.63 (d, J =

5.6 Hz, 6H); 7.30 (t, J = 6.7 Hz, 6H); ^{13}C NMR (101 MHz, CD$_3$CN) δ: 158.7, 150.5, 136.8,

127.7, 124.4,

7.5.3.2 Synthesis of [Os(bpy)$_2$(Bn-pytz)]Cl$_2$

^1H NMR (400 MHz, CD$_3$CN) δ: 8.96 (s, 1H); 8.53 (d, J = 7.9 Hz, 2H); 8.47-8.42 (m, 2H); 8.19

(d, J = 7.4 Hz, 1H); 7.88-7.76 (m, 7H); 7.72 (d, J = 5.6 Hz, 1H); 7.66 (d, J = 5.6 Hz, 1H); 7.51

(d, J = 5.7 Hz, 1H); 7.37-7.29 (m, 6H); 7.25-7.15 (m, 4H); 5.52 (d, J = 11.5 Hz, 2H);

7.5.3.3 Synthesis of [Os(bpy)(Bn-pytz)$_2$]Cl$_2$

^1H NMR (400 MHz, CD$_3$CN) δ: 9.09-8.95 (m, 2H); 8.49-8.39 (m, 2H); 8.25-8.18 (m, 2H);

7.88-7.75 (m, 6H); 7.65-7.60 (m, 2H); 7.37-7.29 (m, 6H); 7.27-7.12 (m, 8H); 5.59-5.49 (m,

4H);

7.5.3.4 Synthesis of [Os(Bn-pytz)$_3$]Cl$_2$

From the NMR spectra the ratio between two isomers *mer: fac* is 1:0.8

^{1}H NMR (400 MHz, CD$_3$CN) δ: 9.26 (s, 1H); 9.18 (s, 1H); 9.15 (s, 3H); 9.06 (s, 1H); 8.3 (d, *J* = 7.9 Hz, 1H); 8.26 (d, *J* = 7.8 Hz, 1H); 8.21 (d, *J* = 7.9 Hz, 3H); 8.15 (d, *J* = 7.9 Hz, 1H); 7.84-7.78 (m, 4H); 7.76-7.71 (m, 6H); 7.66 (t, *J* = 6.3 Hz, 2H); 7.38-7.3 (m, 18H); 7.27-7.25 (m, 4H); 7.22-7.11 (m, 14H); 5.64-5.55 (m, 4H); 5.54 (s, 8H); ^{13}C NMR (101 MHz, CD$_3$CN) δ: 151.5, 151.0, 150.9, 136.9, 136.7, 136.6, 128.6, 128.6, 128.5, 128.4, 127.9, 127.8, 127.4, 125.7, 125.5, 124.8, 122.2, 121.9, 121.4, 121.3, 54.8,

7.5.4 Synthesis of Osmium tridentate Ligand complexes

7.5.4.1 Synthesis of Os(tol-terpy)$_2$(PF$_6$)$_2$[257]
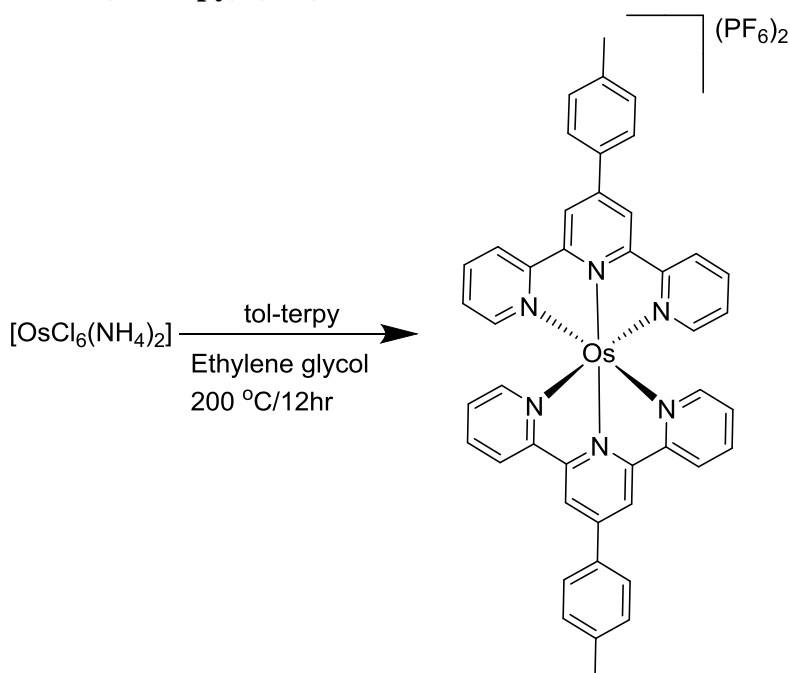
Ammonium hexachloroosmate [(NH$_4$)$_2$OsCl$_6$] (150 mg, 0.341 mmol) and 2.5 eq of 4'-(*p*-tolyl)-2,2':6',2''-terpyridine (toltpy) (310 mg, 0.85 mmol) in ethylene glycol (25 ml) were heated at reflux overnight under N$_2$. The resulting mixture was allowed to cool to room temperature, then 2.5 eq of NH$_4$PF$_6$ (10 ml) was added. The resulting dark brown precipitate was collected by filtration and washed with cold water and diethyl ether then redissolved in acetonitrile. The acetonitrile solution was cooled in the fridge overnight and filtered through celite. Then the

filtrate was recrystallized by the addition of diethylether to give a dark brown powder. Yield = 185 mg, 58% ^{1}H NMR (400 MHz, CD$_3$CN) δ: 9.13 (s, 2H); 8.36 (d, J = 8.0 Hz, 2H); 8.01 (t, J = 8.0 Hz, 1H); 7.59-7.55 (m, 4H); 7.54-7.51 (m, 6H); ^{13}C NMR (101 MHz, CD$_3$CN) δ: 152.0, 150.5, 137.0, 135.7, 129.9, 129.8, 123.7, 120.4, 118.9. ESI HRMS calculated for [C$_{44}$H$_{34}$N$_6$Os]$^{2+}$ m/z = 419.1224, found m/z = 419.1238 [M]$^{2+}$.

7.5.4.2 Synthesis of Os(btzpy)$_2$(PF$_6$)$_2$
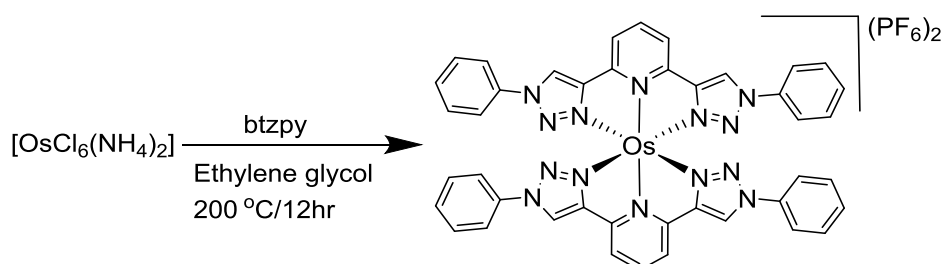
Ammonium Hexachloroosmate [(NH$_4$)$_2$OsCl$_6$] (150 mg, 0.341 mmol) and 2.5 eq of 2,6-bis(1-phenyl-1H-1,2,3-triazol-4-yl)pyridine, (btzpy) (310 mg, 0.85 mmol) in ethylene glycol (25 ml) was heated at reflux overnight under N$_2$. The resulting mixture was allowed to cool to room temperature, then 2.5 eq of NH$_4$PF$_6$ (10 ml) was added. The resulting dark brown precipitate was collected by filtration and washed with cold water and diethyl ether then redissolved in acetonitrile. The acetonitrile solution was cooled in the fridge overnight and filtered. Then the filtrate recrystallized by the addition of diethylether to give a dark brown powder. Yield = 185 mg, 58%. ^{1}H NMR (400 MHz, CD$_3$CN) δ: 9.13 (s, 2H); 8.36 (d, J = 8.0 Hz, 2H); 8.01 (t, J = 8.0 Hz, 1H); 7.59-7.55 (m, 4H); 7.54-7.51 (m, 6H); ^{13}C NMR (101 MHz, CD$_3$CN) δ: 152.01, 150.48, 137.01, 135.69, 129.86, 129.82, 123.73, 120.39, and 118.93. ESI HRMS calculated for [C$_{42}$H$_{30}$N$_{14}$Os]$^{2+}$ m/z = 461.1191, found m/z = 461.1195 (M^{2+}).

7.5.4.3 Synthesis of [Os(btzpy)$_2$]Cl$_2$

A suspension of (100 mg, 0.083 mmol) from [Os(btzpy)$_2$][PF$_6$]$_2$ in methanol (25 ml) was stirred with 2.5 weight equivalents of Amberlite IRA-400 chloride-form ion exchange resin (200 mg) at room temperature in the dark for 24 hrs. The resin was removed by filtration and the solvent then removed by evaporation. The residue was re-dissolved in the minimum volume of H$_2$O (< 10 ml) with subsequent freeze drying affording the chloride salt of the complex [Os(btzpy)$_2$]Cl$_2$ as a powder.^{1}H NMR (400 MHz, d$_6$-DMSO): δ 10.15 (s, 4H); 8.58 (d, J = 8.0 Hz, 4H); 8.21 (t, J = 8.0 Hz, 2H); 7.66 - 7.72 (m, 8H); 7.47 – 7.57 (m, 12H). ^{13}C NMR (101 MHz, d$_6$-DMSO): δ 152.01, 150.32, 137.57, 135.58, 130.08, 130.00, 125.27, 120.46, 119.31. ESI HRMS: calculated for [C$_{42}$H$_{30}$N$_{14}$Os]$^{2+}$ m/z = 461.1191; found m/z = 461.1192 [M]$^{2+}$.

7.6 Synthesis of osmium complexes using triazole-based bridging ligand

7.6.1 Synthesis of [Os(bpy)$_2$]$_2$L](PF$_6$)$_4$
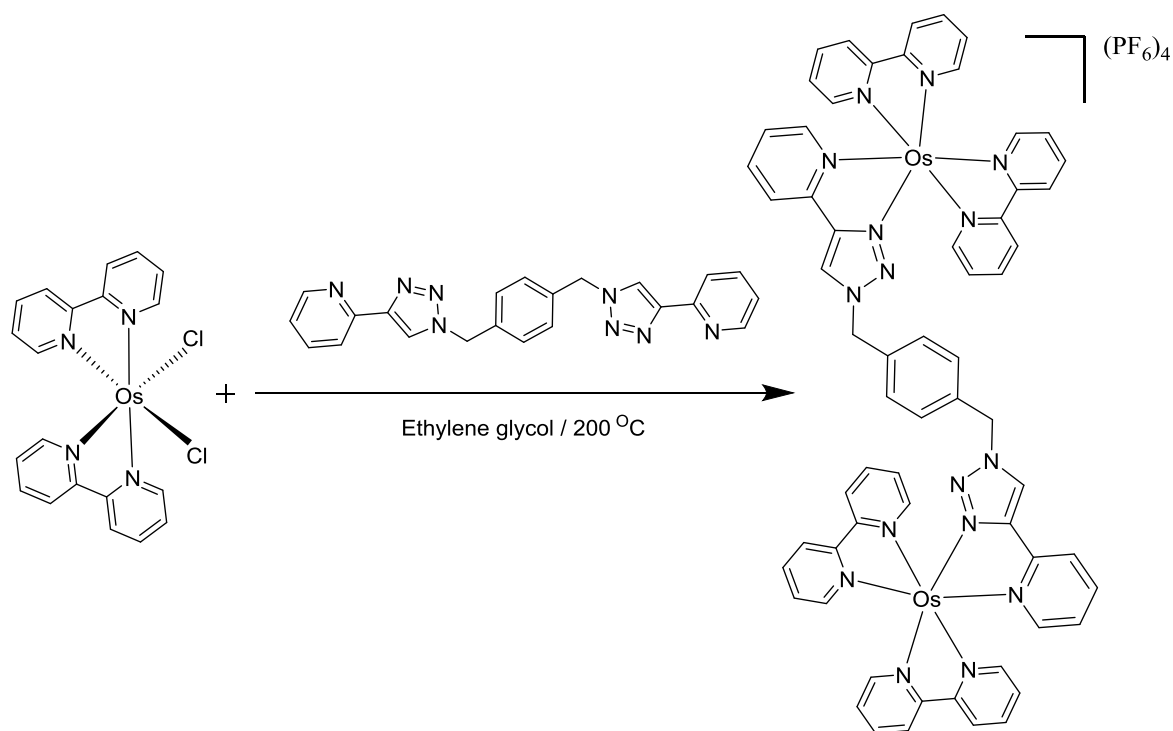
Os(bpy)$_2$Cl (573 mg, 1 mmol), ligand L (197 mg, 0.5 mmol) and AgPF$_6$ (250 mg, 1 mmol) were dissolved in ethylene glycol (20 ml) and refluxed under nitrogen for 24 hrs in the dark. The resulting solution was allowed to cool to room temperature and the precipitate was

separated by vacuum filtration and washed with cold water and diethyl ether .The soleds were

redissolved in acetonitrile and stored in the fridge for 24 hr and filtered through a celite pad to

remove AgCl. Recrystallization from DCM and hexane give the pure product. (Yield = 720

mg, 70%). ^{1}H NMR (400 MHz, CD$_3$CN) δ: 8.62 (d, J = 3.0 Hz, 2H); 8.51 (d, J = 8.1 Hz, 4H);

8.40-8.33 (m, 4H); 8.13 (d, J = 7.9 Hz, 2H); 7.89-7.72 (m, 16H); 7.67 (d, J = 5.8 Hz, 2H); 7.54

(d, J = 5.6 Hz, 2H); 7.36-7.28 (m, 6H); 7.25-7.2 (m, 4H); 7.12 (d, J = 1.8 Hz, 4H); 5.5 (d, J =

4.4 Hz, 4H); ^{13}C NMR (101 MHz, CD$_3$CN) δ: 128.4, 128.4, 128.2, 127.2, 127.0, 126.1, 125.5,

123.4, 122.9, 122.4, 121.4, 54.2, ESI HRMS calculated for [C$_{62}$H$_{50}$N$_{16}$Os$_2$]$^{4+}$ m/z = 350.0905,

found m/z = 350.0903 [M]$^{4+}$.

7.6.2   Synthesis of [Os(Bn-pytz)$_2$]$_2$L](PF$_6$)$_4$
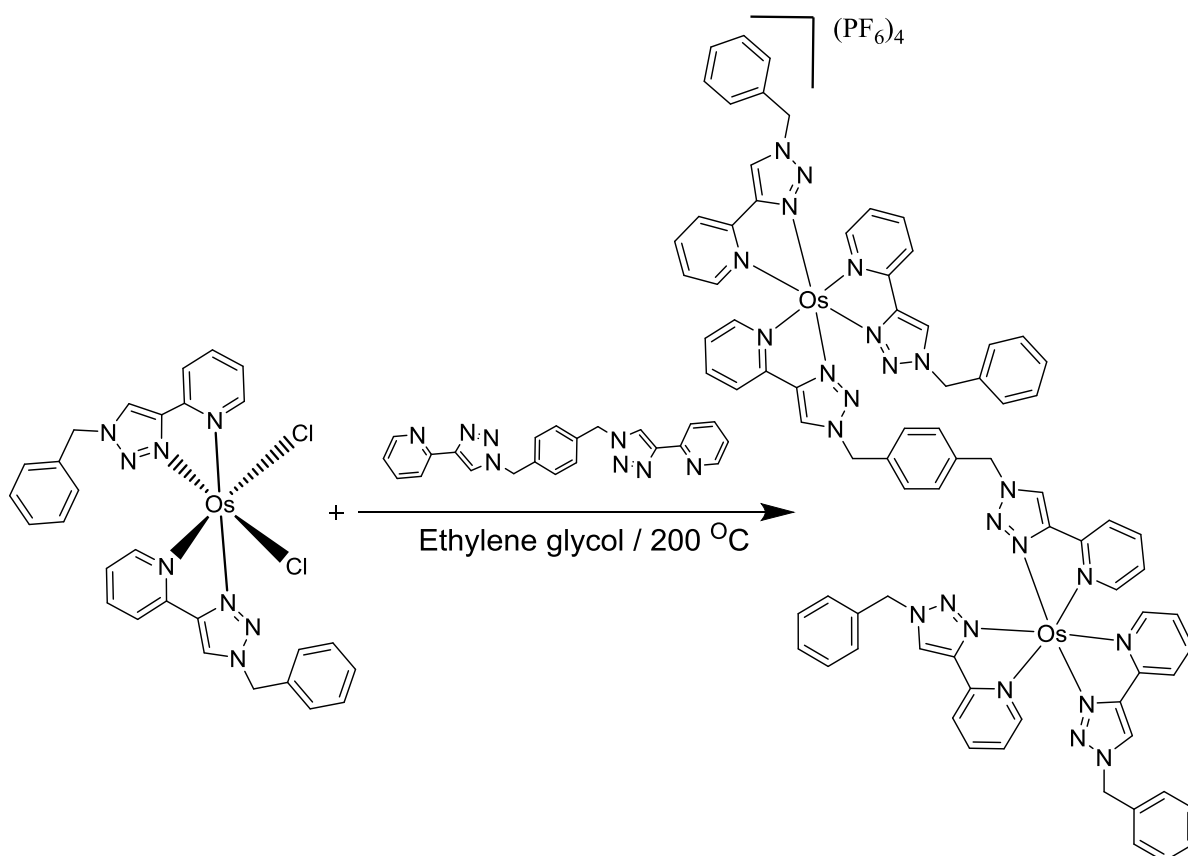
Os(Bn-pytz)$_2$Cl$_2$ (733mg, 1 mmol), ligand L4 (197 mg, 0.5 mmol) and AgPF$_6$ (250 mg, 1

mmol) were dissolved in ethylene glycol (20 ml) and refluxed under nitrogen for 24hrs in the

dark. The resulting solution was allowed to cool to room temperature and the precipitate was separated by vacuum filtration and washed with cold water and diethyl ether. The product was dissolved in acetone and filtered through a celite pad. The filtrate was recrystallized by addition of diethyl ether. The soldes were then redissolved in acetonitrile and stored in fridge for 24 hrs and filtered. Recrystallization from DCM and hexane gave the pure product. (Yield = 760 mg, 70%). ^{1}H NMR (400 MHz, CD$_3$CN) δ: 8.64-8.55 (m, 6H); 8.27 (s, 1H); 8.09-7.95 (m, 6H); 7.84-7.62 (m, 12H); 7.40-7.30 (m, 14H); 7.24-7.09 (m, 15H); 5.61 (d, J = 8.8 Hz, 2H); 5.54-5.47 (m, 10H); ^{13}C NMR (101 MHz, CD$_3$CN) δ: 153.4, 153.2, 152.9, 152.1, 151.6, 151.5, 150.0, 149.8, 149.7, 137.4, 137.3, 134.4, 134.1, 133.7, 129.1, 129.1, 128.9, 128.7, 128.7, 128.4, 128.3, 127.9, 126.2, 125.9, 125.6, 125.5, 125.4, 125.2, 122.9, 122.5, 122.2, 55.6, 55.4, 55.2, 55.0, ESI HRMS calculated for [C$_{78}$H$_{66}$N$_{24}$Os$_2$]$^{4+}$ m/z = 430.6233, found m/z = 430.6277 [M-4Cl]$^{4+}$.

7.7 Synthesis of Iridium Complexes

7.7.1 Synthesis of [{Ir(ppy)$_2$Cl}$_2$][252]
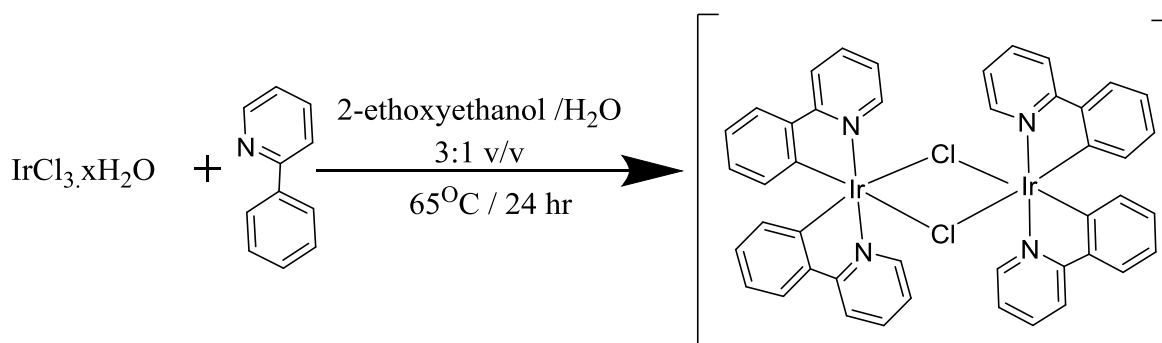
Iridium trichloride hydrate (1.5 g, 0.426 mmol) was combined with 2-phenylpyridine (1.2 ml, 0.84 mmol), dissolved in 60 ml of a mixture of 2-ethoxyethanol: water (3:1 v/v), and refluxed for 24 h. The solution was cooled to room temperature, and the yellow precipitate was collected by filtration. The precipitate was washed with ethanol (30 ml), water (30 ml), acetone (30 ml)

and diethyl ether. (Yield: 3.2 g; 70 %). ^{1}H NMR (400 MHz, (CD$_3$)$_2$SO) δ: 9.82 (d, J = 5.6 Hz,

2H); 9.54 (d, J = 5.5 Hz, 2H); 8.26 (d, J = 8.1 Hz, 2H); 8.17 (d, J = 8.0 Hz, 2H); 8.08 (t, J =

7.5 Hz, 2H); 7.99 (t, J = 7.6 Hz, 2H); 7.79 (d, J = 7.68 Hz, 2H); 7.73 (d, J = 7.68 Hz, 2H); 7.56

(t, J = 6.48 Hz, 2H); 7.44 (t, J = 6.52 Hz, 2H); 6.89 (t, J = 7.32 Hz, 2H); 6.83 (t, J = 7.36 Hz,

2H); 6.76 (t, J = 7.4 Hz, 2H); 6.69 (t, J = 7.4 Hz, 2H); 6.26 (d, J = 7.56 Hz, 2H); 5.67 (d, J =

7.56 Hz, 2H); ^{13}C NMR (101 MHz, (CD$_3$)$_2$SO) δ: 167.8, 167.4, 152.6, 152.5, 151.1, 145.9,

144.2, 143.7, 139.7, 138.6, 131.7, 130.4, 130.1, 129.4, 125.3, 124.3, 124.0, 123.3, 122.7, 122.5,

120.5, 119.9. ESI HRMS calculated for (C$_{45}$H$_{35}$N$_4$Cl$_2$Ir$_2$) m/z = 542.11905, found m/z =

542.11912 [M]$^+$.

7.7.2 Synthesis of [Ir(ppy)$_2$-L-Ir(ppy)$_2$](PF$_6$)$_2$
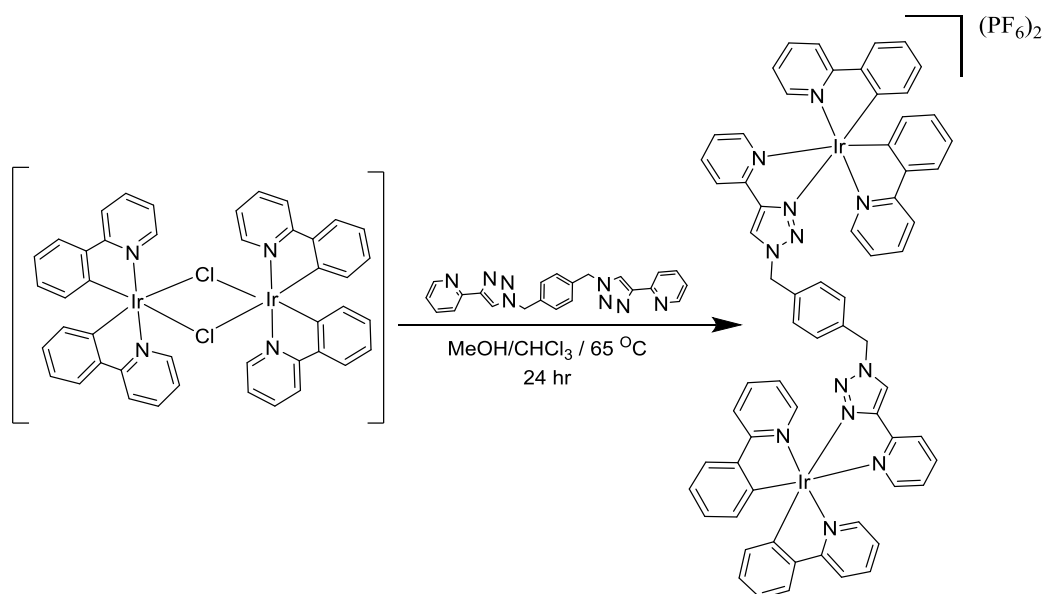
[{Ir(ppy)$_2$Cl}$_2$] (272 mg, 0.25 mmol), L4 (100 mg, 0.25 mmol) and Na$_4$PF$_6$ (250 mg, 1 mmol)

were dissolved in 30 ml of a mixture of methanol: chloroform (1:1) and refluxed under nitrogen

for 24hr. The resulting solution was allowed to cool to room temperature. Diethylether was

added and the yellow precipitate was collected by filtration. The precipitate was washed with

water (5ml) and diethyl ether. The crude product was redissolved in acetonitrile kept in fridge

for 24 hr and filtered. Acetonitrile removed under vacum, then precipitate recrystallized from

(DCM and hexane) (Yield: 265mg; 70%). ^{1}H NMR (400 MHz, CD$_3$CN) δ: 8.66 (s, 1H); 8.65 (s, 1H); 8.12-8.03 (m, 6H); 7.99-7.93 (m, 2H); 7.87-7.78 (m, 8H); 7.74 (d, J = 5.6 Hz, 2H); 7.71-7.66 (m, 2H); 7.61 (d, J = 5.6 Hz, 2H); 7.36 (t, J = 6.4 Hz, 2H); 7.21 (d, J = 4.6 Hz, 4H); 7.08-6.98 (m, 6H); 6.96-6.90 (m, 4H); 6.81 (t, J = 7.44 Hz, 2H); 6.25 (t, J = 6.92 Hz, 4H); 5.59 (s, 4H); ^{13}C NMR (101 MHz, CD$_3$CN) δ: 167.3, 166.9, 150.1, 149.3, 149.0, 149.0, 148.9, 148.6, 146.2, 144.0, 143.9, 139.4, 138.3, 138.1, 134.2, 131.6, 131.1, 130.0, 129.3, 128.6, 128.5, 126.6, 126.1, 126.0, 124.5, 124.1, 123.2, 123.0, 122.6, 122.4, 121.9, 119.5, 119.3, 119.2, 54.5. ESI HRMS calculated for (C$_{66}$H$_{50}$N$_{12}$Ir$_2$) m/z = 696.17411, found m/z = 698.17640 [M]$^{2+}$.

7.7.3 Synthesis of [Ir(ppy)$_2$-L](PF$_6$)
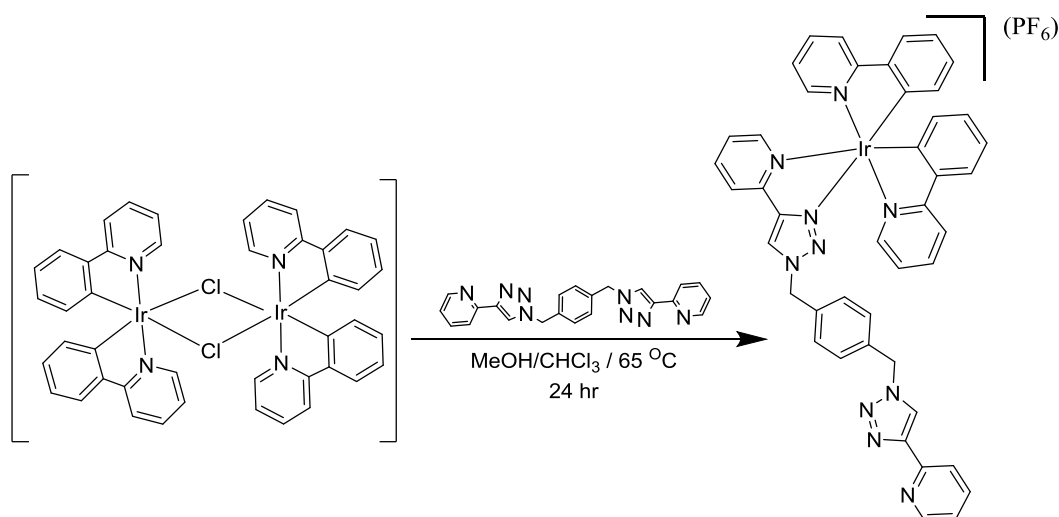
[{Ir(ppy)$_2$Cl}$_2$] (136 mg, 0.25 mmol), L (197 mg, 0.5 mmol) and NaPF$_6$ (250 mg, 1 mmol) were dissolved in 25 ml of mixture of methanol: chloroform (1:1 v/v) and refluxed under nitrogen for 24hrs. The resulting solution was allowed to cool to room temperature. Diethylether was added and the yellow precipitate [Ir(ppy)$_2$-L4](PF$_6$) was collected by filtration and washed with water (5ml), and diethyl ether. The crude product was redissolved in acetonitrile kept in the fridge for 24 hrs and filtered. Acetonitrile was removed under reduced pressure, then the precipitate recrystallized from DCM and hexane. (Yield: 180 mg; 75%). ^{1}H NMR (400 MHz, CD$_3$CN) δ: 8.64 (s, 1H); 8.54 (s, 1H); 8.29 (d, J = 8.4 Hz, 1H); 8.11-7.92 (m,

5H); 7.86-7.76 (m, 5H); 7.71 (d, $J = 5.5$ Hz, 1H); 7.67 (d, $J = 7.5$ Hz, 1H); 7.57 (d, $J = 5.6$ Hz, 1H); 7.35-7.27 (m, 4H); 7.18 (d, $J = 7.1$ Hz, 2H); 7.04-6.95 (m, 3H); 6.92-6.86 (m, 2H); 6.82-6.77 (m, 1H); 6.26-6.20 (m, 2H); 5.61 (d, $J = 5.1$ Hz, 2H); 5.57 (d, $J = 1.5$ Hz, 2H); ^{13}C NMR (101 MHz, CD_3CN) δ: 168.1, 167.7, 150.9, 150.3, 149.8, 149.5, 147.0, 144.9, 144.8, 140.3, 139.1, 139.0, 134.6, 132.4, 132.0, 130.9, 130.2, 129.4, 129.3, 129.2, 127.4, 126.9, 125.4, 124.9, 124.1, 123.9, 123.5, 123.2, 122.8, 120.4, 120.1, 117.9, 55.5. ESI HRMS calculated for ($C_{42}H_{34}N_{12}Ir$) $m/z = 448.13311$, found $m/z = 448.63122$ [M]$^+$.

7.8 Synthesis of Ruthenium Complexes

7.8.1 Synthesis of Ru(bpy)$_2$Cl$_2$[251]
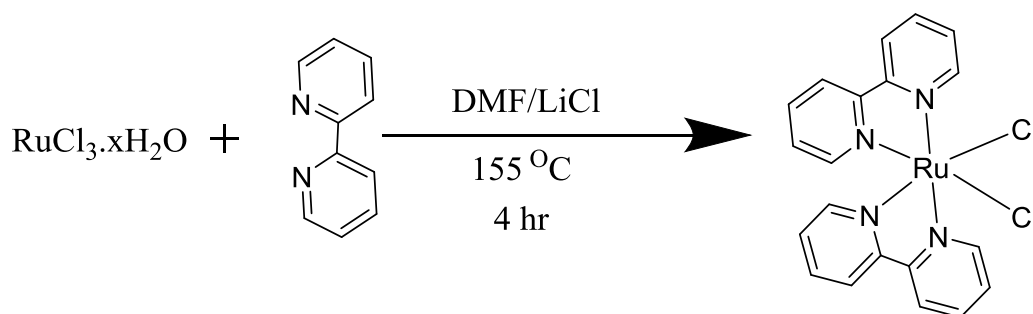
Ru(bpy)$_2$Cl$_2$ was prepared according to the method previously reported,[251] RuCl$_3$·3H$_2$O (3.20 g; 12.15 mmol) and bipyridine (3.78 g; 24.30 mmol) were refluxed under N$_2$ at 155 ^{O}C in 60 ml of DMF for 4 h with magnetic stirring in the dark.. After the reaction mixture had cooled to room temperature, 100 mL of reagent grade acetone was added. and was then cooled to 0°C overnight. The mixture was filtered, yielding a dark green −black product which was recrystallized in LiCl solution (30 g/ 50 ml H$_2$O). The black solid was washed three times with 10 ml portions of cold water followed by three 10 ml portions of diethyl ether, and was subsequently dried under vacuum (Yield: 2.5 g; 40 %).^{1}H NMR (400 MHz, (CD$_3$)$_2$SO) δ: 9.93 (d, $J = 4.1$ Hz, 2H); 8.63 (d, $J = 8.0$ Hz, 2H); 8.49 (d, $J = 7.9$ Hz, 2H); 8.07 (t, $J = 7.6$ Hz, 2H);

7.75 (t, $J = 5.7$ Hz, 2H); 7.65 (t, $J = 7.48$ Hz, 2H); 7.47 (d, $J = 3.16$ Hz, 2H); 7.11 (t, $J = 5.92$ Hz, 2H).

7.8.2   Synthesis of [Ru(bpy)₂-L](PF₆)₂
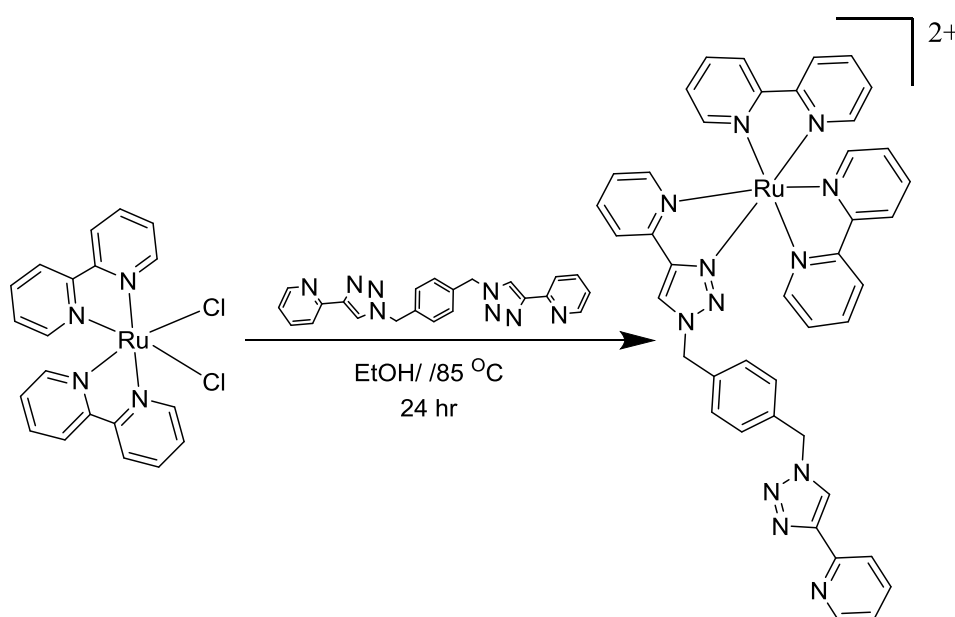
Ru(bpy)$_2$Cl$_2$ (120 mg, 0.25mmol), L (197 mg, 0.5 mmol) were dissolved in ethanol (30 ml) and refluxed in the dark under nitrogen for 24hrs. The resulting solution was allowed to cool to room temperature, then NH$_4$PF$_6$ (250 mg, 1 mmol) was added to the solution and stirred for 45 min. The dark orange precipitate was separated by vacuum filtration and washed with cold water and diethyl ether. The crude product was redissolved in acetonitrile, kept in the fridge for 24 hrs and filtered. Acetonitrile was removed under reduced pressure, then the precipitate recrystallized from DCM and hexane (Yield: 170 mg; 70%) ^{1}H NMR (400 MHz, CD$_3$CN) δ: 8.63 (s, 1H); 8.56 (d, $J = 3.6$ Hz, 1H); 8.49 (t, $J = 7.8$ Hz, 2H); 8.37 (d, $J = 7.9$ Hz, 2H); 8.31 (s, 1H); 8.10-7.94 (m, 7H); 7.87-7.82 (m, 3H); 7.77 (d, $J = 5.4$ Hz, 1H); 7.71 (d, $J = 5.4$ Hz, 1H); 7.57 (d, $J = 5.5$ Hz, 1H); 7.42-7.25 (m, 8H); 7.13 (d, $J = 8.0$ Hz, 2H); 5.62 (s, 2H); 5.51 (d, $J = 1.7$ Hz, 2H); ^{13}C NMR (101 MHz, CD$_3$CN) δ: 156.9, 156.8, 156.6, 151.9, 151.8, 151.7,

151.4, 151.3, 150.4, 147.5, 137.9, 137.4, 137.3, 137.2, 137.0, 136.3, 133.8, 128.4, 128.4, 127.2, 127.1, 127.0, 126.4, 125.7, 125.5, 123.9, 123.8, 123.4, 123.1, 122.8, 122.6, 122.5, 117.0, 54.7, 52.9, ESI HRMS calculated for ($C_{42}H_{34}N_{12}Ru$) m/z = 404.1031, found m/z = 404.10300 $[M]^{2+}$.

7.8.3 Synthesis of [Ru(bpy)₂-L-Ru(bpy)₂](PF₆)₄
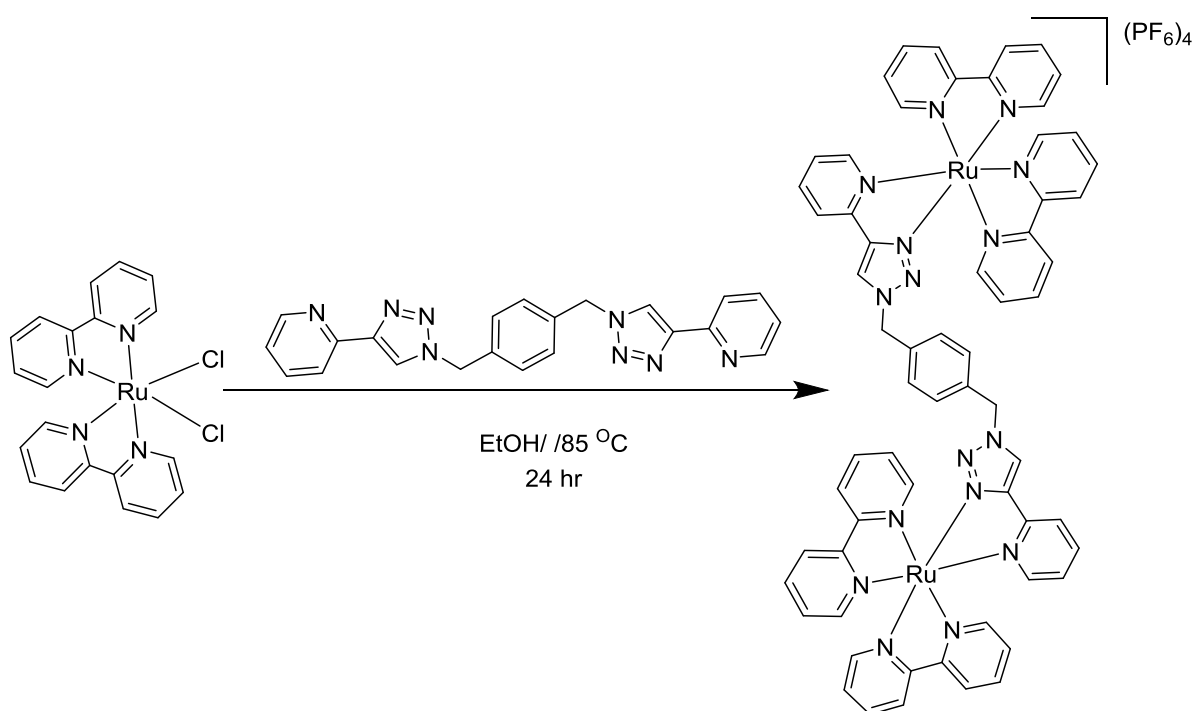
Ru(bpy)₂Cl₂ (242 mg, 0.5mmol), L (197mg, 0.5 mmol) were dissolved in ethanol (30 ml) and refluxed in the dark under nitrogen for 24hrs. The resulting solution was allowed to cool to room temperature. Then NH₄PF₆ (250 mg, 1 mmol) was added to the solution and stirred for 45 min. The dark orange precipitate was separated by vacuum filtration and washed with cold water and diethyl ether. The crude product was redissolved in acetonitrile and kept in fridge for 24 hrs and filtered. Acetonitrile was removed under reduced pressure and the precipitate recrystallized from DCM and hexane (yield: 230 mg; 70. %). ^{1}H NMR (400 MHz, CD₃CN) δ: 8.69 (d, J = 2.88 Hz, 2H); 8.53 (d, J = 7.92 Hz, 4H); 8.42-8.36 (m, 4H); 8.10-8.05 (m, 6H); 8.04-7.96 (m, 6H); 7.85 (t, J = 5.6 Hz, 4H); 7.81 (d, J = 5.4 Hz, 2H); 7.74 (d, J = 5.4 Hz, 2H); 7.60 (d, J = 5.48 Hz, 2H); 7.45-7.37 (m, 6H); 7.34-7.29 (m, 4H); 7.13 (s, 4H); 5.53 (s, 4H);

^{13}C NMR (101 MHz, CD$_3$CN) δ: 157.3, 157.0, 156.9, 156.7, 151.8, 151.8, 151.7, 151.5, 151.4, 150.4, 147.6, 138.0, 137.5, 137.4, 137.3, 134.1, 128.5, 128.5, 127.3, 127.2, 127.1, 126.5, 125.8, 125.6, 125.5, 124.0, 123.9, 123.4, 123.2, 122.5, 117.1, 54.6, ESI HRMS calculated for (C$_{62}$H$_{50}$N$_{16}$Ru$_2$) m/z = 305.56173, found m/z = 305.56216 [M]$^{4+}$.

7.9 - [Ru(bpy)$_2$-L-Ir(ppy)$_2$](PF$_6$)$_3$
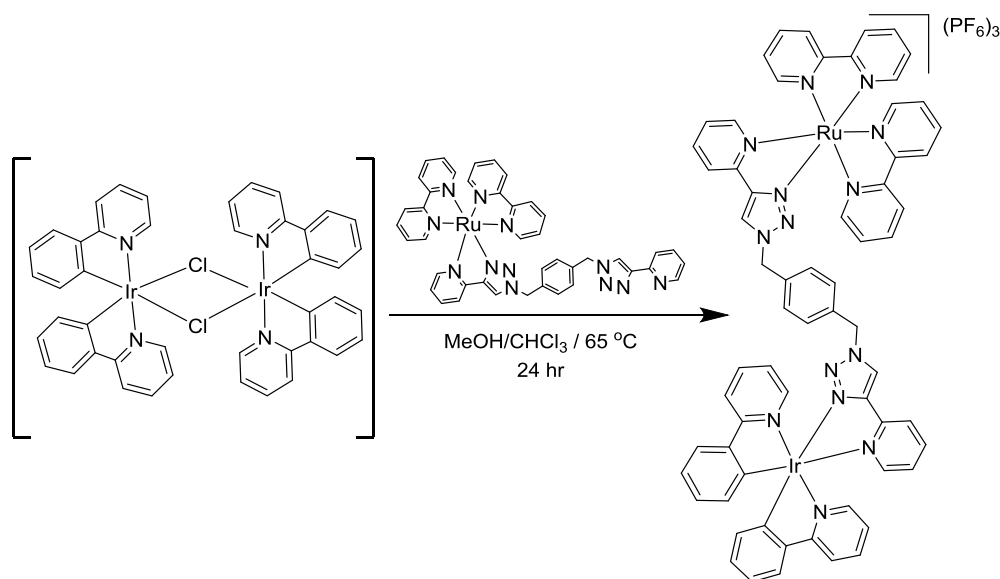
[{Ir(ppy)$_2$Cl}$_2$] (136 mg, 0.125 mmol), [Ru(bpy)$_2$-L4](PF$_6$)$_2$ (100 mg, 0.125 mmol) and NH$_4$PF$_6$ (125 mg, 0.5 mmol) were dissolved in 30 ml of a mixture of methanol: chloroform(1:1 v/v) and refluxed under nitrogen for 24hrs in the dark. The resulting solution was allowed to cool to room temperature, then diethyl ether was added and the orange precipitate was collected by filtration. The precipitate was washed with water (5 ml) and diethyl ether. The crude product was redissolved in acetonitrile kept in the fridge for 24 hrs and filtered. Acetonitrile was removed under reduced pressure, then the precipitate recrystallized from DCM and hexane (Yield: 114 mg; 70%). ^{1}H NMR (400 MHz, CD$_3$CN) δ: 8.69-8.62 (m, 2H); 8.52 (d, J = 5.2 Hz, 2H); 8.36-8.28 (m, 2H); 8.11-7.92 (m, 10H); 7.86-7.59 (m, 12H); 7.42-7.29 (m, 6H); 7.21-6.91 (m, 9H); 6.80 (s, 1H); 6.24 (d, J = 6.9 Hz, 2H); 5.61 (d, J = 5.0 Hz, 2H); 5.54 (d, J = 15.7 Hz,

2H); ^{13}C NMR (100 MHz, CD$_3$CN) δ: 152.2, 151.8, 151.7, 150.4, 149.3, 139.8, 137.8, 131.9, 130.4, 129.7, 128.9, 127.6, 126.1, 124.9, 124.4, 124.3, 124.2, 122.9, 122.7, 122.2, 119.9, 54.8, HRMS calculated for (C$_{64}$H$_{50}$IrN$_{14}$Ru) m/z = 436.4333, found m/z = 436.4335 [M]$^{3+}$.

7.10 **Published Papers**

The following list of publications has risen from this research activity:

7.10.1 Refereed Journal Papers

1- Omar, S. A., Scattergood, P. A., McKenzie, L. K., Bryant, H. E., Weinstein, J. A., & Elliott, P. I. (2016). Towards Water Soluble Mitochondria-Targeting Theranostic Osmium (II) Triazole-Based Complexes. *Molecules*, *21*(10), 1382.

References

1. A. Kumar, S.-S. Sun and A. J. Lees, in *Photophysics of Organometallics*, Springer, 2009, pp. 37-71.
2. N. A. Kane-Maguire, in *Photochemistry and Photophysics of Coordination Compounds I*, Springer, 2007, pp. 37-67.
3. A. D. Kirk, *Chem.Rev.,* 1999, **99**, 1607-1640.
4. M. Wrighton, *Chem.Rev.,* 1974, **74**, 401-430.
5. A. W. Adamson and J. N. Demas, *J. Am. Chem. Soc.*, 1971, **93**, 1800-1801.
6. V. Balzani, N. Sabbatini and F. Scandola, *Chem.Rev.*, 1986, **86**, 319-337.
7. A. Mills and S. Le Hunte, *J. Photochm. photobiol.A.,* 1997, **108**, 1-35.
8. C. C. Mak and H.-F. Chow, *Macromolecules*, 1997, **30**, 1228-1230.
9. J. L. Smithback, J. B. Helms, E. Schutte, S. M. Woessner and B. P. Sullivan, *Inorg. Chem.,* 2006, **45**, 2163-2174.
10. S. y. Takizawa, C. Pérez- Bolívar, P. Anzenbacher and S. Murata, *Eur. J. Inorg. Chem.,*2012, **2012**, 3975-3979.
11. H. Seino, Y. Tanabe, Y. Ishii and M. Hidai, *Inorg. Chem. Acta.,*1998, **280**, 163-171.
12. R. S. Lumpkin, E. M. Kober, L. A. Worl, Z. Murtaza and T. J. Meyer, *J. Phys. Chem.,* 1990, **94**, 239-243.
13. P. K. Chow, G. Cheng, G. S. M. Tong, W. P. To, W. L. Kwong, K. H. Low, C. C. Kwok, C. Ma and C. M. Che, *Angew. Chem. Int. Ed.*, 2015, **127**, 2112-2117.
14. M. Dörr and E. Meggers, *Curr. Opin.Chem. Biol.,*2014, **19**, 76-81.
15. E. Baggaley, J. A. Weinstein and J. G. Williams, in *Luminescent and Photoactive Transition Metal Complexes as Biomolecular Probes and Cellular Reagents*, Springer, 2014, pp. 205-256.
16. M. D. Kärkäs, O. Verho, E. V. Johnston and B. r. Åkermark, *Chem.Rev.,* 2014, **114**, 11863-12001.
17. W. T. Eckenhoff and R. Eisenberg, *Dalton Trans*, 2012, **41**, 13004-13021.
18. J. Kalinowski, V. Fattori, M. Cocchi and J. G. Williams, *Coordin. Chem. Rev.,* 2011, **255**, 2401-2425.
19. A. Hagfeldt, G. Boschloo, L. Sun, L. Kloo and H. Pettersson, *Chem.Rev.,* 2010, **110**, 6595-6663.
20. A. J. McConnell, C. S. Wood, P. P. Neelakandan and J. R. Nitschke, *Chem.Rev.,* 2015, **115**, 7729-7793.
21. E. Baggaley, J. A. Weinstein and J. G. Williams, *Coordin. Chem. Rev.,* 2012, **256**, 1762-1785.
22. T. Yano, S. Hishida, M. Nakai and Y. Nakabayashi, *Inorg. Chem. Acta.,* 2017, **454**, 162-170.
23. G. Hager and G. Crosby, *J. Am. Chem. Soc.*, 1975, **97**, 7031-7037.
24. D. W. Thompson, A. Ito and T. J. Meyer, *Pure and Applied Chemistry*, 2013, **85**, 1257-1305.
25. A. Juris, V. Balzani, F. Barigelletti, S. Campagna, P. l. Belser and A. Von Zelewsky, *Coordin. Chem. Rev.,* 1988, **84**, 85-277.
26. G. Calzaferri and R. Rytz, *J. Phys. Chem.,* 1995, **99**, 12141-12150.
27. K. Rangan, S. M. Arachchige, J. R. Brown and K. J. Brewer, *Energy& Environ. Sci.,*2009, **2**, 410-419.
28. K. King and R. Watts, *J. Am. Chem. Soc.*, 1987, **109**, 1589-1590.
29. H. Wang, Q. Liao, H. Fu, Y. Zeng, Z. Jiang, J. Ma and J. Yao, *J. Mater.Chem.,* 2009, **19**, 89-96.
30. C.-H. Yang, S.-W. Li, Y. Chi, Y.-M. Cheng, Y.-S. Yeh, P.-T. Chou, G.-H. Lee, C.-H. Wang and C.-F. Shu, *Inorg. Chem.,* 2005, **44**, 7770-7780.

31. G. Zhou, W. Y. Wong, B. Yao, Z. Xie and L. Wang, *Angew Chem Int Ed Engl*, 2007, **46**, 1149-1151.

32. S. T. Kochuveedu and D. H. Kim, *Nanoscale*, 2014, **6**, 4966-4984.

33. M. Mauro, A. Aliprandi, D. Septiadi, N. S. Kehr and L. De Cola, *Chem.Soc. Rev.,* 2014, **43**, 4144-4166.

34. J. Leanne B and B. Ross W, *Metal-based drugs*, 2008, **2008**.

35. H. Takeda and O. Ishitani, *Coordin. Chem. Rev.,* 2010, **254**, 346-354.

36. A. Fujishima and K. Honda, *Nature*, 1972, **238**, 37-38.

37. J. Hawecker, J. M. Lehn and R. Ziessel, *Helv. chim. acta.,* 1986, **69**, 1990-2012.

38. H. Hori, F. P. Johnson, K. Koike, O. Ishitani and T. Ibusuki, *J. Photochm. photobiol.A.,* 1996, **96**, 171-174.

39. A. Nakada, K. Koike, T. Nakashima, T. Morimoto and O. Ishitani, *Inorg. Chem.,* 2015, **54**, 1800-1807.

40. Q. Pei, G. Yu, C. Zhang, Y. Yang and A. J. Heeger, *Science*, 1995, **269**, 1086-1088.

41. K. M. Maness, R. H. Terrill, T. J. Meyer, R. W. Murray and R. M. Wightman, *J. Am. Chem. Soc.*, 1996, **118**, 10609-10616.

42. M. S. Lowry and S. Bernhard, *Chem- Eur. J.,* 2006, **12**, 7970-7977.

43. D. A. Bernards, T. Biegala, Z. A. Samuels, J. D. Slinker, G. G. Malliaras, S. Flores-Torres, H. D. Abruna and J. A. Rogers, *Appl. phys.lett.,* 2004, **84**, 3675-3677.

44. J. D. Slinker, J. Rivnay, J. A. DeFranco, D. A. Bernards, A. A. Gorodetsky, S. T. Parker, M. P. Cox, R. Rohl, G. G. Malliaras and S. Flores-Torres, *J. Appl. phys.,* 2006, **99**, 074502.

45. A. Sinopoli, C. J. Wood, E. A. Gibson and P. I. Elliott, *Dyes& Pigments.,* 2017, **140**, 269-277.

46. S. Aghazada, P. Gao, A. Yella, G. Marotta, T. Moehl, J. Teuscher, J. E. Moser, F. De Angelis, M. Gratzel and M. K. Nazeeruddin, *Inorg. Chem.,* 2016, **55**, 6653-6659.

47. M. K. Nazeeruddin, A. Kay, I. Rodicio, R. Humphry-Baker, E. Müller, P. Liska, N. Vlachopoulos and M. Grätzel, *J. Am. Chem. Soc.*, 1993, **115**, 6382-6390.

48. M. Gratzel, *Acc Chem Res*, 2009, **42**, 1788-1798.

49. J. C. Dabrowiak, *Metals in medicine*, John Wiley & Sons, 2017.

50. L. E. Scott and C. Orvig, *Chem.Rev.,* 2009, **109**, 4885-4910.

51. T. W. Hambley, *Dalton Trans.*, 2007, 4929-4937.

52. K. Y. Zhang and K. K. Lo, *Inorg. Chem.,* 2009, **48**, 6011-6025.

53. K. K. Lo, K. Y. Zhang, S. K. Leung and M. C. Tang, *Angew Chem Int Ed Engl*, 2008, **47**, 2213-2216.

54. C. A. Puckett and J. K. Barton, *J Am Chem Soc*, 2009, **131**, 8738-8739.

55. C. A. Puckett, R. J. Ernst and J. K. Barton, *Dalton Trans*, 2010, **39**, 1159-1170.

56. K. A. Stephenson, S. R. Banerjee, T. Besanger, O. O. Sogbein, M. K. Levadala, N. McFarlane, J. A. Lemon, D. R. Boreham, K. P. Maresca and J. D. Brennan, *J. Am. Chem. Soc.*, 2004, **126**, 8598-8599.

57. C. Mari, M. Panigati, L. D'Alfonso, I. Zanoni, D. Donghi, L. Sironi, M. Collini, S. Maiorana, C. Baldoli and G. D'Alfonso, *Organometallics*, 2012, **31**, 5918-5928.

58. A. Byrne, C. Dolan, R. D. Moriarty, A. Martin, U. Neugebauer, R. J. Forster, A. Davies, Y. Volkov and T. E. Keyes, *Dalton Transactions*, 2015, **44**, 14323-14332.

59. E. M. Kober and T. J. Meyer, *Inorg. Chem.,* 1983, **22**, 1614-1616.

60. T. E. Keyes, D. Leane, R. J. Forster, C. G. Coates, J. J. McGarvey, M. N. Nieuwenhuyzen, E. Figgemeier and J. G. Vos, *Inorg. Chem.,* 2002, **41**, 5721-5732.

61. M. Frezza, S. Hindo, D. Chen, A. Davenport, S. Schmitt, D. Tomco and Q. Ping Dou, *Current pharmaceutical design*, 2010, **16**, 1813-1825.

62. Z. Guo and P. J. Sadler, *Advances in Inorg. Chem.,* 1999, **49**, 183-306.

63.   C. X. Zhang and S. J. Lippard, *Curr. Opin.Chem. Biol.,*2003, **7**, 481-489.
64.   P. J. Dyson and G. Sava, *Dalton Trans*, 2006, 1929-1933.
65.   J. M. Hearn, I. Romero-Canelon, B. Qamar, Z. Liu, I. Hands-Portman and P. J. Sadler, *ACS chem.biol.,* 2013, **8**, 2345.
66.   S. Betanzos-Lara, L. Salassa, A. Habtemariam, O. Novakova, A. M. Pizarro, G. J. Clarkson, B. Liskova, V. Brabec and P. J. Sadler, *Organometallics*, 2012, **31**, 3466-3479.
67.   A. F. Peacock, A. Habtemariam, R. Fernandez, V. Walland, F. P. Fabbiani, S. Parsons, R. E. Aird, D. I. Jodrell and P. J. Sadler, *J Am Chem Soc*, 2006, **128**, 1739-1748.
68.   A. M. Funston, C. Cullinane, K. P. Ghiggino, W. D. McFadyen, S. S. Stylli and P. A. Tregloan, *Aust. j.chem.,* 2005, **58**, 206-212.
69.   M. Strianese, A. Basile, A. Mazzone, S. Morello, M. C. Turco and C. Pellecchia, *J Cell Physiol*, 2013, **228**, 2202-2209.
70.   F. S. Mackay, J. A. Woods, H. Moseley, J. Ferguson, A. Dawson, S. Parsons and P. J. Sadler, *Chem- Eur.J.,* 2006, **12**, 3155-3161.
71.   A. Dondoni, *Angew. Chem. Int.Ed.,* 2008, **47**, 8995-8997.
72.   H. C. Kolb, M. G. Finn and K. B. Sharpless, *Angew Chem Int Ed Engl*, 2001, **40**, 2004-2021.
73.   B. R. Buckley and H. Heaney, in *Click Triazoles*, Springer, 2012, pp. 1-29.
74.   J. Totobenazara and A. J. Burke, *Tetrahedron Letters*, 2015, **56**, 2853-2859.
75.   J. E. Moses and A. D. Moorhouse, *Chem. Soc. Rev.*, 2007, **36**, 1249-1262.
76.   S. Narayan, J. Muldoon, M. Finn, V. V. Fokin, H. C. Kolb and K. B. Sharpless, *Angew. Chem. Int.Ed.,* 2005, **44**, 3275-3279.
77.   V. V. Rostovtsev, L. G. Green, V. V. Fokin and K. B. Sharpless, *Angew. Chem. Int. Ed. Engl.*, 2002, **41**, 2596-2599.
78.   E. J. Yoo, M. Ahlquist, S. H. Kim, I. Bae, V. V. Fokin, K. B. Sharpless and S. Chang, *Angew. Chem. Int. Ed. Engl.*, 2007, **46**, 1730-1733.
79.   C. W. Tornoe, C. Christensen and M. Meldal, *J. Org. Chem.*, 2002, **67**, 3057-3064.
80.   J. Košmrlj, *Click triazoles*, Springer, 2012.
81.   H. C. Kolb and K. B. Sharpless, *Drug discovery today*, 2003, **8**, 1128-1137.
82.   K. P. Kaliappan, P. Kalanidhi and S. Mahapatra, *Synlett*, 2009, **2009**, 2162-2166.
83.   P. I. Elliott, *Organometallic. Chem.,* 2014, **39**, 1-25.
84.   P. Wu and V. V. Fokin, *Aldrichim. Acta.,* 2007, **40**, 7-17.
85.   T. Dirk, G. W. Esse, J. Hans and M. Rob, *Chem.Commun.,* 2005, 4581-4583.
86.   J. D. Crowley and D. A. McMorran, in *Click Triazoles*, Springer, 2012, pp. 31-83.
87.   A. Bolje, D. Urankar and J. Košmrlj, *Eur. J.Org Chem.,* 2014, **2014**, 8167-8181.
88.   J. D. Crowley, P. H. Bandeen and L. R. Hanton, *Polyhedron*, 2010, **29**, 70-83.
89.   J. T. Fletcher, B. J. Bumgarner, N. D. Engels and D. A. Skoglund, *Organometallics*, 2008, **27**, 5430-5433.
90.   S. Lee, Y. Hua, H. Park and A. H. Flood, *Org. Lett.,* 2010, **12**, 2100-2102.
91.   Y.-Y. Zhu, G.-T. Wang, R.-X. Wang and Z.-T. Li, *Cryst.Growth & Des.,* 2009, **9**, 4778-4783.
92.   B. Colasson, M. Save, P. Milko, J. Roithova, D. Schroder and O. Reinaud, *Org. Lett.,* 2007, **9**, 4987-4990.
93.   J. P. Byrne, J. A. Kitchen and T. Gunnlaugsson, *Chem. Soc. Rev.*, 2014, **43**, 5302-5325.
94.   B. Happ, C. Friebe, A. Winter, M. D. Hager, R. Hoogenboom and U. S. Schubert, *Chem– Asian. J.,* 2009, **4**, 154-163.
95.   C. E. Welby, S. Grkinic, A. Zahid, B. S. Uppal, E. A. Gibson, C. R. Rice and P. I. Elliott, *Dalton Transactions*, 2012, **41**, 7637-7646.

96. M. Obata, A. Kitamura, A. Mori, C. Kameyama, J. A. Czaplewska, R. Tanaka, I. Kinoshita, T. Kusumoto, H. Hashimoto, M. Harada, Y. Mikata, T. Funabiki and S. Yano, *Dalton Trans*, 2008, 3292-3300.

97. I. Stengel, A. Mishra, N. Pootrakulchote, S.-J. Moon, S. M. Zakeeruddin, M. Grätzel and P. Bäuerle, *J. Mater.Chem.,* 2011, **21**, 3726-3734.

98. B. S. Uppal, R. K. Booth, N. Ali, C. Lockwood, C. R. Rice and P. I. Elliott, *Dalton Trans*, 2011, **40**, 7610-7616.

99. B. M. Suijkerbuijk, B. N. Aerts, H. P. Dijkstra, M. Lutz, A. L. Spek, G. van Koten and R. J. K. Gebbink, *Dalton Transactions*, 2007, 1273-1276.

100. S. Badeche, J. C. Daran, J. Ruiz and D. Astruc, *Inorg. Chem.,* 2008, **47**, 4903-4908.

101. J. D. Crowley and E. L. Gavey, *Dalton Transactions*, 2010, **39**, 4035-4037.

102. C. Maeda, S. Yamaguchi, C. Ikeda, H. Shinokubo and A. Osuka, *Org. Lett.*, 2008, **10**, 549-552.

103. A. Seridi, M. Wolff, A. Boulay, N. Saffon, Y. Coulais, C. Picard, B. Machura and E. Benoist, *Inorg. Chem. Commun.*, 2011, **14**, 238-242.

104. C. Zhang, X. Shen, R. Sakai, M. Gottschaldt, U. S. Schubert, S. Hirohara, M. Tanihara, S. Yano, M. Obata and N. Xiao, *J. Polym. Sci. Pol. Chem.* 2011, **49**, 746-753.

105. S. Zanarini, M. Felici, G. Valenti, M. Marcaccio, L. Prodi, S. Bonacchi, P. Contreras-Carballada, R. M. Williams, M. C. Feiters and R. J. Nolte, *Chem- Eur. J.,* 2011, **17**, 4640-4647.

106. A. Boulay, A. Seridi, C. Zedde, S. Ladeira, C. Picard, L. Maron and E. Benoist, *Eur. J. Inorg. Chem.,* 2010, **2010**, 5058-5062.

107. T. U. Connell, D. J. Hayne, U. Ackermann, H. J. Tochon- Danguy, J. M. White and P. S. Donnelly, *J. Labelled . Compd. Rad.,* 2014, **57**, 262-269.

108. C. Richardson, C. M. Fitchett, F. R. Keene and P. J. Steel, *Dalton Transactions*, 2008, 2534-2537.

109. M. Felici, P. Contreras- Carballada, Y. Vida, J. M. Smits, R. J. Nolte, L. De Cola, R. M. Williams and M. C. Feiters, *Chem- Eur.J.,* 2009, **15**, 13124-13134.

110. M. Felici, P. Contreras-Carballada, J. M. Smits, R. J. Nolte, R. M. Williams, L. De Cola and M. C. Feiters, *Molecules*, 2010, **15**, 2039-2059.

111. M. Mydlak, C. Bizzarri, D. Hartmann, W. Sarfert, G. Schmid and L. De Cola, *Adv. Funct. Mater.,* 2010, **20**, 1812-1820.

112. K. J. Kilpin and J. D. Crowley, *Polyhedron*, 2010, **29**, 3111-3117.

113. A. D'Amora, L. Fanfoni, D. Cozzula, N. Guidolin, E. Zangrando, F. Felluga, S. Gladiali, F. Benedetti and B. Milani, *Organometallics*, 2010, **29**, 4472-4485.

114. D. Schweinfurth, R. Pattacini, S. Strobel and B. Sarkar, *Dalton Transactions*, 2009, 9291-9297.

115. D. Urankar, B. Pinter, A. Pevec, F. De Proft, I. Turel and J. Košmrlj, *Inorg. Chem.,* 2010, **49**, 4820-4829.

116. P. A. Scattergood and P. I. P. Elliott, *Dalton Trans*, 2017.

117. A. Mattiuzzi, I. Jabin, C. Moucheron and A. Kirsch-De Mesmaeker, *Dalton transactions*, 2011, **40**, 7395-7402.

118. U. Monkowius, S. Ritter, B. König, M. Zabel and H. Yersin, *Eur. J. Inorg. Chem.,*2007, **2007**, 4597-4606.

119. C. E. Welby, G. K. Armitage, H. Bartley, A. Wilkinson, A. Sinopoli, B. S. Uppal, C. R. Rice and P. I. Elliott, *Chem- Eur. J.,* 2014, **20**, 8467-8476.

120. D. A. Ross, P. A. Scattergood, A. Babaei, A. Pertegas, H. J. Bolink and P. I. Elliott, *Dalton Trans*, 2016, **45**, 7748-7757.

121. C. E. Welby, L. Gilmartin, R. R. Marriott, A. Zahid, C. R. Rice, E. A. Gibson and P. I. Elliott, *Dalton Transactions*, 2013, **42**, 13527-13536.

122. T. L. Mindt, H. Struthers, L. Brans, T. Anguelov, C. Schweinsberg, V. Maes, D. Tourwé and R. Schibli, *J. Am. Chem. Soc.*, 2006, **128**, 15096-15097.

123. T. L. Mindt, C. Muller, M. Melis, M. de Jong and R. Schibli, *Bioconjug. Chem.*, 2008, **19**, 1689-1695.

124. T. L. Mindt, C. Müller, F. Stuker, J.-F. Salazar, A. Hohn, T. Mueggler, M. Rudin and R. Schibli, *Bioconjug. chem.*, 2009, **20**, 1940-1949.

125. T. L. Mindt, C. Schweinsberg, L. Brans, A. Hagenbach, U. Abram, D. Tourwe, E. Garcia-Garayoa and R. Schibli, *Chem.Med. Chem.*, 2009, **4**, 529-539.

126. H. Struthers, D. Viertl, M. Kosinski, B. Spingler, F. Buchegger and R. Schibli, *Bioconjug.Chem.*, 2010, **21**, 622-634.

127. L. Brans, E. García- Garayoa, C. Schweinsberg, V. Maes, H. Struthers, R. Schibli and D. Tourwé, *Chem.Med.Chem.*, 2010, **5**, 1717-1725.

128. H. Struthers, T. L. Mindt and R. Schibli, *Dalton transactions*, 2010, **39**, 675-696.

129. F. Tinnis and H. Adolfsson, *Org. Biomol. Chem.*, 2010, **8**, 4536-4539.

130. S. Gu, H. Xu, N. Zhang and W. Chen, *Chem. Asian. J.*, 2010, **5**, 1677-1686.

131. N. Chandrasekhar and R. Chandrasekar, *Dalton Transactions*, 2010, **39**, 9872-9878.

132. M. Hebenbrock, L. Stegemann, J. Kosters, N. L. Doltsinis, J. Muller and C. A. Strassert, *Dalton Trans*, 2017, **46**, 3160-3169.

133. Y. Li, J. C. Huffman and A. H. Flood, *Chem.Commun.,* 2007, 2692-2694.

134. R. M. Meudtner, M. Ostermeier, R. Goddard, C. Limberg and S. Hecht, *Chem- Eur.J.,* 2007, **13**, 9834-9840.

135. M. Ostermeier, M. A. Berlin, R. M. Meudtner, S. Demeshko, F. Meyer, C. Limberg and S. Hecht, *Chem- Eur.J.,* 2010, **16**, 10202-10213.

136. P. Danielraj, B. Varghese and S. Sankararaman, *Acta Crystallogr C*, 2010, **66**, m366-370.

137. B. Schulze, C. Friebe, M. D. Hager, A. Winter, R. Hoogenboom, H. Gorls and U. S. Schubert, *Dalton Trans*, 2009, 787-794.

138. W.-W. Yang, L. Wang, Y.-W. Zhong and J. Yao, *Organometallics*, 2011, **30**, 2236-2240.

139. B. Schulze, D. Escudero, C. Friebe, R. Siebert, H. Gorls, U. Kohn, E. Altuntas, A. Baumgaertel, M. D. Hager, A. Winter, B. Dietzek, J. Popp, L. Gonzalez and U. S. Schubert, *Chemistry*, 2011, **17**, 5494-5498.

140. L. Munuera and R. K. O'Reilly, *Dalton Transactions*, 2010, **39**, 388-391.

141. W. S. Brotherton, P. M. Guha, H. Phan, R. J. Clark, M. Shatruk and L. Zhu, *Dalton Trans*, 2011, **40**, 3655-3665.

142. S. Özçubukçu, E. Ozkal, C. Jimeno and M. A. Pericas, *Org. Lett.,* 2009, **11**, 4680-4683.

143. C. Wang, L. Salmon, Q. Li, M. E. Igartua, S. Moya, R. Ciganda, J. Ruiz and D. Astruc, *Inorg. Chem.,* 2016, **55**, 6776-6780.

144. B. Beyer, C. Ulbricht, D. Escudero, C. Friebe, A. Winter, L. González and U. S. Schubert, *Organometallics*, 2009, **28**, 5478-5488.

145. E. Orselli, R. Q. Albuquerque, P. M. Fransen, R. Fröhlich, H. M. Janssen and L. De Cola, *J. Mater.Chem.,* 2008, **18**, 4579-4590.

146. W. Yang and Y. Zhong, *Chinese. J. Chem.,* 2013, **31**, 329-338.

147. S. Liu, P. Müller, M. K. Takase and T. M. Swager, *Inorg. Chem.,* 2011, **50**, 7598-7609.

148. D. V. Partyka, L. Gao, T. S. Teets, J. B. Updegraff III, N. Deligonul and T. G. Gray, *Organometallics*, 2009, **28**, 6171-6182.

149. S. Sinn, B. Schulze, C. Friebe, D. G. Brown, M. Jager, E. Altuntas, J. Kubel, O. Guntner, C. P. Berlinguette, B. Dietzek and U. S. Schubert, *Inorg. Chem.,* 2014, **53**, 2083-2095.

150. S. U. Son, K. H. Park, Y.-S. Lee, B. Y. Kim, C. H. Choi, M. S. Lah, Y. H. Jang, D.-J. Jang and Y. K. Chung, *Inorg. Chem.,* 2004, **43**, 6896-6898.

151. D. G. Brown, N. Sanguantrakun, B. Schulze, U. S. Schubert and C. P. Berlinguette, *J. Am. Chem. Soc.*, 2012, **134**, 12354-12357.

152. H. Iwasaki, Y. Yamada, R. Ishikawa, Y. Koga and K. Matsubara, *Eur. J.Org Chem.,* 2016, **2016**, 1651-1654.

153. A. R. Naziruddin, C. S. Lee, W. J. Lin, B. J. Sun, K. H. Chao, A. H. Chang and W. S. Hwang, *Dalton Trans*, 2016, **45**, 5848-5859.

154. V. Leigh, W. Ghattas, R. Lalrempuia, H. Muller-Bunz, M. T. Pryce and M. Albrecht, *Inorg. Chem.,* 2013, **52**, 5395-5402.

155. Y. Liu, K. S. Kjaer, L. A. Fredin, P. Chabera, T. Harlang, S. E. Canton, S. Lidin, J. Zhang, R. Lomoth, K. E. Bergquist, P. Persson, K. Warnmark and V. Sundstrom, *Chemistry*, 2015, **21**, 3628-3639.

156. M. Navarro, S. Wang, H. Müller-Bunz, G. Redmond, P. Farràs and M. Albrecht, *Organometallics*, 2017, **36**, 1469-1478.

157. E. C. Constable, *Coordin. Chem. Rev.,* 2008, **252**, 842-855.

158. S. Q. Bai, D. J. Young and T. Hor, *Chem. Asian. J.,* 2011, **6**, 292-304.

159. S.-Q. Bai, S. Leelasubcharoen, X. Chen, L. L. Koh, J.-L. Zuo and T. A. Hor, *Cryst.Growth & Des.,* 2010, **10**, 1715-1720.

160. S.-Q. Bai, J. Y. Kwang, L. L. Koh, D. J. Young and T. A. Hor, *Dalton Transactions*, 2010, **39**, 2631-2636.

161. P. S. Donnelly, S. D. Zanatta, S. C. Zammit, J. M. White and S. J. Williams, *Chem.Commun.,* 2008, 2459-2461.

162. L. Wang, W.-W. Yang, R.-H. Zheng, Q. Shi, Y.-W. Zhong and J. Yao, *Inorg. Chem.,* 2011, **50**, 7074-7079.

163. B. Happ, J. Schäfer, C. Friebe, H. Görls, A. Winter, M. D. Hager, J. Popp, B. Dietzek and U. S. Schubert, *Synthesis*, 2012, **44**, 2287-2294.

164. J. D. Crowley and P. H. Bandeen, *Dalton Trans*, 2010, **39**, 612-623.

165. S. K. Vellas, J. E. Lewis, M. Shankar, A. Sagatova, J. D. Tyndall, B. C. Monk, C. M. Fitchett, L. R. Hanton and J. D. Crowley, *Molecules*, 2013, **18**, 6383-6407.

166. M. H. Staegemann, S. Grafe, R. Haag and A. Wiehe, *Org. Biomol. Chem.*, 2016, **14**, 9114-9132.

167. J. Kiwi, K. Kalyanasundaram and M. Grätzel, in *Solar Energy Materials*, Springer, 1982, pp. 37-125.

168. H. Hori, J. Ishihara, K. Koike, K. Takeuchi, T. Ibusuki and O. Ishitani, *J. Photochm. photobiol.A...,*1999, **120**, 119-124.

169. K. Koike, H. Hori, M. Ishizuka, J. R. Westwell, K. Takeuchi, T. Ibusuki, K. Enjouji, H. Konno, K. Sakamoto and O. Ishitani, *Organometallics*, 1997, **16**, 5724-5729.

170. H. Hori, F. P. Johnson, K. Koike, O. Ishitani and T. Ibusuki, *J. Photochm. photobiol.A...,* 1996, **96**, 171-174.

171. N. J. Lundin, A. G. Blackman, K. C. Gordon and D. L. Officer, *Angew. Chem. Int.Ed.,* 2006, **45**, 2582-2584.

172. V. Balzani, A. Credi and M. Venturi, *Chem.Sus.Chem.*, 2008, **1**, 26-58.

173. A. J. Amoroso, R. J. Arthur, M. P. Coogan, V. Fernández-Moreira, A. J. Hayes, D. Lloyd, C. Millet and S. J. Pope, *New. J. Chem.,* 2008, **32**, 1097-1102.

174. M. P. Coogan, V. Fernández-Moreira, J. B. Hess, S. J. Pope and C. Williams, *New. J. Chem.,* 2009, **33**, 1094-1099.

175. V. Fernández-Moreira, F. L. Thorp-Greenwood and M. P. Coogan, *Chem.Commun.,* 2010, **46**, 186-202.

176. A. Coleman, C. Brennan, J. G. Vos and M. T. Pryce, *Coordin. Chem. Rev.,* 2008, **252**, 2585-2595.

177. R. Crabtree and M. Mingos, *Comprehensive organometallic chemistry III*, Elsevier Science, 2007.

178. B. P. Sullivan, *J. Phys. Chem.,* 1989, **93**, 24-26.

179. G. Hughes and M. R. Bryce, *J. Mater.Chem.,* 2005, **15**, 94-107.

180. H. Yersin, *Transition Metal and Rare Earth Compounds*, 2004, 1-26.

181. M. Mauro, E. Q. Procopio, Y. Sun, C. H. Chien, D. Donghi, M. Panigati, P. Mercandelli, P. Mussini, G. D'Alfonso and L. De Cola, *Adv. Funct. Mater.,* 2009, **19**, 2607-2614.

182. S. K. Mizoguchi, A. O. T. Patrocínio and N. Y. M. Iha, *Synthetic Met.*, 2009, **159**, 2315-2317.

183. M. Panigati, M. Mauro, D. Donghi, P. Mercandelli, P. Mussini, L. De Cola and G. D'Alfonso, *Coordin. Chem. Rev.,* 2012, **256**, 1621-1643.

184. J. Li, Z. Si, C. Liu, C. Li, F. Zhao, Y. Duan, P. Chen, S. Liu and B. Li, *Semicond.sci & tech.,* 2007, **22**, 553.

185. J. V. Caspar and T. J. Meyer, *J. Phys. Chem.,* 1983, **87**, 952-957.

186. J. P. Bullock, E. Carter, R. Johnson, A. T. Kennedy, S. E. Key, B. J. Kraft, D. Saxon and P. Underwood, *Inorg. Chem.,* 2008, **47**, 7880-7887.

187. A. J. Amoroso, A. Banu, M. P. Coogan, P. G. Edwards, G. Hossain and K. M. Malik, *Dalton Trans*, 2010, **39**, 6993-7003.

188. J. Van Diemen, J. Haasnoot, R. Hage, E. Müller and J. Reedijk, *Inorg. Chem. Acta.,*1991, **181**, 245-251.

189. K. Kalyanasundaram, *J. Chem. Soc. Farad. T 2.,*1986, **82**, 2401-2415.

190. B. P. Sullivan, C. M. Bolinger, D. Conrad, W. J. Vining and T. J. Meyer, *J. Chem. Soc. Chem.Commun.,* 1985, 1414-1416.

191. L. DellaáCiana, *J. Chem. Soc. Chem., Dalton Transactions*, 1991, 849-858.

192. L. Sacksteder, A. P. Zipp, E. A. Brown, J. Streich, J. Demas and B. DeGraff, *Inorg. Chem.,* 1990, **29**, 4335-4340.

193. V. W.-W. Yam, *Chem.Commun.,* 2001, 789-796.

194. A. Juris, S. Campagna, I. Bidd, J. M. Lehn and R. Ziessel, *Inorg. Chem.,* 1988, **27**, 4007-4011.

195. E. Orselli, G. S. Kottas, A. E. Konradsson, P. Coppo, R. Frohlich, L. de Cola, A. van Dijken, M. Buchel and H. Borner, *Inorg. Chem*, 2007, **46**, 11082-11093.

196. K. Kalyanasundaram and M. Grätzel, *Coordin. Chem. Rev.,* 1998, **177**, 347-414.

197. R. H. Schmehl and K. S. Schanze, *J. Chem. Educ.*, 1997, **74**, 633.

198. L. Hung and C. Chen, *Mat. Sci.Eng. R.,* 2002, **39**, 143-222.

199. D. M. Dattelbaum, E. M. Kober, J. M. Papanikolas and T. J. Meyer, *Chem. phys.,* 2006, **326**, 71-78.

200. E. M. Kober, J. V. Caspar, R. S. Lumpkin and T. J. Meyer, *J. Phys. Chem.,* 1986, **90**, 3722-3734.

201. G. F. Strouse, J. R. Schoonover, R. Duesing, S. Boyde, W. E. J. Jones and T. J. Meyer, *Inorg. Chem.,* 1995, **34**, 473-487.

202. B. Maubert, N. D. McClenaghan, M. T. Indelli and S. Campagna, *J. Phys. Chem. A.,* 2003, **107**, 447-455.

203. D. K. Liu, B. S. Brunschwig, C. Creutz and N. Sutin, *J. Am. Chem. Soc.*, 1986, **108**, 1749-1755.

204. F. Barigelletti, L. Flamigni, V. Balzani, J.-P. Collin, J.-P. Sauvage, A. Sour, E. C. Constable and A. M. C. Thompson, *J. Am. Chem. Soc.*, 1994, **116**, 7692-7699.

205. A. Ito, T. E. Knight, D. J. Stewart, M. K. Brennaman and T. J. Meyer, *J. Phys. Chem. A.*, 2014, **118**, 10326-10332.
206. K. Jahn, V. Buschmann and C. Hille, *Sci Rep*, 2015, **5**, 14334.
207. R. S. Lumpkin, E. M. Kober, L. A. Worl, Z. Murtaza and T. J. Meyer, *J. Phys. Chem.,* 1990, **94**, 239-243.
208. O. J. Stacey and S. J. Pope, *RSC Advances.*, 2013, **3**, 25550-25564.
209. W.-Y. Wong, A. S. Abd-El-Aziz and C. Weder, *Molecular Design and Applications of Photofunctional Polymers and Materials*, Royal Society of Chemistry, 2012.
210. B. Happ, D. Escudero, M. D. Hager, C. Friebe, A. Winter, H. Görls, E. Altuntas, L. González and U. S. Schubert, *J. Org. Chem.,* 2010, **75**, 4025-4038.
211. C. R. Arana and H. D. Abruna, *J. Org. Chem.(USA).,* 1993, **32**.
212. E. Figgemeier, L. Merz, B. Hermann, Y. Zimmermann, C. Housecroft, H.-J. Güntherodt and E. Constable, *J. Phys. Chem. B.*, 2003, **107**, 1157-1162.
213. B. Carlson, G. D. Phelan, W. Kaminsky, L. Dalton, X. Jiang, S. Liu and A. K. Jen, *J. Am. Chem. Soc.*, 2002, **124**, 14162-14172.
214. E. M. Kober, J. V. Caspar, B. P. Sullivan and T. J. Meyer, *Inorg. Chem.,* 1988, **27**, 4587-4598.
215. L. De Cola, V. Balzani, F. Barigelletti, L. Flamigni, P. Belser and S. Bernhard, *Rec. Trav. Chim. Pays-Bas.*, 1995, **114**, 534-541.
216. F. R. Spellman, *Handbook of water and wastewater treatment plant operations*, CRC Press, 2013.
217. H. Sun, H. Guo, W. Wu, X. Liu and J. Zhao, *Dalton Trans*, 2011, **40**, 7834-7841.
218. J. N. Demas, B. DeGraff and P. B. Coleman, *Anal.Chem.*, 1999, **71**, 793A-800A.
219. A. C. Kubler, T. Haase, C. Staff, B. Kahle, M. Rheinwald and J. Muhling, *Laser. Surg. Med.*, 1999, **25**, 60-68.
220. B. G. Maiya, *Resonance*, 2000, **5**, 15-29.
221. J. G. Levy, Seminars in oncology, 1994.
222. C. J. Gomer, A. Ferrario, M. Luna, N. Rucker and S. Wong, *Laser. Surg. Med.*, 2006, **38**, 516-521.
223. R. A. Alderden, M. D. Hall and T. W. Hambley, *J. Chem. Educ.*, 2006, **83**, 728.
224. D. Gaynor and D. M. Griffith, *Dalton Transactions*, 2012, **41**, 13239-13257.
225. D. Kuciauskas, J. E. Monat, R. Villahermosa, H. B. Gray, N. S. Lewis and J. K. McCusker, *J. Phys. Chem. B.*, 2002, **106**, 9347-9358.
226. D. M. D'Alessandro, P. H. Dinolfo, M. S. Davies, J. T. Hupp and F. R. Keene, *Inorg. Chem.,* 2006, **45**, 3261-3274.
227. Y. Sun, L. E. Joyce, N. M. Dickson and C. Turro, *Chem. Commun. (Camb).*, 2010, **46**, 6759-6761.
228. S. A. Omar, P. A. Scattergood, L. K. McKenzie, H. E. Bryant, J. A. Weinstein and P. I. Elliott, *Molecules*, 2016, **21**, 1382.
229. B. Tang, F. Yu, P. Li, L. Tong, X. Duan, T. Xie and X. Wang, *J. Am. Chem. Soc.*, 2009, **131**, 3016-3023.
230. J. r. m. Fortage, G. g. Dupeyre, F. Tuyèras, V. r. Marvaud, P. Ochsenbein, I. Ciofini, M. n. Hromadová, L. Pospísil, A. Arrigo and E. Trovato, *Inorg. Chem.,* 2013, **52**, 11944-11955.
231. J.-Y. Shao and Y.-W. Zhong, *Inorg. Chem.,* 2013, **52**, 6464-6472.
232. S. H. Wadman, M. Lutz, D. M. Tooke, A. L. Spek, F. e. Hartl, R. W. Havenith, G. P. van Klink and G. van Koten, *Inorg. Chem.,* 2009, **48**, 1887-1900.
233. W.-W. Yang, Y.-W. Zhong, S. Yoshikawa, J.-Y. Shao, S. Masaoka, K. Sakai, J. Yao and M.-a. Haga, *Inorg. Chem.,* 2011, **51**, 890-899.
234. X. Zhang, M. Papai, K. B. Moller, J. Zhang and S. E. Canton, *Molecules*, 2016, **21**, 235.

235. C. Kreitner and K. Heinze, *Dalton Trans*, 2016, **45**, 13631-13647.
236. C. B. Anderson, A. B. Elliott, C. J. McAdam, K. C. Gordon and J. D. Crowley, *Organometallics*, 2013, **32**, 788-797.
237. C. Nolte, P. Mayer and B. F. Straub, *Angew. Chem. Int. Ed. Engl.*, 2007, **46**, 2101-2103.
238. J. Winn, A. Pinczewska and S. M. Goldup, *J. Am. Chem. Soc.*, 2013, **135**, 13318-13321.
239. L.-L. Cong, M.-Y. Kang, Y.-F. Ji and Z.-L. Liu, *Acta Crystallogr. E.,* 2012, **68**, m669-m669.
240. B. Baeza, L. Casarrubios, P. Ramírez-López, M. Gómez-Gallego and M. A. Sierra, *Organometallics*, 2009, **28**, 956-959.
241. B. S. Uppal, A. Zahid and P. I. Elliott, *Eur. J. Inorg. Chem.,*2013, **2013**, 2571-2579.
242. R. A. Vasdev, D. Preston, S. Ø. Scottwell, H. J. Brooks, J. D. Crowley and M. P. Schramm, *Molecules*, 2016, **21**, 1548.
243. S. V. Kumar, W. K. Lo, H. J. Brooks and J. D. Crowley, *Inorg. Chem. Acta.,*2015, **425**, 1-6.
244. S. V. Kumar, S. O. Scottwell, E. Waugh, C. J. McAdam, L. R. Hanton, H. J. Brooks and J. D. Crowley, *Inorg. Chem.,* 2016, **55**, 9767-9777.
245. L. Favereau, A. Makhal, D. Provost, Y. Pellegrin, E. Blart, E. Göransson, L. Hammarström and F. Odobel, *Phys. Chem. Chem. phys.,* 2017, **19**, 4778-4786.
246. W. K. Lo, G. S. Huff, J. R. Cubanski, A. D. Kennedy, C. J. McAdam, D. A. McMorran, K. C. Gordon and J. D. Crowley, *Inorg. Chem.,* 2015, **54**, 1572-1587.
247. C. E. Welby, G. K. Armitage, H. Bartley, A. Sinopoli, B. S. Uppal and P. I. Elliott, *Photochem & Photobio. S.*, 2014, **13**, 735-738.
248. H. Y. Ching, X. Wang, M. He, N. Perujo Holland, R. Guillot, C. Slim, S. Griveau, H. C. Bertrand, C. Policar, F. Bedioui and M. Fontecave, *Inorg. Chem.,* 2017, **56**, 2966-2976.
249. T. J. Meyer and M. H. Huynh, *Inorg. Chem.,* 2003, **42**, 8140-8160.
250. N. D. McDaniel, F. J. Coughlin, L. L. Tinker and S. Bernhard, *J. Am. Chem. Soc.*, 2008, **130**, 210-217.
251. V. Aranyos, A. Hagfeldt, H. Grennberg and E. Figgemeier, *Polyhedron*, 2004, **23**, 589-598.
252. S. Sprouse, K. King, P. Spellane and R. J. Watts, *J. Am. Chem. Soc.;(USA)*, 1984, **106**.
253. S. Diring, R. Ziessel, F. Barigelletti, A. Barbieri and B. Ventura, *Chem- Eur.J.,* 2010, **16**, 9226-9236.
254. R. L. Bretz, *J.Electroanal.Chem.*, 1995, **388**, 123-132.
255. L. Chen, D. Huang, S. Ren, T. Dong, Y. Chi and G. Chen, *Nanoscale*, 2013, **5**, 225-230.
256. L. A. Büldt, A. Prescimone, M. Neuburger and O. S. Wenger, *Eur. J. Inorg. Chem.,*2015, **2015**, 4666-4677.
257. T. W. Hamann, F. Gstrein, B. S. Brunschwig and N. S. Lewis, *J. Am. Chem. Soc.*, 2005, **127**, 7815-7824.